INVESTIGATION OF CAI/SI OPERATIONS IN A FOUR-CYLINDER DIRECT INJECTION GASOLINE ENGINE

A thesis submitted for the degree of Doctor of Philosophy

By

Navin Kalian

School of Engineering and Design
Brunel University
United Kingdom

July 2006

Brunel University

School of Engineering and Design

United Kingdom

Navin Kalian

Investigation of CAI/SI Operations in a Four-Cylinder, Direct Injection Gasoline

Engine

July 2006

Abstract

A four-cylinder, four-stroke, gasoline engine with direct injection fuel was commissioned and used to achieve CAI combustion. CAI combustion was achieved by employing short-duration, low-lift camshafts and early exhaust valve closure. Trapping sufficient volumes of exhaust residual provided the necessary thermal energy needed to initiate auto-ignition.

The effects of valve opening durations on the CAI operation range were investigated at different air/fuel ratios, valve timings and injection timings. Furthermore the effect on engine performance, exhaust emissions, fuel consumption and combustion characteristics were also investigated.

Methods which could be used for CAI combustion region enlargement were also studied. These included spark-assisted CAI at different EVC timings and valve durations, CAI operation at 2000 rpm and CAI combustion at late fuel injection timings.

Acknowledgements

If a thousand mile journey starts with a first step then it must end with a last step. I would like to thank everyone who helped me with each of my steps through my PhD journey.

First and foremost I would like to offer my sincere gratitude to Professor Hua Zhao for giving me the opportunity to study in his esteemed engines group and allowing me to study technology-leading prototype engines and equipment. Furthermore, for allowing me to attend international conferences and gaining valuable experience in presenting.

I would also like to express my gratefulness to Dr Xi Jiang, who has given sound academic advice and provided guidance throughout my time at Brunel.

I would further like to thank the technicians and everyone in the lab, namely: Bob Webb for his help in ordering sensors and equipment and generally helping with any queries regarding administration matters. Andy Selway for machining various engine components, building engine rigs and giving practical trouble shooting advice with engine problems. I would like to offer my gratitude to Clive Barrett for helping with wiring sensors, making various electrical boxes for the data acquisition system and fault finding. I would like to thank John Langdon and Paul from stores for providing tools and fixtures. Len for milling the Ford engine cylinder head to a high degree of accuracy.

I would also like to take this opportunity to thank my colleagues for their support and advice during this project, namely Cao Li, Chris Marriner, Changho Yang, Mario Martins and Kayiu Mann. I would like to thank Richard Standing for his collaboration and detailing of the Ford Engine.

Last but not least, I would also like to express my gratitude to my parents, who have morally supported me throughout my education and built a solid foundation from which I can work.

Nomenclature

General Abbreviations

AFR	Air/Fuel Ratio
AI	Auto-Ignition
ARC	Active Radical Combustion
ATDC	Active Thermo Atmosphere Combustion
ATDC	After Top Dead Center
BDC	Bottom Dead Center
BMEP	Brake Mean Effective Pressure
BSCO	Brake Specific Carbon Monoxide
BSFC	Brake Specific Fuel Consumption
BSHC	Brake Specific Hydro-Carbons
BSNO	Brake Specific Nitrogen Oxides
BTDC	Before Top Dead Center
CA	Crank Angle
CAI	Controlled Auto-Ignition
CARB	Californian Air Resource Board
CI	Compression Ignition
CIHC	Compression Ignition Homogeneous Charge
CPS	Cam Profile Switching
CR	Compression Ratio
DI	Direct Injection
DISI	Direct Injection Spark Ignition
ECU	Electronic Control Unit
EGR	Exhaust Gas Re-circulation
EOI	End of Injection
EV	Electric Vehicle
EVC	Exhaust Valve Closing
EVO	Exhaust Valve Opening
GDI	Gasoline Direct Injection

GIMEP	Gross Indicated Mean Effective Pressure
HCCI	Homogeneous Charge Compression Ignition
HRR	Heat Release Rate
HSDI	High Speed Direct Injection
IC	Internal Combustion
IMEP	Indicated Mean Effective Pressure
ISCO	Indicated Specific Carbon Monoxide
ISFC	Indicated Specific Fuel Consumption
ISHC	Indicated Specific Hydro-carbons
ISNO	Indicated Specific Nitrogen Oxides
IVC	Intake Valve Closing
IVO	Intake Valve Opening
LEV	Low Emission Vehicle
MBT	Minimum Spark Advance for Best Torque
MFB	Mass Fraction Burn
NIMEP	Net Indicated Mean Effective Pressure
NOx	Nitrogen Oxides
PC	Personal Computer
PFI	Port Fuel Injection
PM	Particulate Matter
PMEP	Pumping Mean Effective Pressure
ppm	Parts per Million
PRF	Primary Reference Fuel
RGF	Residual Gas Fraction
RON	Research Octane Number
rpm	Revolutions per Minute
SA-CAI	Spark Assisted Controlled Auto-Ignition
SI	Spark Ignition
SOI	Start of Injection
SULEV	Super Low Emissions Vehicle
TDC	Top Dead Center
uHC	Unburned Hydrocarbons
VCT	Variable Cam Timing

VVA	Variable Valve Actuation
VOC	Volatile Organic Compounds
WOT	Wide Open Throttle
ZEV	Zero Emission Vehicle

Contents   Page Number

Chapter 1

Introduction

Chapter 1 Introduction

1.1 Introduction

The introduction of Internal Combustion (IC) engines, over a century ago, has provided a robust and relatively inexpensive means of transportation. Indeed the operating principal of an IC engine has also not changed since their introduction. Gasoline IC engines utilize the four-stroke 'Otto' cycle which was developed around 1867 by Nikolaus Agust Otto. Initially, research and development on IC engines concentrated on improving performance and efficiency. However, after a century of use, it became apparent that IC engine emissions contributed towards global warming and other environmental impact. Coupled with dwindling oil reserves, it became apparent that IC engine research and development had to be shifted towards reducing engine-out emissions and fuel consumption. World-wide various emission legislation has been put in place, in a concerted effort to motivate vehicle manufacturers to produce cleaner and more fuel efficient vehicles. Although other technologies exist, such as fuel cells and electric vehicles, which in theory seem to offer a viable power-plant alternative to the IC engine; these technologies still have related short comings. These namely are high cost, efficiency and power density concerns, well to wheel emission issues, hydrogen storage and lack of infrastructure to support these technologies.

In the absence of any feasible alternatives to the IC engine, the last two decades have seen immense steps towards the reduction of emissions and fuel consumption while at the same time enhancing power output. These improvements have been realized due to the application of new technologies to the IC engine, such as three-way catalysts and improved engine management systems. Furthermore, other innovative developments are under progress and expected to be introduced in the near future, these include gasoline direct injection systems, cylinder de-activation, flexible valve operation and cam profile switching. Based on current trends and tightening emission legislation, it can be expected that future IC engines will incorporate technologies which will allow them to be considerably cleaner and have better fuel economy than current IC engines.

Indeed, an alternative combustion technology, known as Controlled Auto-Ignition (CAI) or Homogeneous Charge Compression Ignition (HCCI), is being researched which has high efficiency yet experiences lower NOx emissions and reduced fuel consumption compared with SI engines at a given load. This technology provides a method to meet current and future emission legislation, whilst dismissing the need for expensive, complex and inefficient three-way exhaust gas after-treatment systems.

CAI combustion can be achieved by controlling the temperature, pressure and composition of the fuel and air mixture so that it spontaneously ignites in the engine. To this end, researchers use various methods of achieving CAI combustion, one such method which could be incorporated into present production engines and involve minimum modification is the use of a variable valve timing system which can trap large amounts of burned gas prior to induction. This provides both the thermal energy needed to initiate combustion and the high levels of charge dilution required to control the subsequent heat release rate to sustainable levels. The use of trapped residuals occupying the combustion chamber results in a decreased achievable load. Therefore, in order to provide an engine capable of meeting the wide range load expected from current production engines and to capitalize on low emissions; it is envisaged that an engine capable of SI-HCCI switching would be needed. SI operation would be used at high and low loads and HCCI operation would be utilized at mid-range loads.

Initial research separated SI operation with the use of high-lift, long-duration camshafts and CAI operation with the use of low-lift, short-duration camshafts. However, it becomes apparent that SI operation can also be achieved with low-lift, short-duration camshafts. Therefore providing an enlarged scope for seamless transitioning, i.e. switching from low-lift, short-duration SI combustion to CAI combustion.

For CAI combustion, the gas exchange process and hence engine load, is controlled primarily by valve timing, therefore its effect on CAI combustion with regards to engine performance, exhaust emissions and operating range were investigated. A GDI injection

system and hence injection timing offers further flexibility over ignition phasing and therefore was studied as a means of combustion control.

1.2 Objectives of Project

The objectives of this project are to:

1   Demonstrate CAI operation in a production type multi-cylinder engine using short-duration, low-lift camshafts and trapping exhaust residual.

2   Investigate CAI, SI and CAI/SI regions using different camshaft profiles and examine the effect on exhaust emissions, fuel consumption and combustion characteristics.

3   Develop potential strategy for transitioning between SI/CAI operation.

4   Explore the potential for enlarged CAI operation through the investigation of spark-assisted CAI combustion at different EVC timings and valve durations, increased engine speed and late fuel injections.

1.3 Outline of Thesis

Following this introduction, Chapter two is a review of relevant literature relating to the project and is split into three main parts. First of all, the current and future emissions legislation with regard to vehicles is outlined in order to give context for the motivation for research and development of IC engines. Next, the historic and current development of CAI technology and various methods available to achieve CAI combustion are discussed briefly. Finally, issues involved with transitioning from SI to CAI and back to SI operation are discussed.

The basics and operation of experimental setup and test facilities used to obtain all measurements and data are described in Chapter 3. The key mechanisms namely, the direct injection system, the ECU and control system, and the variable valve timing mechanism used to undertake the research are described. Finally the equipment and sensors used to control and monitor the engine are also listed.

Chapter 4 details the data acquisition system used to obtain pressure data and methods used to validate acquired data. Furthermore, load, specific fuel consumption as well as specific emission calculations are listed. Finally, the method used to obtain the heat release rate and the 10%, 50% and 90% MFB are also given.

Chapter 5 introduces the research methodology used to undertake testing, thereafter the effects of valve duration on CAI combustion are investigated. An initial load-speed map and load-valve timing map is provided so that the operating region for the research engine can be established. Contour maps are used to represent engine performance and emission data for the SI, Spark-assisted and CAI combustion regions for both shorter and longer duration CAI camshafts at lambda 1.0. The effects of air/fuel ratio at lambda 1.2 on CAI combustion are also investigated in Chapter 5. Testing was carried out for all possible IVO-EVC valve timing combinations including SI combustion, spark-assisted combustion and CAI combustion for both shorter and longer CAI camshafts. Contour maps were plotted and performance and emission characteristics were studied.

Areas which offer potential for CAI combustion region enlargement were studied in Chapter 6. It was decided from observational and simulation work that the areas that merited further investigation were spark-assisted CAI, high speed CAI combustion and the effects of late injection on CAI combustion.

Chapter 7 presents the general conclusions that can be drawn as a result of the knowledge learned during this project. This chapter also contains recommendations for future work and avenues worthy of exploration in order to progress CAI engine research further.

Chapter 2

Literature Review

Chapter 2 Literature Review

2.1 Introduction

There is currently an urgent need to reduce world wide fuel consumption, green house gas emissions and car exhaust emissions. Transport accounted for about 24 per cent of UK greenhouse gas emissions in 2002. Carbon dioxide is the most significant greenhouse gas emitted, accounting for about 80 per cent of emissions from the transport sector in 2002 [1]. It is predicted that carbon dioxide emissions from road transport is expected to grow by 9 per cent or so between 2000 and 2010.

Many technologies and concepts have received attention from the media, as potential solutions for reducing fuel consumption and car exhaust emissions. However, there are still many issues which have to be resolved before these technologies can reach mass production. Technologies such as fuel cells and all-electric vehicles require substantial infrastructure re-construction, from fuel supply through to technology maintenance work. In comparison the internal combustion engine offers flexibility for further development with little alteration to current infrastructure. Alternative and renewable fuels can be used, variable valve technologies (VVT, electro-hydraulic valves) can be adopted, a range of exhaust after-treatment catalysts utilized. Indeed the IC engine can be developed further to incorporate a new combustion technique referred to as Homogeneous Charge Compression Ignition (HCCI). This study investigates the benefits of HCCI combustion such as improved fuel consumption and lower emissions compared with standard SI combustion. As with most technologies there are issues which need to be overcome before production status can be reached. This study also examines how these issues can be resolved gradually and within the foreseeable future; hence providing the next generation of highly efficient and low emission engines.

2.2 Emission Standards Worldwide

The main pollutants arising from burning fossil fuel are carbon monoxide (CO), oxides of nitrogen (NOx), unburnt hydrocarbons (uHC) and fine particulates. The effects of these pollutants can be divided into local and environmental effects. At a local level, NOx and VOCs (emitted at ground level) can react with atmospheric oxygen in the presence of sunlight to contribute to the formation of ozone and the formation of acid rain leading to water quality problems. Combustion of Hydrocarbons under rich conditions leads to the incomplete carbon oxidation (CO_2) resulting in the formation of carbon monoxide (CO). This gas when inhaled causes respiratory problems, reduced flow of oxygen in the bloodstream and can impair mental functions and visual perception. On an environmental level, emissions of CO_2 and unburnt hydrocarbons are blamed for accelerating Global Warming through increasing the Earth's Greenhouse effect.

Emissions, such as NOx, CO and VOC, emitted from hydrocarbon fuelled powerplants, have been dramatically reduced over the years through continued improvement of exhaust gas after-treatment technologies such as catalytic converters. In the last 30 years, reduction has been motivated by a continual tightening of the legislation regulating the emissions of these pollutants. This has been enforced in all developed countries and some developing countries.

Car manufacturers worldwide, follow either national emission standards or Euro standards. In Japan in 1976, the Central Environment Council came out with the Motor Vehicle Exhaust Emission Regulations, which comprehensively set the standards for NOx, HC and CO both for gasoline and diesel-fed vehicles. In November 1997, a report was produced outlining more stringent regulations and setting the path for stricter emission standards.

The United States has two sets of standards: Tier 1 and Tier 2 which have been defined for light-duty vehicles in the Clean Air Act Amendments (CAAA) of 1990. The Tier 1 regulations were published in 1991 and fully implemented in 1997. The Tier 2 standards were adopted in 1999, phased-in beginning in 2004. Tier II regulations are 50 to 95 percent lower than Tier I, depending on the pollutant and vehicle class [2]. In California, the

Californian Air Resources Board (CARB) has specified additional standards to Tier I regulations. Car manufacturers are required to produce a percentage of vehicles certified to increasingly more stringent emission categories, generally based on vehicle fleet emission averages. The current California emission standards are expressed through the following emission categories: Tier 1, Transitional Low Emission Vehicles (TLEV), Low Emission Vehicles (LEV), Ultra Low Emission Vehicles (ULEV), Super Ultra Low Emission Vehicles (SULEV) and Zero Emission Vehicles (ZEV).

In China, Vehicle and engine emission standards are adopted at a national level by the State Environmental Protection Administration (SEPA). First emission regulations became effective in the 1990's. Chinese standards are based on European regulations, which are being adopted with a certain time delay. It is planned that Beijing will implement Euro 4 standards for light duty vehicles by 2008, the year of the Beijing Olympics.

Since the year 2000, India started adopting European emission and fuel regulations for four-wheeled light-duty and heavy-duty vehicles. In 2003, the National Auto Fuel Policy was announced, which envisages a phased program for introducing Euro 2 - 4 emission and fuel regulations by 2010.

Table 2.1 Current and future EU and CARB legislated emissions levels for passenger cars [3],[4].

Euro Standard	Year	Engine type	CO (g/km)	HC/NMOG (g/km)	NOx (g/km)	HC+NOx (g/km)	PM (g/km)
Euro III	2001	SI	2.3	0.2	0.15	-	-
		CI	0.64	-	0.5	0.56	0.05
Euro IV	2005	SI	1.00	0.1	0.08	-	-
		CI	0.5	-	0.25	0.3	0.025
Euro V	2008	SI	-	0.05	0.08	-	0.0025
		CI	-	0.05	0.08	-	0.0025

*After 100,000 miles

Directive 98/69 specified Euro III emission levels in Europe, effective from 1st January 2001 and Euro IV emission levels introduced from 1st January 2005 and fully effective from 1st January 2007. Table 2.1 lists the various Euro standards and the permissible pollutant output (g/km). It can be seen that Euro IV emissions are approximately one quarter of Euro I emissions. The upcoming Euro V emissions coming into force in 2008, are even more stringent for both SI and CI engines. Permitted levels of HC, NOx and PM are 0.05, 0.08 and 0.0025 g/km consecutively, for HC this is a reduction of 66% and for PM a reduction of 90% over Euro IV emissions. Therefore, there is a need to drastically modify existing SI and CI engines in order to comply with strict upcoming regulations. To this end, there are on-going research projects world wide investigating methods to reduce emissions.

Ultimately the objective of emission legislation is to push technology to the point where a practical, affordable zero emission vehicle (ZEV) with acceptable performance becomes a reality. Technology exists which provides a powerplant for road going vehicles whilst producing zero emissions. One such ZEV technology which has been developed at a conceptual stage is fuel cell technology. A fuel cell uses an electrochemical reaction to create electricity using hydrogen and ambient air, resulting in water vapor as the only emission. A fuel cell consists of two electrodes sandwiched around an electrolyte. Oxygen passes over one electrode and hydrogen over the other, generating electricity, water and heat. Hydrogen fuel is fed into the anode of the fuel cell. Oxygen (or air) enters the fuel cell through the cathode, encouraged by a catalyst, the hydrogen atom splits into a proton and an electron, which take different paths to the cathode. The electrons create a separate current that can be utilized before they return to the cathode, to be reunited with the hydrogen and oxygen in a molecule of water. Fundamentally this technology only produces water vapor as an emission. However, obstacles that exist with hydrogen fuel cell technology which make it a highly unlikely candidate for mass transport purposes at the present time are: the onboard storage of hydrogen at high pressure raising safety issues, mass production of hydrogen, and fuel supply infrastructure overhaul.

Another technology which is being developed to provide a reduction in emissions and a path towards ZEV's is the use of battery power. This is in the form of a Hybrid Electric Vehicle (HEV) which combines an internal combustion engine with a battery driving an electric motor. The battery is kept recharged by an engine-driven generator. The electric motor is used for low speed ranges and assisting the combustion engine at high speeds, allowing downsizing of both components. Due to the stop-start ability of an electric motor the engine can be shut-off when the vehicle comes to a stop and restarted when the accelerator is pressed; preventing wasted energy from idling. Fuel economy can be increased through regenerative braking; the energy that is recovered during braking is stored by the battery and is later used. Toyota Prius, have a 201 volt, 1.3kWh battery pack mounted under the rear passenger seat. Speeds of only 42 mph can be realized on pure battery power, and that is if the battery is fully charged and the engine is warmed up.

Although exhaust emissions are reduced for HEV, based on the fact that battery operation does not produce exhaust emissions, there are still issues of emissions generated from electricity production. Furthermore, the lack of battery technology is one of the limitations of the HEV and the all-electric vehicle (EV) preventing mass-production. The types of batteries that are being tested and used are high-powered lead acid, nickel-metal hydride, lithium ion, and lithium polymer. Each has associated disadvantages including: the amount of power, cost, safety, reliability, specific energy, cold temperature performance, high temperature performance, calendar life, cycle life, heat generation, self-discharge, and abuse tolerance. The extra weight of battery packs and additional electric motor and associated high cost would limit HEV to a niche market.

2.3 Current Gasoline Engine Technologies

After investigating alternative powerplants, it is apparent that there is no readily available technology which offers a simple alternative. Therefore, a great deal of research has been dedicated to traditional SI and CI engine technology to improve emissions and fuel consumption. Indeed, the adoption of the 3-way catalytic converter has allowed gasoline engine-out emissions of CO, uHC and NOx to be reduced by over 90%. However, so that

11

the catalyst can operate efficiently, engine operation has to be maintained within a few percent of stoichiometry. This degree of AFR precision is beyond the capabilities of the traditional carburetor and so has been replaced by electronically controlled closed loop fuel injection systems. This has added significantly to vehicle cost, furthermore continuous stoichiometric operation prevents the engine from operating with a lean AFR at part load, leading to a small but significant increase in overall fuel consumption.

In order to vary engine load in SI engines, air flow and fuel flow must be controlled simultaneously. Furthermore, the 3-way catalyst must operate with homogeneous charge and at $\lambda = 1.0$. Intake throttling is used to control airflow intake, leading to an increase in pumping losses that reduce engine efficiency by up to 20%. However High Speed Direct Injection (HSDI), and stratified charge gasoline direct injection (GDI) engines, permit lean combustion by allowing fuel flow rate (and hence load), to be varied independently of airflow. Significant reductions in fuel consumption, particularly at part load can be achieved. Ultimately, though 3-way catalysts are limited to operation at stoichiometry, therefore the fuel savings of using a GDI engine at lean lambda is offset by the fact that catalysts are rendered inefficient at reducing NOx emissions away from $\lambda = 1$. Even though the technology to achieve NOx reduction from lean burn engines is available [5], it is currently very expensive and can suffer from durability problems.

A new type of technology which reduces the need for 3-way catalysts and allows operation over different Air Fuel Ratio's whilst offering a vast reduction in emissions and improved efficiency is Homogeneous Charge Compression Ignition (HCCI) also known as Controlled Auto-Ignition (CAI). These engines are not radically different from spark ignition engines found in production cars today. It is the actual combustion method which separates CAI engines from standard SI engines. Controlled Auto-ignition is achieved by subjecting part or the entire cylinder contents to temperatures above those required for auto-ignition of the reacting species.

2.4 Controlled Auto-Ignition Combustion/ Homogeneous Charge Compression Ignition (HCCI)

2.4.1 Benefits of HCCI combustion

The concept of CAI/HCCI combustion can be traced back to about 20 years ago when Onishi et al. (1979) [6] discovered an alternative combustion method within 2-stroke engines that allowed a remarkable improvement in emissions and fuel consumption. Identifying a new lean combustion process for internal combustion engines, they called it 'Active Thermo-Atmospheric Combustion' (ATAC). ATAC differs from conventional gasoline engine combustion in that combustion reactions occur spontaneously at many locations within the combustion chamber sometimes leading to erratic combustion. To Onishi et al. it was not clear where combustion commenced due to the gradual change in combustion pressure. They found that with this combustion mode, there was no discernible flame front propagating through the combustion chamber similar to SI engines. They also found that ATAC differs from diesel combustion in that the fuel and air are uniformly mixed. Therefore, Onishi et al. considered ATAC as a third combustion process of the internal combustion engine. Onishi et al. found that stable combustion could be achieved with a lean mixture at part–throttle operation. Indeed production engines were produced within the Japanese market [7,8] which utilized CAI/HCCI combustion at light-load conditions and reverted to conventional SI combustion systems at high load.

Despite the advantages of operating two-stroke engines in CAI/HCCI combustion mode, there still exists many problems which make it unsuitable for mainstream automotive applications. Firstly during the intake process, due to the lack of low pressure, fresh charge has to be pumped into the cylinder. In most cases, this is achieved by initially inducting the fresh charge into the crankcase as the piston rises and subsequently using crankcase pressure generated by the descending piston to push the charge into the cylinder. However, this configuration prevents the use of a closed, re-circulating lubrication system, meaning a total loss system where lubricating oil is mixed with fuel, causing extremely high levels of uHC emissions. A separate pump to drive in the charge must be used to overcome this

problem, leading to increased costs, complexity, weight and parasitic losses that increase fuel consumption. Furthermore, there are associated drivability issues, since the influence of gas flow dynamics on the gas exchange process dictates that torque is strongly related to engine speed. Also, during high load operation, there are unacceptable levels of uHC emissions, due to fuel 'short circuiting' caused by the simultaneous opening of the intake and exhaust ports.

With CAI/HCCI combustion evidently offering fuel efficiency and emissions improvement for two-stroke engines, researchers focused their attention on CAI/HCCI combustion within four-stroke engines. Four-stroke engines are more suited for automotive applications and the benefits of being able to run these engines in CAI/HCCI combustion mode are numerous. The single largest attraction of HCCI combustion is that it can reduce NOx emissions by 90-98% [9-13]. The underlying mechanism responsible for this reduction in NOx emissions is the absence of high temperature regions with the combustion. HCCI combustion reactions occur at the global air-fuel ratio, which is typically quite lean, and at a temperature significantly below those encountered within the reaction zone in diesel or spark-ignition engines [14].

Particulate matter emission levels are also low for HCCI combustion. HCCI combustion takes place at near homogeneous conditions throughout the mixture. Since there is no fuel-rich diffusion burning taking place, the particulate emissions are at near zero levels. In principle, homogeneous mixtures of fuel and air do not produce particles of significant size (e.g. mass) [15].

HCCI combustion benefits from high thermal efficiency. Large amounts of charge dilution dramatically reduce the peak burned gas temperature, which in turn reduces the closed-cycle heat losses and increases the indicated thermal efficiency to levels approaching those of a diesel engine [16].

Another benefit of HCCI combustion is improved fuel economy, Fuerhapter et al. [17] states that the fuel consumption benefit of such a combustion process comes from more or

less unthrottled operation and a high efficiency combustion. The controlled auto-ignition combustion is characterized by thermodynamically optimized combustion timing and very fast combustion and high heat release rates. So far new technologies for spark-ignition engines, including stratified-charge direct-injection spark-ignition (SC-DISI) engines, can only improve fuel economy up to 10-12% over European regulatory drive cycles [18]. The highest fuel consumption improvement potential is provided by lean stratified combustion systems. The relative expensive exhaust gas after-treatment and the sensitivity to the fuel quality especially the sulfur content, congests a world wide application of these systems [19]. HCCI combustion can achieve fuel savings of upto 20% compared with SI engine combustion at the same load [20].

2.4.2 Approaches to CAI/HCCI Combustion Gasoline engines

The many benefits of CAI/HCCI combustion provide motivation for researchers to realize this combustion within four-stroke engines; ultimately developing methods to achieve CAI/HCCI within production engines. The initial approach of achieving CAI/HCCCI combustion utilized intake charge heating, this involved the use of an electrical heater to heat the intake air and provide the thermal energy needed for the charge to auto-ignite. Najt and Foster [21], used this method to highly dilute charge compositions to control the subsequent heat release. Even though initiating CAI/HCCI combustion through intake charge heating has been used in many subsequent studies, this method has limited automotive applications. The drawback is that energy is needed for intake air heating, unless heat can be recovered from engine coolant or exhaust gas, an auxiliary heat system most likely powered by extra fuel would be needed. Hence the fuel efficiency benefits of CAI/HCCI combustion would be offset against the extra energy required to heat the intake air. Also owing to the highly transient nature of automotive applications the large thermal inertias associated with heating the intake charge will make control of CAI/HCCI combustion with this method very hard to achieve. Nevertheless, Najt and Foster's work established the potential of CAI/HCCI combustion to reduce fuel consumption in four-stroke engines.

Variable compression ratio can also be used to initiate CAI/HCCI combustion. Increasing the compression ratio allows fuels to ignite more readily. Mariott et al. [22] found that higher compression ratio resulted in optimum intake air temperature and higher intake air density. The Ricardo E6 single cylinder engine has been used to demonstrate the use of variable compression ratio for auto-ignition. However, since changing the engine's compression ratio requires overcoming the force of cylinder pressure, a reliable VCR device, which can fine tune the engine compression ratio and has fast response, has yet to be demonstrated [18]. Furthermore, using a VCR engine to achieve CAI/HCCI would substantially increase the cost of the engine.

CAI/HCCI combustion can also be achieved through the use of different fuels, allowing greater flexibility in realizing combustion. Research studies on primary reference fuels (PRFs) indicated that the auto-ignition behaviour of a fuel depends largely on its composition, molecular size and structure [23] allowing various fuels to be suitable for CAI/HCCI combustion. Jun et al. [24] and Yap et al. [25] have shown that natural gas could be used in a CAI/HCCI four-stroke engine. Pucker et al. [26] reported that methanol appears to offer a wider operating range, smoother combustion and faster heat release than gasoline for CAI/HCCI combustion applications. In addition to being able to use different fuels for CAI/HCCI combustion instigation, fuel additives can be added to gasoline to alter combustion behaviour. Gong et al. [27] used a Di Tertiary Butyl Peroxide (DTBP) additive along with gasoline to investigate the effects on CAI/HCCI. They found that DTBP affects fuel oxidation by causing higher in-cylinder temperature and hence increased oxidation. They also found that increasing the concentration of DTBP retards ignition timing. The use of different fuels and fuel additives play an important role in offering flexibility over the CAI/HCCI process. However, the introduction of new fuels or additives require infrastructure overhaul and is expensive.

It is apparent that the main challenge for triggering auto-ignition is obtaining sufficient thermal energy. Researchers turned their attention to burned exhaust gas which provided a ready source of thermal energy which did not incur any energy penalties like intake air heating. Initial efforts involved re-circulating exhaust gas from the exhaust manifold

16

through an EGR runner back into the intake manifold. Thring et al. [28] were the pioneer of this technique using external EGR on a SWRI Labeco CLR engine and accomplishing CAI/HCCI combustion. However, it is apparent that external EGR has inherent problems the main being that a dead volume of exhaust gases are present in the EGR runner. This causes cycle to cycle variations and heat losses as the exhaust gas is passed through the EGR runner. Furthermore, regulating the amount of EGR gas is difficult and involves difficult bypass valves. A method which offers more flexibility is the use of internal EGR through the use of negative valve overlap. With this method, the exhaust valve is closed early and a volume of exhaust gas is trapped, the intake valve is opened late preventing blow-back in the intake manifold [29]. The more advanced EVC, the greater the volume of trapped residual.

Investigators involved in the 4-SPACE [30] project realized CAI/HCCI combustion of gasoline at the part load, low speed range of the engine using fixed camshafts, but with shorter than normal valve opening duration and lower than normal valve lift. They coined the term Controlled Auto-Ignition (CAI) which has become synonyms for HCCI combustion generated by trapping residuals. Due to this reason the author will refer to HCCI combustion as CAI combustion within the results and discussions chapter. Furthermore, HCCI combustion implies that the charge is homogeneously mixed, however with GDI engines, at late injection the charge can be stratified. Therefore, the author believes that CAI is a more accurate term to describe the combustion process.

With the advent of variable valve timing systems, the scope for CAI combustion increased drastically. A second residual trapping method was proposed, namely the re-breathing method, which allows the exhaust valve to open during the intake stroke and thus induct previously emitted exhaust gas.

Over the last few years, the IEGR method of initiating and controlling CAI combustion has been agreed as the most feasible method which offers the best chance of CAI combustion being realised for automotive applications. Furthermore, this method offers the easiest route in terms of implementation in current production engines. Apart from the addition of

a new valve train and control system, there is no need for any changes to the vehicle or engine architecture.

2.4.3 Challenges concerning HCCI combustion

There exist many methods to initiate CAI combustion and the emission and fuel economy improvements remain a motivational factor for adopting this concept in production engines. However, CAI combustion presents several hurdles and challenges which must be overcome if CAI combustion is to be considered for application to commercial engines. CAI/HCCI combustion is governed by chemical kinetics and has no flame propagation, the principle of SI combustion. CAI/HCCI combustion is achieved by controlling the temperature, pressure and composition of the air and fuel mixture so that it spontaneously ignites in the engine [31]. Therefore determining the phasing and rate of combustion presents many difficulties. Several potential methods exist which can be used to control CAI combustion ignition timing. Christensen et al. [32] lists the following parameters as controlling factors:

- Compression Ratio
- Inlet Mixture Temperature
- Inlet Manifold Pressure
- Fuel type/blend
- Air/Fuel Ratio
- EGR rate
- Engine Speed
- Coolant Temperature

The method with the most practical basis of achieving CAI is using variable valve timing (VVT), this allows limited control of combustion phasing by changing the effective compression ratio and/or the amount of hot exhaust gases retained in the cylinder [33-34]. Therefore additional methods are needed to control combustion phasing and burn rate. Various methods have been implemented which involve practical and conceivable changes

18

to the current production IC engines. One such method is injecting fuel directly into the cylinder, this provides the potential to control combustion by altering the local fuel concentration via varying the injection timing. The gas temperature may also be altered through charge cooling from fuel evaporation. Early fuel injection provides adequate time for fuel to vaporize and mix with the air to achieve a homogeneous charge. Late pilot fuel injection into the combustion chamber during the compression stroke can control the HCCI combustion by increasing the local fuel concentration in some regions of the combustion chamber. Urushihara et al. [35] directly injected fuel into the residual in-cylinder gas during the negative valve overlap interval for the purpose of reforming it by using the high temperature resulting from exhaust gas recompression. They found that with this strategy, the HCCI combustion region was expanded drastically without any increase in NOx emissions.

Another challenge with CAI/HCCI combustion is that CO and uHC emission levels of CAI combustion can reach or even surpass those of SI engines. The source of these emissions has generally been considered to be incomplete combustion in crevices and/or near walls where the mixture is cooler [36]. Through the investigation of single and multi zone models Martinez-Frias et al. [37] reason that uHC and CO emissions result from cold mass in crevices and boundary layers, which are too cold to burn to completion. The use of a relatively cheap 3-way catalyst can curb CO and uHC emissions.

One of the major hurdles blocking progression to commercial production of CAI/HCCI engines is the limited operating boundary compared with traditional SI operation. Due to the trapping of exhaust gas residual, there arises a CAI/HCCI combustion region with a subsequent boundary where EGR percentage and equivalence ratio define and ultimately limit this boundary. CAI/HCCI combustion is limited by three regions of unsatisfactory operation identified primarily by Thring et al. [28]. These are the 'misfire region,' 'power-limited region,' and the 'knock region.' In the misfire region, either the mixture is too rich or the EGR percentage is excessive for consistent combustion resulting in engine misfire. In the power-limited region either the mixture is too lean, or the EGR percentage is excessive for the indicated power to exceed the friction power. In the knock region, under

19

rich conditions and low EGR percentage combustion is so rapid that the engine is very noisy and knock is occurring.
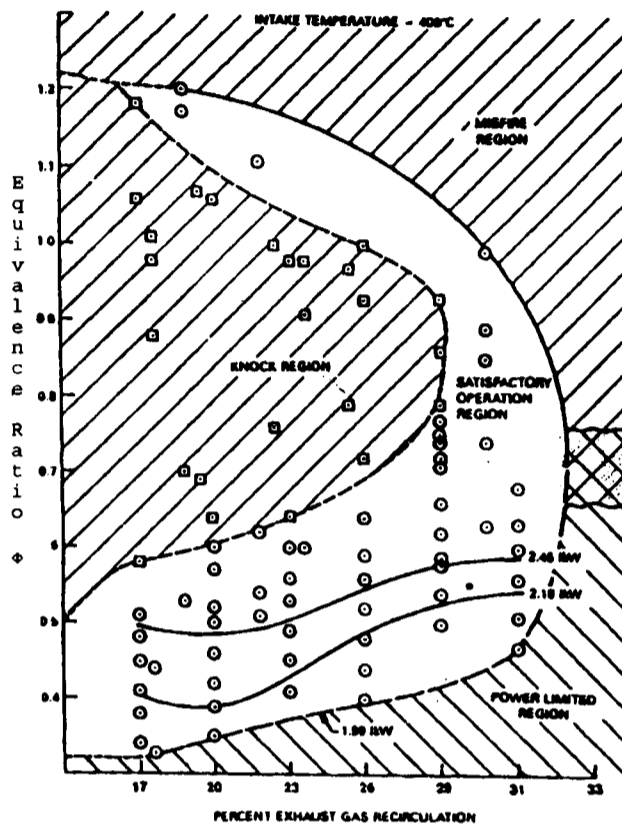

Figure 2.1 Typical HCCI Operation Map indicating boundary regions [28]

The CAI/HCCI combustion region can also be appreciated further by describing the effects of EGR percentage on load and speed. Minimum load is limited by misfire, at these conditions there is a lot of residual gas but the exhaust gas temperature is too low to initiate auto-ignition. Maximum load is restricted by airflow, at these conditions the airflow is the maximum that the engine can breathe due to reduced valve lifts used for a negative valve overlap configuration to achieve CAI/HCCI combustion.

At low equivalence ratios and low EGR percentage i.e. high loads, HCCI engines are extremely loud and measured in-cylinder pressure traces show strong oscillations resembling those for a knocking spark ignited engine [38]. Yelvington et al. developed numerical simulations used to predict the viable operating range of HCCI combustion and the reason for knock being a limiting factor. They reasoned that CAI/HCCI knock originates because of local inter-pressures due to very fast chemical heat-release. Indeed,

20

the potential method of using boosting to increase the CAI/HCCI combustion boundary also suffers from high cylinder inter-pressures (around 250 bar for 2 bar boost pressure), which can cause premature engine failure. Furthermore, a drawback to encroaching the high load boundary using boosting is the gas exchange process limited by EGR percentage. Olsson et al. [39] have demonstrated that high load CAI/HCCI combustion is viable by applying boost. However, they found in most cases that gas exchange efficiencies was load limiting.

It is apparent that to increase the boundary of the CAI/HCCI combustion region whilst also obtaining control over the auto-ignition process, a combination of technologies is required.

2.4.4 Transitioning from SI to HCCI mode

Various technologies can be used to enlarge the CAI/HCCI combustion region, as described, but ultimately due to the limited operating region of HCCI combustion, a SI/CAI hybrid engine would need to be used. SI combustion could be used for cold start and high loads and CAI/HCCI combustion can be used for operation at low to mid-range loads. This would allow the emission and fuel consumption improvements with CAI/HCCI combustion at low-mid loads while maintaining the full load operating range of the IC engine at high load using SI combustion.

Researchers have investigated the effects and feasibility of transitioning from SI combustion to CAI/HCCI combustion and back to SI combustion [40]. Comprehensive work involving SI-HCCI-SI mode change was carried out by Koopmans et al [41]. They identified three transition modes:

1. Transition from HCCI part load to SI high load conditions and vice versa.
2. Transition from HCCI low to middle speed range to SI high speed range and vice versa.
3. Transition from SI operation to HCCI operation.

Transition mode 3 proved the most difficult to achieve. Koopmans et al. states that the gain in fuel conversion efficiency has to be known or predicted in order to adjust the fuel flow and avoid a torque jump. The authors found that with the proper setting of the control parameters, no problems with mode change were encountered.

Sun et al. [42] undertook transitioning a HCCI engine along a given power curve of 3.5 kW to 30 kW. In order to set smooth transition from one point to the next, the fuelling rate, boost level, EGR intake charge and coolant temperature were varied accordingly. They achieved ramping up time of 5 seconds and ramping down time of 1 second. The work carried out paved the way for using CAI/HCCI engines as a potential power plant for a hybrid vehicle.

A method which has been viewed as a potential way in which SI-HCCI-SI transition can be made is through the use of a cam profile switching (CPS) system. On both the intake and exhaust camshafts there are two lobes on each camshaft with two different valve profiles. There is a low-lift, short-duration lobe for CAI/HCCI operation and a high-lift, long-duration lobe for SI operation. Milovanovic et al. [43] used an engine with such capabilities, there was a fully variable valve timing system with cam profile switching (CPS) capabilities to transition from SI-HCCI-SI modes. The authors investigated the influence of engine torque, power, combustion stability and maximum rate of pressure rise (MRPR) controlling parameters regarding transition smoothness. For cold start and mode transition, the research engine is started in SI mode and when the coolant temperature reaches 90°C, there is a mode transition from SI to HCCI achieved by first reducing the valve lift and then advancing exhaust valve timing and trapping exhaust residual; realizing HCCI combustion within one engine cycle. Changing from HCCI to SI was not so smooth and the authors reported a considerable change in the engine torque and uHC. This was due to the unsynchronised valve profile changes, throttle response and unadjusted fuelling rate that in turn caused a very weak combustion or misfire or both. It was found that throttle response was more influential on the SI-HCCI-SI transition process than valve profile switching. Furthermore, Milovanovic et al. found that during transitioning from HCCI back to SI, the uHC values experienced a sharp rise during the first few cycles in SI mode before reaching

a stable value. When transitioning from SI to HCCI mode, there was not an immediate drop in NOx values when HCCI mode was realised. Instead, there was a few cycles lapse before NOx values dropped to the level of those expected for HCCI.

The SI-HCCI-SI transition methodology provides a feasible method in which the benefits of HCCI combustion can be utilized while high loads can still be achieved with SI combustion.

2.4.5 Feedback Control Systems for HCCI combustion

It becomes apparent if HCCI combustion is to see use in automotive applications that a system has to be implemented that could take into account transient operation and select the right operational mode, i.e. SI or HCCI combustion mode without any interaction by the driver. Furthermore this system would also have to have capabilities which can select the right values for optimum ignition time; it is obvious that a system with a feedback control system is required. Researchers have begun to develop feedback systems, however, these systems are still at a primitive stage in comparison to how intricate these systems need to be. Nevertheless, work has been carried out which can give an insight into the requirements and sophistication of a feedback controller.

Haraldsson et al. [44] applied a state feedback based closed-loop combustion control (CLCC) using Fast Thermal Management (FTM). Using this control method the European EC2000 drive cycle was mimicked. The CLCC was designed to keep a desired CA50 at all times and compare this to the set point for the cylinder in question. The result was sent to the PID controller where a duty cycle for a PWM signal is calculated. The hot air throttle receives the PWM with the calculated duty cycle, while the cold air throttle works with an inverse duty cycle i.e. if the hot throttle is wide open the cold one is shut. Ultimately, the load controller handled load steps and speed ramps satisfactorily and has a time constant of 5 to 6 engine cycles or 0.30 to 0.36 seconds at 2000 rpm. In their research, a combination of CAI/HCCI and SI operation is shown to be superior to scaled CAI/HCCI approach, which suffers from low mechanical efficiency at low load. It was demonstrated that both

23

CO and NOx emissions are well below the Euro IV limits. HC emissions were slightly above the limit when calculated without cold start. The authors concluded that for improvements in fuel consumption the current PID and state feedback controllers were sufficient. However, emissions could be decreased further using an improved controller.

Mathews et al. [45] have also developed a controller to simulate drive-by-wire conditions where the driver commands the engine torque output according to the perceived vehicle speed. Ultimately, they developed a load following controller with a table-lookup feed-forward component and a feed-back component based on the cumulative difference between the targeted and measured output. Matthews et al. were able to follow the commanded values of NIMEP not fuel equivalence ratio (ϕ) dynamically under timing varying operating conditions. The temperature was modulated between 100°C and 120°C. The speed was modulated from 1350 to 1650 rpm. The ϕ target was at stoichiometric. A transition time of 0.25 seconds was used to vary NIMEP with a 3 second lapse between each transition.

Fuerhapter et al. [17], studied whether a closed loop combustion control is necessary and if it has to be cylinder individual. A possible solution is provided in the way of a cylinder pressure signal which gives the possibility of a real combustion control. However, there are still cost issues involved with mass production of these sensors. Fuerhapter et al. also designed a block diagram which represented a transition algorithm. In this they took into account EVC position for stationary CAI/HCCI operation and EVC position for the first CAI/HCCI cycle. They included a correction for first cycle value by actual load temperature history. They included a parameter for transition function which was cycle based.

A feedback control system is a method in which CAI/HCCI combustion can be controlled in order for it to be used within production engines. Other technologies are emerging as a possibility for enlarging the CAI/HCCI combustion region.

2.4.6 Emerging HCCI Technology

Various authors are using novel methods of investigating CAI/HCCI combustion, which may be considered unconventional. These methods involve techniques utilizing spark to aid HCCI combustion, using two fuel injectors for each cylinder and using 2-stroke/4-stroke engines. These techniques veer off the conventional CAI/HCCI combustion path yet still cover interesting concepts which could be used to expand the CAI/HCCI combustion region.

Hyvönen et al. [46] studied operating conditions using spark assisted CAI/HCCI combustion. They state that spark assistance has a clear effect on CAI/HCCI combustion initiation up to lambda values of about 3. Furthermore, slightly lower compression ratio or inlet air temperature are needed for the same operating point with spark assistance compared to pure auto-ignited CAI/HCCI. The combustion fluctuations are higher with spark assistance than without, due to cycle-to-cycle differences in combustion phasing that are introduced with the initial SI flame kernel development. With spark assistance NOx emissions were 10-20 ppm higher compared with conventional CAI/HCCI. It is reasoned that high temperature is reached locally in the spark ignition flame kernel, despite the mean cylinder temperature is the same in both cases. Using spark assistance for controlling the combustion phasing between mode transfer from HCCI to SI leads to large combustion fluctuations in the intermediate combustion region. These intermediate combustion cycles have to be minimised during combustion mode transfer. Ultimately Hyvönen et al. say that closed loop controls of several parameters are needed to make a smooth and fast combustion mode transfer possible.

Another technique which has been used to increase both the lower and upper limits of CAI/HCCI combustion is through regulating coolant water temperature. This method is practical and can be implemented within production IC engines based on the cooling water system already used within production engines. Milovanovic et al. [47] controlled coolant temperature to extend the operating range of CAI/HCCI combustion, varying cooling water temperature from 65°C to 90°C in order to investigate whether the boundary region of

CAI/HCCI could be enlarged. They found that cooling water temperature had a significant effect on ISFC, ISNOx and ISHC. Decreasing cooling water temperature increased ISHC and ISNOx due to enhanced heat transfer and thus reduced temperature near the cylinder walls and hence the existence of colder boundary layers that suppress the fuel oxidation process. Lower coolant temperature reduced fuel consumption. This was reasoned due to improved combustion and thermal efficiencies (due to improved combustion stability). The results obtained indicated that with reducing coolant temperature, the upper limit can be extended up to 14% while with increasing the coolant temperature the lower limit can be extended up to 28%. Although it is envisaged that controlling cooling water temperature in a production HCCI engine where load and speed is changing constantly is difficult to implement. The authors have reported that it could be possible for a BMW ECU to control a thermostat and electric water pump using a control algorithm to manage coolant flow in response to engine speed, load and outside temperature.

There are several methods in which the CAI/HCCI region can be expanded. Aroonsrisopon et al. [48] states that the stratified charge shows potential as a viable enhancement for CAI/HCCI combustion at the lean low-load limit. Two Mitsubishi GDI injectors were installed in their test engine; one injector was assembled in the combustion chamber in the existing spark plug hole and provides charge stratification via Direct Injection. A second injector used for homogeneous charge was installed upstream before the intake tank and was called the premixed injector (PI). They reported that stratified charge shows potential as a viable enhancement for CAI/HCCI combustion at the lean limit. The combustion becomes more stable with more stratified charge. They found that at the rich limit, the stratification was limited by the high-pressure rise rate and high CO and NOx emissions.

Urushihara et al. [49] also used two injectors to implement a novel method in which, there was a direct injector coupled with a port fuel injector. The direct injector injected near the spark plug causing a stratified mixture. The port fuel injector injected a homogeneous mixture. The stratified charge, near the spark plug, instigated CAI/HCCI combustion within the combustion chamber due to higher pressure and temperature. SI-CI combustion (the name dubbed by the authors) reduced the mixture temperature needed at the onset of

compression for obtaining stable and moderate combustion. As a result the maximum IMEP obtained with CI combustion improved. However the authors found that NOx emissions are produced by SI flame propagated combustion and the NOx emissions level is higher than that of the HCCI combustion.

Another novel method discussed by Osbourne et al. [50] is the prospect of two-stroke/four-stroke switching engines. Using a poppet valve combustion system with capability for both 2-stroke and 4-stroke combustion, it is envisaged that the CAI/HCCI boundary region can be increased. It is thought that two-stroke operation will prove useful for highest specific load for CAI/HCCI engines in passenger cars. Two-stroke operation also offers exceptional torque at low engine speeds, making it attractive for downsized engine concepts. Four-stroke operation has proved to be useful for low/mid load ranges and low/medium speeds. Therefore it appears that a two-stroke/four-stroke concept would drastically increase the CAI/HCCI boundary region. In their research Osbourne et al. reported that engine speeds of 3250 rpm were achieved and higher speeds were limited only by valve train considerations.

It is important that researchers study methods which veer of the normal accepted path for CAI/HCCI combustion. This helps bring about techniques which can enlarge the standard operational region of CAI/HCCI combustion. The purpose of CAI/HCCI combustion is to reduce emissions and improve fuel economy, the method in which this is achieved and whether or not it is conventional CAI/HCCI combustion is less important.

2.5 Motivation

One of the most feasible methods of achieving CAI/HCCI combustion, as discussed in the literature survey, is the use of trapping exhaust gas within the combustion chamber by closing exhaust valves early. Percentage of trapped residual, based on EVC time, valve lift and valve duration, limits the operating region. Usually a shorter than normal valve opening duration and lower than normal valve lift strategy is used. In this study modified valve profiles for both intake and exhaust camshafts will be used to investigate their effect

on CAI operation. Other methods have been identified as possible solutions to increasing the operating region, among which spark assistance has the potential to expand the CAI/HCCI region near the misfire limit and will be investigated. Direct injection has also been demonstrated to be a very useful means to control CAI combustion and hence a systematic investigation of injection will be included in the current study. Split injection has the potential benefits of charge reforming/cooling and stratified charge to be realised. Due to the hardware limitation, individual effect of early injection and late injection, as they would be used in a split injection strategy will be studied.

2.6 Summary

This literature survey has highlighted the need for a gasoline engine which has low emission output and can adhere to tightening legislation, while delivering reduced fuel consumption over an acceptable load and speed range. There are many prevailing technologies, i.e. hydrogen fuel cells and HEV's, which offer the potential of low emissions, however, as reported in the literature survey, they have associated hurdles which need to be overcome before they are considered for automotive applications.

The ongoing research with SI and CI production engines has highlighted that developments can be made to reduce emissions and fuel consumption within these engines, without the need for expensive infrastructure overhaul. The literature review has shown that the greatest emissions and fuel consumption reductions can be sought with CAI/HCCI combustion technology. This technology does not involve the need for expensive exhaust after-treatment systems nor does it require major alterations to existing production engines. However, CAI/HCCI technology still has several issues that must be addressed if this technology is to see service within automotive applications. Combustion phasing and limited operating range are the main challenges associated with CAI/HCCI combustion. It has been demonstrated that a VVT mechanism can be used to achieve CAI/HCCI combustion whilst gasoline direct injection technology offers control over combustion phasing. Spark assistance, split and late injection help expand the operating region. Therefore, investigation of a GDI engine with a VVT mechanism would be useful, with

importance being given to studying combustion phasing control and combustion region expansion.

Chapter 3

Experimental Set-up and Test Facility

Chapter 3   Experimental Set-up and Test Facility

3.1 Introduction

This chapter describes the basics and operation of experimental setup and test facilities used to obtain all measurements and data. The key mechanisms namely, the direct injection system, the ECU and control system, and the variable valve timing mechanism used to undertake the research are described. Finally the equipment and sensors used to control and monitor the engine are also listed.

3.2 Ford 1.6 L Sigma DI Gasoline Engine

A 1.6L Ford pre-production prototype Direct Injection Gasoline engine, supplied by Ford Motor Company was used to obtain all the results presented in this thesis (Table 3.1). The cylinder block was based on a standard Ford 1.6L Zetec-SE engine found in production models like the Puma™ and Focus™. Compared with its production type counterpart, the cylinder head had two main modifications to allow control for CAI combustion and to undertake the specific direct injection and valve timing research intended to be carried out at Brunel.

The first modification of the cylinder head, commissioned by Ford Motor Comapany, was a Variable Cam Timing (VCT) system, consisting of a solenoid valve actuator regulating a spline type VVT sprocket, which was installed on both the intake and exhaust sides. Corresponding oil passageways bored from a lubrication supply passageway was used to supply oil to the VVT mechanism.

The other cylinder head modification was the installation of a direct injection fuel supply, commissioned by Bosch GmbH. An injector was installed in each cylinder with a 70° spray cone angle. Fuel was supplied via a low pressure (4 bar) fuel pump, powered from a 12V supply, to a cam driven pump, where fuel is pressurized at 100 bar along a common rail.

An Injector Driver Unit was used to compute the desired fuel injection time and amount and send this signal to the injector.

The engine was installed in a dedicated test cell within Brunel's engine research lab. The test cell provides the engine with an industrial extraction fan facility, fuelling from an 80 gallon underground gasoline tank and cooling water from an independent water circuit. Adjustable engine mounting was used to seat the engine and couple it to a dynamometer on independent mounting.

Table 3.1: Ford test Engine Specifications

Engine Type	Inline 4-cylinder
Bore (mm)	79
Stroke (mm)	81.4
Displacement (cm^3)	1596
Compression ratio	11.5
Fuel Supply	Direct Injection
Fuel Injector (Spray cone angle)	Swirl Injector (70°)
Fuel Rail Pressure	10MPa
Fuel	Gasoline 95 RON

3.3 Engine Control and Operation

This section details the different systems used to control and operate the engine. The systems used to operate the engine and ensure safe running were: cooling water supply, air intake system, engine lubrication and fuel supply. The actual control systems which are used to control engine parameters specifically for testing purposes are also discussed in the chapter; these are the Engine management system, VVT mechanism, direct injection system and the dynamometer.

3.3.1 Engine Water Cooling
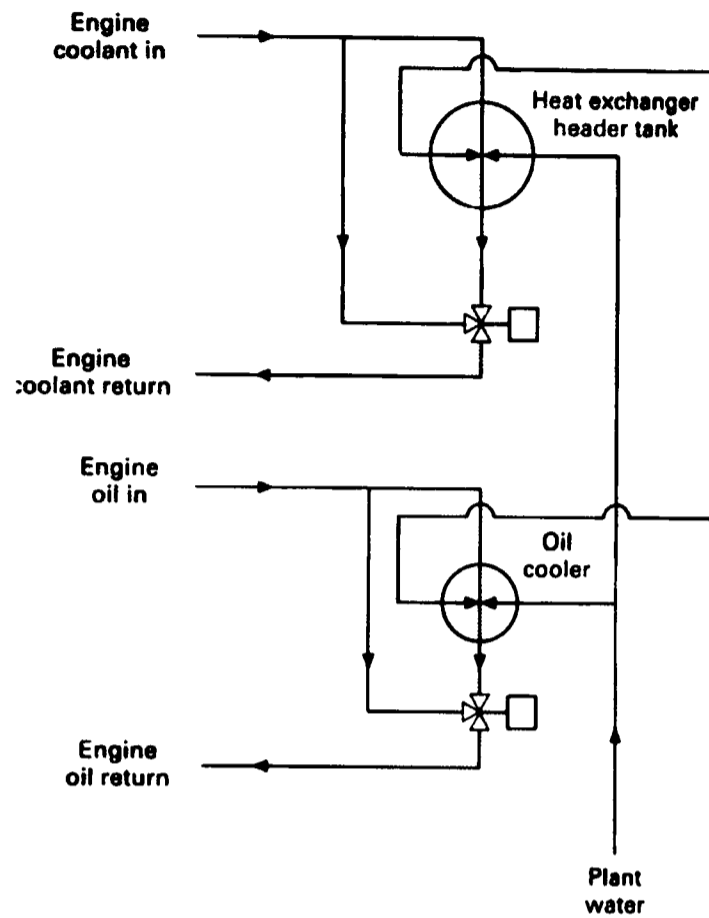
Figure 3.1 Cooling water circuit schematic

Attention was first given to a cooling water circuit which prevented the engine from overheating. In terms of experimentation this also allows a steady operating temperature of 90°C, replicating standard engine temperatures. Engine water cooling was achieved through a heat exchanger, a schematic representation is displayed in Figure 3.1. A three-way thermostatically controlled valve was used to introduce cool water to the engine and maintain stable operating temperatures. The cold water flowrate through the heat exchanger could be controlled via a valve allowing control over engine cooling water temperature. The higher the cold water flowrate through the heat exchanger, the cooler the engine cooling water. The thermostat opened when the engine water temperature reached 95°C pulling in cool water and reaching a stable temperature. A separate water supply was fed to cool the dynamometer.

3.3.2 Air Intake System

The system that was devised next and used for operation purposes to provide the necessary pollutant-free air is the air intake system. The system used replicated the intake system used on a road-going car, apart from the airflow meter. A paper-element type air filter made of resin impregnated paper was used for air filtering. A standard intake tube led into the air filter housing, the clean air then flowed through the airflow meter before flowing into the intake manifold. The air filter housing, intake tube and air filter were the same as the intake system used for a standard Ford Fiesta with a 1.4L Zetec engine. Since the engine was naturally aspirated there was no need for auxiliary air supply.

3.3.3 Engine lubrication and oil cooling

Attention also had to be given to engine lubrication in order to avoid premature engine failure, this was achieved using 10W/40 Grade engine motor oil. This was provided via an oil pump which pumped oil to all moving parts. The oil passages in the cylinder block were based on a production type Ford 1.6L Zetec engine. However, because of the modified cylinder head with variable valve timing mechanism, a special oil passage way was bored to allow oil to reach here.

3.3.4 Fuel Supply System

For purposes of investigating the effects of direct injection on CAI combustion, a direct injection fuel system was used. This section discusses the fuelling system used to inject directly into the cylinder and the injectors used for DI purposes.

A low pressure pump powered from a 12V supply is used to supply fuel from the tank to the high-pressure pump, Figure 3.2. The high-pressure pump is driven by the camshaft and delivers an engine speed-dependent fuel quantity.

High pressure supply

Temperature sensor

Fuel pressure sensor

Pressure control valve
incl. low pressure
return
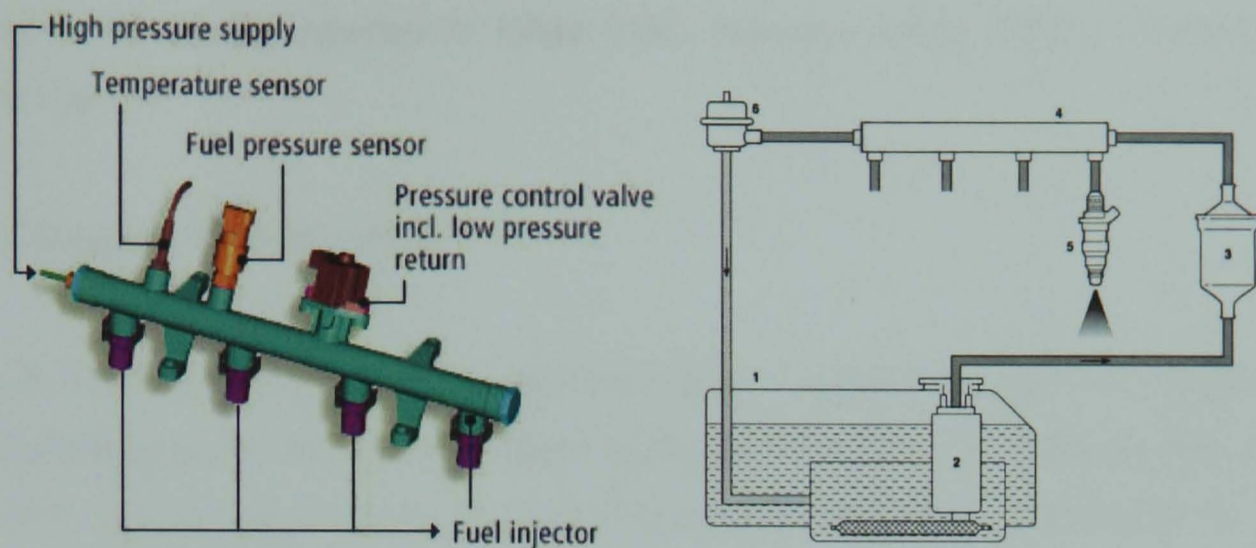
Fuel injector

Figure 3.2 Diagram of the fuel rail and also a schematic of the fuel system [51]

The high-pressure pump then distributes the fuel along the common rail to the high-pressure injectors. It is important that the rail guides a defined fuel pressure to the high-pressure injectors and provides adequate volume to compensate for pressure pulsations.

The injectors were installed in the cylinder head, with care taken for positioning purposes. The injector, Figure 3.3, consists of housing, a valve seat, a nozzle needle, a spring and a coil to create the magnetic field. If the coil is energized, the nozzle needle is raised against the spring pressure by the valve seat so that the fuel flows into the combustion chamber. When the electrical current is switched off, the nozzle needle is pressed by the spring pressure into the valve seat and interrupts the fuel flow.

PIN

Closing spring

Magneto armature

Adjustment disc

Seat Carrier

Valve needle

Guide plate

Swirl plate

Seat plate

Adjustment nozzle

Housing lid

Coil

Valve housing

O-ring

Teflon-ring
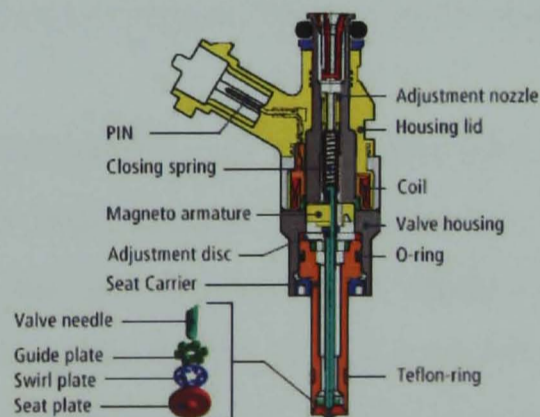
Figure 3.3 Cut-away diagram of injector [51]

Injection timing is defined as the duration and angular position of the injection pulse in relation to top dead center. In the results presented, the convention used to present injection

timing is referencing injection to intake TDC. Injection before TDC is denoted with a minus sign.

3.3.5 Engine Management

After the correct operating systems had been setup, a method to control the engine had to be implemented; to this end an engine management system was devised. This allowed complete control over the engine via a DOS based computer interface and an ECU.

Communication with the engine was achieved through the ECU, this involved receiving data from the engine and sending commands to the engine. A standard PC was used to relay data to and from the ECU which then communicated with the engine. The injection was the only parameter which was controlled by a secondary system, the Injector driver Unit (IDU). The ECU could be connected to the parallel port on the computer via a MAC module, the MAC required a permanent 12V power supply. It was envisaged that a break-out box was needed for systems diagnostics. A break-out box could monitor signals sent from the engine to the ECU and vice versa. The box proved an invaluable source for identifying and repairing faulty sensors. Furthermore, the box could also be used to interrupt signals sent from the ECU to the engine through the use of a switch. This was useful for the controlling of spark and establishing whether pure CAI combustion was occurring. Figure 3.4 provides a schematic diagram of the engine management system.

In order to communicate with the ECU and relay commands the Bosch ETAS tools VS-100 engine management system was installed on the computer. The system could be used to control: the air-fuel ratio, the fuel injection time, spark ignition timing and the charge motion valve opening position. The ECU was used to monitor the speed, airflow, camshaft position and throttle position. There was the facility to control and monitor various other parameters, however, these did not have to be altered after initial set-up.

The VS-100 program was binary coded and every value had to be inputted in binary form (Table 3.2a and 3.2b). A value could be used to switch on desired and selected functions.

Each switch activated a function; for example if the binary number 57 was inputted, this would activate switch 1, 4, 5 and 6 and corresponding functions, leaving the others inactivated.
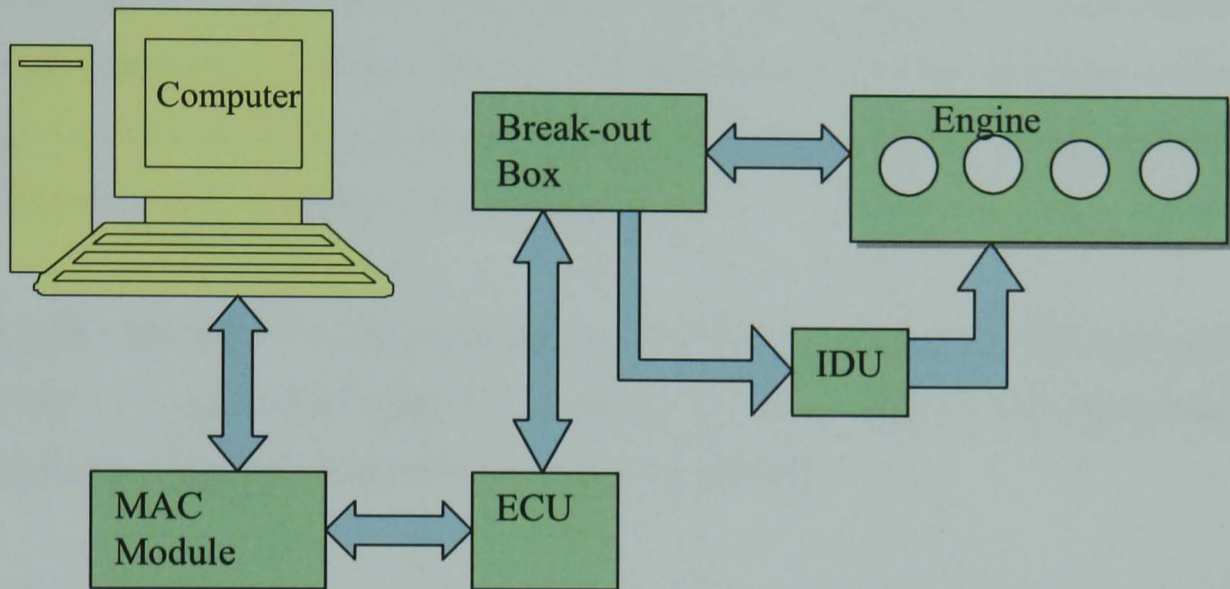
Figure 3.4: Schematic representation of engine management system

Table 3.2a Binary Value and corresponding switch

Binary Value	Switch/Function
1	1
2	2
4	3
8	4

Table 3.2b Binary Value and corresponding switch

Binary Value	Switch/Function
16	5
32	6
64	7
128	8

Camshaft position sensor

So that the engine management system can monitor camshaft position, a Hall sensor was used (Figure 3.5). Two Hall sensors were installed, one on the intake camshaft side and one on the exhaust camshaft side. This consists of a Hall element with a semiconductor wafer through which current flows. This ferromagnetic Hall element responds to activation by a trigger wheel rotating in unison with the camshaft by generating voltage at right angles to the direction of the current passing through it.

The basic procedure for determining the camshaft position is for the microprocessor to respond to trigger-wheel gaps by checking for Hall voltage and determining whether cylinder no. 1 is in the compression or the power stroke.

Special trigger-wheel designs allow the camshaft signal to be used as an emergency back-up in the event of crankshaft sensor failure. However, the resolution provided by the camshaft signal is much too low to allow its use as a permanent replacement for the crankshaft rpm sensor.
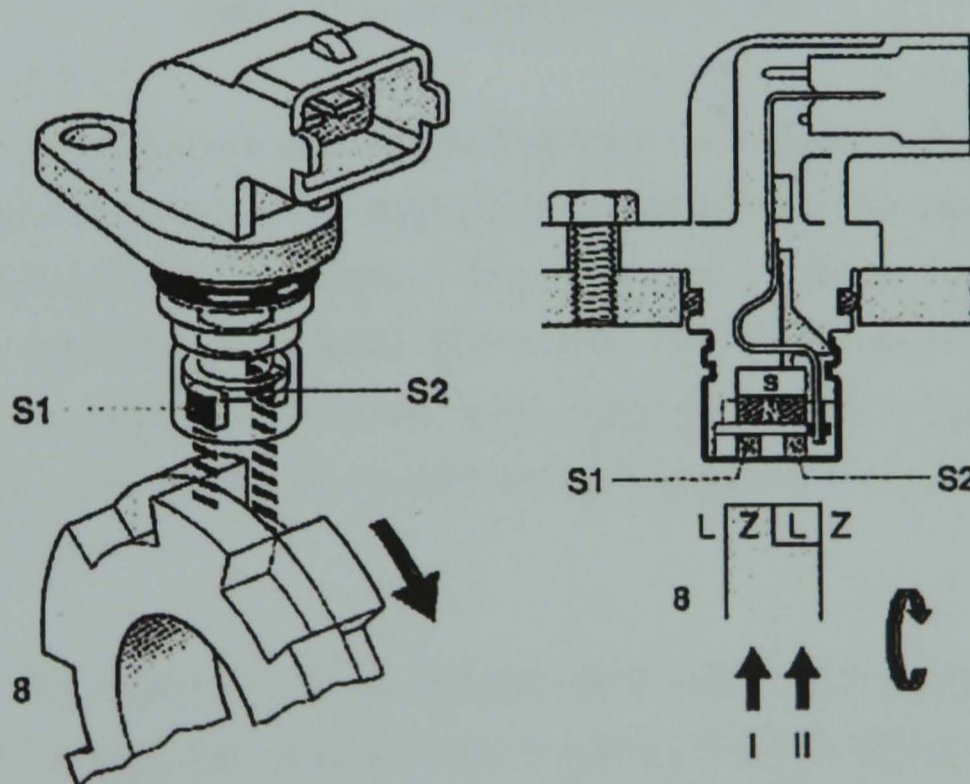
Figure 3.5 Differential Hall-effect sensor [52]

38

Crankshaft position sensor
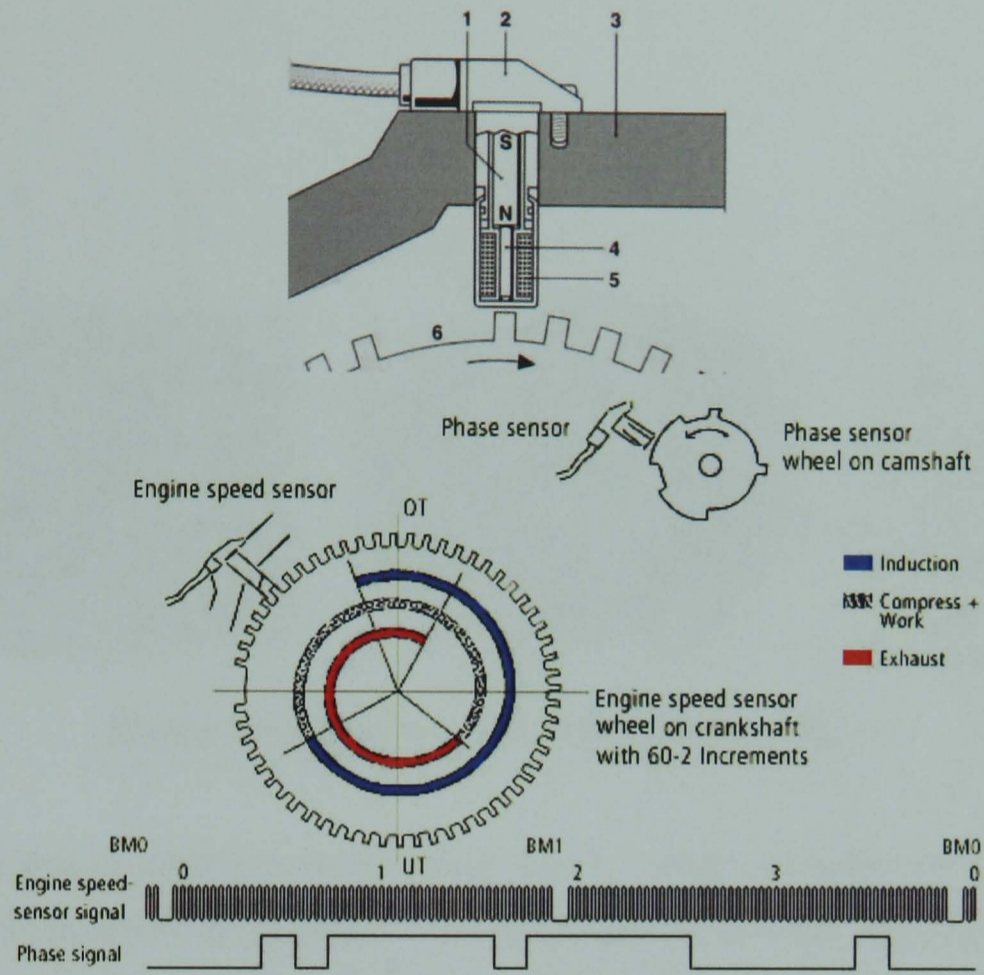
Figure 3.6 Crankshaft Position sensor

The engine's rotational speed and crankshaft position were determined via a crankshaft position sensor and relayed to the engine management system. The sensor is mounted directly opposite one of the 360 flywheel teeth. The sensor contains a ferromagnetic ring gear, which is installed on the flywheel of the engine. The flywheel has a deliberate tooth missing from its periphery. An inductive speed sensor registers the equally-spaced tooth sequence. This sensor consists of a permanent magnet and a soft-iron core with copper winding (Figure 3.6).

The magnetic flux field at the sensor responds as the teeth on the sensor gear pass by, generating AC voltage. This continues until it reaches the missing tooth and the ECU registers a response. The ECU synchronizes the crankshaft position according to this point in time.

Throttle

1. Bottom section of the central injection unit
2. Throttle-valve shaft
3. Wiper arm
4. Wiper
5. Resistance Track 1
6. Collector Track 1
7. Resistance Track 2
8. Collector Track 2
9. Toroidal seal ring
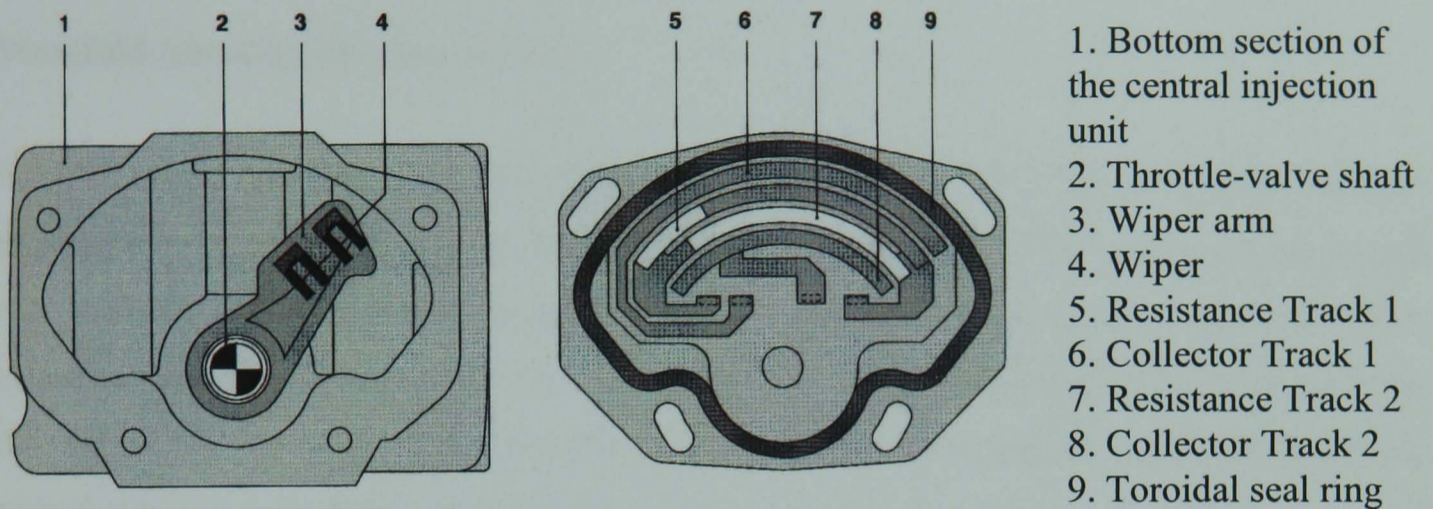
Figure 3.7 Throttle-valve potentiometer [52]

The throttle signal is sent by the engine management system to determine throttle opening. A value can be inputted in the Bosch VS100 program to alter the angle, with Wide Open Throttle being the default position. Throttle angle could also be changed manually through a purpose built slider. It was necessary to use throttling for initial start-up purposes.

The throttle consisted of a potentiometer wiper arm, Figure 3.7, fastened to the throttle-valve shaft. The potentiometer wiper arm has resistance tracks connected to an electric motor. A 5 V supply was distributed between the resistance tracks; the ratio of distributed voltage determined the throttle angle.

Charge Motion Valve

The charge motion valve can be used by the engine management system to control the intensity of the charge movement. The valve is operated by a motor which can vary the angle of a plate and influence the motion of the charge. The intake manifold consisted of two ports near the intake valve, one port can be partially blocked creating high charge movement. In stratified mode, this inducted air motion assures the mixture transportation to the spark plug and supports mixture preparation. For regions of low engine-speed and

torque the charge motion valve is partially closed, whereas in homogeneous operating mode the charge motion valve was fully opened and there was no introduction of swirl motion.

Manifold Absolute Pressure sensor

A MAP sensor was pre-installed directly on the intake manifold and provided an absolute pressure measurement during various engine operating loads. This corresponding signal was sent to the engine management system which could be used along with other measurements by the control system to calculate fuel injection timings and ignition timings. The sensor element is made up of a silicon chip, into which a pressure diaphragm has been etched. Pressure changes can be registered as changes in resistance. The evaluation and calibration circuitry are integrated on the chip.

3.3.6 Variable Valve Timing Mechanism

In order to undertake CAI combustion, control of valve timing was necessary. Advancing or retarding both intake and exhaust position was undertaken through the use of a variable valve timing sprocket mechanism (Figure 3.8). A custom made intake and exhaust sprocket mechanism was developed by INA Germany which was slotted onto the respective camshaft (Figure 3.9). A mount was designed to house the camshaft angle actuator which supplied oil to the sprocket and the camshaft. A change in the position of the sprocket pulley relative to the camshaft was achieved due to a change in the oil pressure supplied by the camshaft angle actuator. The camshaft angle actuator consisted of a solenoid valve operated by a square wave signal. The valve could be controlled to open by very small increments controlling the flow off oil to the variable valve timing mechanism. Oil also acted as a lubricant but its main purpose was to supply a set volume of oil to the VVT mechanism and control the camshaft shift angle. The greater the flow of oil, the greater the camshaft shift. The camshaft was controlled by the VS100 Bosch control program;

however an additional box was developed to control the square-wave signal to the actuator in case of malfunction by the program.
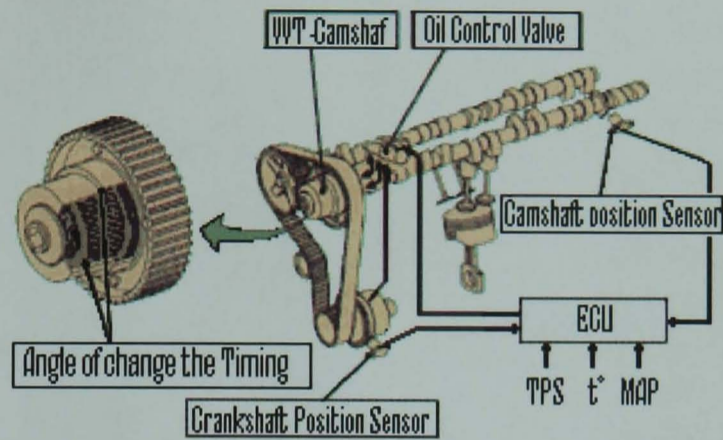
Figure 3.8 Diagram of VVT mechanism Sprocket fitting on camshaft [52]

1. Bearing Bush
2. Stopping Ring
3. Piston Plate
4. Tube
5. Spline bush
6. Damping ring
7. Housing
8. Bell Gear
9. Spring
10. Screw
11. O-ring seal
12. Spline Flange
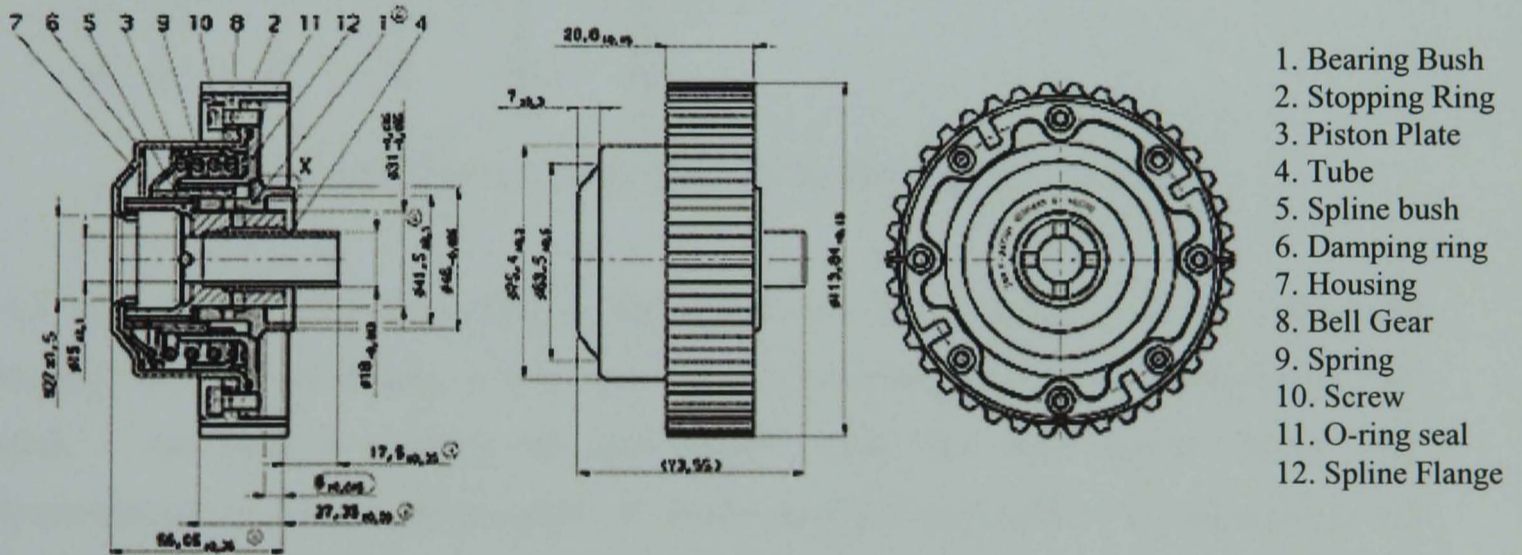
Figure 3.9 Sectioned Drawing of VVT Mechanism Sprocket and oil passageways [52]

3.3.7 Dynamometer

1. Rotor
2. Rotor Shaft
3. Coupling Flange
4. Water Outlet with thermostat
5. Excitation Coil
6. Dynamometer housing
7. Cooling Chamber
8. Air gap
9. Speed pick-up
10. Flexure Support
11. Base
12. Water Inlet
13. Joint
14. Water outlet pipe
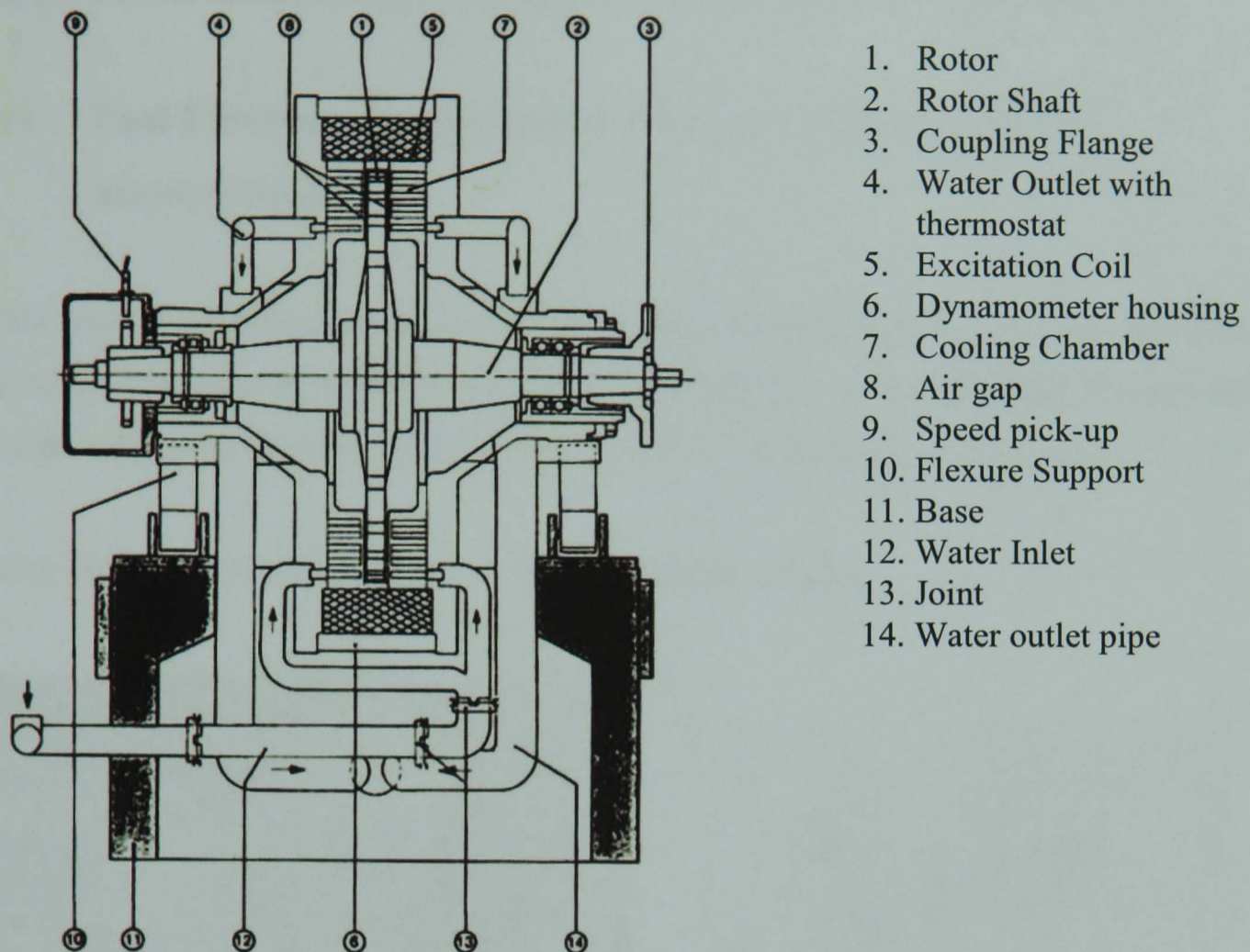
Figure 3.10 Typical Eddy Current dynamometer layout [51]

The final control method applied to the engine involved measuring power output and running constant speed tests. A Heenan & Froude eddy-current engine dynamometer type Mark 1 was used to perform all experimental work. The eddy current steady state dynamometer operates on the principle of electro-magnetic induction to develop torque and dissipate power, Figure 3.10. A toothed rotor of high permeability steel rotates with a fine clearance between water-cooled steel loss plates. A magnetic field parallel to the machine axis is generated by two annular coils and motion of the rotor gives rise to changes in the distribution of magnetic flux in the loss plates.

This in turn gives rise to circulating eddy currents and the dissipation of power in the form of electrical resistive losses. Energy is transferred in the form of heat to cooling water circulating through passages in the loss plates, while some cooling is achieved by the radial

flow of air in the gaps between rotor and plates. Power is controlled by varying the current supplied to the annular exciting coils, and very rapid load changes are possible.

3.4 Fuel Flowrate, Temperature, Pressure, AFR and fuelling measurement

This section discusses the devices used for measurement purposes, namely: fuel and air flowrate, temperature, engine speed, pressure and AFR. In addition to these measurements, a data acquisition system was also implemented; this is discussed in chapter 4.

3.4.1 Fuel Flowrate and Air-mass Flowrate measurement
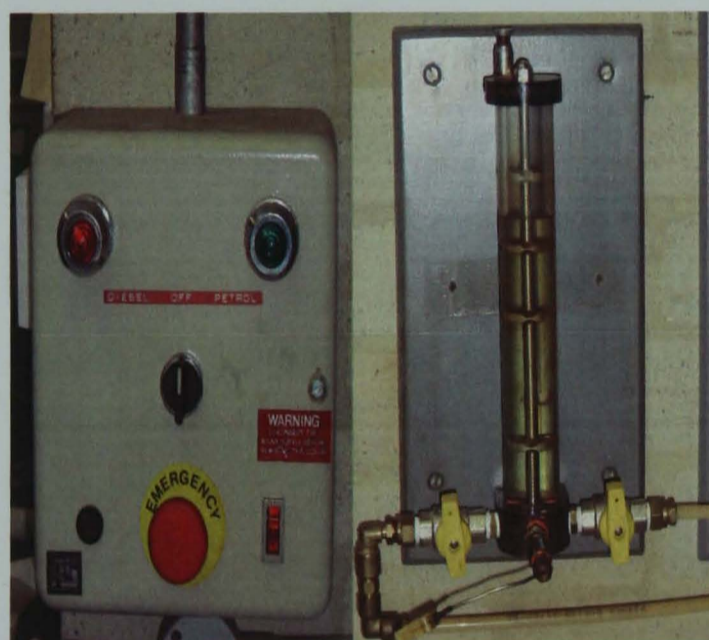
Figure 3.11 Mains Safety Power Supply switch **Figure 3.12 Air-mass**
(left), 100cc Plint and Partners Burette (right) **flowmeter [53]**
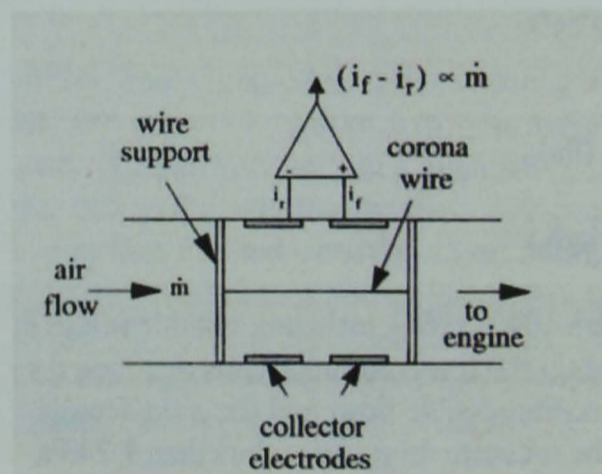
Fuel readings were taken using a 100 cc Plint and Partners burette. Figure 3.11 shows the apparatus used to rig the burette. A mains safety power supply switch was used to open a valve to allow standard gasoline fuel to flow to the engine bay. Secondly a manual valve was used to allow the fuel to flow through the burette on-route to the engine. The burette itself had two valves, which basically allowed the burette to be filled to the 100 cc mark,

then the supply valve to the burette would be closed and the delivery valve would be left open. The time taken for 100 cc of fuel to be used by the engine would be measured using a standard stop watch.

A Lucas Dawe Corona Discharge meter, type 1642A was used to measure the instantaneous airflow rate, Figure 3.12. The meter was installed between the air filter and the throttle valve and registered the air-mass flow (kg/h) drawn in by the engine. A corona wire sits within the meter and is maintained at a high voltage of around 10 kV, this causes ionization of the air within the meter and a corona discharge. As a result, an ion flow is established between the wire and the two tubular collector electrodes [53]. As air flows through the meter, the ion streams flowing to the two electrodes are deflected causing an imbalance between the ion currents flowing to the two electrodes. The difference in the two current flows is proportional to the air mass flow rate through the meter.

3.4.2 Temperature Measurements

Standard RS K type thermocouples were used to measure temperature. Thermocouples consist of two wires of dissimilar metals joined near the measurement point. The output is a small voltage measured between the two wires (Figure 3.13). This voltage can be converted to a calibrated temperature and displayed on a digital display.

Four thermocouples were mounted in each runner of the exhaust manifold. Two thermocouples were installed in the runners of the intake manifold. Since there was little variation in inlet temperature throughout the intake manifold it was deemed adequate to use two thermocouples. Another thermocouple was used to measure the cooling water temperature. This thermocouple was used to monitor the engine temperature and rule when CAI combustion was possible. The thermocouples were linked into a digital display unit where the various temperatures could be noted.
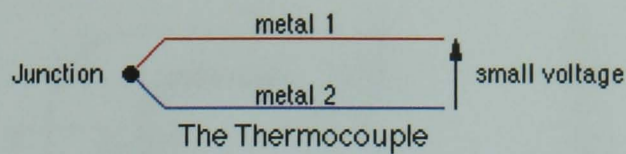
Figure 3.13 Schematic diagram of a standard bimetal thermocouple

3.4.3 Shaft Encoder

A shaft encoder supplied by Encoder Technology, type EC 58 was used to measure rotational speed, and indicate TDC. The encoder was driven directly by the crank shaft and had a resolution of 720, and produced two pluses per degree of crankshaft rotation giving a clock speed. The optoelectronic type shaft encoder consists of a plastic disc driven by the crankshaft with a photographically produced pattern of transparent and opaque areas, through which light is directed to photosensors [54]. The encoder produces two main signals: the first is a train of clock pulses and the second is a single pulse per revolution of the crankshaft. The single pulse was aligned with the intake stroke top dead centre and used as the cycle reference for the Data Acquisition System.

3.4.4 Pressure Inducer

The Kistler 6061B piezoelectric transducer (Figure 3.14) was installed in cylinder 1 to measure in-cylinder pressure. In a piezoelectric pressure transducer, a pressure-sensing diaphragm transduces the force to a stack of disks made of piezoelectric ceramics or crystalline quartz. The electrical charges, picked up from the faces of the stack, are proportional to the pressure.
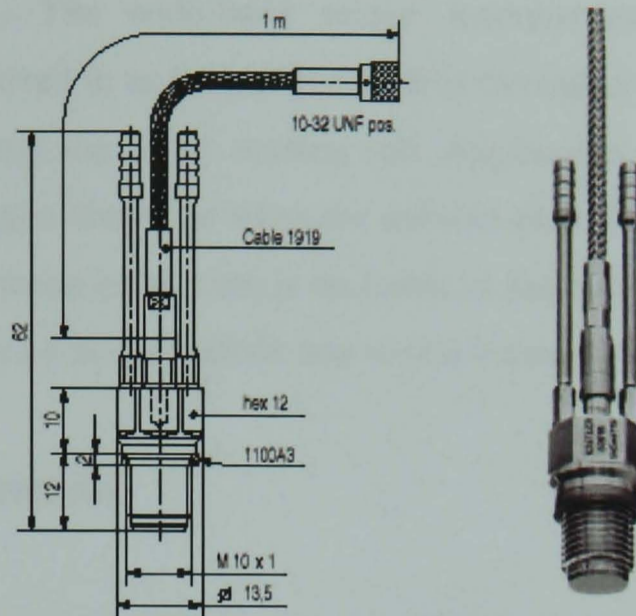
Figure 3.14 Schematic of Kistler 6061B piezoelectric transducer (left), photo of Kistler 6061B (right) [54]

The transducer is of the high impedance type and requires a charge amplifier (Kistler Type 501) for charge-to-voltage conversion. The measurement range was 0-100 bar gauge, a sensitivity of -6 pC/bar and a operating temperature range of -50 to 350°C.

3.4.5 Lambda Sensor

1. Sensing cell
2. Reference cell
3. Heater
4. Diffusion gap
5. Pump cell
6. Exhaust pipe
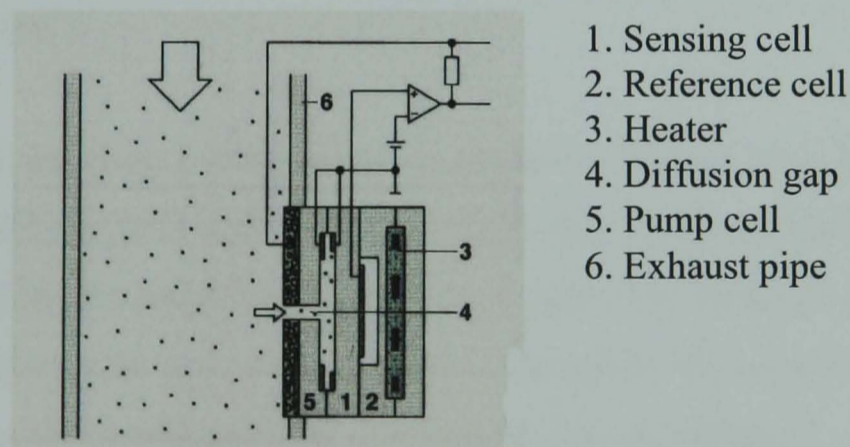
Figure 3.15 Lambda Oxygen Sensor: Position in exhaust pipe [55]

A Horiba MEXA-110λ AFR Analyzer unit was used to display the lambda reading. A UEGO wide-band sensor (Figure 3.15) was installed in the exhaust pipe and had a capability of measuring excess air ratio (lambda) from 0.00-9.99 and oxygen concentration

47

(O_2) from 0-25 vol%. The wide-band sensor incorporates a sensing cell and an electrochemical cell referred to as the pump cell. It is through a small slot in the pump cell that the exhaust gas enters the actual sensing cell. Application of pumping voltage to the pump cell results in oxygen discharge when the exhaust gas is lean and oxygen induction if it is rich. The resulting pumping current is an index of the excess-air factor in the exhaust gas. For experimentation purposes lambda was varied between λ=1.0 and λ=1.2.

3.5 Exhaust Measurement

Exhaust measurement was undertaken with the Horiba Mexa 7000 series analysers. The analysers could display CO, CO_2, O_2, uHC and NO_x emissions onscreen. This section discusses the different set-up of each analyser and the principle behind collecting emission data.

3.5.1 Horiba AIA-72: CO and CO_2 measurement

The AIA-72 unit consists of a NDIR (non-dispersive infrared) analyser used to measure the concentration of CO and CO2. NDIR analysers absorb infrared energy at specific wavelengths with the degree of absorption being proportional to the concentration of gases at constant pressure.

A typical NDIR analyser configuration is shown in Figure 3.16, consisting of a light source, sample cell, detector and electrical system. The infrared beam from the light source passes through both the sample and comparison cells. The detector consists of two cells, either side of a moveable membrane, in which the gas to be measured is sealed. The gas enclosed in each cell absorbs infrared radiation as heat and expands. The infrared radiation is transmitted intermittently by a light chopper, so the change of gas concentration in the sample cell can be detected as electrical output by the displacement of the moveable membrane.
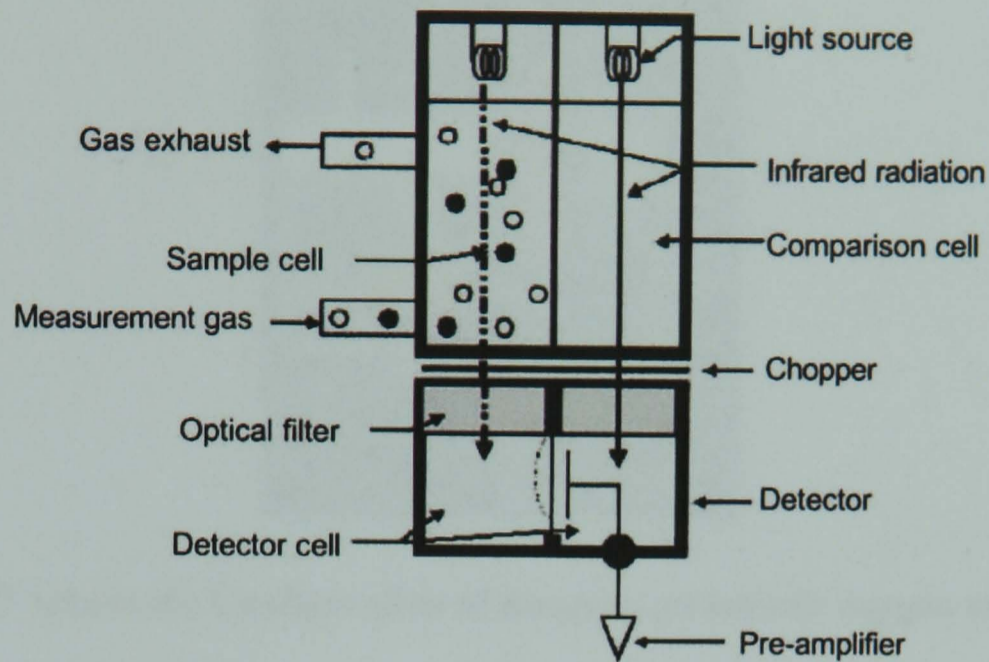
Figure 3.16 Schematic Configuration of NDIR configuration used for CO and CO$_2$ measurement [55]

3.5.2 Horiba MPA-720: O$_2$ measurement

The MPA-720 is used to measure the concentration of oxygen (O$_2$) in the sample gas using magneto-pneumatic detection (MPD). Magneto-pneumatic detection relies on the fact that oxygen has a much greater response to a magnetic field than other gases.

The principle of a magneto-pneumatic oxygen analyzer is shown in Figure 3.17. AC current flows in the electromagnet so an alternating field appears between the poles of the electromagnet. When the sample gas flows in the magnetic field, the pressure around the magnetic poles changes according to the concentration of oxygen. This is because oxygen whose susceptibility is high is attracted by the magnetic poles. This pressure change is detected by a condenser microphone as an alternating signal as electric capacity changes.
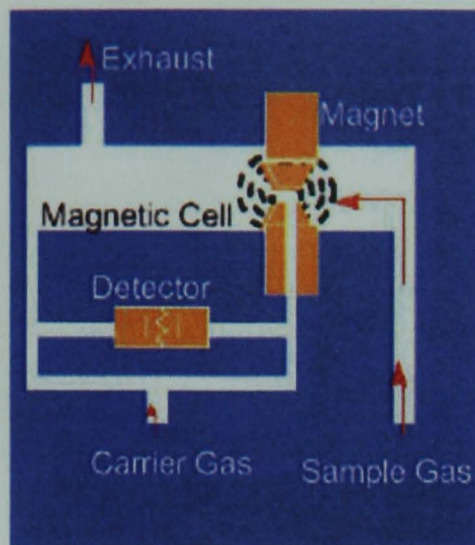
Fig 3.17 Schematic Configuration of magneto-pneumatic oxygen analyser

3.5.3 Horiba FIA-720: Unburnt Hydrocarbon measurement

The FIA- 720 is designed to measure the concentration of total hydrocarbon (uHC) using hydrogen flame ionisation detection (FID). Hydrogen flame ionisation uses the phenomenon in which ions, generated by the heat energy when hydrocarbons are introduced into a hydrogen flame, are proportional to the number of carbon atoms in the sample. It is widely used for the measurement of exhaust gases from engines because it is sensitive to almost all HC compounds.

The configuration of the FID is shown in Figure 3.18. H_2 and air are supplied to the burner nozzle and a hydrogen flame is formed. Two electrodes are fitted on either side of the flame, and a DC voltage is applied. The sample gas is mixed with the fuel H_2 and introduced to the hydrogen flame. It is thermally dissociated and generates ions in the high-temperature area. The ions generated migrate to the electrodes and are detected as current. The characteristic of this method is that the detector output is nearly in proportion to the number of carbon atoms and so is used for measurement of total hydrocarbons (uHC).
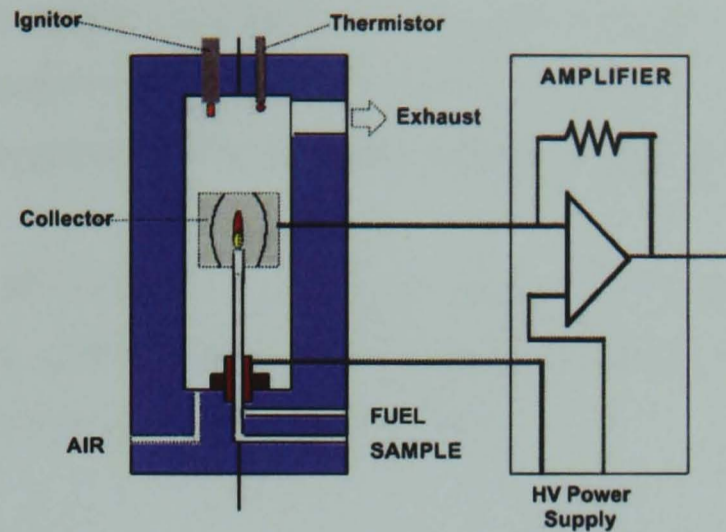
Figure 3.18 Schematic configuration of Flame Ionisation Detector (FID) used for uHC measurement

3.5.4 Horiba CLA-720A: NO and NOx measurement

CLA-720A is designed to measure the concentration of NO and NOx using chemiluminescence (detector: CLD). It is widely used as the measurement method of NO and NOx in exhaust gases from engines because it is highly sensitive to NO and is not interfered by other components easily.

When sample gas with NO and ozone gas (O_3) gas is mixed in a reactor, NO is oxidized and is transformed to NO_2.

$$NO + O_3 \rightarrow NO_2 + O_2$$
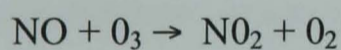
A part of NO_2 that is generated here is in excited state, which means its energy is higher than normal. Excited NO_2 molecules release excited energy as light when returning to the ground state.

$$NO + O_3 \rightarrow NO_2 * + O_2 \qquad NO_2 *: NO_2 \text{ molecules in excited state}$$

$$NO_2 * \rightarrow NO_2 + \text{light photon}$$
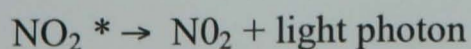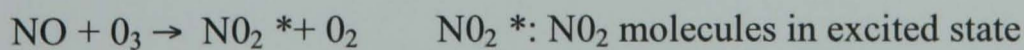
This phenomenon is called chemiluminescence, and the degree of light is directly proportional to the quantity of NO molecules before the reaction. Thus, NO concentration in the sample can be acquired by measuring the amount of light emission.

Some of the excited N0 molecules lose excited energy by collision with other molecules before returning to the ground state without emitting light. In this case, N0 re-turns to the ground state, but chemiluminescence does not occur.

N0 * + M → N0 + M
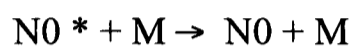
M : Other molecules

The probability of energy loss depends on the kind of the collision partner, and sometimes CLD's sensitivity to NO differs depending on the kind and concentration of the co-existing gas components. It is known that the probability of energy loss by CO_2 and H_2O is larger than that by N_2 and O_2 in the components of engine exhaust gas normally, and that the change of CO_2 and H_2O concentration in the sample tends to cause the change of NO sensitivity.

3.6 Summary

This chapter details the equipment used for measurement and control purposes, this includes the sensors used to control and monitor the engine Furthermore, the advanced systems used for the specific research, presented in this thesis, are also listed, namely the direct injection system, the engine management system, and the variable valve timing mechanism.

Chapter 4

Data Post Processing and Analysis

Chapter 4   Data Post Processing and Analysis

4.1 Introduction

Data was collected from the equipment and instruments detailed in Chapter 3, with attention given to ensuring that data was accumulated in a consistent manner with no bias. To ensure consistent data post processing rigid methods were used for analysis purposes and any theoretical material used is supported academically. This chapter describes the method used to analyse all collected data. Obtaining data included two methods; the first was noting values at a certain steady-state point and the second involved using a data acquisition system to obtain pressure data from the pressure transducer, described in Chapter 3, synchronising the data with piston geometry and processing it further.

Pressure data was collected, displayed and analyzed through the data acquisition software package LabVIEW™ Version 6.0 (Figure 4.1). LabVIEW™ was used to process the gathered data further using its built-in mathematical functions. Pressure data was processed and the values for: load (NIMEP), percentage of trapped residuals and 10%, 50% and 90% MFB were calculated within LabVIEW™. In the subsequent sections the theoretical basis used to calculate load, trapped residual and MFB is outlined, along with calculations for brake emissions, brake specific fuel consumption and heat release.

4.2 Data Acquisition System

Since the pressure data formed the framework for the data acquisition system, it was important to establish the correct criteria for obtaining pressure data. Pressure versus crank angle can be obtained to a certain degree of accuracy according to Heywood [56], as long as the following steps are carried out:

Figure 4.1 Front panel of the LabVIEW DAQ™ Program displaying IMEP, 10%, 50% and 90% MFB

(1) the correct reference pressure is used to convert the measured pressure signals to the absolute pressures; (2) the pressure versus crank angle (or volume) phasing is accurate to within about 0.2°; (3) the clearance volume is estimated with sufficient accuracy; (4) transducer temperature variations due to variation in wall heat flux during the engine cycle are held to a minimum.

The criterion listed by Heywood was followed, and through the use of an oscilloscope the pressure data was validated. Furthermore, the front screen of the Labview™ program used to obtain pressure data (figure 4.1) had a toggle button on the pressure volume diagram to view Log P versus Log V plots which ensured the quality of pressure data.
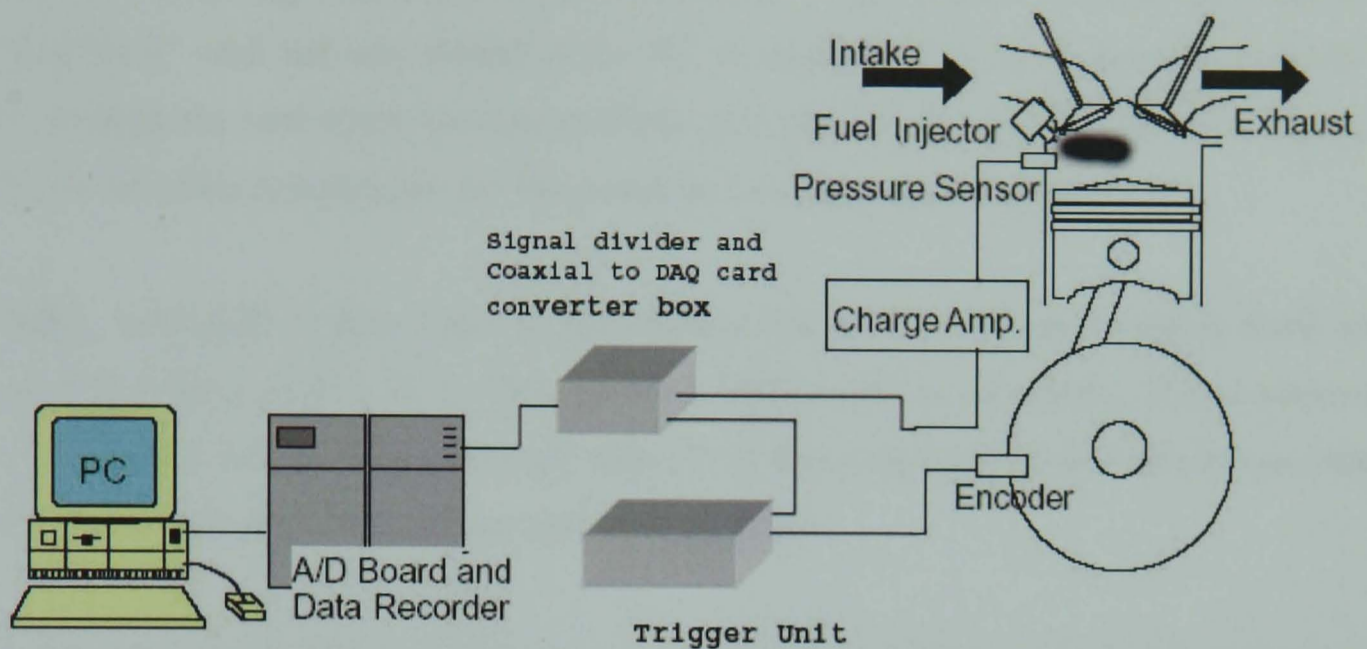
Figure 4.2 DAQ set-up incorporating NI™ card and LabVIEW™

In order to use the software LabVIEW™ for data acquisition purposes, a National Instruments™ PCIMI016-1 card was used which to communicated with a Pentium II™ 400 MHz specification Personal Computer (PC).

The LabVIEW™ program used was labelled "runme.vi" and was written by John Williams formerly of Brunel University and was used for obtaining all pressure data. The main data collected was for pressure which was obtained from the Kistler pressure transducer (section 3.2.5). In order to reference the data, a shaft encoder supplied a clock and trigger signal for purposes of identifying TDC and supplying a signal every 0.5 CA deg. A separate trigger unit was built to provide the trigger on the correct revolution, the shaft encoder provides a signal every 360°, but an engine cycle consists of two revolutions. Therefore the trigger unit identified a TDC every engine cycle, ideally this should be intake TDC, however if the signal provided was compression TDC then the trigger phasing could be adjusted through the front panel of the LabVIEW™ program; values of either 252 or 612 were entered in the "trigger position before compression TDC" box on the front panel and provided the correct phasing. The trigger unit signal, a clock signal and the pressure transducer data were provided through co-axial cable, these were converted through a specially built box and

allowed interfacing with the National Instruments™ A/D board. The A/D card was a PCI 'plugNplay' card and was slotted in the PC, obtained data could be communicated to the PC through the card where the data could be fully processed using LabVIEW™. Figure 4.2 shows the schematic diagram for the complete data acquisition system.

Within LabVIEW™ data could be presented in the form of pressure against crank angle and furthermore IMEP, 10%, 50% and 90% MFB could be calculated. The pressure data was analysed further using Microsoft Excel™ or Microcal Origin 6.0™ where heat release rate and in-cylinder temperatures could be calculated.

A separate LabVIEW™ program was used to determine when knocking was occurring and whether it was at an acceptable level. Audible knocking combustion can arise from the auto-ignition and rapid consumption of all or part of the cylinder charge. Spatial charge consumption can exceed the velocity of sound during this process, which sets up pressure oscillations that are internally reflected within the combustion chamber. Pressure wave energy is dissipated at the combustion chamber walls, exciting the structure at its natural frequency. The in-cylinder transducer is capable of measuring the pressure oscillations to a high accuracy, and the intensity measured does not depend greatly on the specific location of the transducer [55]. The technique requires finding the frequency range in which the measured knock intensity is highest. For the Ford Zetec 1.6L chamber, this frequency is in the region of 13 kHz to 18 kHz.

An independent program is used for determining knocking, where a pressure sample is collected at high frequency, the resulting vector is fed into a digital band-pass filter, which removes frequencies below 13 kHz and above 20 kHz. This allows the knock trace to be separated from the low-frequency pressure trace and the high-frequency noise. An intensity threshold is manually set to separate knocking from non-knocking cycles. If the knock trace exceeds this threshold (0.5 bar), then the software indicates that knocking combustion has occurred. When sampling a number of engine cycles the software calculates the ratio of knocking cycles to the number sampled, and this is termed the Knock Occurrence Frequency (KOF). The KOF is a good measure of whether the engine is deemed 'knocking'

or not. For the purposes of the test carried out in this study, combustion is reported as 'knocking' if the KOF exceeds 10% for an intensity threshold of 0.5 bar.

4.3 Load Calculations

The following section discusses the calculations used for load consideration namely NIMEP and BMEP. The calculation for pumping work is also given.

4.3.1 IMEP
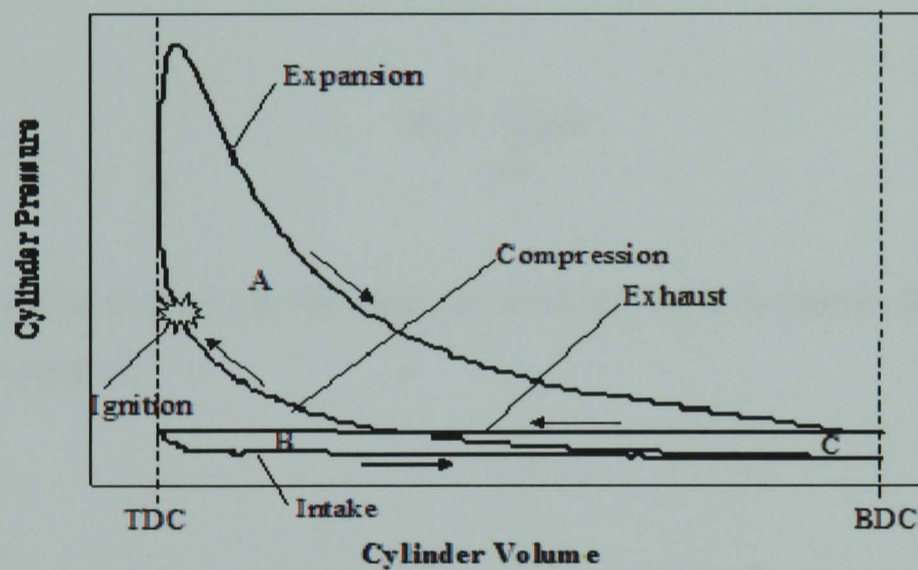
Figure 4.3 Example of a p-V diagram for a SI four-stroke cycle engine

The output from the engine can be expressed in terms of load or as NIMEP, PMEP and Gross IMEP. Figure 4.3 shows a representation of a typical PV diagram. Area A and Area C represents the gross Indicated Work per cycle; work delivered to the piston over the compression and expansion strokes. Area B and Area C represents the Pumping work per cycle; work delivered to the piston over the induction and exhaust strokes. The Net work per cycle, is the work delivered to the piston over the entire four-stroke cycle, taking into consideration gross indicated work and pumping work.

Pumping work is the work per cycle done by the piston on the in-cylinder gases during the induction and exhaust strokes and can be obtained by integrating around the p-V diagram over the exhaust and intake strokes:

$$W_p = \int_{bcd} pdV \qquad (4.1)$$

The gross indicated work per cycle is calculated from the compression and expansion strokes:

$$W_{i,g} = \int_{deab} pdV \qquad (4.2)$$

For the four-stroke engine, the net indicated work per cycle is also used, and it is calculated from the four strokes:

$$W_{i,n} = \int_{dedea} pdV \qquad (4.3)$$

and $W_{i,n}$ equals (area A - area B).

NIMEP is calculated by dividing the Net Indicated Work by the displaced volume, V_d indicating a value independent of engine size.

$$NIMEP = \frac{W_i}{V_d} \qquad (4.4)$$

Similarly Gross Indicated Mean Effective Pressure is calculated by dividing the Gross Indicated Work by the displaced volume, V_d.

$$GIMEP = \frac{W_i}{V_d} \tag{4.5}$$

Finally pumping work can be calculated from subtracting NIMEP from Gross IMEP:

$$gross \text{ imep} = \text{net imep} + \text{pmep} \tag{4.6}$$

4.3.2 BMEP

The mean effective pressure (work per cycle divided by the cylinder volume displaced per cycle) can also be expressed in terms of torque allowing the Brake Mean Effective Pressure to be calculated.

$$BMEP \text{ (Pa)} = \frac{P \text{ (W)} \times n_r}{V_d(dm^3)N(rev/s)} \tag{4.7}$$

where
n_r = 2 crank revolutions for each power stroke per cylinder
V_d = displaced volume = 1596 cc
P = Power (kW) delivered by the engine and absorbed by the dynamometer

$$P = 2\pi NT \tag{4.8}$$

Substituting for P

$$BMEP \text{ (bar)} = \frac{4\pi T}{0.001596 \times 10^5}$$

where
T = torque exerted by the engine

4.4 Fuel Consumption

Consideration was next given to fuel consumption, which is converted to kg/s and then allowing BSFC to be calculated, this allows like-for-like comparison between different geometry engines.

4.4.1 Fuel Flow rate

The fuel flow rate is calculated in kg/s, where a time is recorded for the consumption of 100 cc of fuel and converted to m^3/s

$$\dot{m}_f = \rho \times \frac{0.0001}{\text{time taken}} \qquad (4.9)$$

where

$\dot{m}_f$ = mass flowrate of fuel (kg/s)

ρ = density of gasoline = 760 kg/m^3

Time taken (s) for the consumption of 100 cc fuel measured from burette during testing

4.4.2 BSFC

The brake specific fuel consumption is given as the fuel flow rate per unit power output and measures how efficiently an engine produces work based on the fuel supplied.

$$bsfc = \frac{\dot{m}_f}{P} \qquad (4.10)$$

Substituting for P

$$bsfc = \frac{\dot{m}_F}{2\pi NT}$$

where
N = 1500 rpm = 25 revs/s
m_f is converted to g/hr
Power (W)
Torque (Nm) exerted by the engine

$$bsfc = \frac{\dot{m}_f \times 3600 \times 1000}{2 \times 25 \times \pi \times T} \qquad (4.11)$$

4.5 Emissions

Emissions are an obvious indication of the amount of pollutant released from an engine. However, these values need to be converted to specific values to provide a basis for comparison with different engines. This section lists how emission values either in ppm or % are converted to indicted, brake and gross indicated specific values.
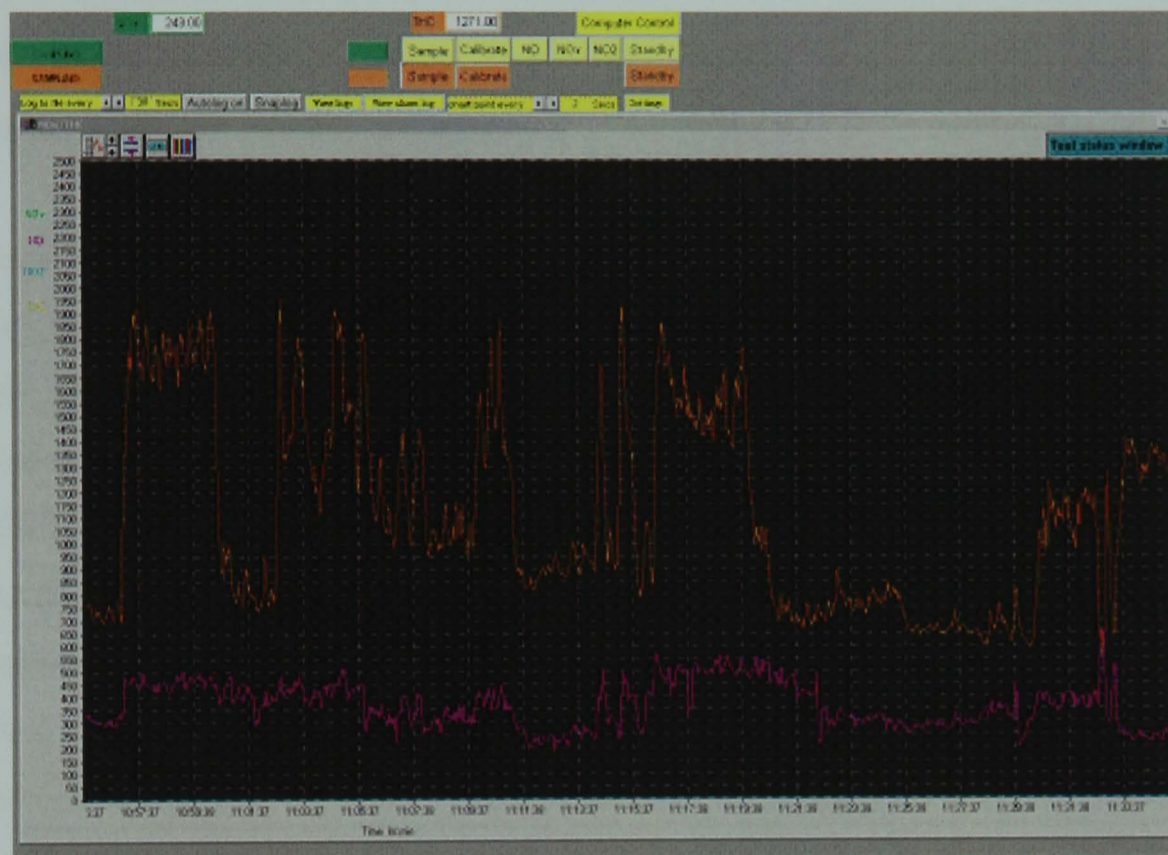
Figure 4.3 Screen Image showing the NOx and uHC (ppm) against time

The Horiba MEXA 7000 series analyzer was used to collect emissions data (Chapter 3) and had the ability to display onscreen the emission data for CO, CO_2, O_2, uHC and NO_x against time (Figure 4.3). This allowed an averaged raw emission value to be read compared with an instantaneous reading observed solely from the LED display of the Signal Analysers.

4.5.1 BSNO, BSHC, BSCO

The collected emission data was processed through the spreadsheet package Microsoft Excel™ using a matrix function to analyze the bulk data. A Microsoft Excel™ spreadsheet, written by Aaron Oakley formerly of Brunel University, was standardised and titled as "specific emissions.xls." Raw data for CO, CO_2, O_2, uHC and NO_x could be entered in either PPM or percent within this spreadsheet and BSFC values were entered as g/kW.h. The spreadsheet made the instantaneous calculations and Brake Specific Emission values were displayed on the "specific emissions" tab within the spreadsheet.

Raw emissions data observed during engine testing are recorded on a volumetric basis (ppm, %); hence the quantity of any species is therefore dependent on the total exhaust flow rate. In SI engines, the exhaust flow per cycle, excluding speed considerations, is dependent on engine load, ultimately determined by the intake throttle position. Diesel and un-throttled CAI engines, however, exhibit roughly constant exhaust flow per cycle characteristics, determined only by restrictions imposed by intake design and valve configuration. Emissions are expressed on a gravimetric basis, requiring emissions to be normalised. The most common practice is to normalise the volumetric emissions to the indicated or brake-power values. Raw emission data was converted to brake specific values first, then converted to Indicated Specific values. The generic equation used to calculate Brake Specific emission values, where x is the emission of interest is given below:

$$BS(x) = \frac{[(n_p - n_R) * vol(x)*M_x}{n_{Ra}(M_c + bM_H + cM_o)} * BSFC \qquad (4.12)$$

where

x = emission of interest
$vol(x)$ = mole fraction quantity of x
M_x = molar mass of emission concerned
n_p = number of moles of products
n_R = number of moles of reactants
a = wet molar fraction of fuel
b = Hydrogen/Carbon ratio

c	= Oxygen/Carbon ratio
M_c	= molar mass of carbon
M_H	= molar mass of hydrogen
M_o	= molar mass of oxygen

4.5.2 ISFC, ISNO, ISHC, ISCO

As mentioned in section 4.4.1, it is useful to normalize brake specific values and present them as indicated specific values. The method used to achieve this is given below. The ISNOx, ISHC and ISCO as delivered over the entire four strokes of the cycle, per unit displaced volume is given in 4.13.

$$isfc = \frac{bsfc * bmep}{imep}, \quad ishc = \frac{bshc * bmep}{imep}, \quad isnox = \frac{bsno_x * bmep}{imep}, \quad isco = \frac{bsco * bmep}{imep}$$

$$(4.13)$$

4.5.3 GSIFC, GSINO, GSIHC, GSICO

Gross specific indicated values are also useful characteristics and give an indication of the specific emission or SFC over the compression and expansion stroke. The GSIFC, GSINO, GSIHC and GSICO as delivered over the compression and expansion strokes, per cycle per unit displaced volume is given in 4.14.

$$gisfc = \frac{bsfc * bmep}{gross\ imep}, \quad gishc = \frac{bshc * bmep}{gross\ imep}, \quad gisnox = \frac{bsno_x * bmep}{gross\ imep}, \quad gisco = \frac{bsco * bmep}{gross\ imep}$$

$$(4.14)$$

4.6 Trapped residual and Heat Release calculations

4.6.1 Trapped Residual

The initiation of CAI combustion in this research is through the use of advancing exhaust valve closing and trapping residuals. Therefore knowing the volume of trapped residual is vital in analyzing CAI combustion. Equation 4.15 was used to calculate the volume of trapped residuals at EVC. The in-cylinder pressure value used for the calculations was measured at EVC using a pressure transducer. The cylinder volume was calculated at EVC, based on engine geometry and EVC timing. The temperature was assumed to be the burnt gas temperature at EVC, measured by the thermocouples installed in the exhaust manifold. Therefore, the amount of residuals at EVC was assumed to be the total residual mass for the whole cycle. Using fuel flow data and the lambda value, the mass of fresh charge in the cylinder could be calculated. The ratio of Trapped Residuals to Total In-Cylinder Charge could be calculated from the known masses of residual and fresh charge.

$$PV = m_r RT \qquad (4.15)$$

where, P = in-cylinder pressure
V = cylinder volume
m_r = mass of trapped residuals
R = specific gas constant
T = burnt gas temperature

4.6.2 Heat Release Analysis

In order to characterize combustion events within both SI and CI engines, heat release analysis is used; heat release analysis can also be used for characterizing combustion events for CAI combustion. The amount of heat that would have to be added to the cylinder to produce the observed pressure variation is calculated. It is assumed that there is a single zone combustion chamber and hence reactants and products are fully mixed, and no

temperature gradient exists. It is also assumed that there is no difference in the properties of the reactants and products. The first law of thermodynamics is applied to the cylinder contents, which represents a closed system during the combustion.

$$\partial Q_{hr} = dU + \partial W + \partial Q_{ht} \tag{4.16}$$

where

$$\partial W = pdV \tag{4.17}$$

$$dU = mc_v dT \tag{4.18}$$

$$mdT = \frac{[pdV + Vdp]}{R} \tag{4.19}$$

Combining equations 4.18 and 4.19 in terms of dU, substituting terms into equation 4.16 and writing on an angle incremental basis gives:

$$\frac{dQ_n}{d\theta} = \frac{dQ_{hr}}{d\theta} - \frac{dQ_{ht}}{d\theta} = \frac{\gamma}{\gamma - 1} p \frac{dV}{d\theta} + \frac{\gamma}{\gamma - 1} V \frac{dp}{d\theta} \tag{4.20}$$

Where γ is the ratio of specific heats and is equal to cp/cv, γ is almost always assumed to be constant and in the range of 1.3 to 1.35. $dQ_n/d\Theta$ is the net heat release rate and obtained from the measured pressure array, the calculated volume array, an estimation of average ratio of specific heat values during compression and expansion, and arrays that define the rate of change of pressure and volume with respect to crank angle [57].

4.6.3 CA 10% MFB, CA 50% MFB and CA 90% MFB

The integration of Equation 4.16 with respect to crank angle will yield a cumulative heat release function, from which the normalized mass fraction burned (MFB) curve can be obtained. Based on the mass fraction burnt curves, the CA at 10% MFB, 50% MFB and

66

90% MFB can be calculated. Burned mass fraction (MFB) curves can be used to quantify ignition timing and combustion duration. In the case of SI operation, the 'flame development angle', and the 'rapid burn angle', are defined as the 0-10% MFB CA and the 10-90% MFB CA respectively.

4.7 Summary

This chapter details the analysis used for the various data presented in this thesis. It is important that all data presented is quantified for CAI combustion, although certain equations may be true for SI combustion, this may not be the case for CAI combustion. This chapter therefore attempts to clarify the reasoning for using these equations and their relevance to CAI combustion data presented in chapter 5.

Chapter 5

CAI Combustion Engine Performance and Emissions

Chapter 5 CAI Combustion Engine Performance and Emissions

5.1 Introduction

There are various methods available to achieve CAI combustion as mentioned in chapter 2. The method chosen to initiate CAI combustion was the trapping of large amounts of exhaust residual in the cylinder. This was possible through the early closure of low-lift, short-duration exhaust valves. Retention of exhaust residuals provides sufficient thermal energy to enable the charge to auto-ignite and the necessary dilution for control of heat release rate. This chapter introduces the research methodology used to undertake testing, thereafter the effects of valve duration on CAI combustion are investigated, an initial load-speed map and load-valve timing map is provided, thereafter contour maps are used to represent engine performance data.

5.2 Negative Valve Overlap Approach for CAI Combustion

Trapping large quantities of exhaust gas residuals in the cylinder to initiate CAI combustion, inadvertently controls subsequent heat release rate. Closing exhaust valves early ensures that a sufficient quantity of exhaust gas is trapped, as a result intake valve opening has to be retarded to reduce back flow into the inlet manifold. The use of standard long duration, high lift SI camshaft profiles would result in exhaust valves opening half way through the expansion stroke and the intake valves closing half way through the compression stroke. It was therefore necessary to use a pair of short duration camshafts produced by re-profiling a standard pair of SI camshafts. Figure 5.1 shows a schematic diagram highlighting the difference in valve duration and lift between standard CAI camshafts and standard SI camshafts.

Previous work undertaken on this engine [57] involved investigating the effects of direct fuel injection on CAI combustion characteristics at lambda 1.0, 1.1, 1.2 and 1.3. The characteristics studied were: engine power output, fuel consumption, exhaust emissions and

operating region, where a pair of low lift camshafts (2mm 110 CA deg for exhaust and 2mm 120 CA deg for intake) were used. In an attempt to optimize the operating region, various exhaust and inlet strategies were employed.
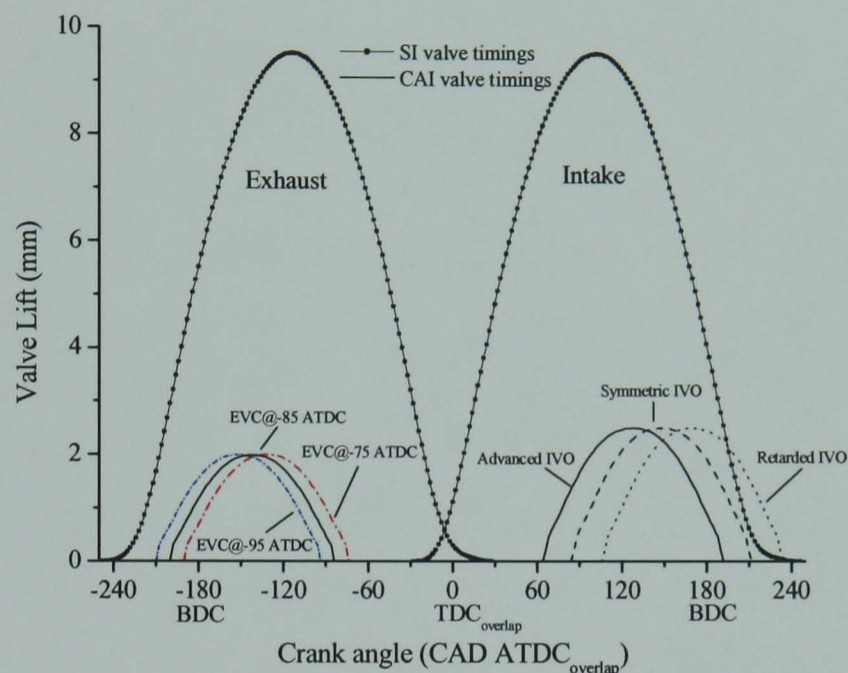
Figure 5.1 Indication of typical SI and CAI valve configuration

It became apparent that the deployment of the very short duration intake camshafts restricted the amount of inducted fresh air; the deployment of short duration exhaust camshaft restricted the amount of trapped exhaust gas. Therefore, it was envisaged that the use of longer duration intake and exhaust camshafts would extend the possible operational region of CAI combustion for this experimental engine.

The initial camshafts used had a duration of 110 CA deg and lift of 2mm for the exhaust camshaft and a duration of 120 CA deg and lift of 2mm for the intake. The second pair of camshafts used for comparison purposes had a duration of 130 CA deg and lift of 3mm for the exhaust and 140 CA deg and lift of 3mm for the intake. The rate of change of lift is very small during the first and last few degrees of the camshaft duration. As a consequence it is hard to accurately define the camshaft duration and timing at zero lift. It is estimated that approximately 10 CA deg of rotation is required to generate the first and the last

0.1mm of valve lift. The re-profiling of standard SI camshafts resulted in maximum valve lift from 9mm to 2mm for the shorter CAI camshafts and 3mm for the longer CAI camshafts in order to meet the duration criteria. This was based on re-profiling requirements rather a maximum or minimum lift requirement for CAI combustion.

The default valve positions were based on previous work carried out on a 4-cylinder PFI engine at Brunel University. The default positions chosen were exhaust valve closing at 55 CA deg BTDC and intake valve opening at 60 CA deg ATDC for both the shorter and longer CAI camshafts. It is noted that the intake TDC is used as the reference throughout the text unless it is otherwise specified. The VCT mechanism allowed increments of 1 CA change for advancing exhaust valve closing and retarding intake valve opening. It was decided that increments of 10 CA change in valve timing would be sufficient for test purposes. Figure 5.2 shows all the possible valve timing combinations possible with the initial set of camshafts with the shorter CAI duration. Figure 5.3 shows all the possible durations with the longer CAI profile camshafts. The VCT mechanism had the ability to be advanced by 60 CA deg for the exhaust closing and retarded 50 CA deg for the intake opening. Therefore the maximum EVC value was 115 CA deg BTDC and the maximum IVO value was 110 CA deg ATDC for both the shorter and longer CAI camshafts. It was possible to set different default values for EVC and IVO by turning the cylinder 1 piston to the CA deg desired for either IVO or EVC. For IVO the piston was turned a set number of CA deg after intake TDC and for EVC the piston was positioned a set number of CA deg before intake TDC. The cambelt was then removed and the camshaft in question rotated to the desired position where cylinder 1 lobes were touching cylinder 1 tappets and in a position ready to either open the intake valves or close the exhaust valves. For exact precision a Verne™ gauge was placed on the tappets and opening and closing movement was noted with relation to piston 1 TDC.
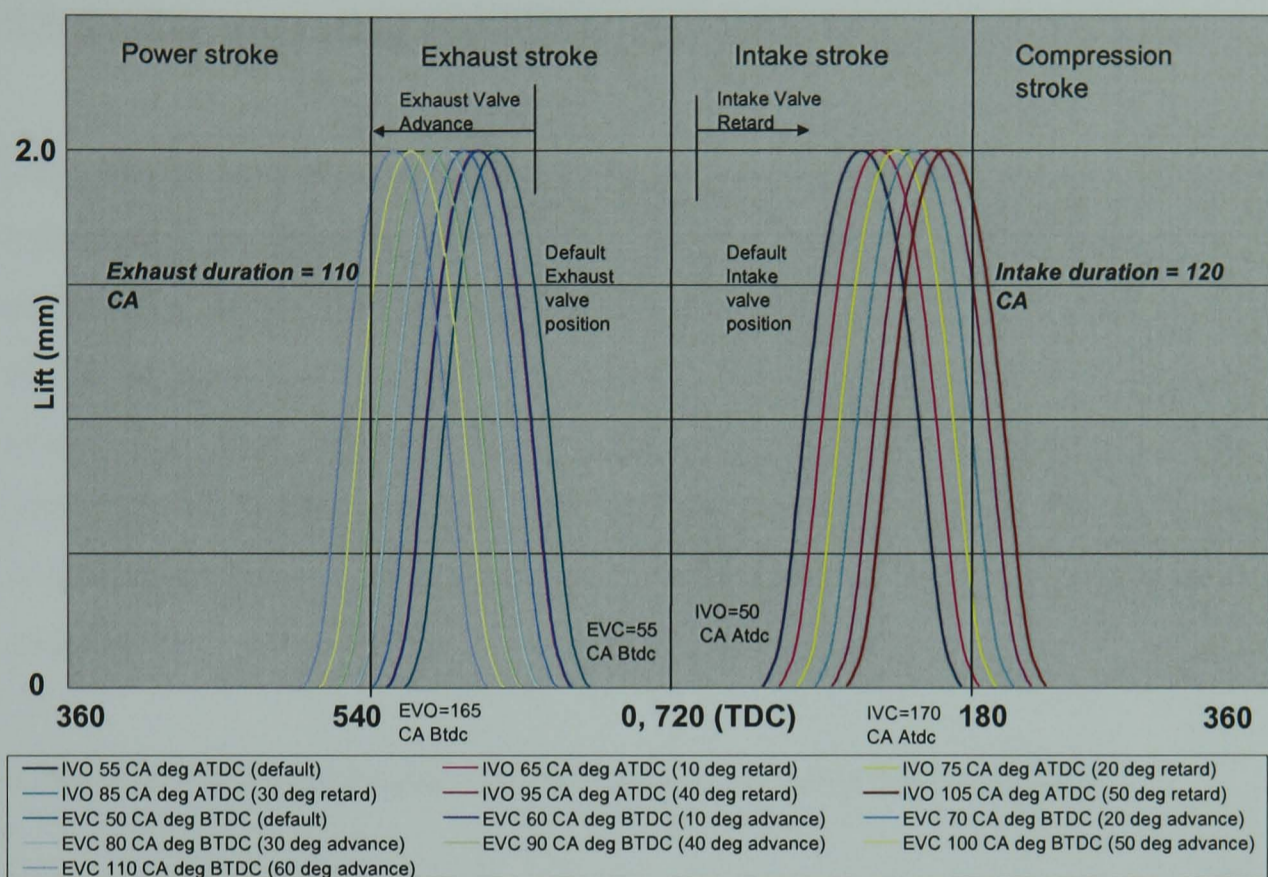
Figure 5.2 Intake and Exhaust valve profiles for entire range of VVT mechanism for shorter CAI camshafts
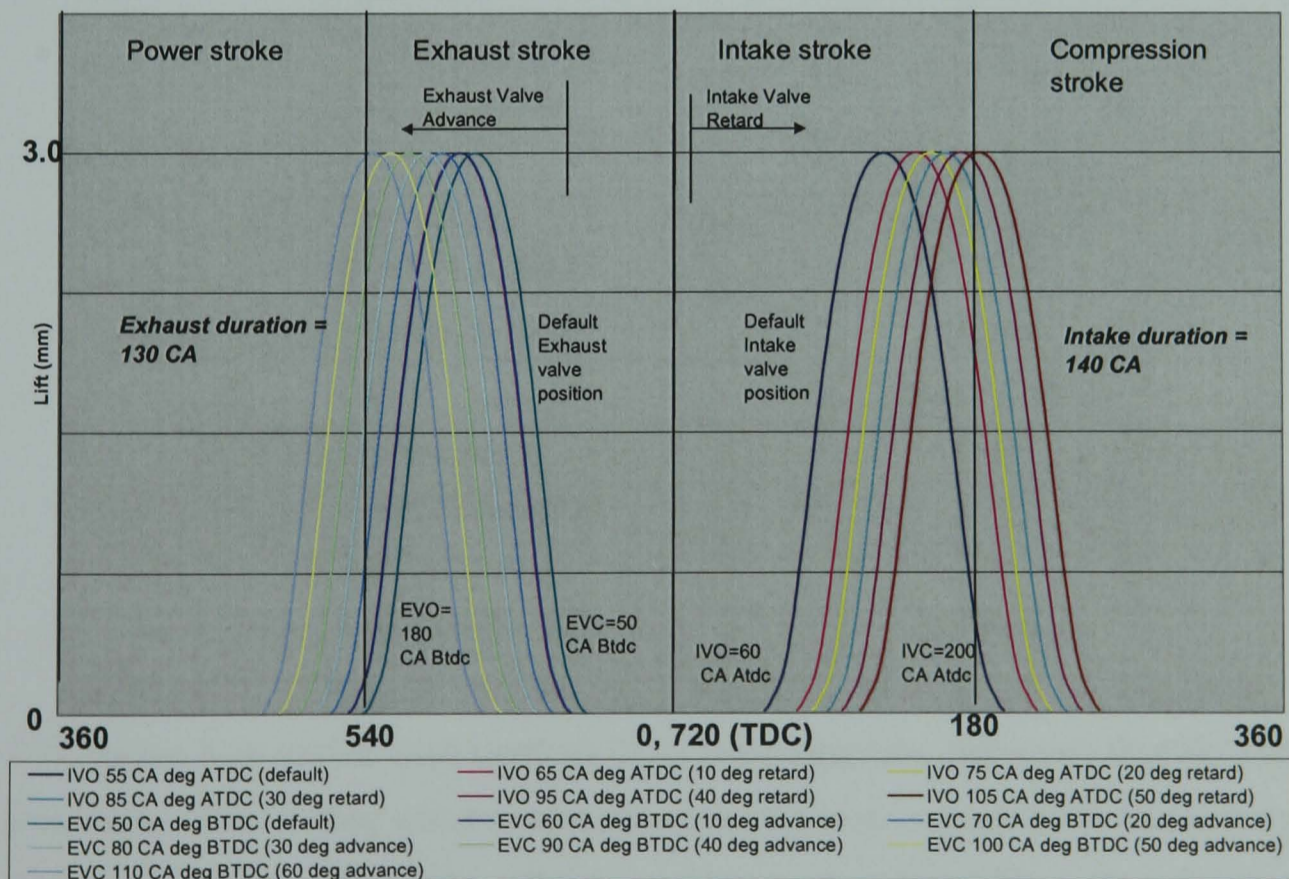
Figure 5.3 Intake and Exhaust valve profiles for entire range of the VVT mechanism for the longer CAI camshaft

5.3 Engine operating conditions and experimental procedure

The cylinder head incorporated standard spark plugs used for initial SI startup. The engine was started in SI mode, with IVO in the least retarded position and EVC in the least advanced position. Although this combustion phenomenon is referred to as spark ignition, this is not entirely true. The low-lift and short duration camshafts used in the experimental engine are in a negative valve overlap configuration compared with positive valve configuration for high-lift, long duration SI camshafts. Therefore the gas exchange process is different even for the default CAI camshafts position compared with normal SI camshafts.

Table 5.1: Ford test Engine Specifications and operating conditions

Engine Type	Inline 4-cylinder
Bore (mm)	79
Stroke (mm)	81.4
Displacement (cm^3)	1596
Compression ratio	11.5
Fuel Supply	Direct Injection
Fuel Injector (Spray cone angle)	Swirl Injector (70°)
Fuel Rail Pressure	10MPa
Fuel	Gasoline 95 RON
Oil Temperature	96°C
Coolant Temperature	80°C
Inlet Temperature	22°C
Operational speed	1500 rpm

The engine was started with spark at TDC (compression), part-open throttle and cold start conditions. The cooling water temperature was allowed to reach 80°C before it was deemed that EVC could be advanced to allow pure CAI mode to be realized. The throttle was left at the wide open position and the spark was turned off. Table 5.1 lists the operating conditions and engine specifications used during testing.
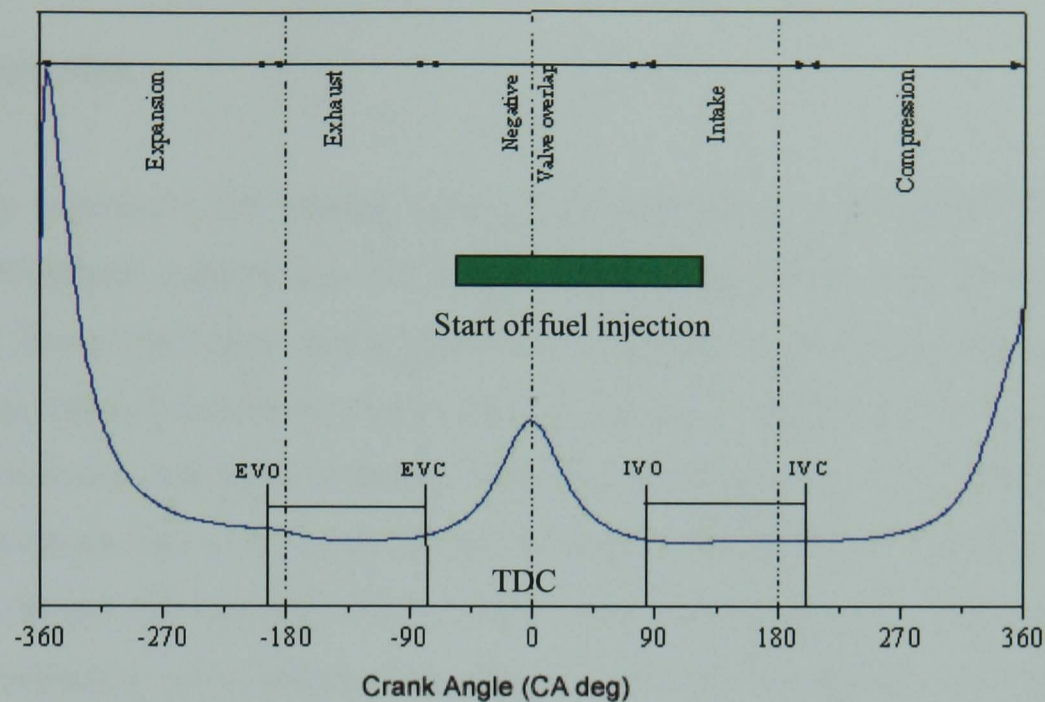
Figure 5.4 Schematic Indication of range of Start of Fuel Injection during CAI combustion mode for experimental Ford Engine

Once testing commenced which occurred when an IVO and EVC time had been selected and deemed that neither knocking nor misfire was occurring then injection timing was varied from -30 to 120 CA deg ATDC in increments of 30 CA deg. The software limited any further retarding of SOI in CAI combustion mode. Figure 5.4 shows the range of injection possible in CAI combustion mode. During testing, lambda values were monitored and if required the fuelling would be slightly altered to keep lambda constant. Results were only recorded when the engine was operating in a steady state with no erratic behavior. At each injection time, a time was recorded for how long it took to consume 100 cc of fuel and the airflow rate was noted. Nitric Oxides were measured using a Horiba CLA-720A analyzer and unburned hydrocarbons were measured using a Horiba FIA-720 analyzer. A Kistler 6061B pressure transducer was used to acquire in-cylinder pressure measurements. This data was then processed and recorded using LabVIEW™, a data acquisition software system. The program recorded pressure against crank angle, the IMEP and 10%, 50% and 90% MFB for 100 cycles.

5.4 Overview of engine operating modes with CAI camshafts

5.4.1 Introduction

This section introduces the starting point of analysis which established CAI combustion engine performance outputs for the shorter duration camshafts and the longer duration camshafts. The performance characteristics investigated were: engine power output, fuel consumption, exhaust emissions and operating region. As mentioned from previous work, direct fuel injection and valve strategies can be used to optimize and extend the operating region. Therefore maps were produced for the entire spectrum of IVO against EVC timings at SOI -30, 30 and 120 CA deg ATDC, with a particular performance characteristic plotted for each operational valve timing. This allowed a holistic comparison between the shorter and longer valve durations to be reached.

Conventional engine work dictates that an engine speed-load map is produced in which specific emissions and performance contours are plotted. It was envisaged that the engine would be run at different speeds with the relevant contour plotted. However, due to the reduction in the valve lift brought about because of duration reductions, it was physically not possible for the engine to induct enough fresh charge to run at high speeds. For the shorter duration CAI camshafts a speed of 1750 RPM was possible, higher speeds could only be achieved through SI combustion. For the longer duration CAI camshafts a speed of 2000 RPM was possible, speeds over this again utilized only SI combustion. Therefore for analysis purposes, it was decided that a contour map of EVC versus IVO plotted for a specific value would provide a detailed analysis of the operational region of both sets of camshafts.

An initial map of equivalence ratio against trapped residual is provided for both the shorter and longer camshafts. A load-speed map is also provided which indicates the operational region of both the shorter and longer CAI camshafts. Contour maps are then used as a comparative tool for comparing the effects of valve opening duration on CAI combustion.

CAI combustion characteristic analysis is also undertaken; where heat release data and mass fraction burnt data is examined.

5.4.2 Combustion modes with CAI Camshafts

As discussed in Chapter 2, Thring et al. [28] showed that the operating region for CAI/HCCI combustion is limited by three limits: the knock limit, misfire limit and the power limited region. Thring et al. used a SWRI Labeco CLR engine, achieving CAI/HCCI combustion with the use of external EGR. Ultimately the volume of exhaust residual was limited by an EGR valve which allows as much or as little EGR to be used for CAI/HCCI combustion. The volume of EGR determines the CAI boundary region for the engine, as long as no auxiliary system is used i.e. intake air heating. Using the method of NVO to trap residuals, the CAI combustion region is limited by the range of EVC and IVO timings permissible by the variable valve timing system. Through the VVT system, the valve duration and lift determines the full operating range of the engine, including a SI region and a spark assisted region.

Figure 5.5 and Figure 5.6 show a chart of lambda against percentage of in-cylinder residuals for the experimental engine plotted for the shorter and longer CAI camshaft at 1500 rpm, lambda 1.0 to 1.2 and for SOI -30 to 170 CA deg ATDC. On the chart there is an indication of where SI combustion is occurring, here it is considered that combustion is initiated by spark alone and continues by flame propagation. There is not enough residual to initiate auto-ignition but the charge is fuel rich enough for SI combustion to occur. SI combustion is associated with high NOx levels. However, for low-lift, short-duration camshafts with NVO configuration there will be proportionally less NOx emissions due to some trapped residual than the conventional SI operation with normal valve lifts. Therefore, it is apparent that further investigation is needed to study this area. There also exists a spark-assisted CAI combustion region where spark is used. However, combustion does not occur purely by flame propagation but through a combination of auto-ignition combustion and flame propagation. In the spark-assisted region there is not enough thermal energy to

allow auto-ignition to occur alone but the charge is too diluted to allow complete flame propagation to occur.
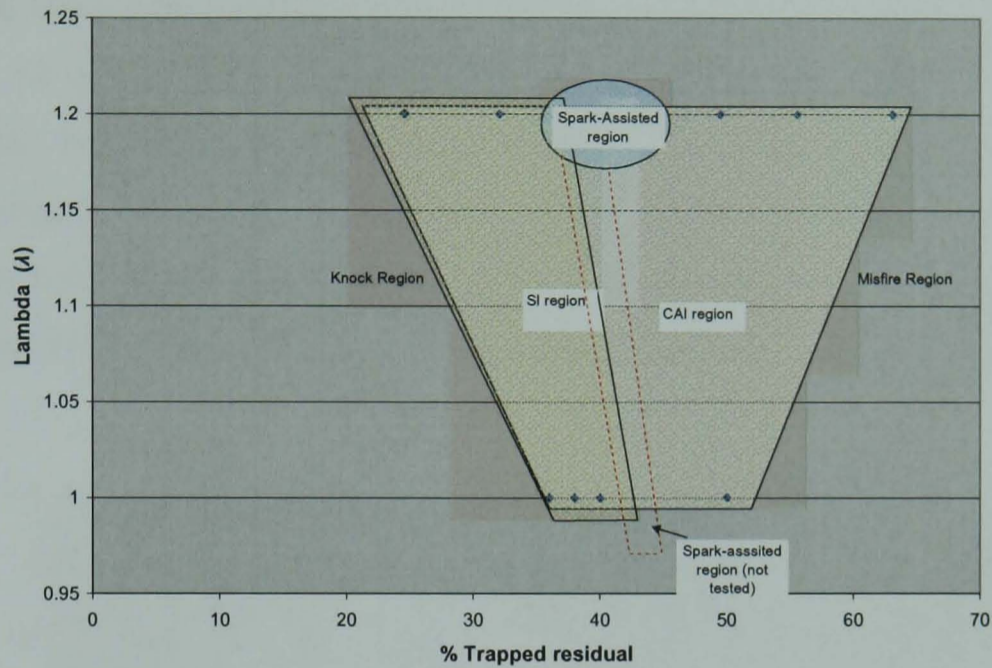
Figure 5.5 Combustion modes for the shorter CAI camshaft at 1500 rpm
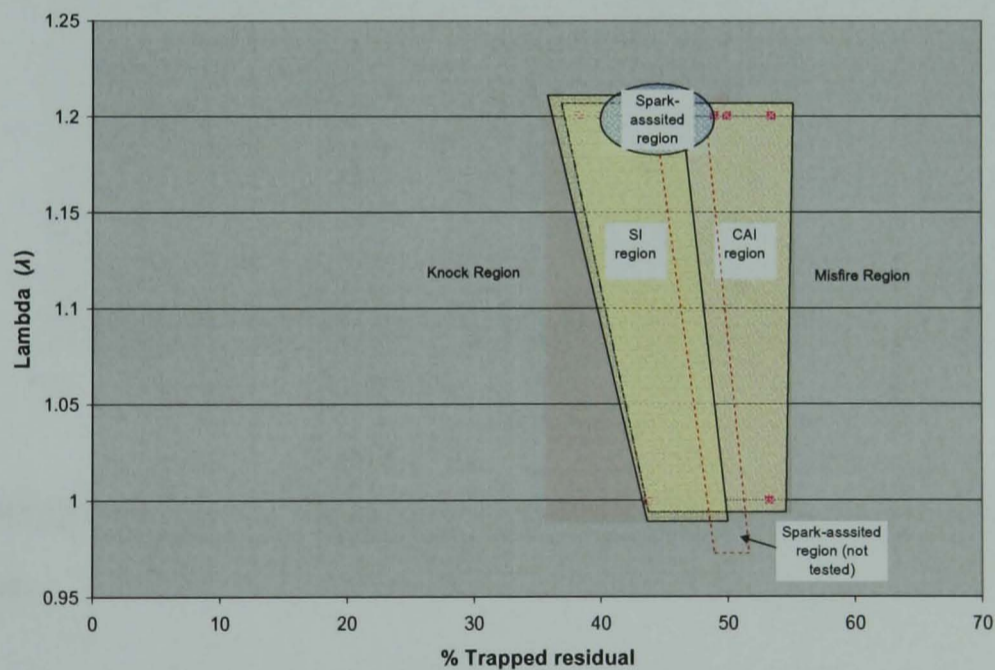
Figure 5.6 Combustion modes for the longer CAI camshaft at 1500 rpm

5.4.3 CAI Operational region at lambda = 1.0

At lambda 1.0, initial tests were undertaken to deem whether different speeds could be achieved for the shorter and longer CAI camshafts. It was found that speeds up to 2000 rpm were possible with the longer CAI camshafts, where there was a degree of CAI combustion

77

taking place at 2000 rpm. More importantly since the intake valve lift was higher than the shorter camshafts, extra charge could be inducted. For the shorter CAI camshaft, speeds up to 1750 RPM were only possible where CAI combustion was occurring. Retarded EVC allowed only SI combustion, advancing EVC caused trappings of high levels of residual due to low lift and hence there was not enough fresh charge inducted to initiate any combustion. Figure 5.7 shows the boundary region of CAI combustion with regards to load-speed for both the shorter and longer CAI camshafts. It can be observed that for the longer CAI camshafts, the load boundary is lower than the shorter CAI camshafts.
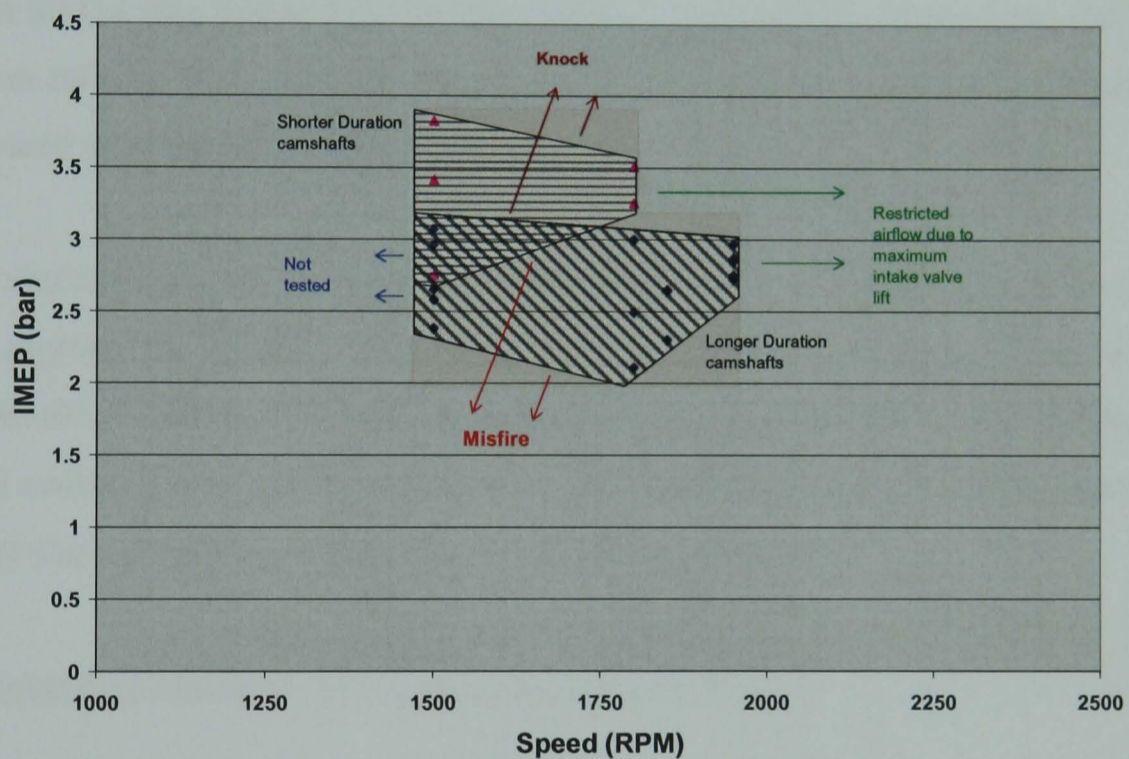
Figure 5.7 NIMEP range Vs. Speed for both duration camshafts at lambda = 1.0 for CAI operation

From Figure 5.7, it can be seen that three limits have been identified. These are the knock limit, the misfire limit and the restricted airflow limit. Speeds below 1500 rpm were not tested at, therefore it is not possible to indicate a boundary. It is speculated that speeds of approximately 1000 rpm would be possible for both the longer and shorter CAI camshafts, speeds below this would require immense frictional forces to be overcome causing engine misfire.

The limits vary between the shorter and the longer CAI camshafts. Higher speeds are possible for the longer CAI camshaft since the higher lift allows the breathing of extra air compared with the shorter CAI camshafts. The misfire limit is lower for the longer CAI camshaft since extra residual is trapped at a given Exhaust Valve Closing compared with the shorter CAI camshafts. This could be caused by the early opening of the exhaust valves and hence higher residual gas temperature, leading to more favorable auto-ignition conditions at low load operations (e.g. at EVC = 75 CA deg ATDC, the exhaust temperature for the longer CAI camshafts is 667K, for the shorter CAI camshafts the exhaust temperature is 654K). The knock limit is higher for the shorter CAI camshaft since IVC occurs 20 CA deg before IVC for the longer CAI camshafts. This causes the effective compression ratio to be higher for the shorter CAI camshafts, leading to a higher knock limit compared with the longer CAI camshaft.

The CAI boundary region for both the shorter and longer camshafts can be investigated further by plotting the NIMEP range at different valve timings. Figure 5.8 and 5.9 shows each conceivable NIMEP value (bar) at each valve timing at lambda 1.0 for the shorter and longer CAI camshaft consecutively. It is noted that for each EVC/IVO combustion, NIMEP value varies due to injection timing, which will be discussed later.

5.4.3.1 Shorter CAI camshaft operational range at Lambda 1.0

Previous work [57] determined that CAI combustion at lambda 1.0 only occurred for the shorter CAI camshafts at EVC 95 and 105 CA deg BTDC. At EVC 105 CA deg BTDC, IVO timings of 70, 80, 90 and 100 CA deg ATDC were possible. It is noted that for EVC/IVO combination the NIMEP values could be altered by injection timings. At IVO 70 CA deg ATDC the upper end of operation was limited by knocking combustion (at a fuel injection of 130 CA deg ATDC). As IVO is retarded the effective compression ratio decreases in accordance, hence at EVC 105 CA deg BTDC, IVO timings of 80, 90 and 100 CA deg were possible. However, retarding IVO beyond this (110 CA deg) caused misfire. At EVC 95 CA deg BTDC, it was reported that CAI could only be operated at an IVO timing of 110 CA deg ATDC when the effective compression ratio was low enough to

avoid knocking combustion. Any EVC timings retarded beyond 95 CA deg BTDC did not trap sufficient levels of exhaust residual to initiate CAI combustion. However, for purposes of presenting a complete operational map, tests for EVC timings of 75 and 85 CA deg BTDC were conducted, where SI combustion was occurring. It was deemed that this would provide useful information for the possibility of transitioning from low-lift, short-duration SI combustion to CAI combustion, compared with the conventional method of switching from high-lift, long duration SI combustion to CAI combustion. It was deemed that SI combustion was occurring based on a few factors, firstly combustion only occurred if the spark signal was switched on and secondly the resulting combustion produced extremely high levels of NOx.
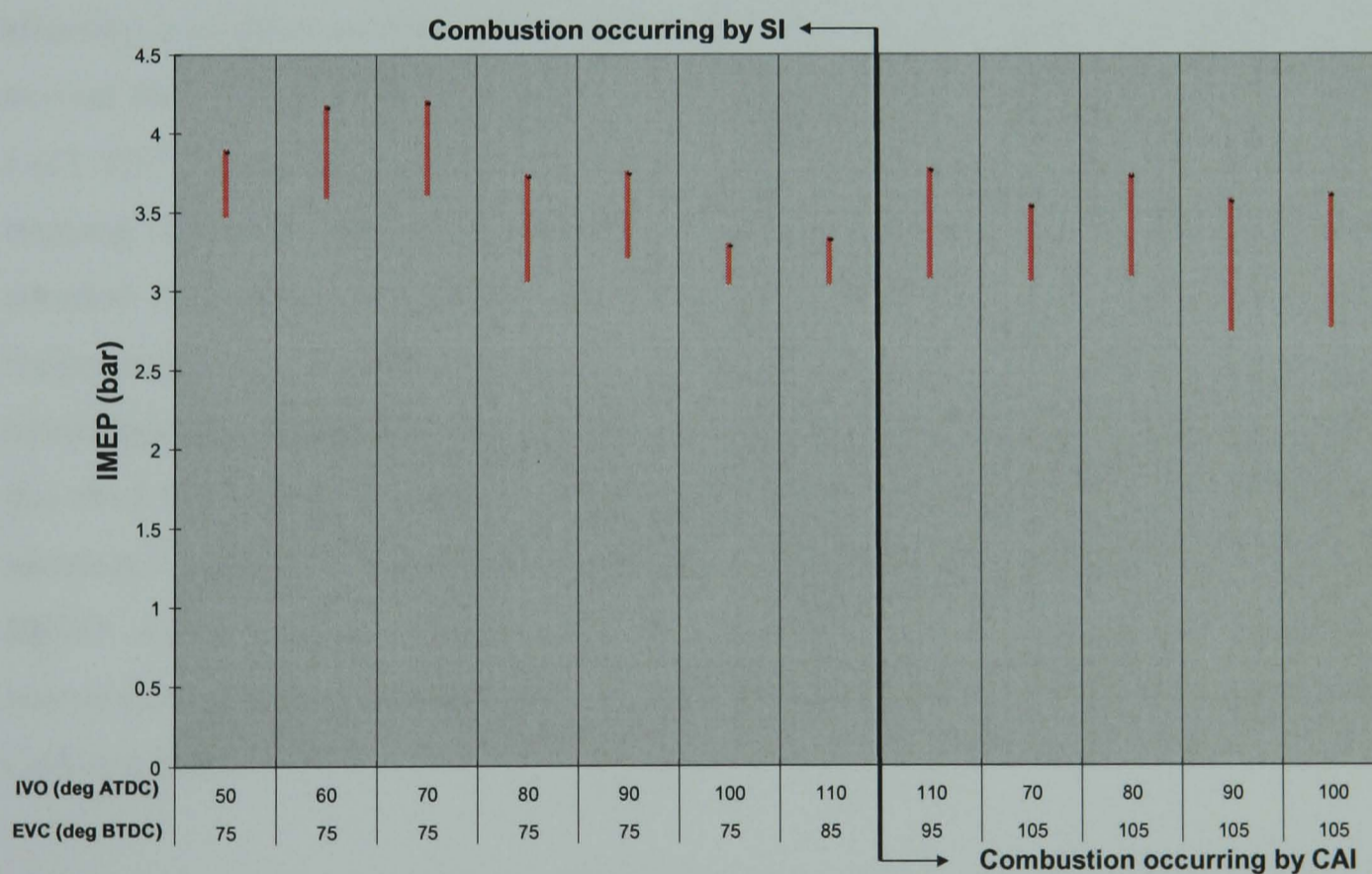
Figure 5.8 NIMEP range Vs. Operating points at lambda = 1.0, shorter CAI camshafts at 1500 rpm

5.4.3.2 Longer CAI camshaft operational range at lambda 1.0

For the longer CAI camshafts at lambda 1.0, CAI combustion occurred at EVC timings of 75, 85 and 95 CA deg BTDC. At EVC 95 CA deg BTDC, an IVO timing of 90 CA deg ATDC could only be used to achieve CAI combustion. If the IVO timing was retarded beyond this point, then IVC would occur further into the compression stroke, hence reducing the effective compression ratio. Advancing IVO timing beyond 90 CA deg ATDC caused misfire to occur in some cycles, which could be caused by the heat loss of residual gas involved in the backflow into the intake port.

At EVC 85 CA deg BTDC, IVO timings of 60, 70, 80 and 90 CA deg ATDC were permissible. Again retarding IVO timing beyond 90 CA deg resulted in a decreased effective compression ratio and hence misfire. It was found that advancing IVO timing beyond 60 CA deg ATDC resulted in knocking combustion, this was determined using a LabVIEW™ program (discussed in Chapter 3). The final EVC timing which allowed the trapping of enough residual to permit CAI combustion was 75 CA deg BTDC. The most retarded IVO timing permissible was 100 CA deg ATDC and the most advanced IVO timing permissible was 60 CA deg ATDC. Retarding IVO timing resulted in misfire and advancing IVO timing resulted in knocking combustion. It is perhaps interesting to notice that the EVO timings to achieve CAI operation for both long and short CAI camshafts are identical, i.e. 235 CA deg BTDC or 55 CA deg BBDC and 225 CA BTDC or 45 CA deg BBDC. As the exhaust valve opening has a large effect on the exhaust gas and hence the temperature of trapped residual gas, these results indicate the significance of temperature in CAI operation.

EVC timings of 55 and 65 CA deg BTDC experienced SI combustion, here the spark signal was switched on and the NOx values were extremely high. The IVO timings selected for SI combustion were determined by whether knocking was occurring. At an EVC timing of 55 CA deg BTDC, IVO timings of 60, 70, 80, 90, 100 and 110 CA deg ATDC were permissible. Advancing EVC timing to 65 CA deg BTDC, increased the percentage of trapped residual and hence the valve timings at which combustion by pure flame

propagation was occurring was limited. IVO timings of 80, 90 and 100 CA deg ATDC experienced SI combustion at EVC 65 CA deg ATDC.

IVO (deg ATDC)	70	80	90	100	110	80	90	100	60	70	80	90	100	60	70	80	90	90
EVC (deg BTDC)	55	55	55	55	55	65	65	65	75	75	75	75	75	85	85	85	85	95
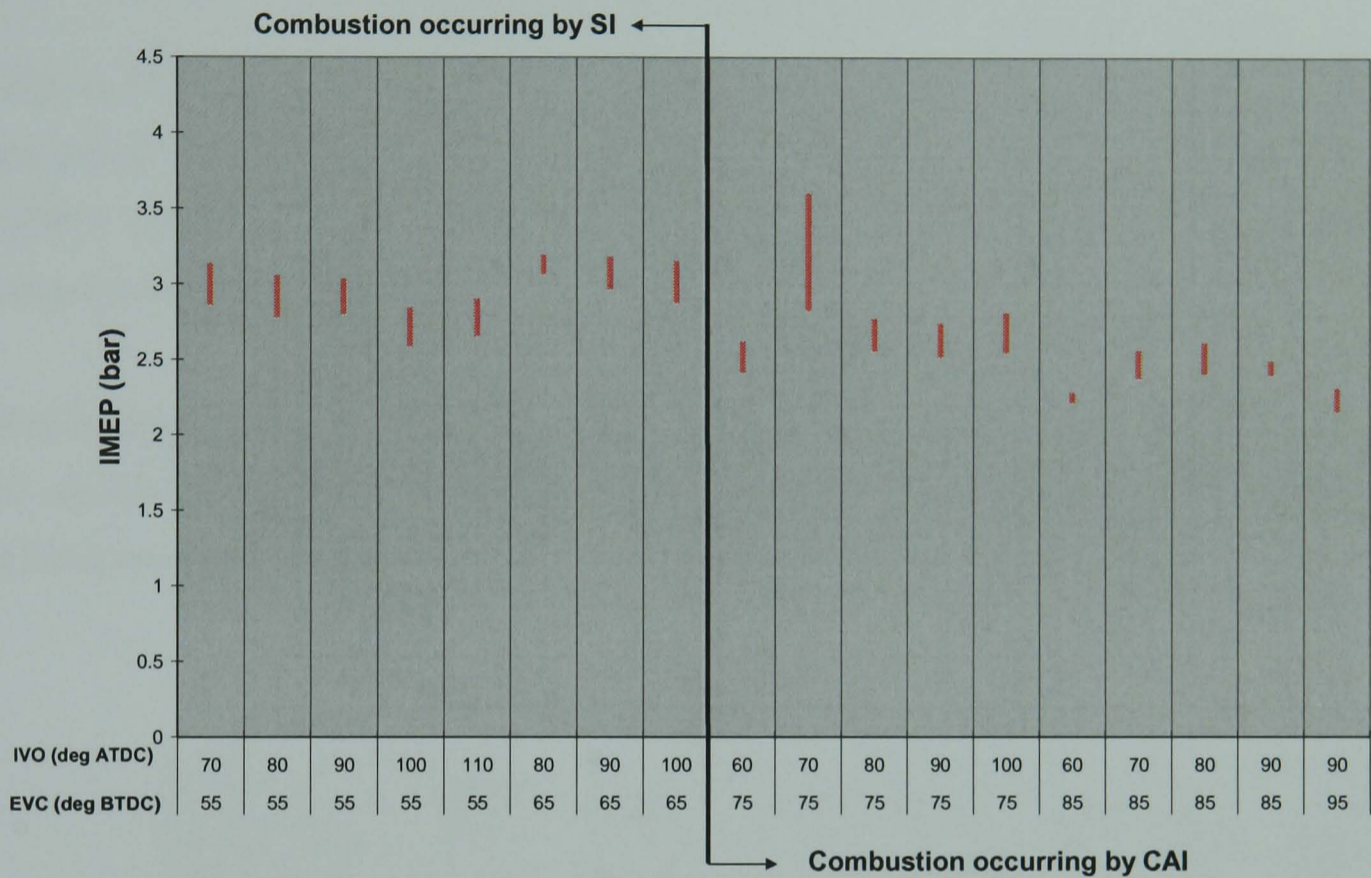
Figure 5.9 NIMEP range Vs. Operating points at lambda = 1.0, longer CAI camshafts at 1500 rpm

5.4.4 Operational region lambda = 1.2

To indicate the operational region for both the shorter and longer CAI camshafts, the NIMEP (bar) at different valve timings was plotted (Figure 5.10 and 5.11).

5.4.4.1 Shorter CAI camshaft operational range at lambda 1.2

From Figure 5.10, it can be seen that three different EVC timings could be tested at which CAI combustion occurred; these EVC timings were 85, 95 and 105 CA deg BTDC. It was reported that at EVC 85 CA deg BTDC, only two IVO timing could be tested, 80 and 100

82

CA deg ATDC. If the IVO timing was further retarded (e.g. to 110 CA deg ATDC) the engine would misfire. This is due to two factors, the reduction in the effective compression ratio and the lower levels of Trapped Residuals. If the IVO timing was advanced (e.g. to 90 CA de ATDC or less) then knocking combustion occurs.

With an EVC of 95 CA deg ATDC four different IVO timings could be tested (70, 80, 90 and 100 CA deg ATDC). It was found that further retarding of the IVO (e.g. to 100 CA deg ATDC) resulted in misfire and further advancing of the IVO (e.g. to 60 CA deg ATDC) caused knocking combustion.

With an EVC timing of 105 CA deg BTDC three different IVO timings could be tested (70, 80 and 90 CA deg ATDC). The IVO timing could not be retarded further (to 100 CA deg ATDC) because of misfire.
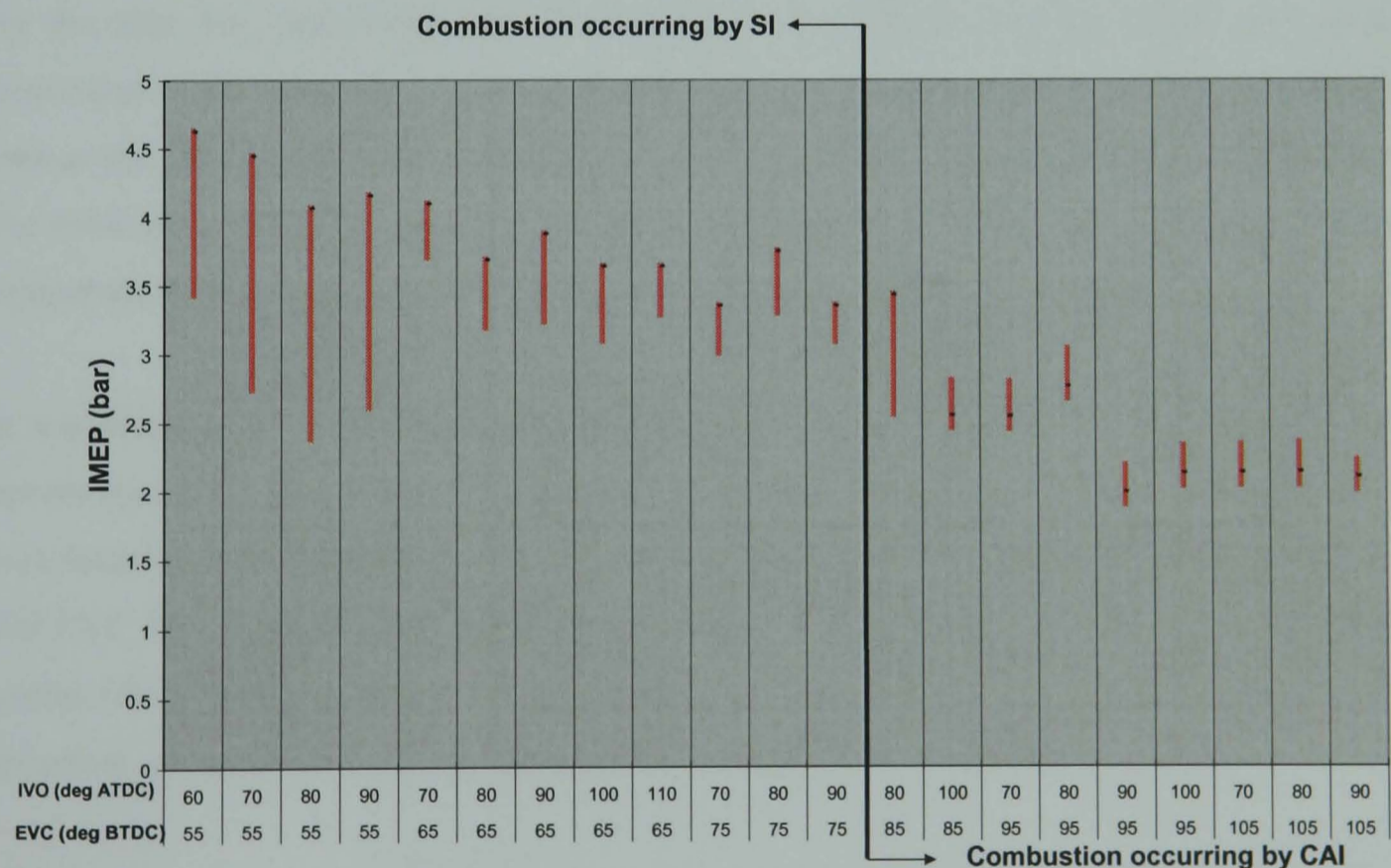
Figure 5.10 NIMEP range Vs. Operating points at lambda = 1.2, shorter CAI camshafts at 1500 rpm

5.4.4.2 Longer CAI camshaft operational range at lambda 1.2

Figure 5.11 shows the NIMEP (bar) range for the longer CAI camshaft at lambda 1.2 for various valve timings, at EVC 75, 85, 95 and 105 CA deg ATDC combustion is occurring by CAI combustion. At an EVC timing of 105 CA deg BTDC, two IVO timings, 90 and 100 CA deg ATDC, can be used to initiate combustion. Retarding IVO beyond 100 CA deg ATDC reduced the effective compression ratio and hence combustion would experience misfire. Advanced IVO timings (e.g. 80 CA deg ATDC) brought about asymmetric valve timings and resulted in misfire.

At EVC 75, 85 and 95 CA deg BTDC, IVO timings of 90, 100 and 110 CA deg ATDC were achievable. It was found again that retarding IVO (e.g. 120 CA deg ATDC) caused the effective compression ratio to decrease and hence misfire would occur. Advancing IVO timing (e.g. 80 CA deg ATDC) resulted in knocking combustion. This is probably caused by the heat loss associated with the backflow of residuals into the intake port at the beginning of the inlet valve opening results in lower charge temperature. This is probably true as the IVO is much more advanced compared with the symmetric timings. In addition, the most advanced EVC produces the highest residuals and hence lower load and residual temperature, therefore it would be most sensitive to the charge temperature.

It was found at EVC 75 CA deg BTDC, IVO 90 CA deg ATDC, that knocking was more severe than EVC 95 CA deg BTDC, IVO 90 CA deg ATDC. At EVC 75 CA deg BTDC, it was found that for an average of a 100 cycles, there was 78 cycles where knock occurred. For EVC 95 CA deg BTDC, it was found that for an average of a 100 cycles, there was 61 cycles where knock occurred. The knock criterion had been set for a 50 cycles out of a 100, therefore advanced IVO timings beyond 90 CA deg ATDC could not be tested.

The above results have shown that the retarded IVO timing always leads to misfire, due to lower effective CR ratio but advancing IVO has the opposing effect on the most advanced EVC and retarded EVCs. Advancing IVO for the most advanced EVC causes misfire

84

whereas for the retarded EVCs and advanced IVO leads to knock combustion. In this case, the engine is operating at higher load, the increase in effective CR may be more important.

For advanced EVC timings of 55 and 65 CA deg, stable combustion could only be achieved using spark ignition. Again, the LabVIEW™ program was used to determine knocking, therefore for EVC 55 CA deg BTDC, IVO timings of 60 and 70 CA deg ATDC could only be tested at. For EVC 65 CA deg BTDC, IVO timings of 60, 70, 80, 90, 100 and 110 CA deg ATDC could be tested at.
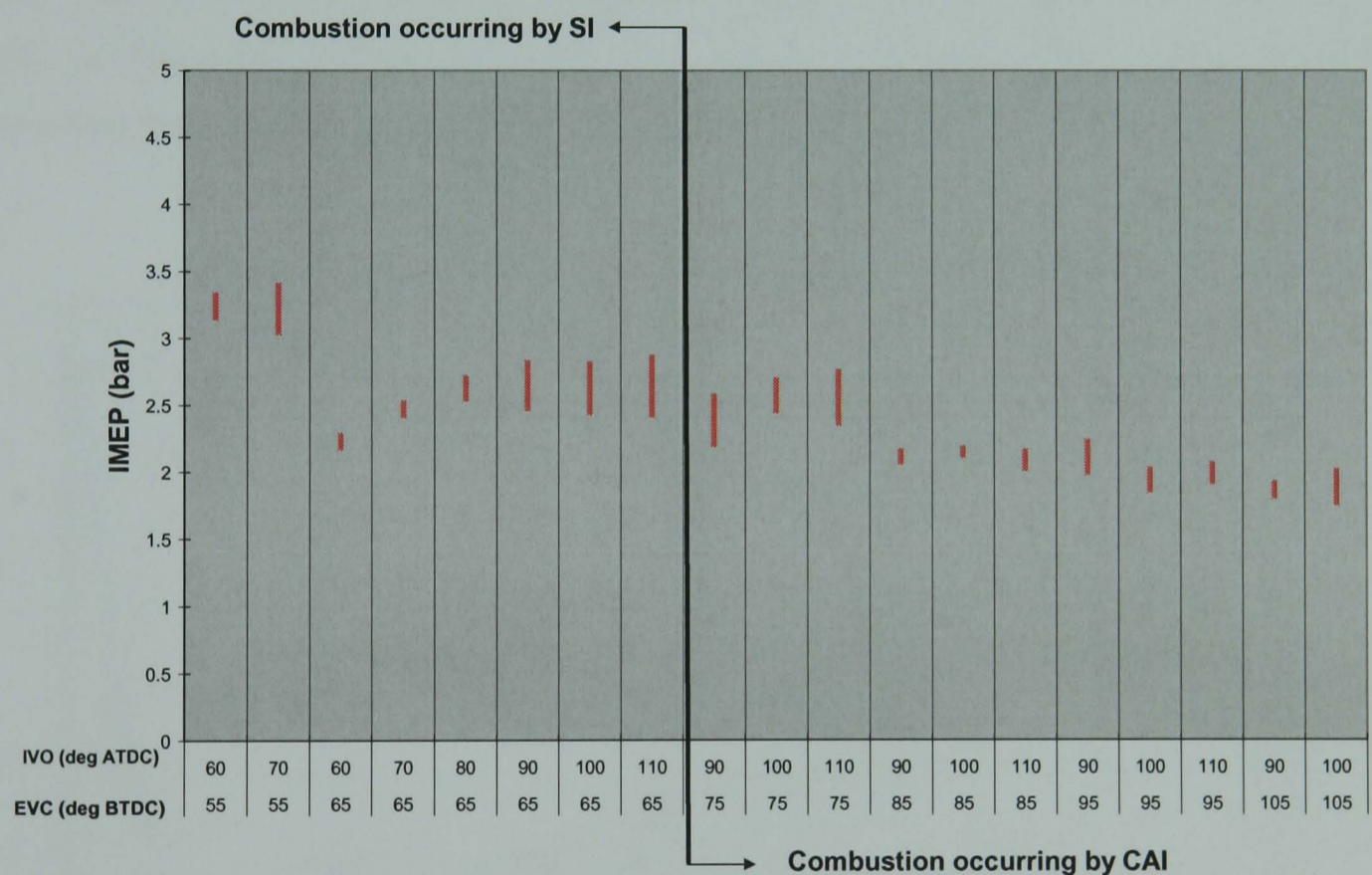
Figure 5.11 NIMEP range Vs. Operating points at lambda = 1.2, longer CAI camshafts at 1500 rpm

5.5 Effects of Camshaft design and Injection Timing at lambda =1.0

5.5.1 Introduction

Work undertaken on the Ford research engine, has shown that start of fuel injection can control the phasing of CAI combustion. Three different fuel injection timings were chosen: injection during the Negative Valve Overlap re-compression period before intake TDC (SOI -30 CA deg ATDC), injection during the Negative Valve Overlap re-expansion period after intake TDC (SOI 30 CA deg ATDC) and injection after Intake Valve Opening (SOI 120 CA deg ATDC). Figure 5.12 shows a schematic representation of where these fuel injections are in relation to CAI combustion events.
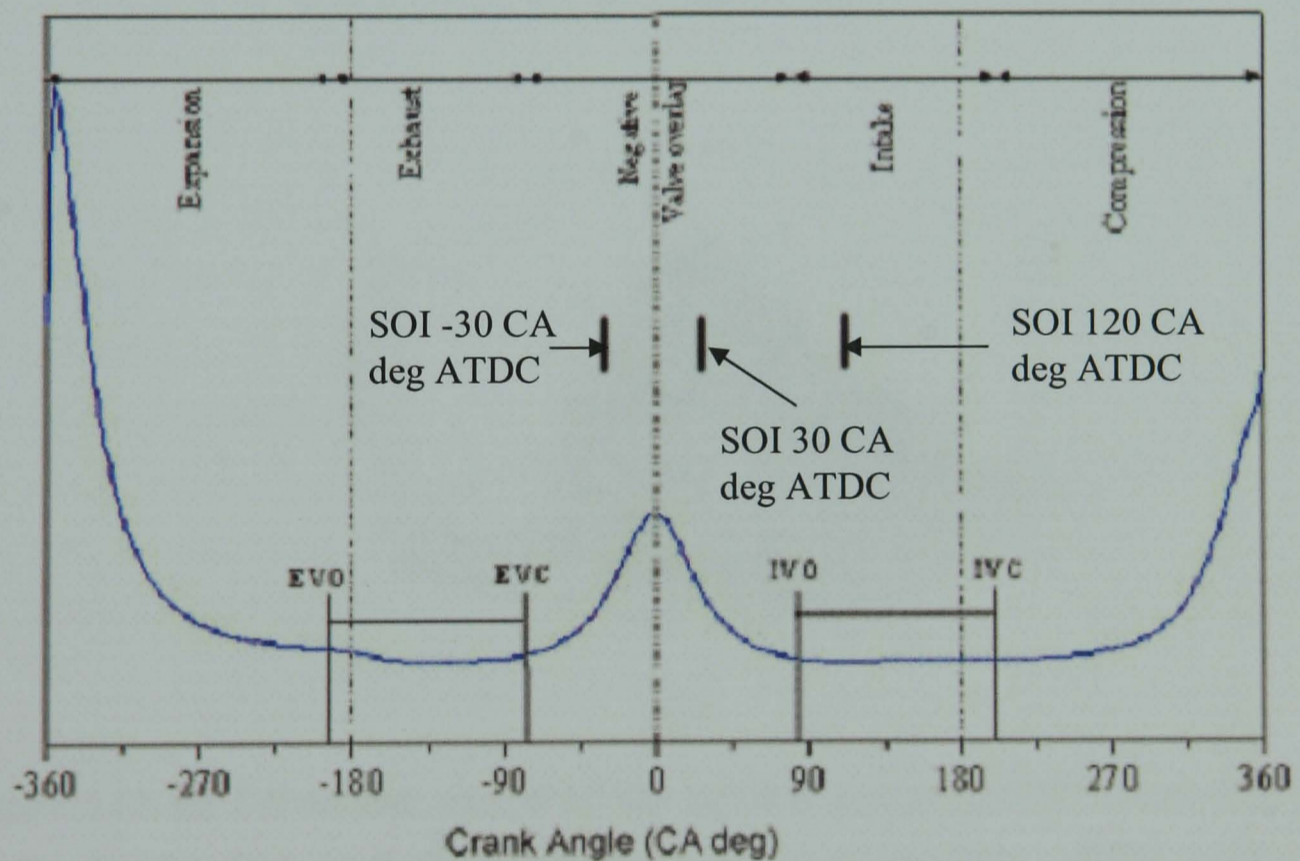
Figure 5.12: Indication of fuel injection at -30, 30 and 120 CA deg ATDC.

In previous work, Indicated Specific Values were plotted against Start of Fuel Injection. This method is useful for a fundamental study. However, to represent the full operational

range and present the data for direct comparison purposes, it was envisaged that data should be plotted as contour maps. Uniplot™ was used for plotting contour maps, the Indicated Specific values at a certain IVO and EVC timing was plotted. Figure 5.13 shows an example of such a map, with the SI and CAI combustion regions marked.
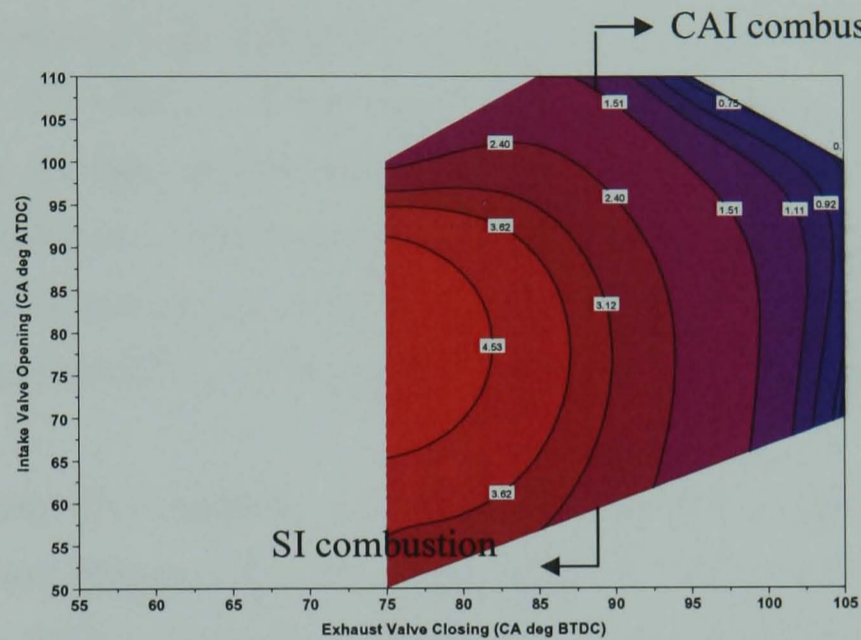
(a)
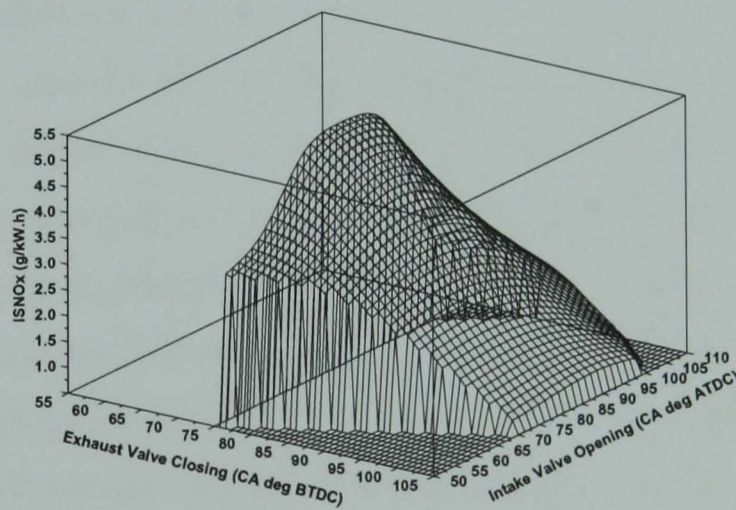
(b)

Figure 5.13, (a) 2-D contour plot of ISNOx (g/kW.h) values for EVC versus IVO for the shorter duration CAI camshafts at lambda 1.0. (b) 3-D representation of 2-D contour plot in (a)

5.5.2 Effect of Camshaft design and Injection Timings on Engine Performance at Lambda =1.0

For the shorter CAI camshafts, SOI -30 and 30 CA deg ATDC produced the lowest NIMEP range of values compared with SOI 120 CA deg ATDC (Figure 5.14 (a-c)). The NIMEP range for SOI -30 CA ATDC is 3.02 bar to 3.43, for SOI 30 CA deg ATDC the NIMEP range is 3.10 bar to 3.40 bar, whereas SOI 120 CA deg ATDC the NIMEP range is 3.14 bar to 3.71 bar. The variation in NIMEP at different injection timings can be largely attributed to pumping losses. From Figure 5.15 (a-c), it is apparent that the highest pumping losses occur at SOI -30 and 30 CA deg ATDC compared with SOI 120 CA deg ATDC.

Similar to the shorter CAI camshaft, the longer CAI camshafts also produce some of the lowest NIMEP values (Figure 5.16 (a-c)) at SOI -30 and 30 CA deg ATDC compared with SOI 120 CA deg ATDC. Again, the difference in NIMEP values at different injection timings is due to higher pumping losses (Figure 5.17 (a-c)). Injection during the negative valve overlap re-compression period (SOI -30 CA deg ATDC) results in the charge cooling phenomenon, as fuel is injected into the high temperature residual gas, the evaporation of fuel droplets results in lower in-cylinder pressure. As the fuel evaporation mainly takes place after TDC during the re-expansion process, the re-expansion work becomes lower than the re-compression work, hence higher pumping losses. Injecting at 30 CA deg ATDC also leads to lower expansion pressure, however, this is later in the cycle and hence the duration of higher pumping losses is shorter than at SOI -30 CA deg ATDC. Injecting at 120 CA deg ATDC, does not have any effect on the pumping loss during the NVO period.

A comparison of NIMEP values at SOI -30, 30 and 120 CA deg ATDC between shorter and longer CAI camshafts shows that for the entire valve timing range, the shorter CAI camshafts have a higher NIMEP. This is true at all three injection times and at all overlapping valve timing combinations. For example at EVC 95 CA deg BTDC, IVO 90 CA deg ATDC and SOI 30 CA deg ATDC, the NIMEP for the shorter CAI camshafts is 3.12 bar, whereas for the longer CAI camshafts the NIMEP is 2.21 bar; almost a 1 bar drop. The reason for the lower NIMEP values for the longer CAI camshaft is due to a few

reasons. Firstly, EVO for the longer CAI camshaft occurs 20 CA deg before EVO for the shorter CAI camshaft. Meaning that the exhaust valve opens earlier during the power stroke, taking away positive work generated during this stroke. Pumping losses are much higher for the longer CAI camshaft over the valve timing range. Furthermore, the effective compression ratio is lower for the longer CAI camshaft as IVC is retarded by 20 CA deg.

Another main reason for lower NIMEP values for the longer CAI camshaft at SOI -30, 30 and 120 CA deg ATDC compared with the shorter CAI camshaft is due to the higher percentage of trapped residual at the same valve timings (Figure 5.18 (a-c) and Figure 5.19 (a-c)). For example at EVC 95 CA deg BTDC, IVO 90 CA deg ATDC, the percentage of trapped residual for the shorter CAI camshaft is 45.6%, for the longer CAI camshaft the percentage is 52.7%. This trend is true for all valve timings, on average the difference is approximately 7% higher residual for the longer CAI camshaft compared with the shorter CAI camshaft at a given valve timing. The higher percentage of trapped residual results in less inducted fresh charge, hence lower NIMEP values. The reason for higher trapped residual for the longer CAI camshaft is due to the fact that at EVC, the in-cylinder pressure is higher for the longer duration camshaft compared with the shorter duration camshaft, therefore at IVO there will be less inducted fresh charge.

On comparison of NIMEP values during SI and CAI operation, it is apparent that the highest NIMEP value is found for SI combustion. CAI combustion is dependent on the amount of trapped residual and is achieved by advancing EVC timing. Therefore, for SI combustion there is a higher volume of inducted fresh charge, which allows for higher NIMEP values. For the shorter CAI camshaft, the NIMEP values for SI operation range between 3.02 and 3.73 bar, whereas for CAI operation NIMEP values range between 3.12 and 3.41 bar, using optimum values over the SOI range. For the longer CAI camshafts, the NIMEP values for SI operation range between 2.66 and 3.14 bar, whereas for CAI operation NIMEP values range between 2.30 and 2.98 bar, again using optimum values over the SOI range. It can be noticed that for both camshafts, there is an overlap of NIMEP values for SI and CAI combustion. This overlap provides a mechanism for achieving a transition from SI to CAI combustion and back to SI combustion. For example for the

shorter CAI camshaft at EVC 85 CA deg BTDC, IVO 90 CA deg ATDC, SOI 120 CA deg ATDC using SI operation, the NIMEP value is 3.41 bar, at EVC 100 CA deg BTDC and IVO 85 CA deg ATDC using CAI operation the NIMEP value is also 3.41 bar. Therefore a seamless transition maintaining a fixed load, can be made from SI combustion to CAI combustion allowing the benefits of low NOx values to be realized.

SI combustion ◄—► CAI combustion
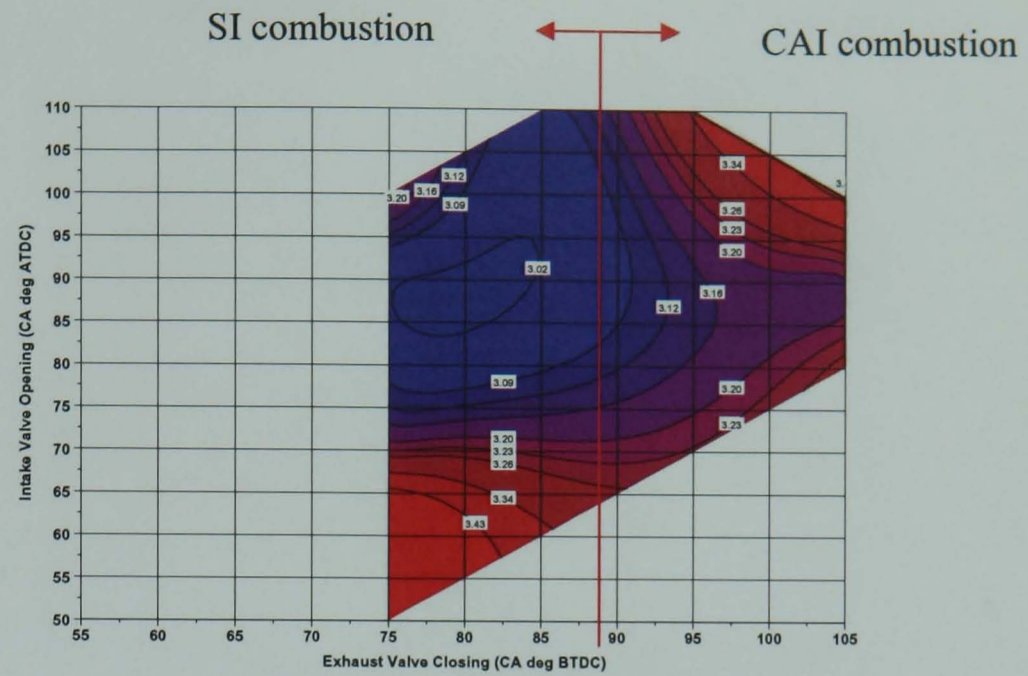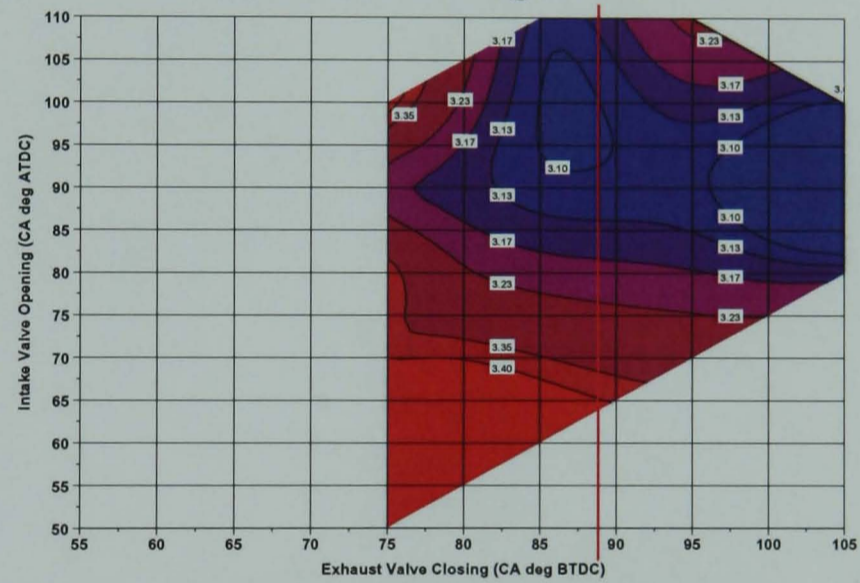
(a) SOI -30 CA deg ATDC

(b) SOI 30 CA deg ATDC
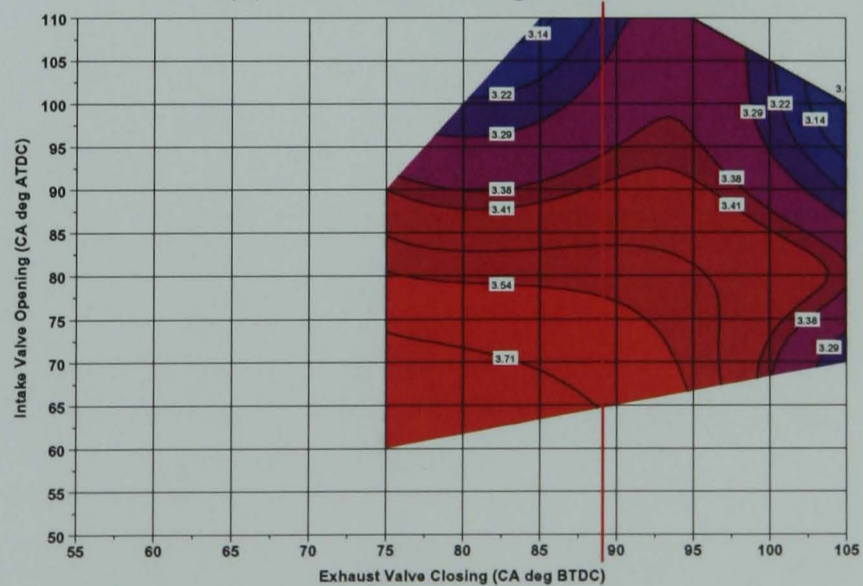
(c) SOI 120 CA deg ATDC

Figure 5.14 (a-c) NIMEP (bar) at EVC versus IVO timings for the shorter CAI
camshaft at lambda 1.0
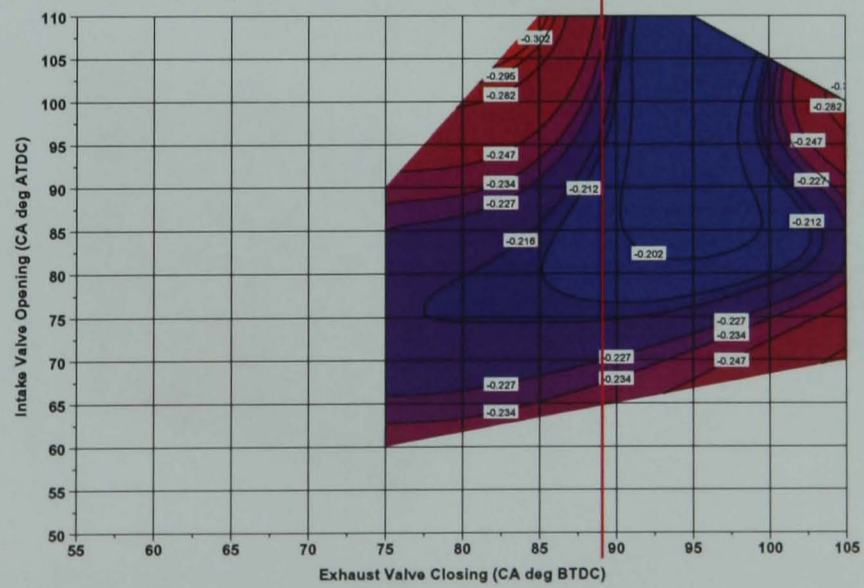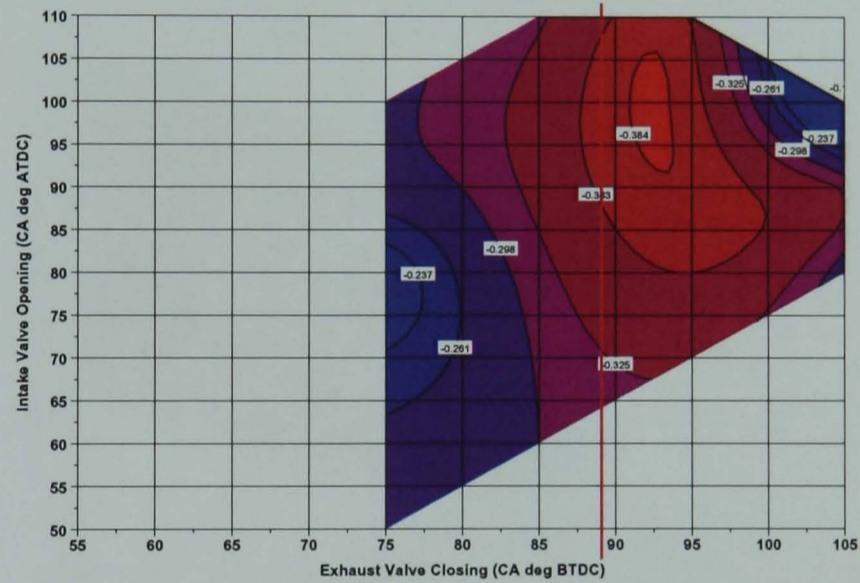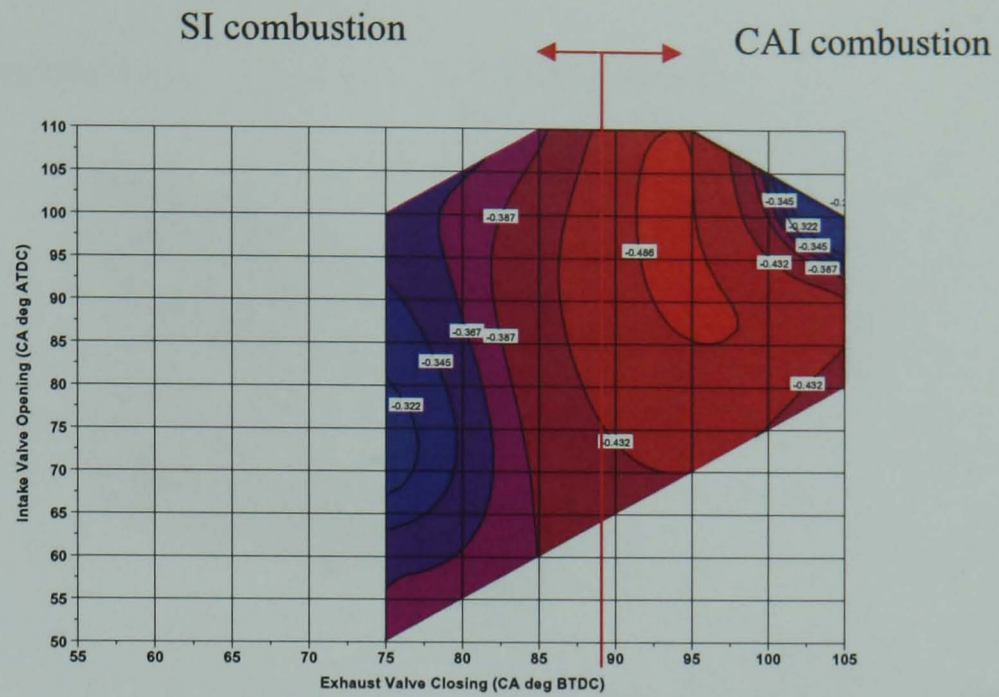
Figure 5.15 (a-c) Pumping losses (bar) at EVC versus IVO timings for the shorter CAI camshaft at lambda 1.0

SI combustion ←→ CAI combustion
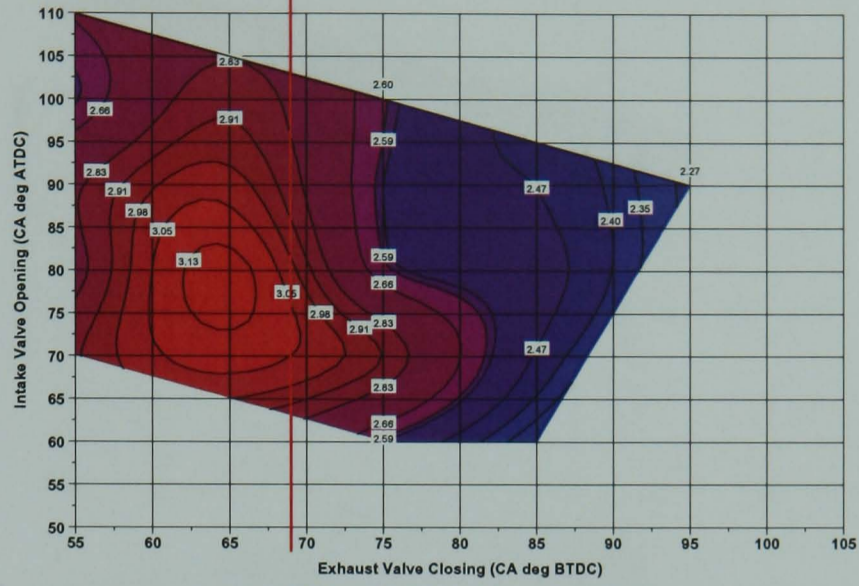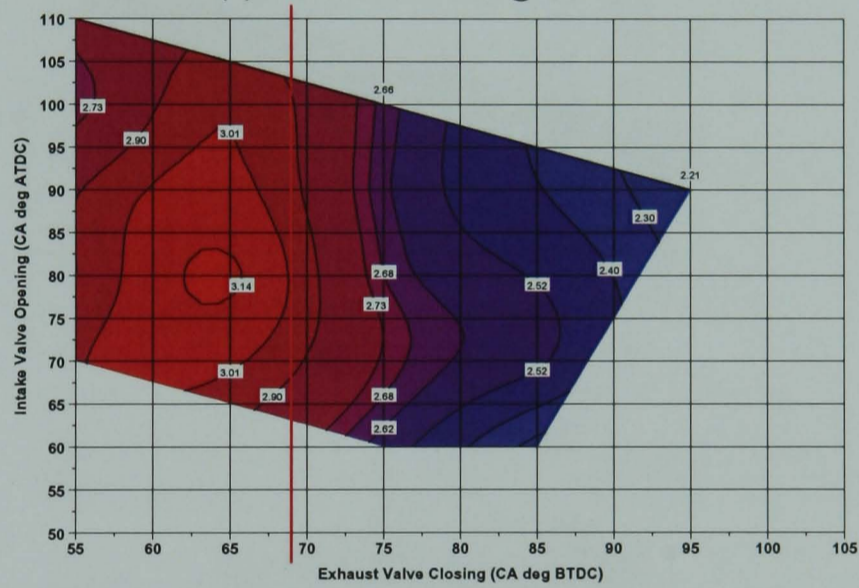
(a) SOI -30 CA deg ATDC
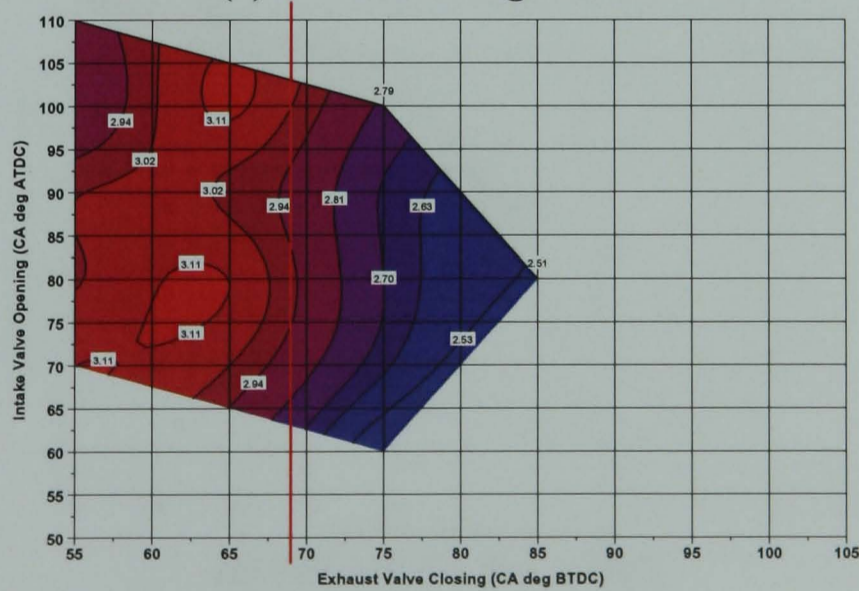
(b) SOI 30 CA deg ATDC

(c) SOI 120 CA deg ATDC

Figure 5.16 (a-c) NIMEP (bar) at EVC versus IVO timings for the longer CAI camshaft at lambda 1.0
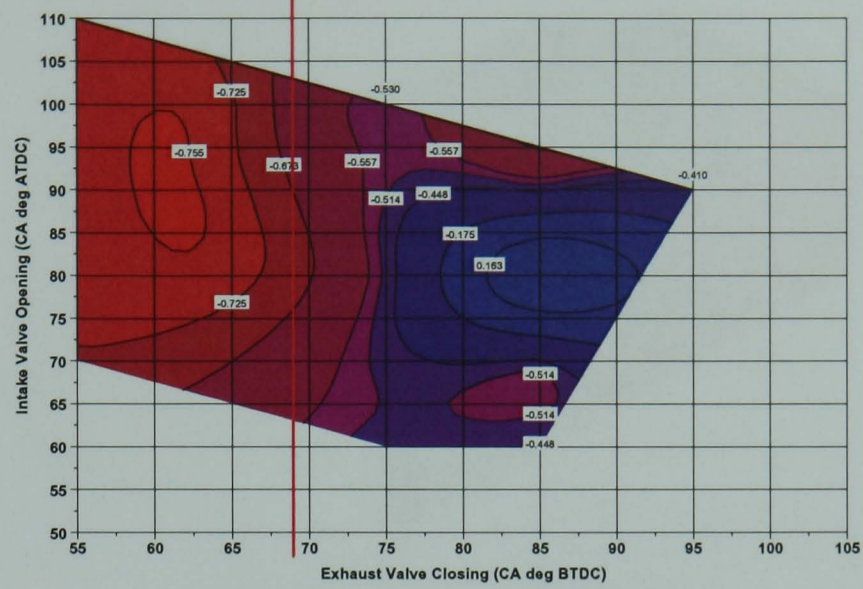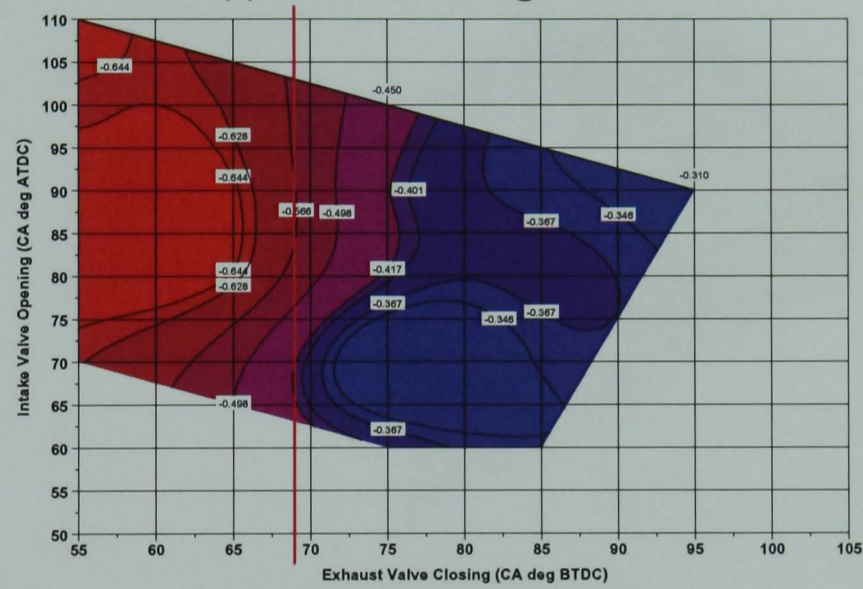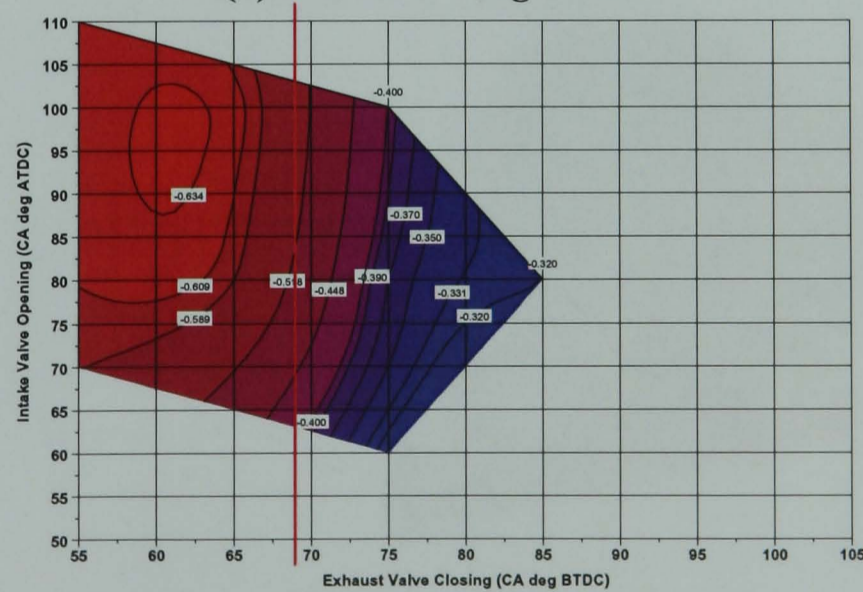
Figure 5.17 (a-c) Pumping losses (bar) at EVC versus IVO timings for the longer CAI camshaft at lambda 1.0

Figure 5.18 (a-c) Percentage of Trapped Residual at EVC versus IVO timings for the shorter CAI camshaft at lambda 1.0

95

SI combustion ←→ CAI combustion
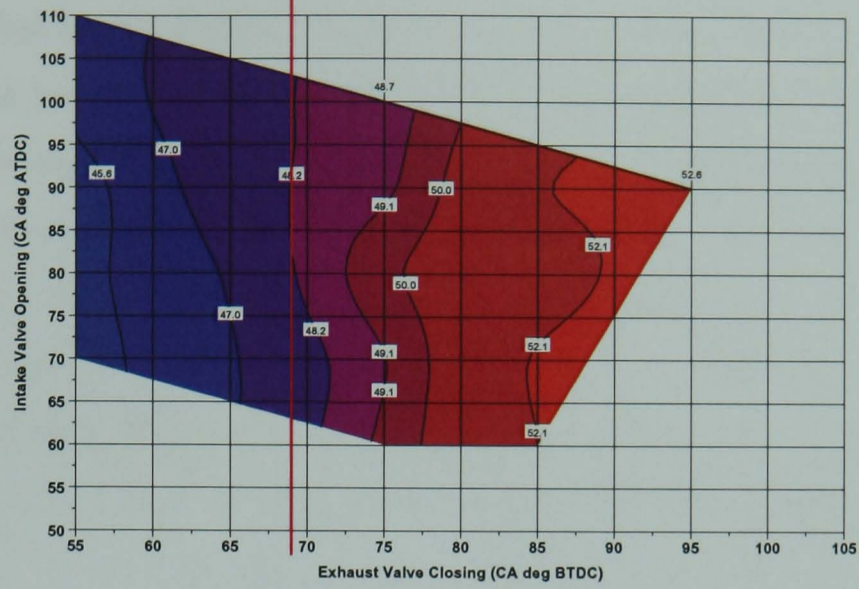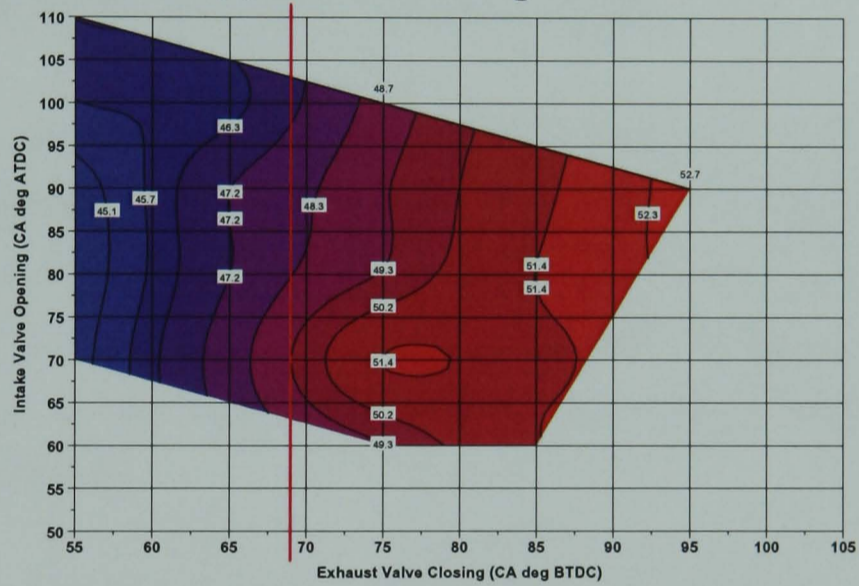
(a) SOI -30 CA deg ATDC

(b) SOI 30 CA deg ATDC
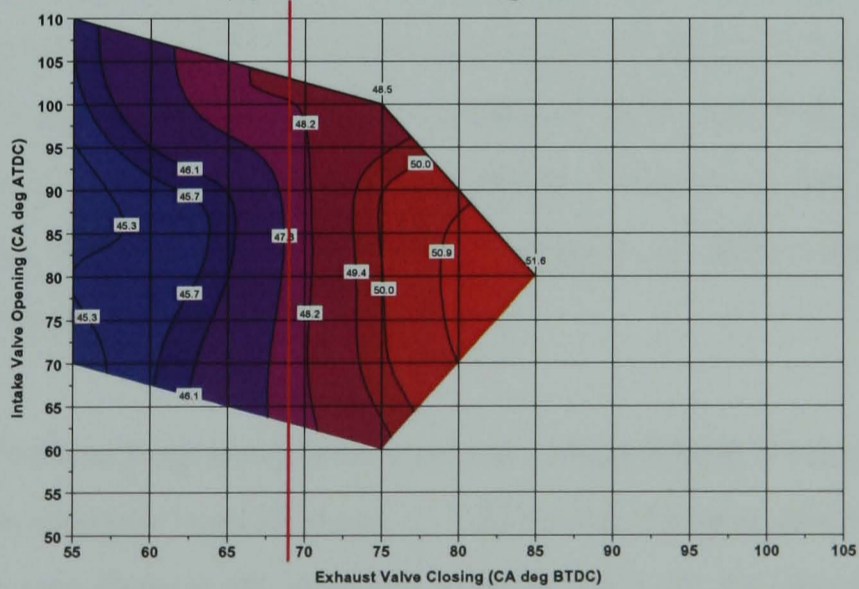
(c) SOI 120 CA deg ATDC

Figure 5.19 (a-c) Percentage of Trapped Residual at EVC versus IVO timings for the longer CAI camshaft at lambda 1.0

It was reported that higher NIMEP values were observed for the shorter CAI camshafts compared with the longer CAI camshafts due to a smaller percentage of trapped residual at a fixed EVC. On investigation of the pressure trace during the expansion and exhaust stroke (Figure 5.20 and Figure 5.21), it appears that for the longer CAI camshafts, the in-cylinder pressure is higher during the exhaust stroke compared with the shorter CAI camshafts. There appears to be a reduction of the volume of exhaust gas exhausted leaving the engine. A possible explanation is due to the interaction of exhaust gas within the exhaust manifold after it has been expelled from each individual cylinder.

5.5.2.1 Effects of Injection Timing on Combustion at Lambda = 1.0

Tables 5.2-5.7 show MFB data and peak in-cylinder pressure data at SOI -30, 30 and 120 CA deg ATDC respectively for both the shorter and longer CAI camshafts. It appears that as combustion shifts from SI mode to CAI mode that the 10% MFB angle retards towards Top Dead Center (compression stroke). This would support the argument that combustion is occurring by auto-ignition for the high-lighted CAI combustion range for both the shorter and longer CAI camshafts.

For SI combustion, ignition timing was maintained at 20 CA deg BTDC (compression), the 10% MFB angle is advanced for SI Combustion compared with CAI combustion; this again is observed for the shorter and longer CAI camshafts. However, in some cases it is noted that the main combustion period (10 – 90% MFB) is shorter in the presence of spark-ignition, indicating that spark-assisted CAI is present in these cases, which will be discussed in great detail in Chapter 6.

Tables 5.2-5.7 also show peak in-cylinder pressure and peak heat release rate. It is observed that as combustion changes from SI mode to CAI mode, the peak in-cylinder pressure and peak heat release rate drop at all injection timings for both the shorter and longer CAI camshafts. As EVC timing is advanced, extra exhaust residual is trapped decreasing the amount of fresh charge that can be inducted. The decrease in fresh charge limits the potential energy released from combustion and hence causes a drop in peak in-cylinder

pressure and peak heat release rate as EVC is advanced. Figures 5.22-5.29 shows how heat release rate varies at different SOI timings and different EVC timings for both the shorter and longer CAI camshafts. From the graphs, it can be seen that as SOI is retarded, the heat release rate also follows the general trend of becoming retarded. Furthermore, at SOI -30 CA deg ATDC, the peak heat release rate value is the highest compared with SOI 30 and 120 CA deg ATDC. Injection during the re-compression period allows the longest time for charge mixing, furthermore the upward piston motion during the exhaust stroke contributes to even better mixing. Even more importantly as Cao et al. [58] have shown, the early injection allows more time for active intermediates to form, leading to earlier auto-ignition.
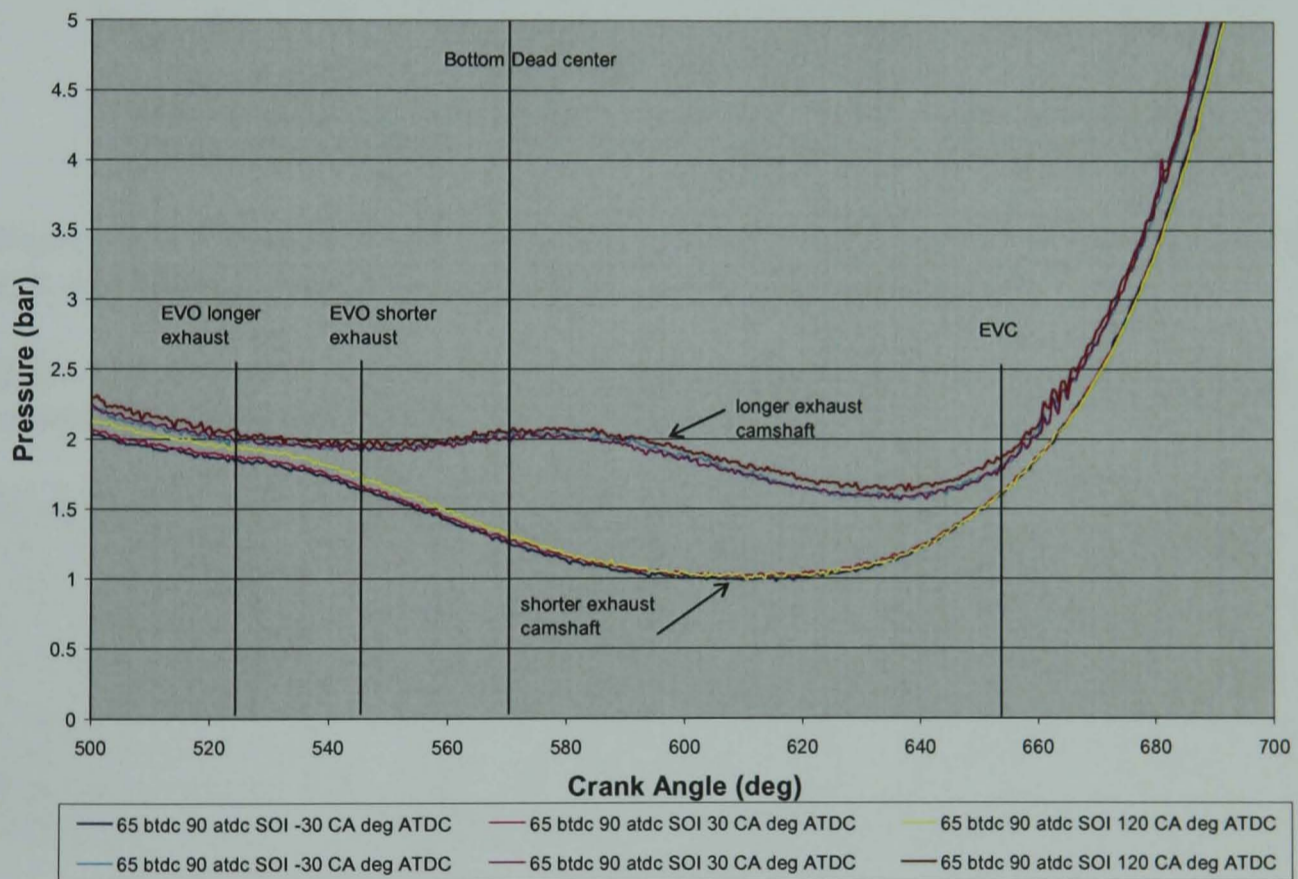
Figure 5.20 Pressure versus Crank angle during the re-compression period at EVC 65 CA deg BTDC, IVO 90 CA deg ATDC, 1500 rpm, lambda 1.0
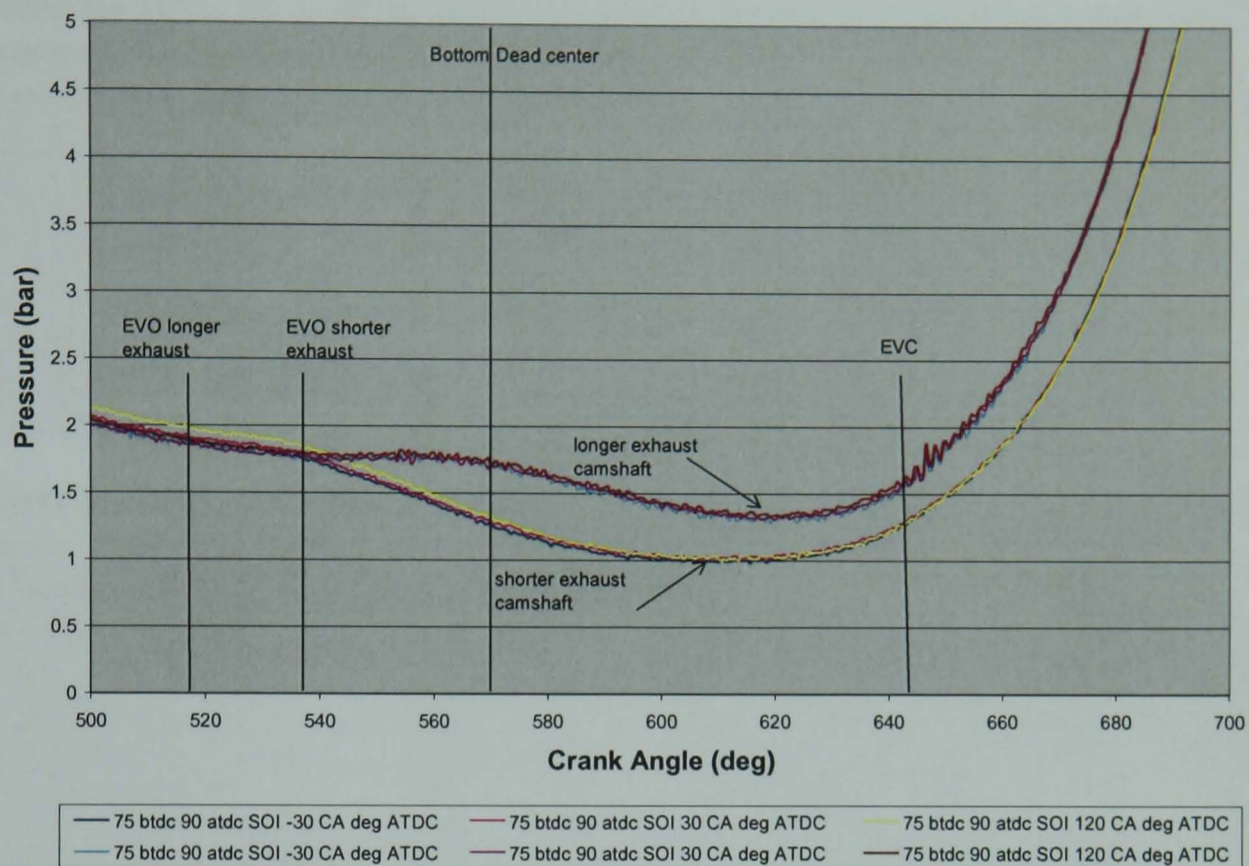
Figure 5.21 Pressure versus Crank angle during the re-compression period at EVC 75 CA deg BTDC, IVO 90 CA deg ATDC, 1500 rpm, lambda 1.0

Table 5.2 10%, 90% MFB, burn duration and peak in-cylinder pressure for the shorter CAI camshaft at SOI -30 CA deg ATDC

SI combustion - Ignition Timing 20 CA deg BTDC								CAI combustion			
EVC (CA deg BTDC)	75	75	75	75	75	75	85	95	105	105	105
IVO (CA deg ATDC)	50	60	70	80	90	100	110	110	80	90	100
10 % MFB (CA ATDC)	356	356	356	355	355	362	363	368	360	362	362
90 % MFB (CA ATDC)	377	406	381	376	375	373	376	380	365	369	370
Burn Duration (CA)	21	50	25	21	20	11	13	12	5	7	8
Peak In-cylinder Pressure	44	48	44	44	43	40	31	31	43	41	40
Peak heat release rate (J/CA)	51	67	77	70	65	68	35	40	72	62	53
COV (%)	2.53	2.96	3.81	3.72	4.56	2.63	0.75	1.2	1.9	1.7	1.03

Table 5.3 10%, 90% MFB, burn duration and peak in-cylinder pressure for the shorter CAI camshaft at SOI 30 CA deg ATDC

SI combustion - Ignition Timing 20 CA deg BTDC								CAI combustion			
EVC (CA deg BTDC)	75	75	75	75	75	75	85	95	105	105	105
IVO (CA deg ATDC)	50	60	70	80	90	100	110	110	80	90	100
10 % MFB (CA ATDC)	357	357	357	357	356	362	364	369	361	361	363
90 % MFB (CA ATDC)	372	398	379	376	380	370	384	383	367	368	371
Burn Duration (CA)	15	41	12	19	24	12	22	14	6	7	8
Peak In-cylinder Pressure	43	47	44	44	42	39	26	28	41	39	37
Peak heat release rate (J/CA)	57	67	76	66	70	64	27	32	60	57	50
COV (%)	2.38	2.81	3.33	3.44	3.43	1.90	2.56	1.6	1.73	1.26	0.91

99

Table 5.4 10%, 90% MFB, burn duration and peak in-cylinder pressure for the shorter CAI camshaft at SOI 120 CA deg ATDC

SI combustion- Ignition Timing 20 CA deg BTDC						CAI combustion			
EVC (CA deg BTDC)	75	75	75	75	75	85	95	105	105	105
IVO (CA deg ATDC)	60	70	80	90	100	110	110	80	90	100
10 % MFB (CA ATDC)	357	358	356	357	363	360	362	363	365	366
90 % MFB (CA ATDC)	379	371	373	375	391	384	370	370	373	377
Burn Duration (CA)	12	13	17	18	28	24	12	7	8	11
Peak In-cylinder Pressure	36	41	43	42	41	39	40	40	36	35
Peak heat release rate (J/CA)	24	51	53	62	57	17	58	59	47	37
COV (%)	3.16	2.67	3.36	3.19	10.6	9.87	1.96	2.17	1.76	1.35

Table 5.5 10%, 90% MFB, burn duration and peak in-cylinder pressure for the longer CAI camshaft at SOI -30 CA deg ATDC

SI combustion- Ignition Timing 20 CA deg BTDC								
EVC (CA deg BTDC)	55	55	55	55	55	65	65	65
IVO (CA deg ATDC)	70	80	90	100	110	80	90	100
10 % MFB (CA ATDC)	353	350	351	347	350	353	345	347
90 % MFB (CA ATDC)	366	371	364	373	371	384	386	386
Burn Duration (CA)	13	21	13	26	21	31	41	39
Peak In-cylinder Pressure	44	44	43	40	41	41	41	41
Peak heat release rate (J/CA)	60	58	58	41	44	47	45	47
COV (%)	2.35	2.58	2.39	2.71	2.21	2.41	2.34	2.40

CAI combustion									
EVC (CA deg BTDC)	75	75	75	75	75	85	85	85	85	95
IVO (CA deg ATDC)	60	70	80	90	100	60	70	80	90	90
10 % MFB (CA ATDC)	362	362	360	361	363	358	355	363	358	358
90 % MFB (CA ATDC)	378	383	382	382	377	369	367	383	377	372
Burn Duration (CA)	16	21	22	21	14	11	12	20	19	14
Peak In-cylinder Pressure	34	37	38	37	33	28	33	35	34	31
Peak heat release rate (J/CA)	48	33	38	37	39	37	35	30	28	28
COV (%)	0.99	1.25	1.46	1.32	0.81	4.62	1.33	1.23	5.34	1.96

Table 5.6 10%, 90% MFB, burn duration and peak in-cylinder pressure for the longer CAI camshaft at SOI 30 CA deg ATDC

SI combustion- Ignition Timing 20 CA deg BTDC								
EVC (CA deg BTDC)	55	55	55	55	55	65	65	65
IVO (CA deg ATDC)	70	80	90	100	110	80	90	100
10 % MFB (CA ATDC)	353	352	350	346	346	350	352	346
90 % MFB (CA ATDC)	371	372	373	379	375	383	383	382
Burn Duration (CA)	18	20	23	33	29	33	31	36
Peak In-cylinder Pressure	40	43	43	40	40	39	39	40
Peak heat release rate (J/CA)	38	54	53	38	39	41	40	46
COV (%)	2.25	2.40	2.14	2.21	1.94	2.22	2.21	1.87

CAI combustion								
EVC (CA deg BTDC)	75	75	75	75	75	85	85	85	95
IVO (CA deg ATDC)	60	70	80	90	100	60	70	80	90
10 % MFB (CA ATDC)	356	357	356	357	361	358	363	359	358
90 % MFB (CA ATDC)	381	380	377	378	380	378	381	379	377
Burn Duration (CA)	25	23	21	21	21	20	18	20	19
Peak In-cylinder Pressure	31	34	36	35	30	26	32	33	28

Peak heat release rate (J/CA)	29	32	34	34	34	24	30	24	23
COV (%)	1.26	2.12	0.96	1.09	1.26	2.11	1.50	1.14	2.56

Table 5.7 10%, 90% MFB, burn duration and peak in-cylinder pressure for the longer CAI camshaft at SOI 120 CA deg ATDC

SI combustion- Ignition Timing 20 CA deg BTDC								
EVC (CA deg BTDC)	55	55	55	55	55	65	65	65
IVO (CA deg ATDC)	70	80	90	100	110	80	90	100
10 % MFB (CA ATDC)	350	353	352	348	349	352	355	354
90 % MFB (CA ATDC)	373	370	370	379	382	382	384	386
Burn Duration (CA)	23	17	18	31	33	30	29	32
Peak In-cylinder Pressure	41	42	43	39	39	37	39	38
Peak heat release rate (J/CA)	41	47	46	35	35	40	38	35
COV (%)	2.49	2.05	2.04	2.29	1.84	2.24	1.88	1.84
CAI combustion								
EVC (CA deg BTDC)	75		75		75		75		75		85
IVO (CA deg ATDC)	60		70		80		90		100		80
10 % MFB (CA ATDC)	362		356		355		359		364		361
90 % MFB (CA ATDC)	386		380		379		379		380		384
Burn Duration (CA)	24		24		24		20		16		23
Peak In-cylinder Pressure	26		31		34		33		31		30
Peak heat release rate (J/CA)	23		24		26		26		34		20
COV (%)	10.42		2.82		2.04		1.57		1.26		2.85
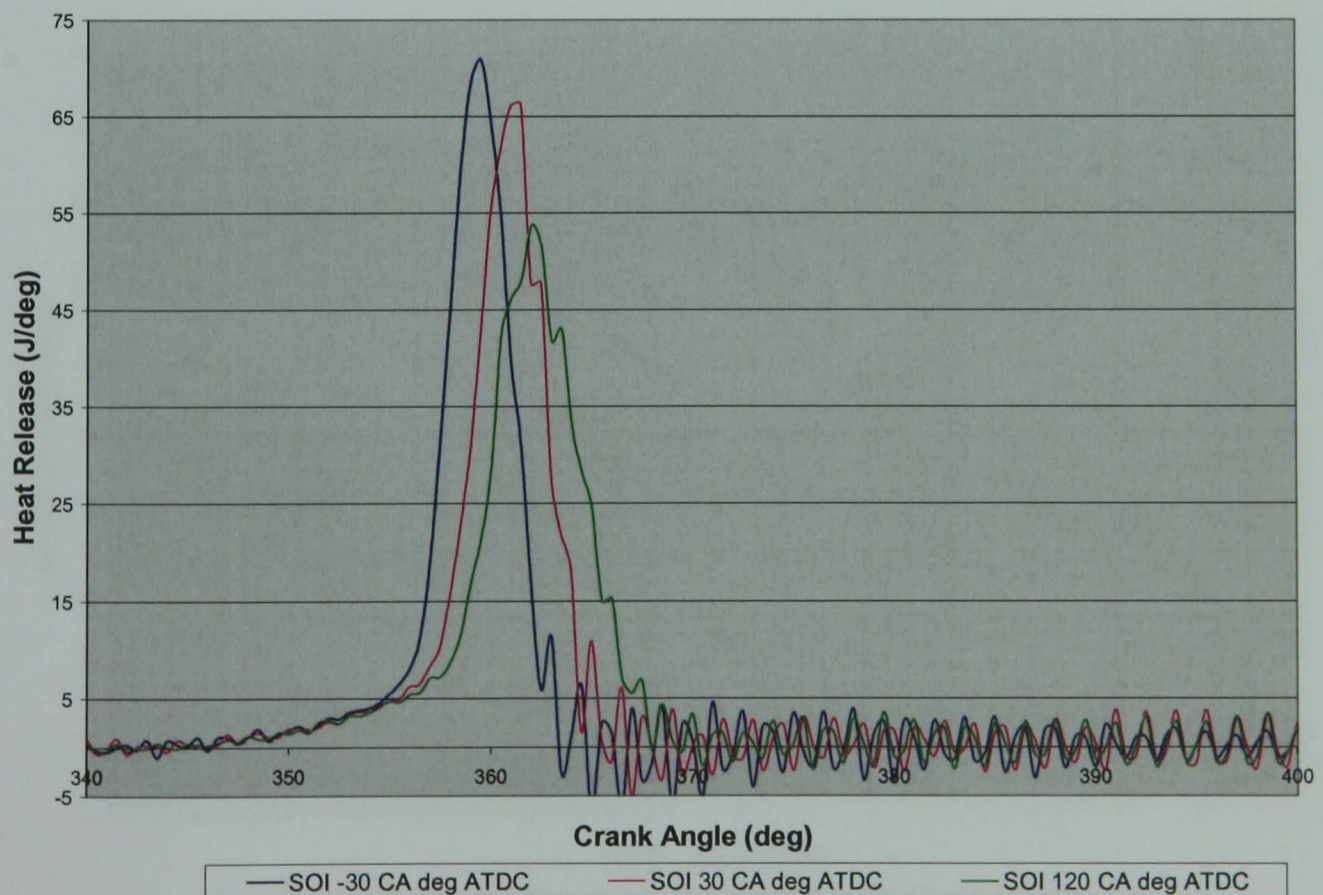
Figure 5.22 Heat Release versus Crank angle for the shorter CAI camshafts at EVC 75 CA deg BTDC, IVO 80 CA deg ATDC, 1500 rpm, lambda 1.0
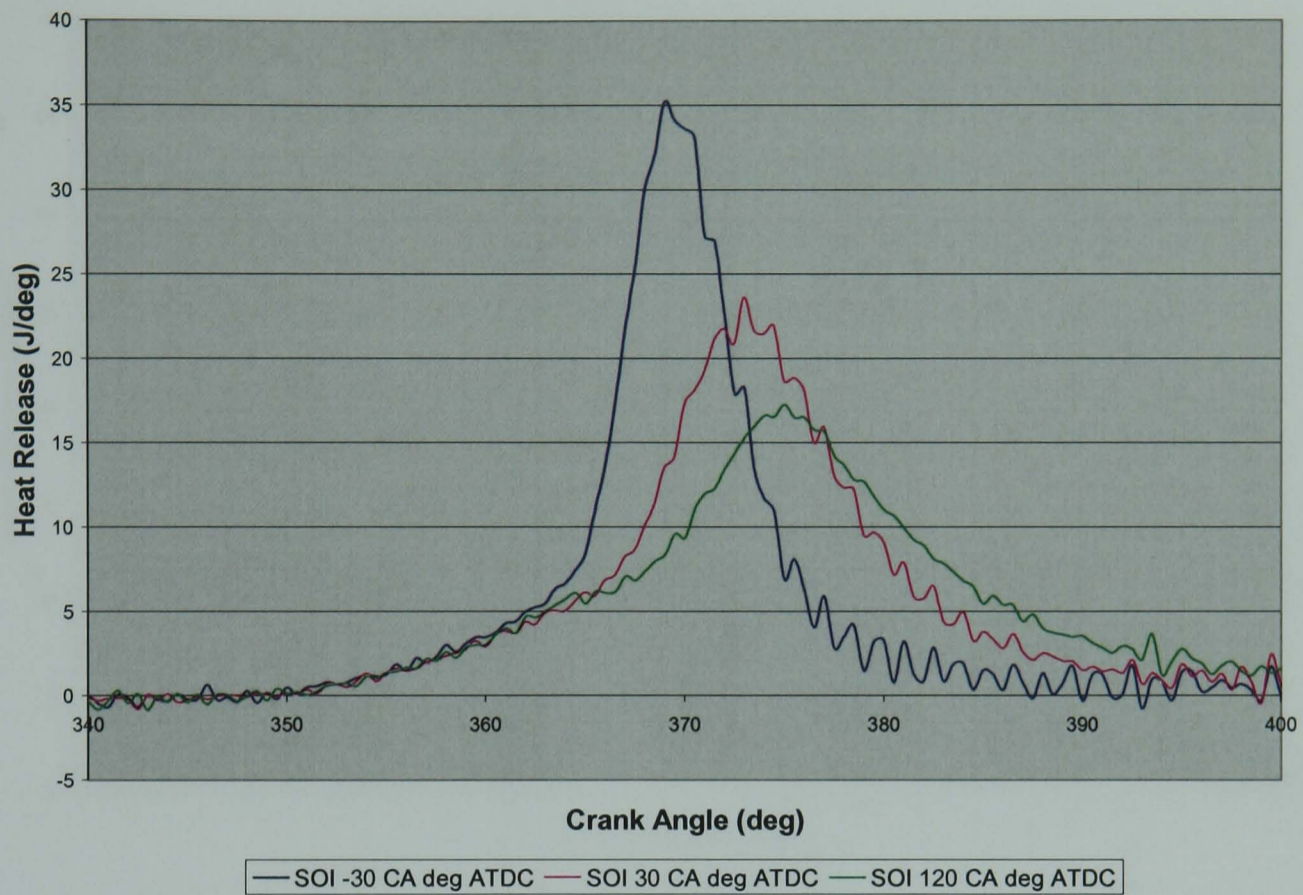
Figure 5.23 Heat Release versus Crank angle for the shorter CAI camshafts at EVC 85 CA deg BTDC, IVO 110 CA deg ATDC, 1500 rpm, lambda 1.0
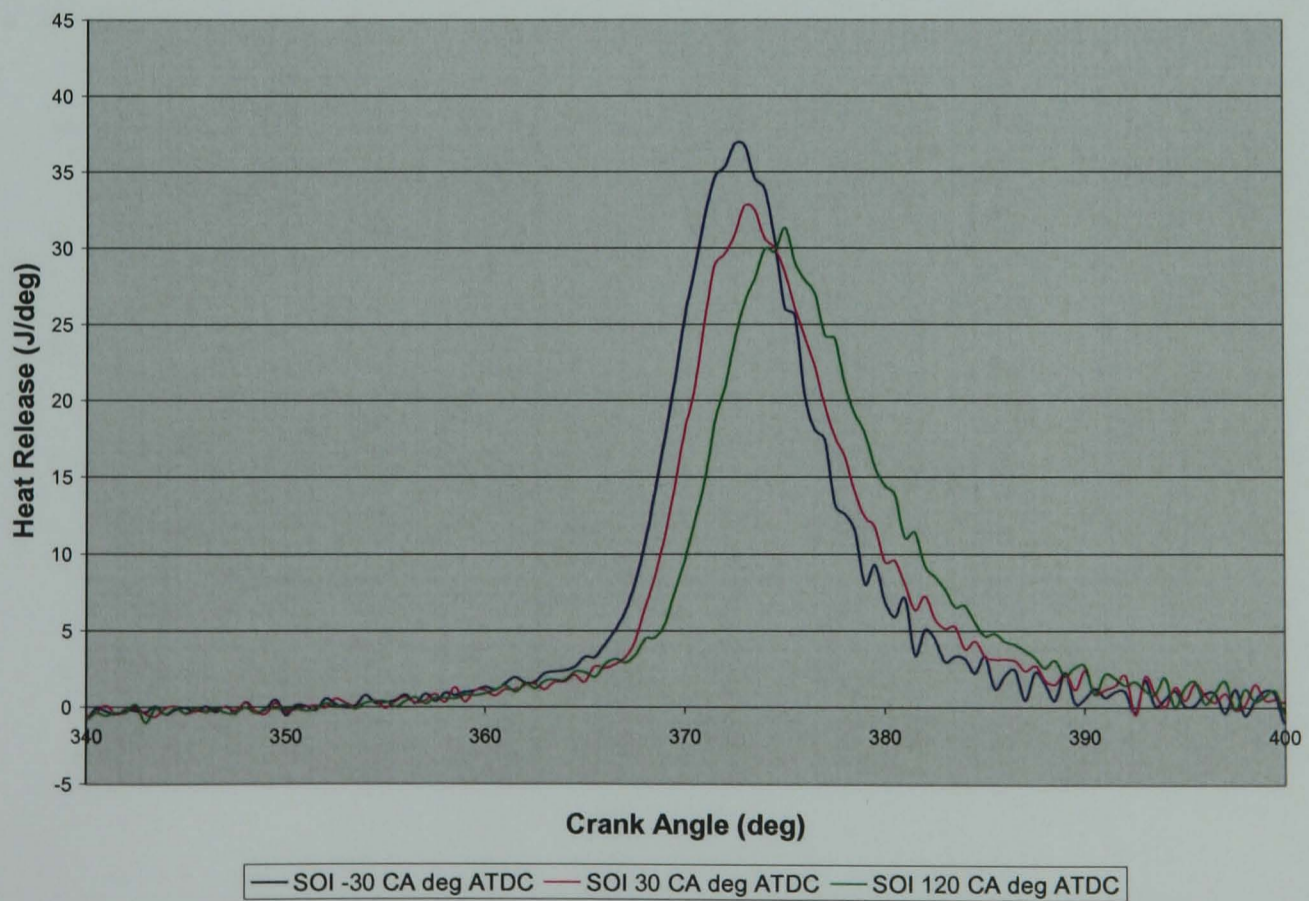
Figure 5.24 Heat Release versus Crank angle for the shorter CAI camshafts at EVC 95 CA deg BTDC, IVO 110 CA deg ATDC, 1500 rpm, lambda 1.0
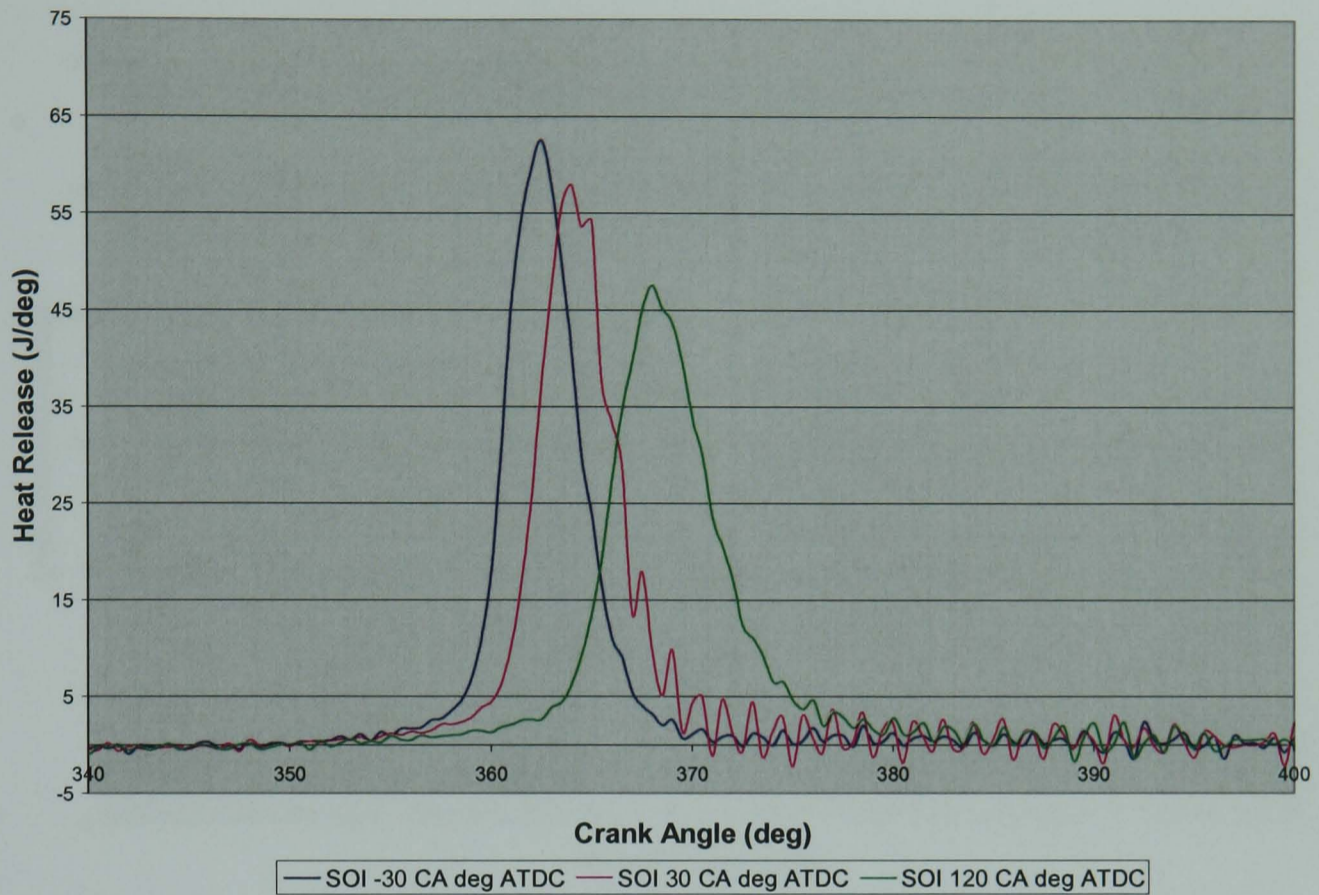
Figure 5.25 Heat Release versus Crank angle for the shorter CAI camshafts at EVC 105 CA deg BTDC, IVO 80 CA deg ATDC, 1500 rpm, lambda 1.0
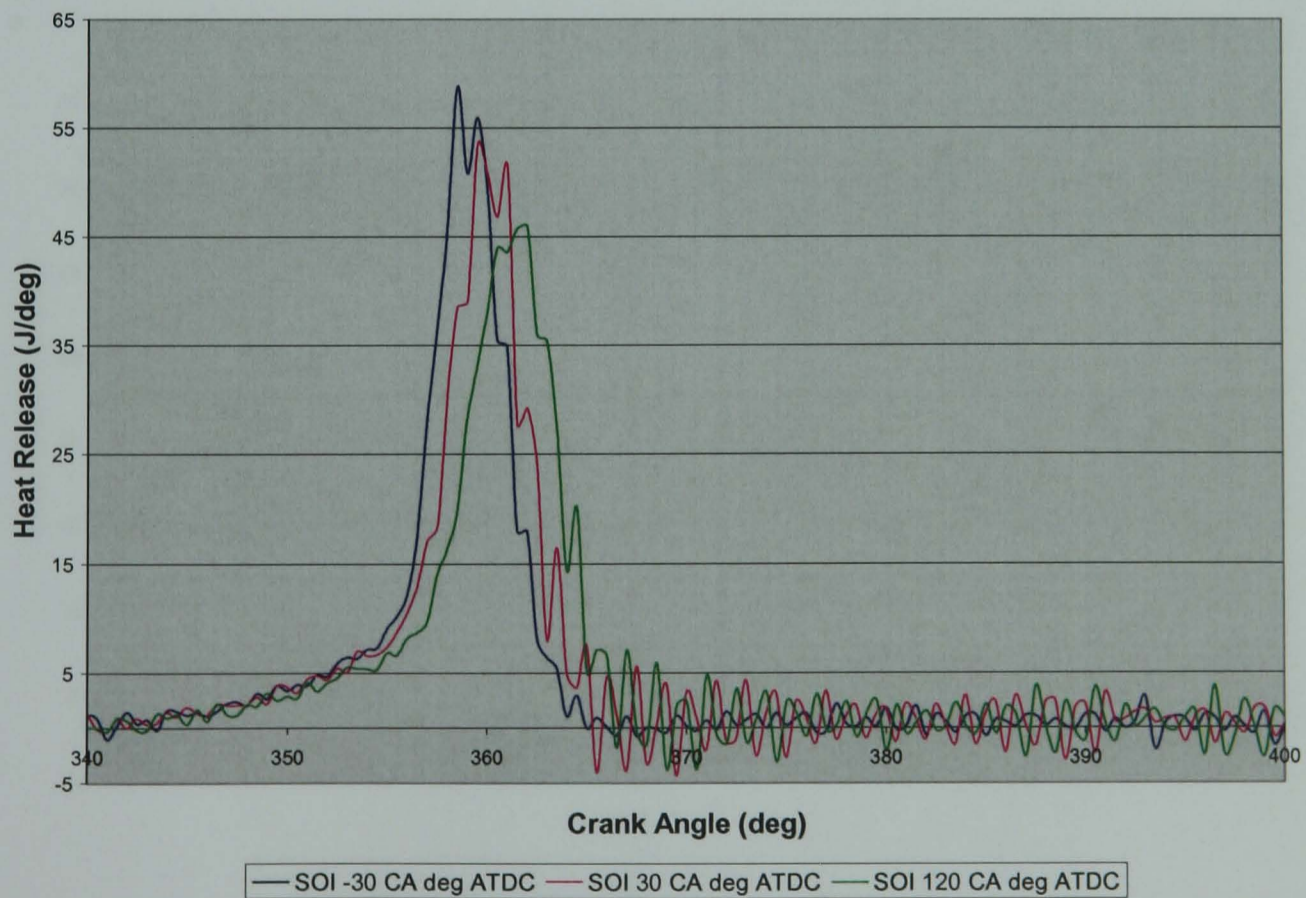
Figure 5.26 Heat Release versus Crank angle for the longer CAI camshafts at EVC 55 CA deg BTDC, IVO 90 CA deg ATDC, 1500 rpm, lambda 1.0
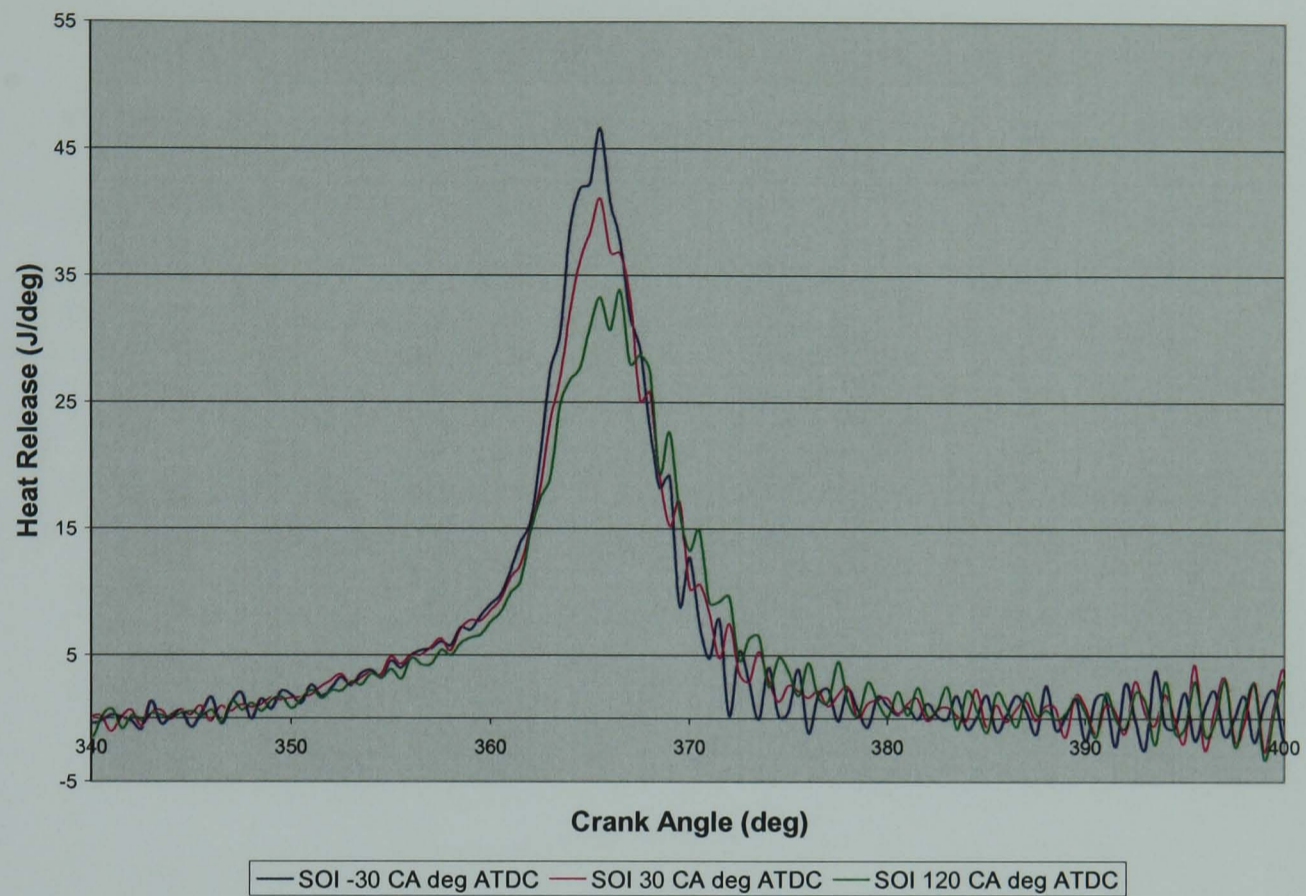
Figure 5.27 Heat Release versus Crank angle for the longer CAI camshafts at EVC 65 CA deg BTDC, IVO 90 CA deg ATDC, 1500 rpm, lambda 1.0
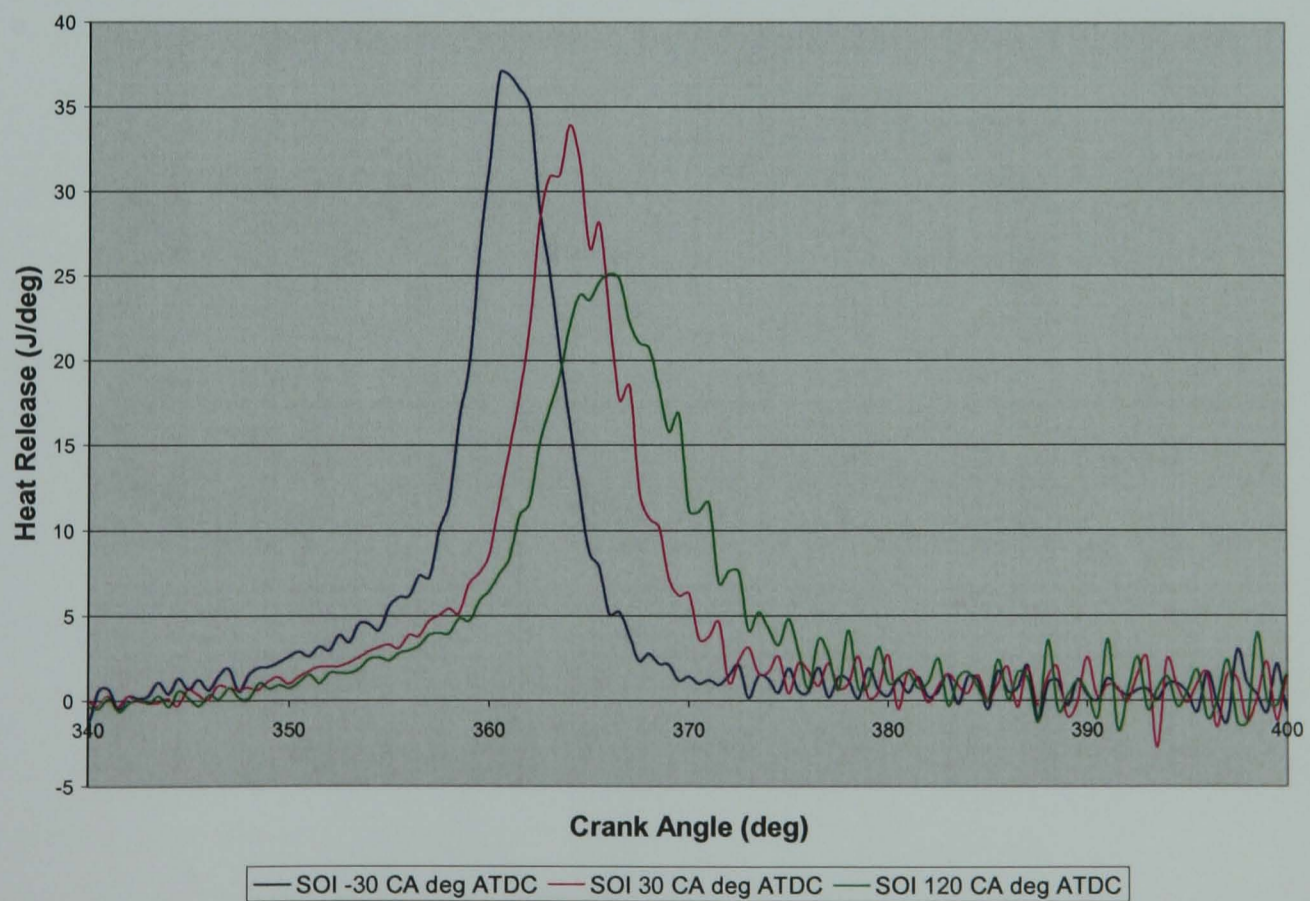
Figure 5.28 Heat Release versus Crank angle for the longer CAI camshafts at EVC 75 CA deg BTDC, IVO 90 CA deg ATDC, 1500 rpm, lambda 1.0
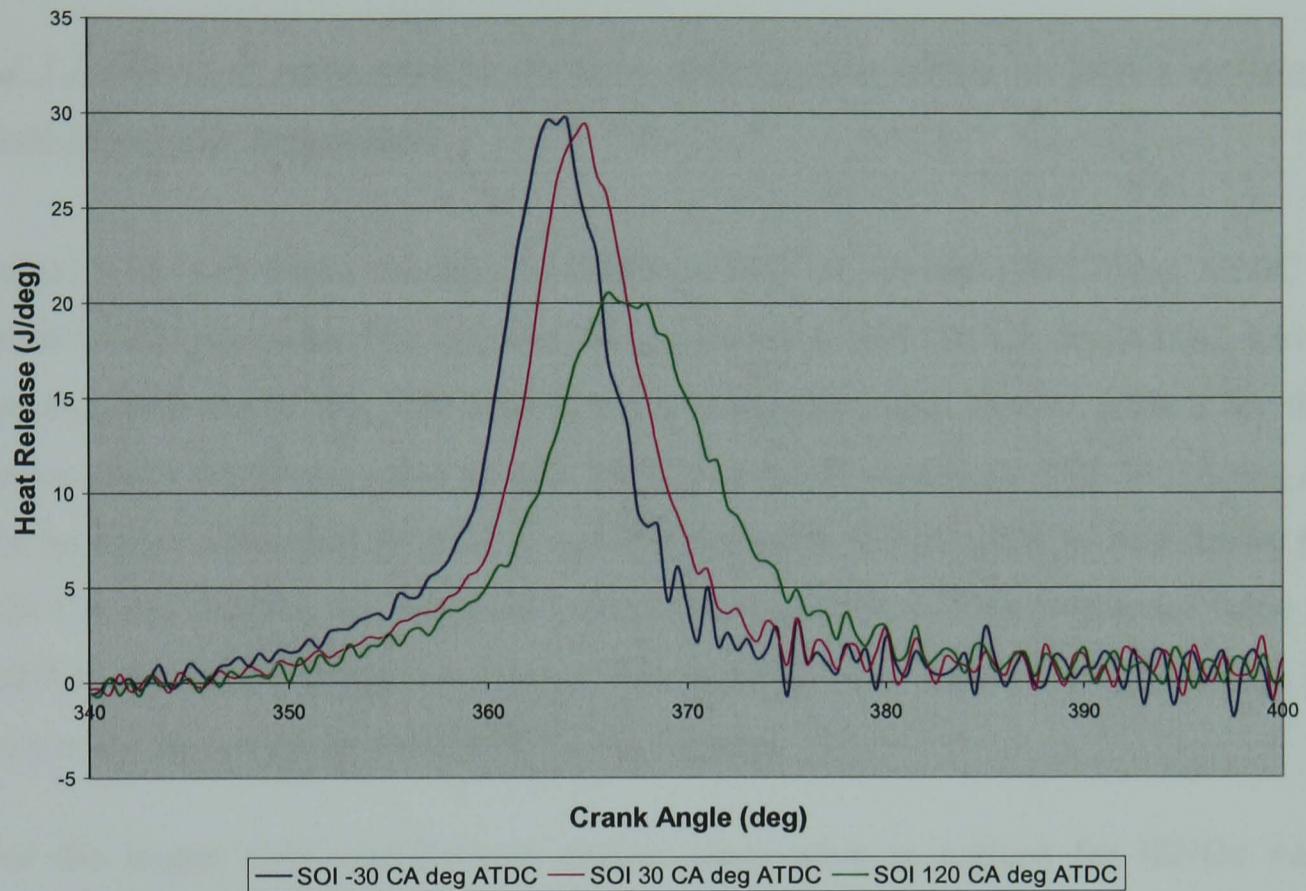
Figure 5.29 Heat Release versus Crank angle for the longer CAI camshafts at EVC 85 CA deg BTDC, IVO 90 CA deg ATDC, 1500 rpm, lambda 1.0

5.5.3 Effects of Camshaft design and Injection Timing on Emissions at lambda = 1.0

5.5.3.1 Effects of valve opening duration and injection timing on ISNOx emissions and Peak In-cylinder temperature

Figure 5.30 (a-c) shows the maps of ISNOx at SOI -30, 30 and 120 CA deg ATDC for the shorter CAI camshafts. The range of ISNOx values at SOI -30 CA deg ATDC, taking into account both the SI and CAI region, has a minimum value of 0.92 g/kW.h for the CAI region and a maximum value of 4.53 g/kW.h in the SI region. At SOI 30 CA deg ATDC, the minimum value is 0.57 g/kW.h and the maximum is 3.98 g/kW.h. And finally for SOI 120 CA deg ATDC, the minimum value is 0.38 g/kW.h and the maximum value is 3.13 g/kW.h. Therefore, it appears that at fuel injection after Intake Valve Opening, ISNOx values are the lowest for both the CAI and SI range.

For the longer CAI camshafts, a similar observation is noticed for ISNOx values at different fuel injection timings. However, at SOI 120 CA deg ATDC, EVC timings cannot be advanced further than 85 CA deg BTDC. At EVC 85 CA deg BTDC and IVO 80 CA deg ATDC, for SOI 120 CA deg ATDC the ISNOx value is 0.3 g/kW.h, whereas for SOI -30 and 30 CA deg ATDC, the ISNOx value is 0.55 g/kW.h and 0.32 g/kW.h respectively. Therefore, again it appears that for SOI after Intake Valve Opening, ISNOx values are lower compared with earlier injection.

It is evident that overall the ISNOx values at lambda 1.0, are lower for the longer duration CAI camshafts compared with the shorter duration camshafts. The reason for this is that bulk in-cylinder temperatures are lower for the longer CAI camshafts (Figure 5.33 (a-c)) compared with the shorter CAI camshafts (Figure 5.32 (a-c)). Since, the longer intake camshafts is extended by 20 CA deg, IVC is occurring 20 CA deg later in the compression stroke at a given valve timing compared with the shorter CAI camshaft. This means that the in-cylinder pressure is lower for the longer CAI camshafts and hence the bulk temperature will be lower. ISNOx is determined by in-cylinder temperature, the lower the temperature, the lower the ISNOx values.

The effects of valve timings on the peak cylinder charge temperature are different for the short and long CAI camshafts. As shown in Figure 5.32 (a-c), the peak temperature is mainly affected by the IVO timing; the more retarded the IVO timing the lower the peak temperature due to lower effective compression ratio. In comparison, the EVC timing has a small effect; the more advanced the EVC the lower the peak temperature probably due to higher percentage of residuals.

Furthermore, it appears that for the longer CAI camshafts at EVC timings that are not as advanced as the shorter CAI camshafts, the ISNOx values are lower. For example at EVC 75 CA deg BTDC, IVO 80 CA deg ATDC and SOI 30 CA deg ATDC, the ISNOx value for the shorter CAI camshaft is 3.98 g/kW.h, whereas for the longer CAI camshaft this value is 0.7 g/kW.h. As discussed there is a higher percentage of trapped residual for the longer CAI camshaft compared with the shorter CAI camshaft at a given valve timing. The higher the percentage of trapped residual, the lower the in-cylinder temperature and hence lower the value of ISNOx.

For both the shorter and longer CAI camshafts at SOI -30, 30 and 120 CA deg ATDC, ISNOx values are higher for SI combustion compared with CAI combustion even though in-cylinder temperatures are similar for the two modes. This is due to the fact that the actual peak gas temperature is much higher for SI combustion compared with CAI combustion. The values of in-cylinder temperature are based on the ideal gas law and are spatially averaged for the entire combustion chamber.

5.5.3.2 Effects of valve opening duration and injection timing on ISHC emissions

ISHC emissions follow the opposite trend when compared with ISNOx emissions (Figure 5.34 (a-c) and Figure 5.35 (a-c)). The lower in-cylinder temperature, observed for CAI combustion leads to high ISHC values. For the shorter CAI camshafts at SOI -30 CA deg ATDC, the lowest ISHC value, obtained within SI region is 1.29 g/kW.h, the highest value obtained during CAI operation is 2.81 g/kW.h. At SOI 30 CA deg ATDC, the lowest value is 1.21 g/kW.h and the highest is 3.71 g/kW.h. And finally at SOI 120 CA deg ATDC, the

lowest ISHC value is 1.2 g/kW.h and the highest is 3.5 g/kW.h. Therefore, the overall lowest range of ISHC values with the CAI operation at a particular valve timing is observed at -30 CA deg ATDC. For the longer CAI camshafts a similar trend is observed, at a given valve timing ISHC values of CAI operation are low for SOI -30 CA deg ATDC compared with later fuel injection. For example, at EVC 75 CA deg BTDC, IVO 80 CA deg ATDC, the ISHC value at -30, 30 and 120 CA deg ATDC are 3.1 g/kW.h, 3.4 g/kW.h and 3.4 g/kW.h respectively. However, unlike the shorter CAI camshafts, there does not seem to be a clear trend that when EVC is advanced, ISHC increases. There appears to be certain areas on the EVC-IVO map where ISHC values are affected by IVO timings.

The shorter CAI camshafts have lower ISHC values compared with the longer CAI camshafts. ISHC values range from 1.2 g/kW.h to 3.71 g/kW.h for the shorter CAI camshafts, compared with ISHC values of 2.0 g/kW.h to 5.1 g/kW.h for the longer CAI camshafts. This range of values takes into account both SI and CAI combustion and also SOI at -30, 30 and 120 CA deg ATDC. The reason for the higher range of ISHC values for the longer duration CAI camshafts is due to the fact that bulk in-cylinder temperatures are lower compared with the shorter CAI camshafts. The in-cylinder temperature range for the longer CAI camshaft is 1141K to 1684K, for the shorter CAI camshafts the range is 1533K to 1903K. The lower temperatures for the longer CAI camshafts are again a result of greater volumes of trapped residual at a given valve timing compared with the shorter CAI camshafts.

Examination of ISHC values for SI and CAI combustion reveals that ISHC values are higher for CAI combustion compared with SI combustion. This again is due to actual peak gas temperature being much higher for SI combustion compared with CAI combustion. The higher in-cylinder temperature allows greater quantities of fuel to be burned lowering uHC emissions.

5.5.3.3 Effects of valve opening duration and injection timing on ISCO emissions

Unlike ISHC and ISNOx values, ISCO values are not entirely dependent on temperatures during the combustion process. CO is a product of incomplete oxidation.

Injection timing plays a crucial role in determining CO production, during the CAI operation for the shorter CAI camshafts (Figure 5.36 (a-c)) at SOI -30 CA deg ATDC, ISCO values range between 1.29 g/kW.h and 2.81 g/kW.h. Retarding SOI to 30 CA deg ATDC, causes ISCO values to increase drastically, the lowest ISCO value is 2.18 g/kW.h whereas the highest is 16.51 g/kW.h. Retarding SOI even further to 120 CA deg ATDC, causes ISCO values to increase even further. The lowest ISCO value is 4 g/kW.h and the highest is 37 g/kW.h. There is a similar scenario for the longer CAI camshafts (Figure 5.37 (a-c)), ISCO values increase as SOI is retarded. At EVC 75 CA deg BTDC, IVO 70 CA deg ATDC and SOI -30 CA deg ATDC, the ISCO value is 10.1 g/kW.h. At the same valve timing, for SOI 30 and 120 CA deg ATDC, this value increases to 10.2 g/kW.h and 22.6 g/kW.h respectively. The increase in ISCO values with SOI 120 CA deg ATDC as injection timing is retarded can be explained by less time for charge mixing at later injections, decreasing homogeneity and locally rich combustion. But it is not clear what is the cause in higher CO emissions at SOI 30 CA deg ATDC than that at SOI -30CA deg ATDC.

ISCO values are higher for the longer CAI camshafts compared with the shorter CAI camshafts, due to higher in-cylinder temperatures for the shorter CAI camshafts. The higher in-cylinder temperatures result in lower ISCO values due to a more favorable environment for CO to be oxidized to CO_2.

ISCO values are generally lower for SI operation compared with CAI operation for the shorter CAI camshafts. The opposite trend is seen with the longer CAI camshafts, i.e. CAI operation produces less CO emission than SI as indicated by the dominant blue region in the CAI mode. The opposing trend in ISCO values seen for the two CAI camshafts may be explained by referring to Table 5.2 – 5.7. It is noted that the end of SI combustion is later than the end of CAI combustion for the shorter CAI camshafts and vice versa for the long

CAI camshafts. The delayed end of combustion leads to higher gas temperature during the expansion stroke, and hence better CO to CO_2 oxidation. As a result, the CAI operation produces less CO than SI operation for the longer CAI camshafts and more CO than SI operation for the shorter CAI camshafts.
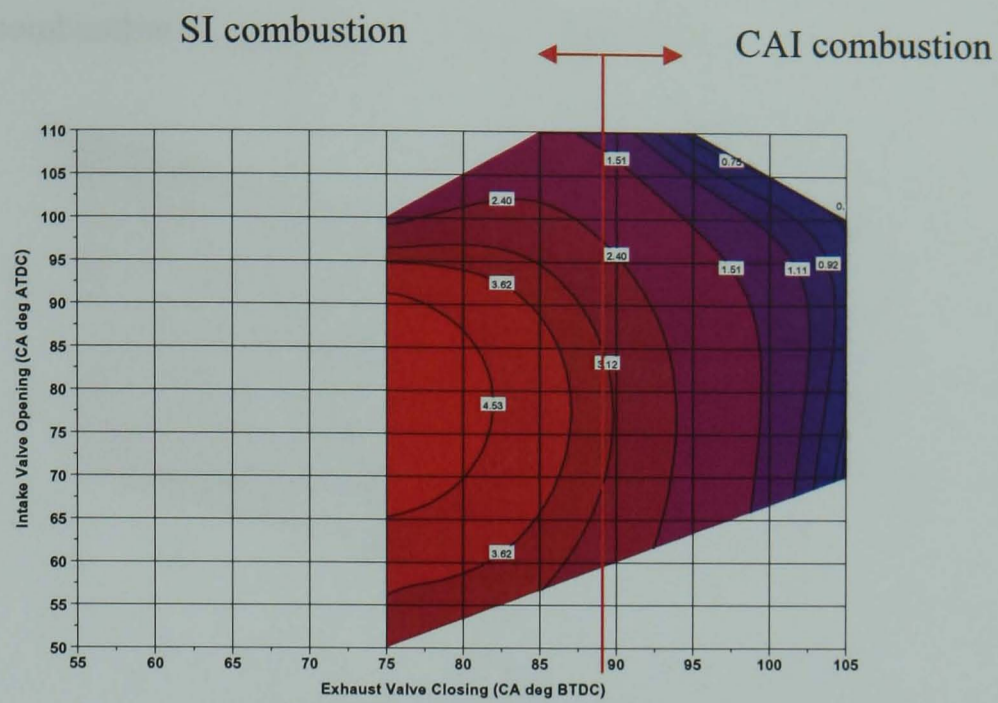
(a) SOI -30 CA deg ATDC
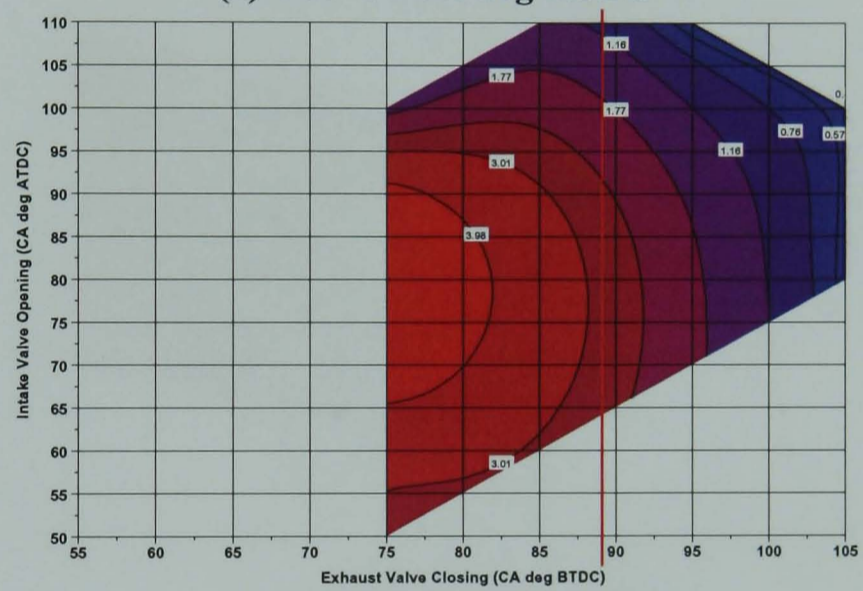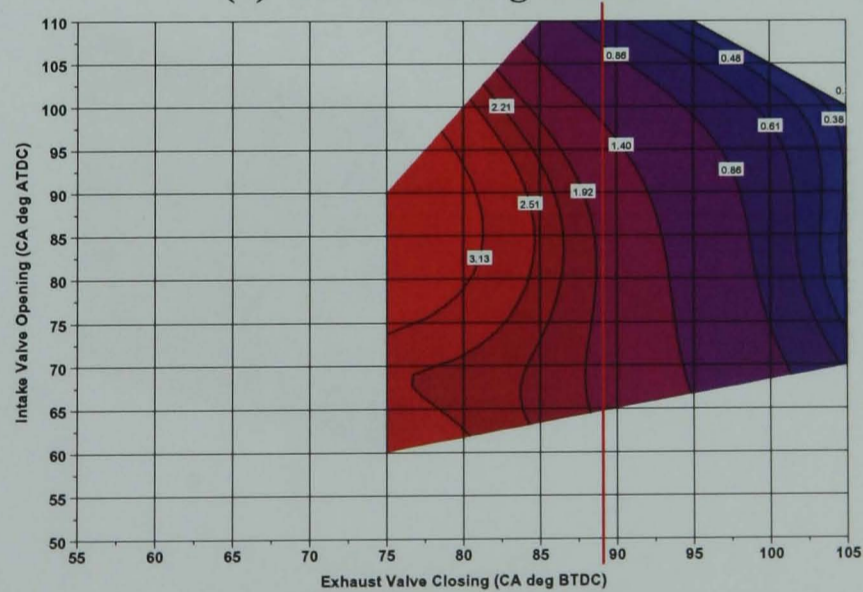
(b) SOI 30 CA deg ATDC

(c) SOI 120 CA deg ATDC

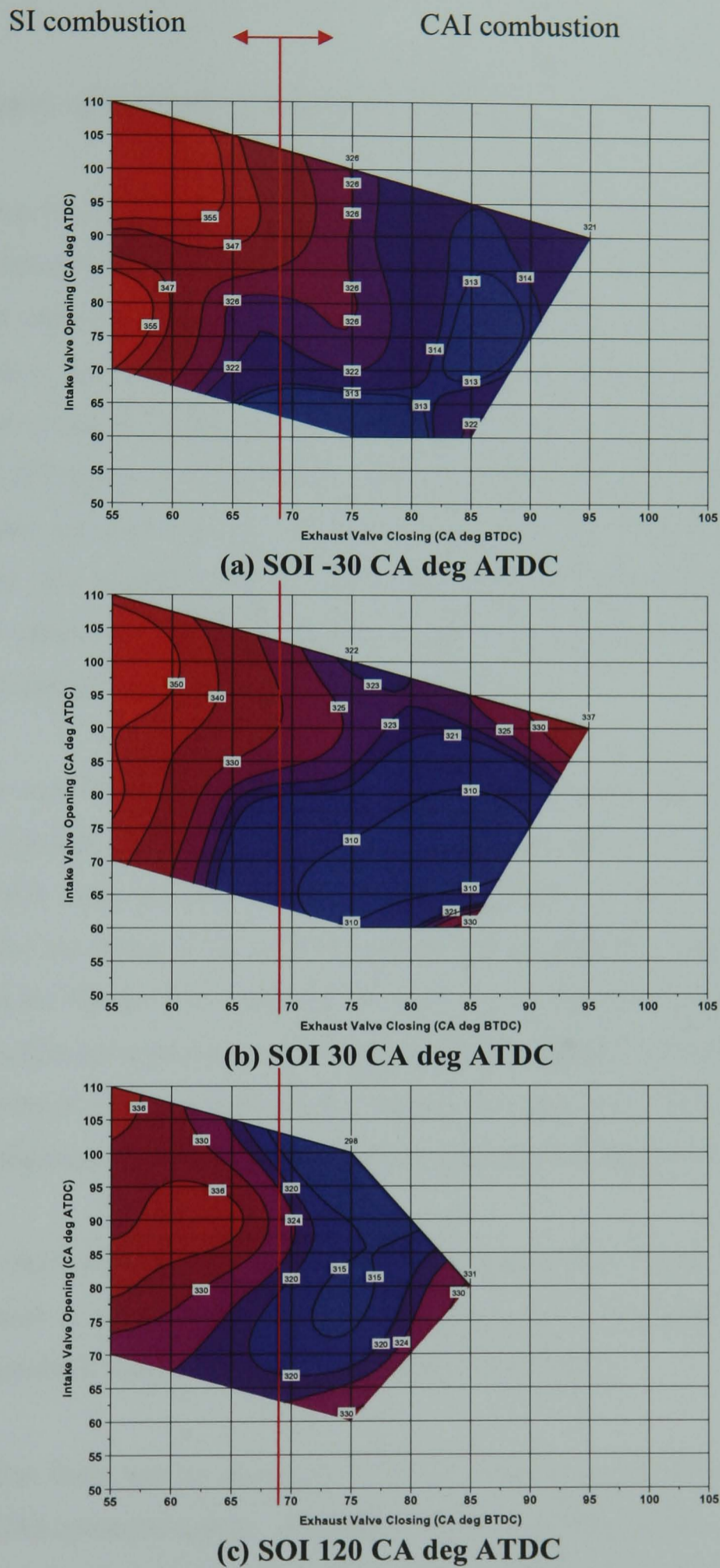Figure 5.30 (a-c) ISNOx (g/kW.h) at EVC versus IVO timings for the shorter CAI camshaft at lambda 1.0

SI combustion ←→ CAI combustion
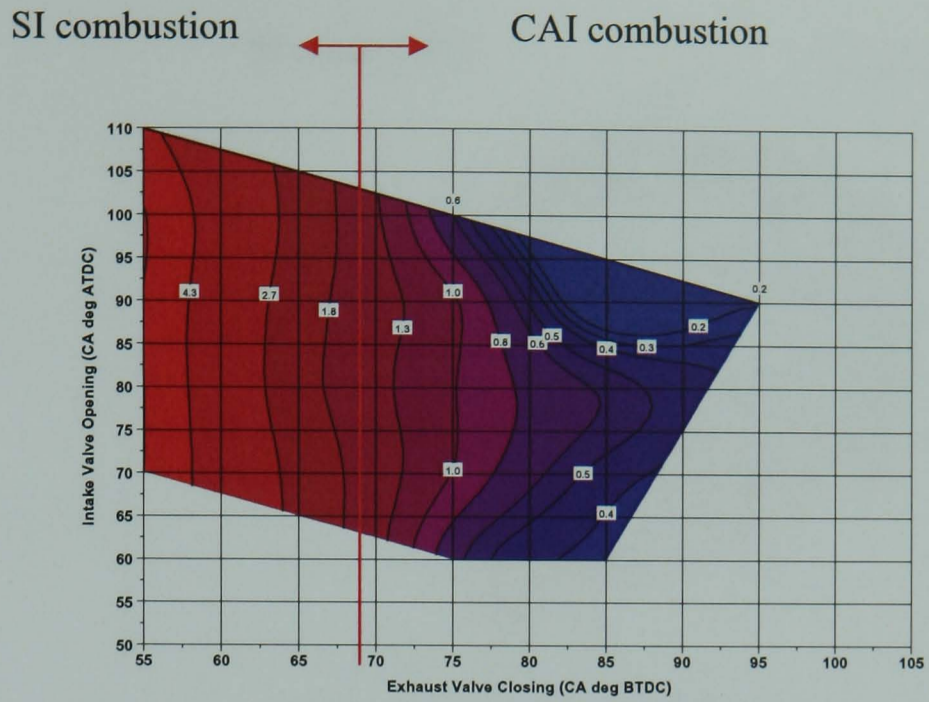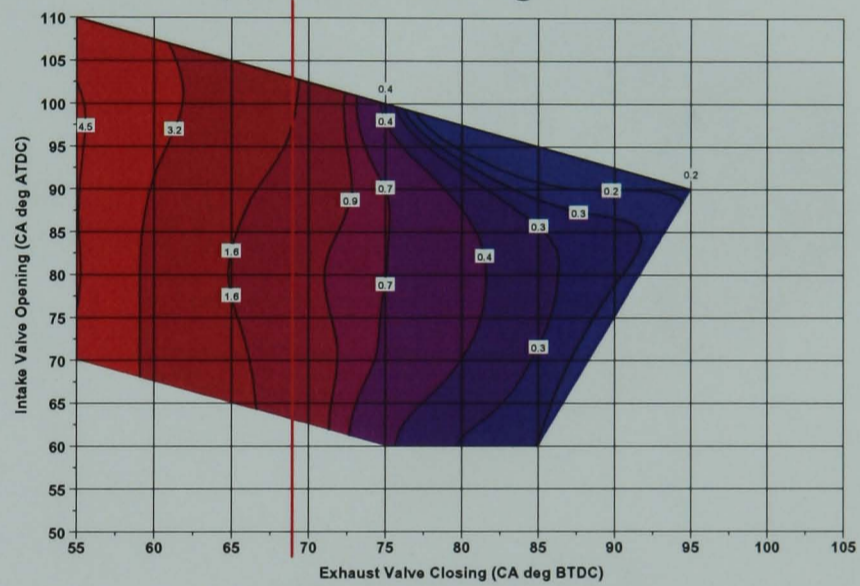
(a) SOI -30 CA deg ATDC

(b) SOI 30 CA deg ATDC
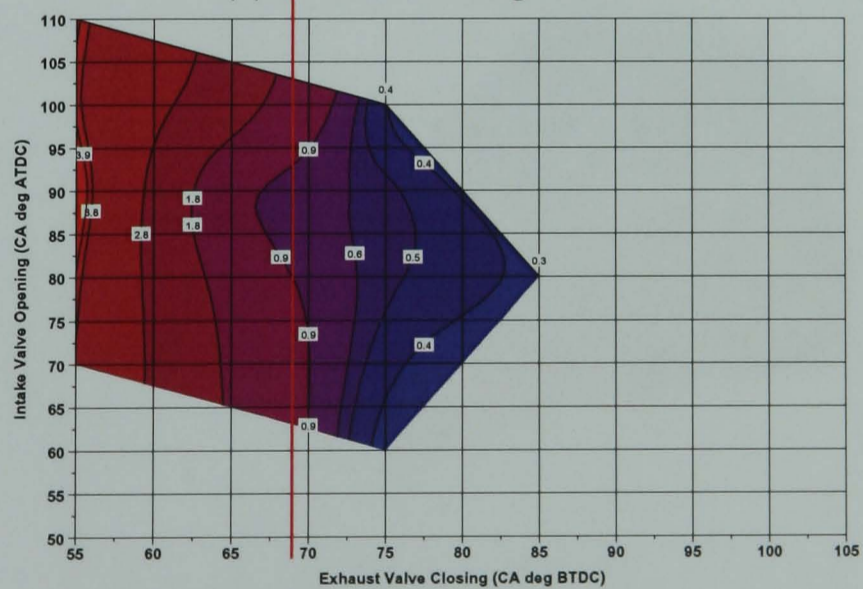
(c) SOI 120 CA deg ATDC

Figure 5.31 (a-c) ISNOx (g/kW.h) at EVC versus IVO timings for the longer CAI camshaft at lambda 1.0

112

(a) SOI -30 CA deg ATDC

(b) SOI 30 CA deg ATDC
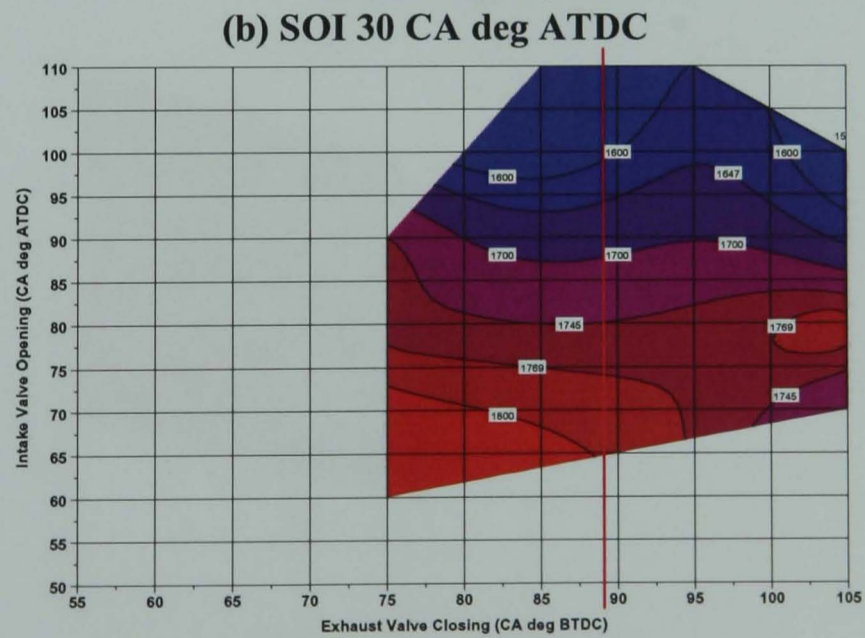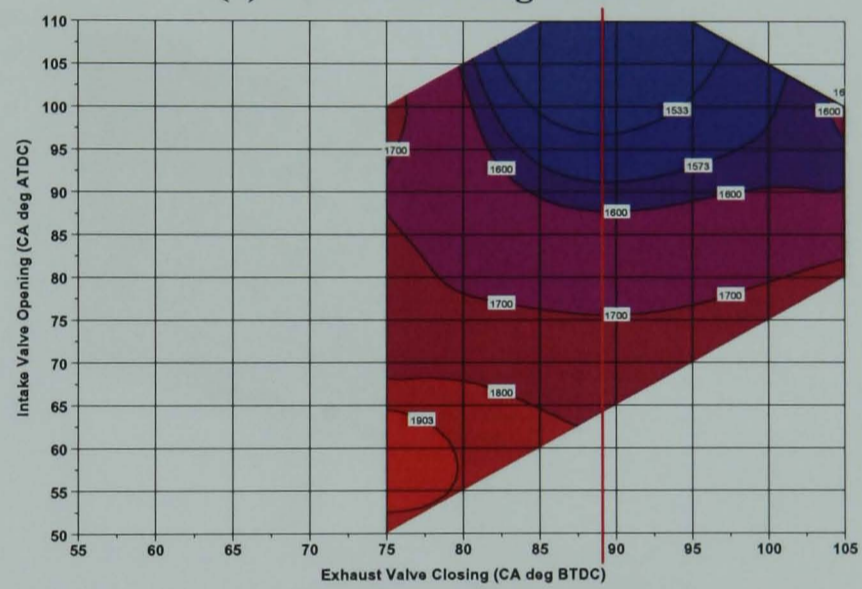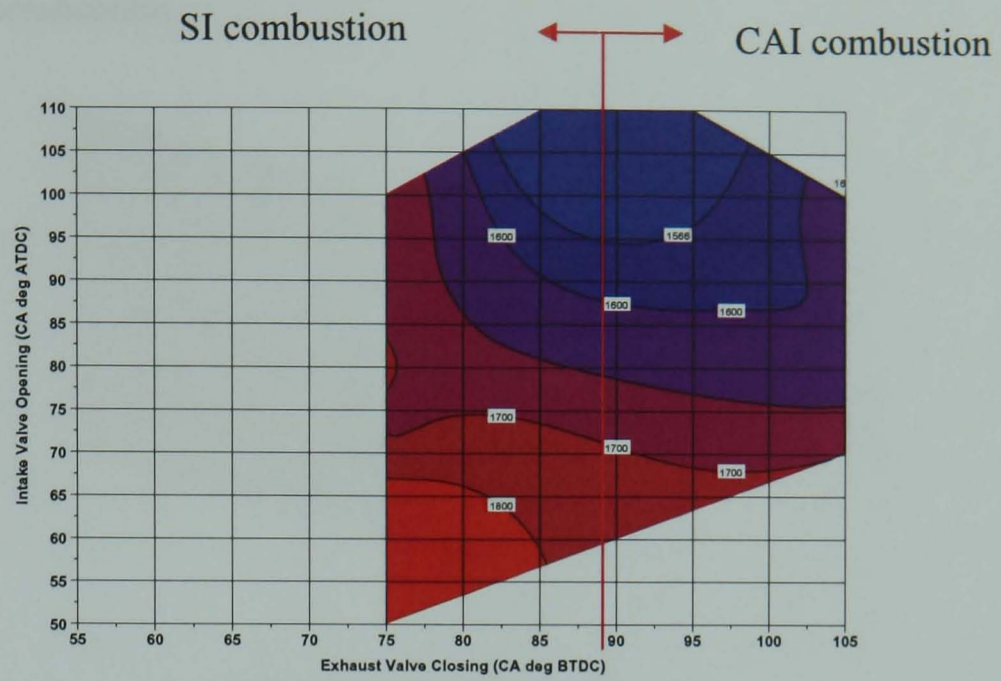
(c) SOI 120 CA deg ATDC

Figure 5.32 (a-c) Averaged Peak In-cylinder Temperature (K) at EVC versus IVO timings for the shorter CAI camshaft at lambda 1.0

113

SI combustion ◄───► CAI combustion
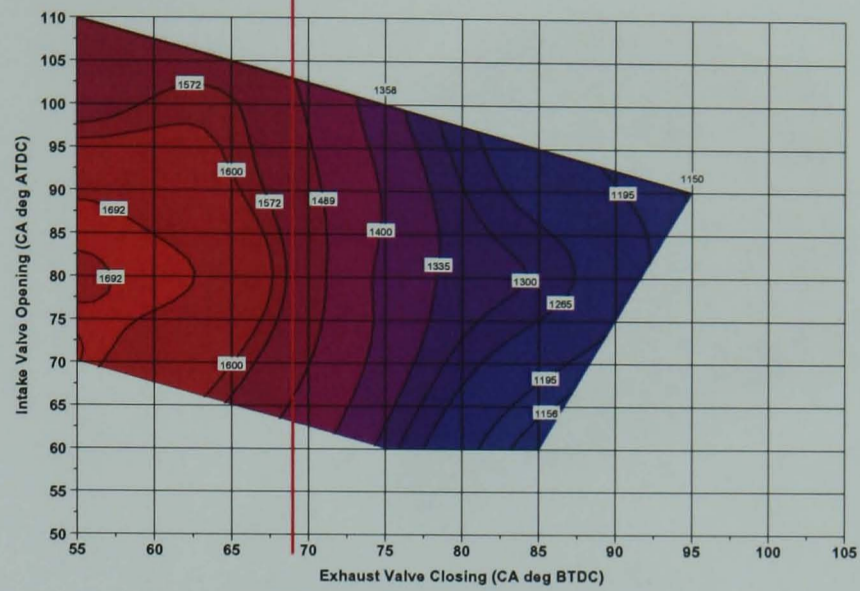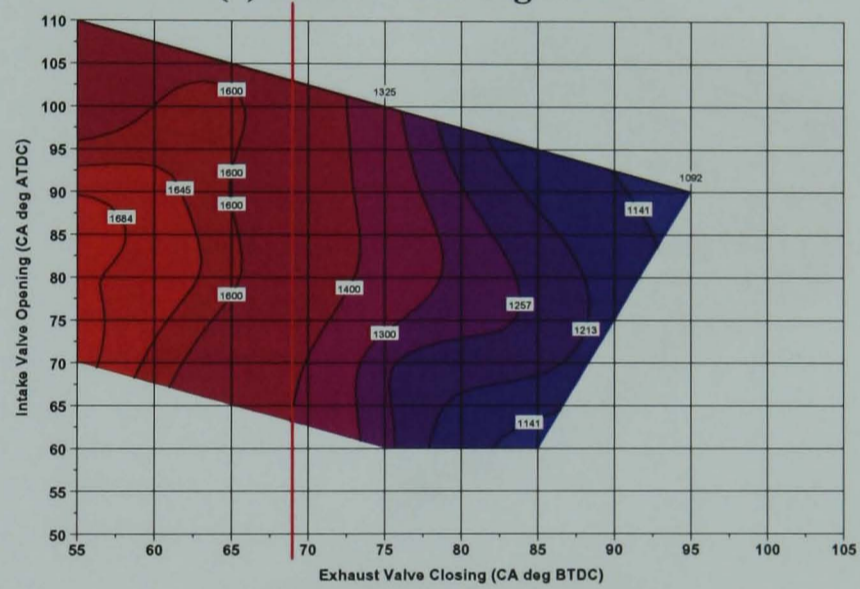
(a) SOI -30 CA deg ATDC
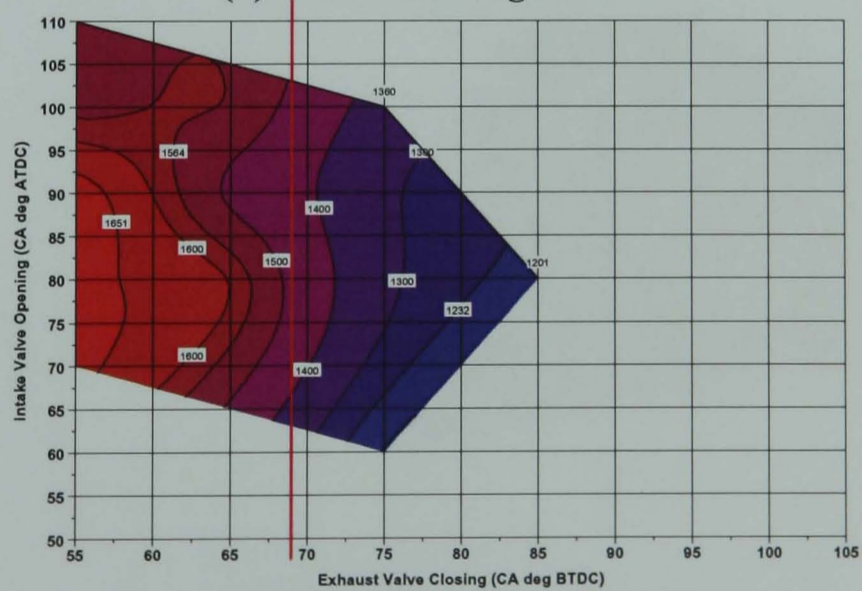
(b) SOI 30 CA deg ATDC

(c) SOI 120 CA deg ATDC

Figure 5.33 (a-c) Averaged Peak In-cylinder Temperature (K) at EVC versus IVO timings for the longer CAI camshaft at lambda 1.0

114
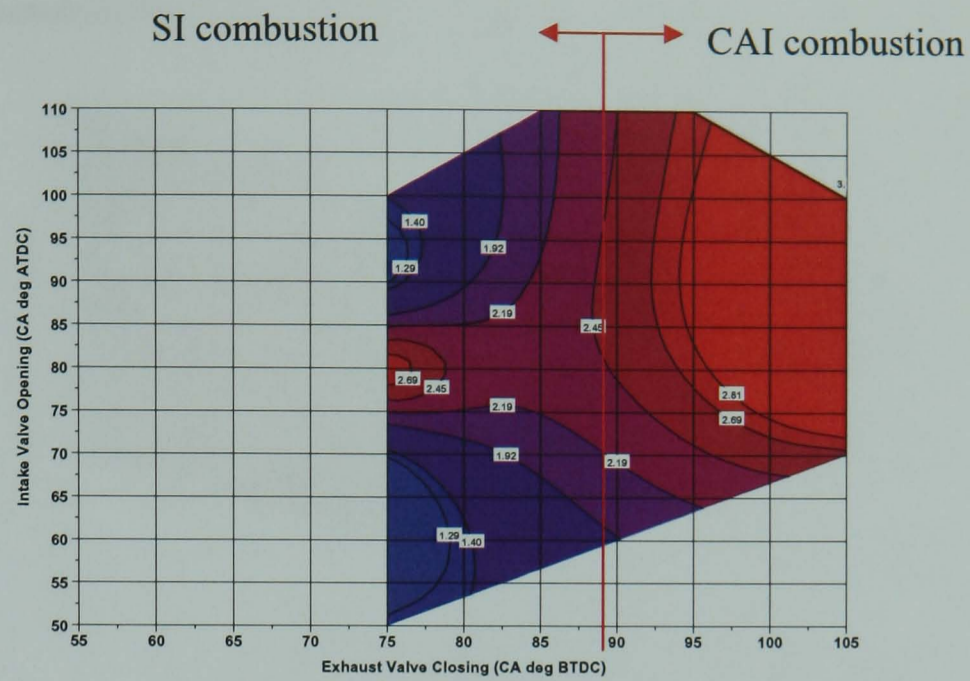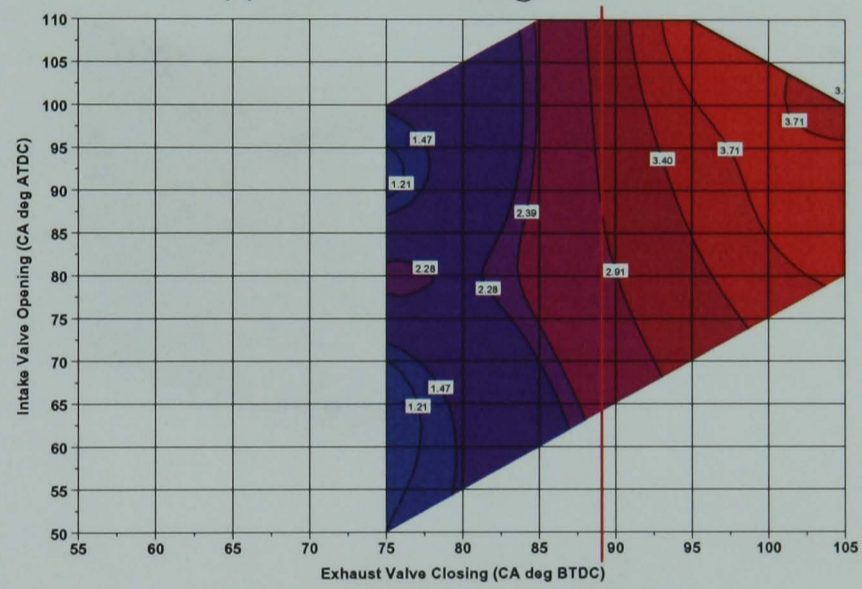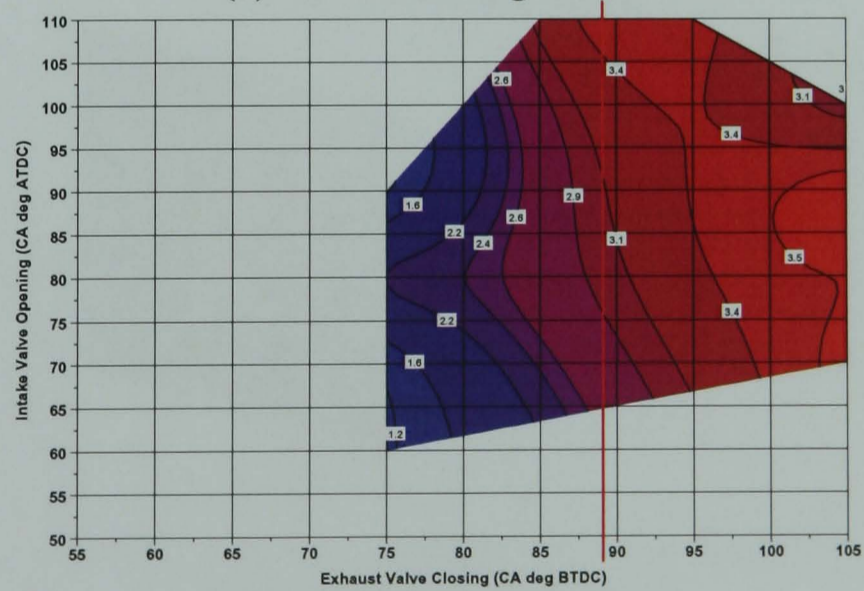
Figure 5.34 (a-c) ISHC (g/kW.h) at EVC versus IVO timings for the shorter CAI camshaft at lambda 1.0

SI combustion ← → CAI combustion
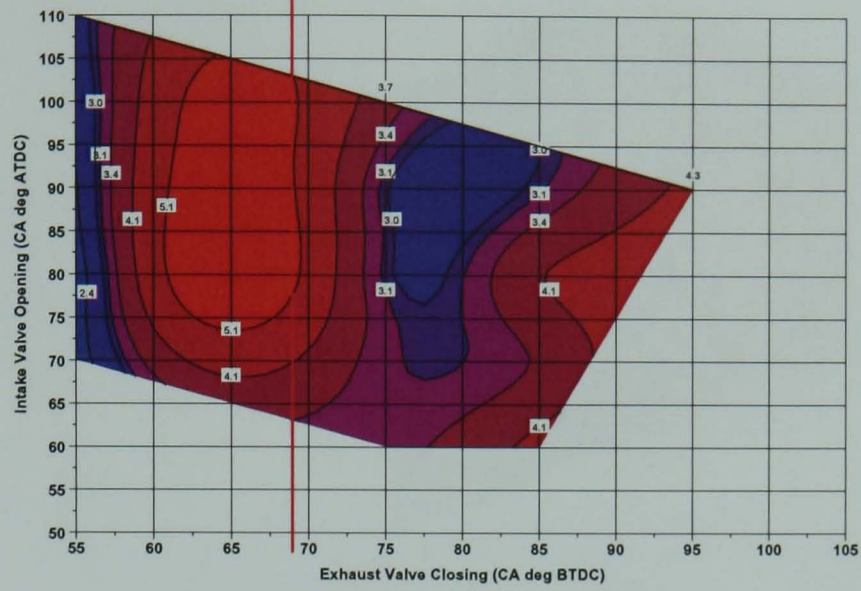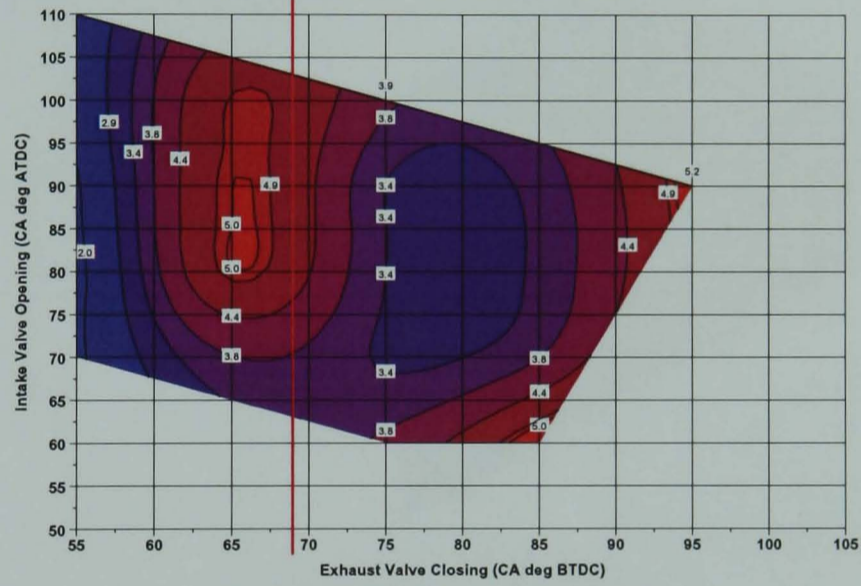
(a) SOI -30 CA deg ATDC
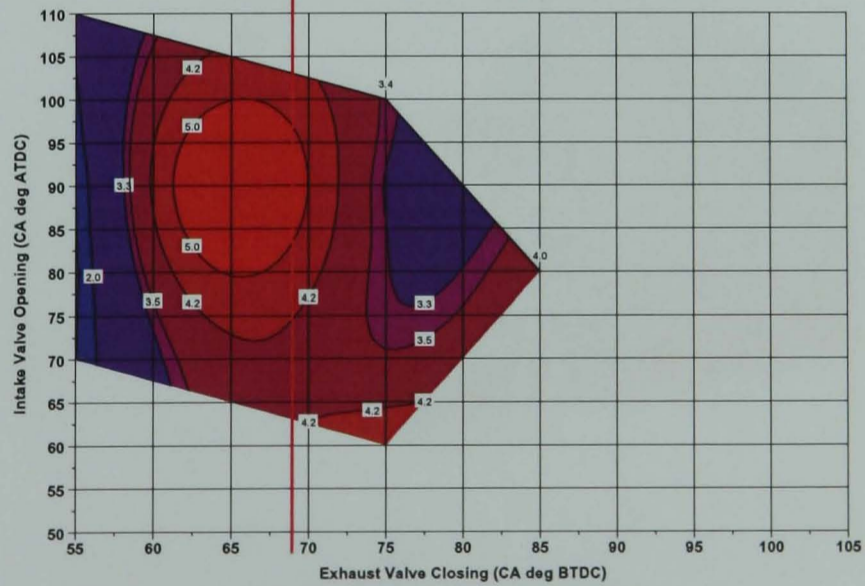
(b) SOI 30 CA deg ATDC

(c) SOI 120 CA deg ATDC

Figure 5.35 (a-c) ISHC (g/kW.h) at EVC versus IVO timings for the longer CAI camshaft at lambda 1.0

SI combustion ←——→ CAI combustion
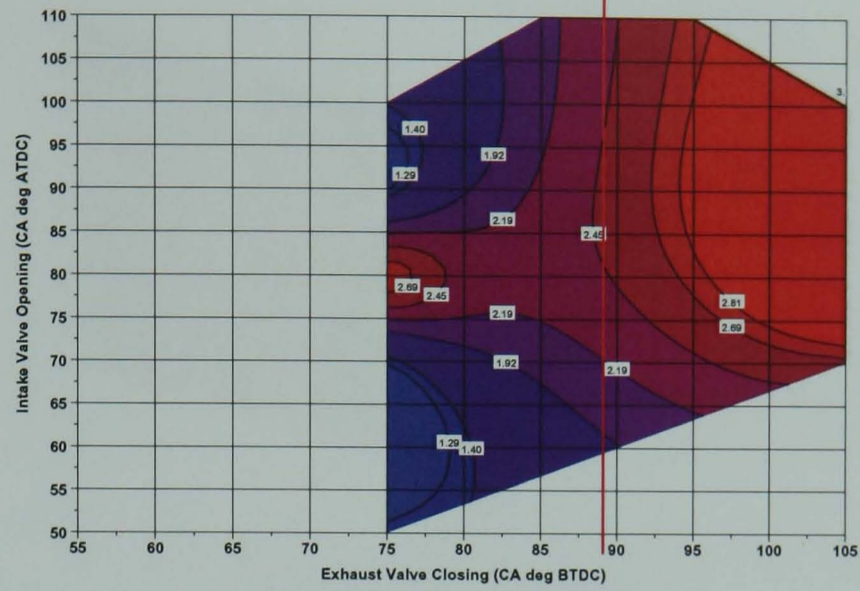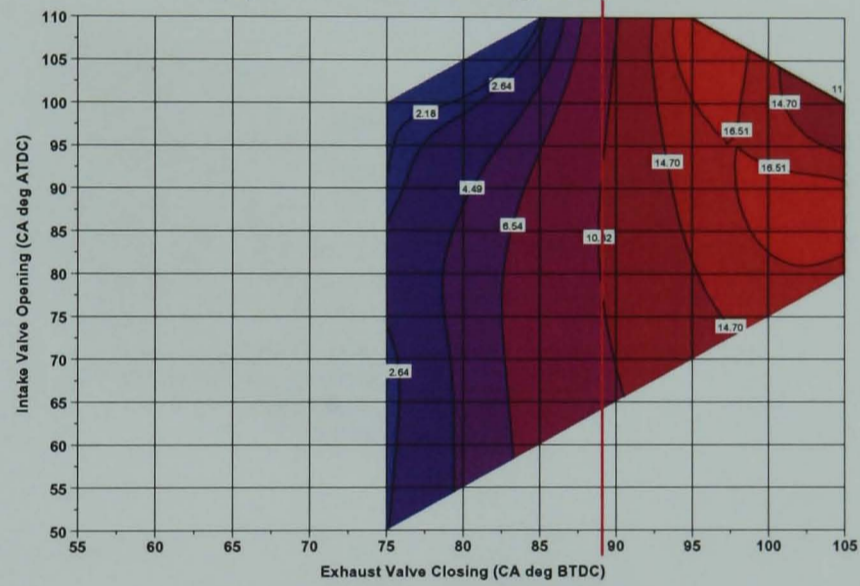
(a) SOI -30 CA deg ATDC
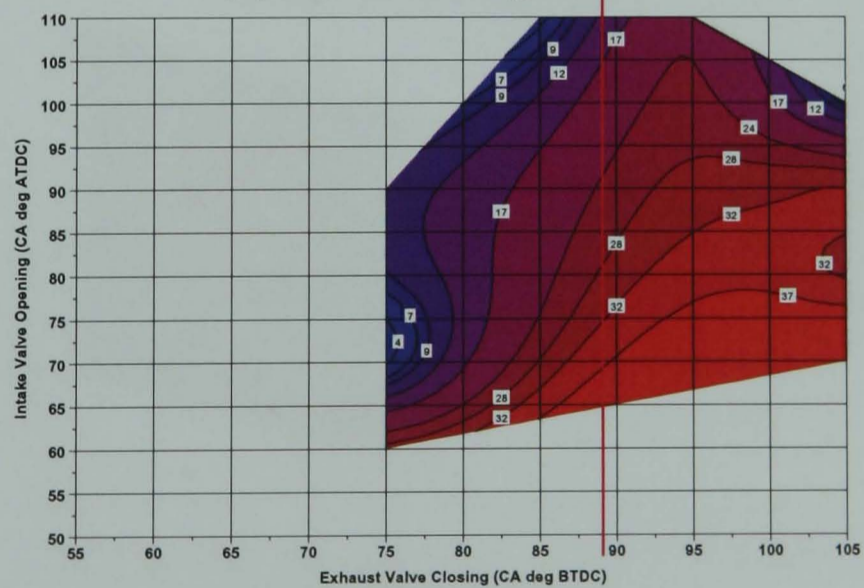
(b) SOI 30 CA deg ATDC

(c) SOI 120 CA deg ATDC

Figure 5.36 (a-c) ISCO (g/kW.h) at EVC versus IVO timings for the shorter CAI camshaft at lambda 1.0

117
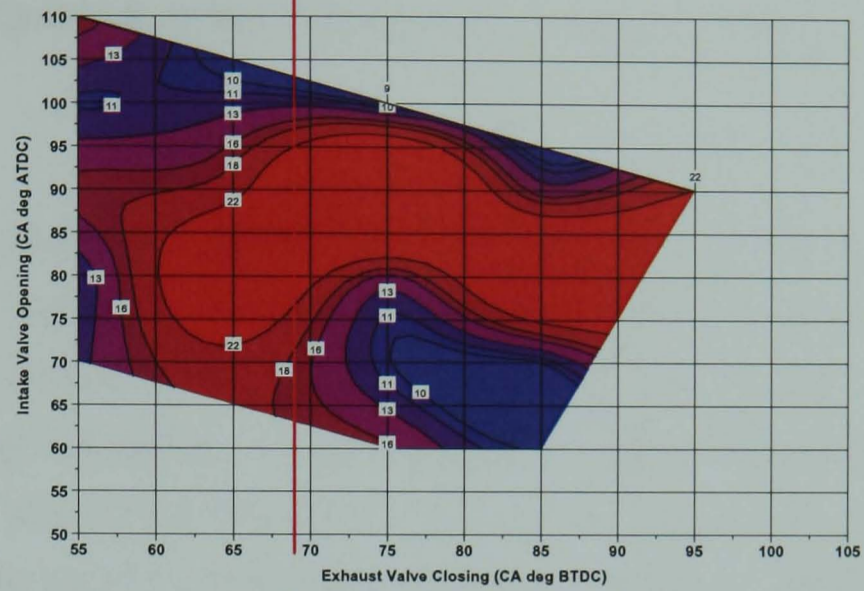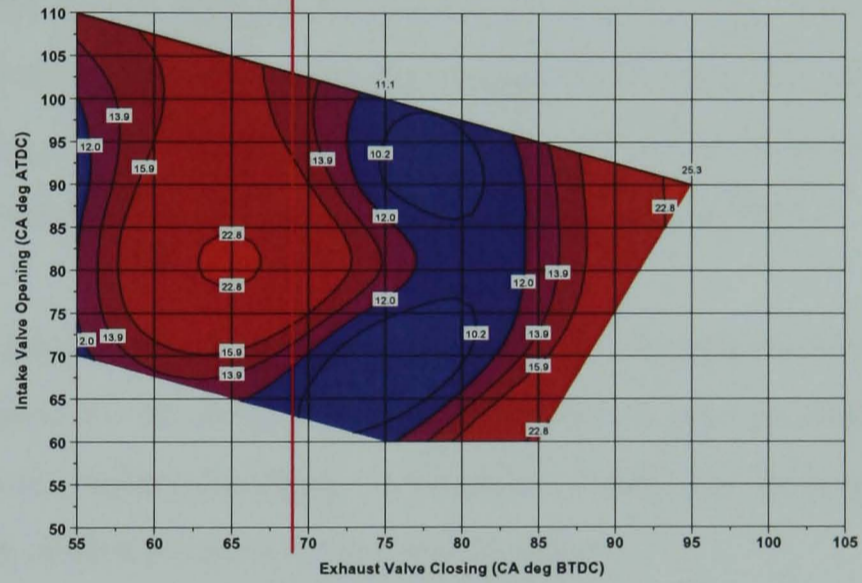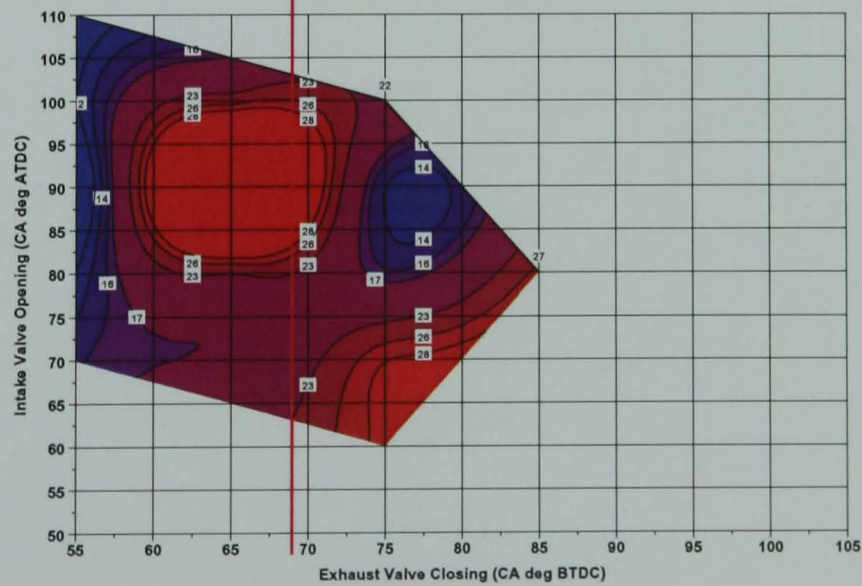
Figure 5.37 (a-c) ISCO (g/kW.h) at EVC versus IVO timings for the longer CAI camshaft at lambda 1.0

5.5.4 Effects of Camshaft design and Injection Timing on ISFC values at Lambda = 1.0

Figure 5.38 (a-c) shows that ISFC values at specific valve timings for the shorter CAI camshafts. There appears to be a general trend that as EVC is advanced, ISFC values decrease. At SOI -30 CA deg ATDC, ISFC values range from 264 g/kW.h to 330 g/kW.h. As injection timing is retarded, it appears that ISFC values decrease for any given valve timing case. For SOI 30 CA deg ATDC, ISFC values range from 260 g/kW.h to 310 g/kW.h. Finally for the SOI 120 CA deg ATDC, ISFC values range from 253 g/kW.h to 306 g/kW.h. For the longer duration camshafts, Figure 5.39 (a-c), a similar observation is made. For EVC 85 CA deg BTDC, IVO 80 CA deg ATDC, the ISFC value is 313 g/kW.h at SOI -30 CA deg ATDC. At the same valve timing case at SOI 30 and 120 CA deg ATDC, the ISFC values are 310 g/kW.h and 331 g/kW.h respectively.

ISFC values are greater for the longer CAI camshafts compared with the shorter CAI camshafts. The reason for this is that higher pumping losses are associated with longer CAI camshafts. As shown, higher percentage of trapped residuals for the longer CAI camshafts leads to more work needed to expel the in-cylinder gases.

SI combustion ←→ CAI combustion
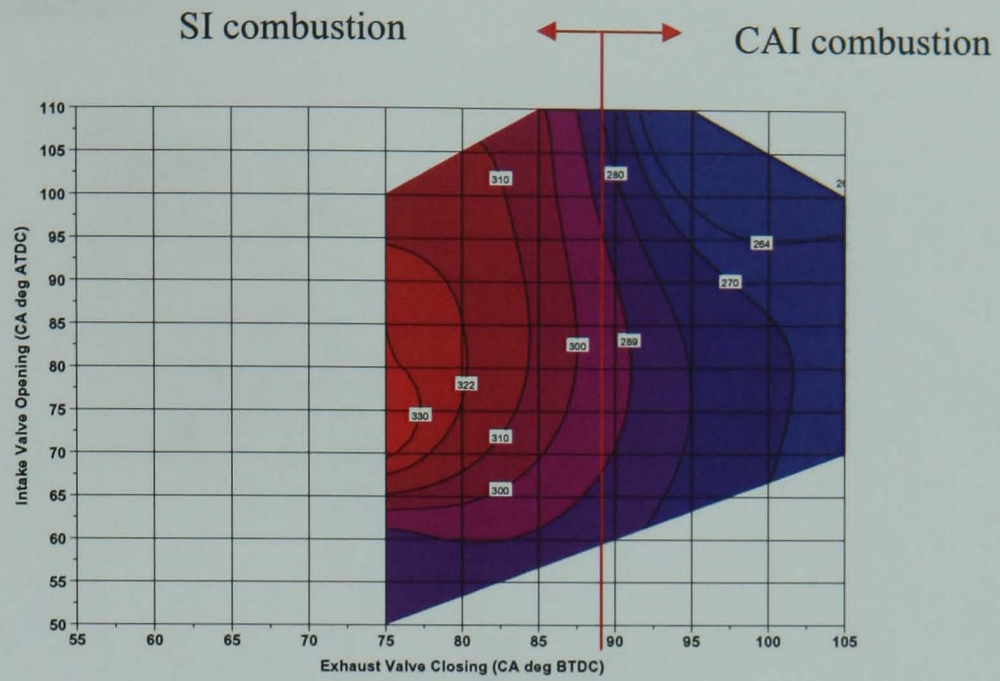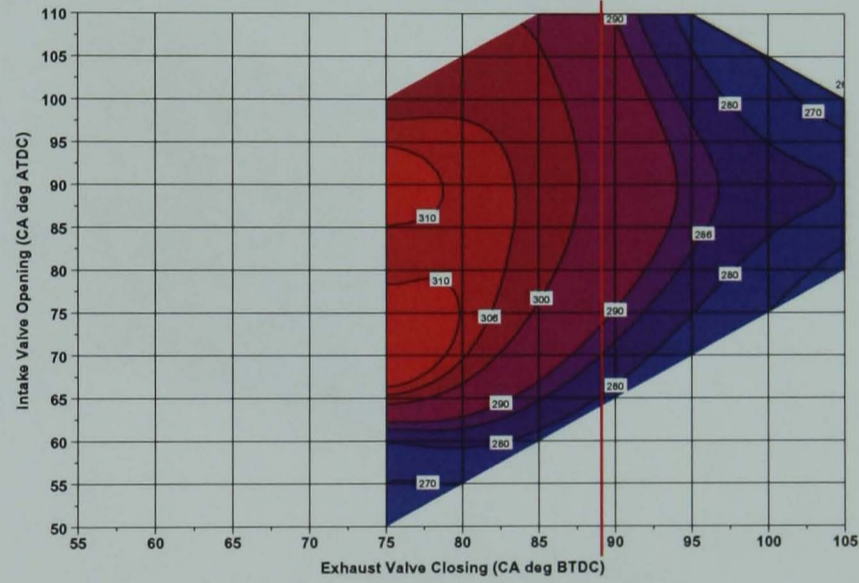
(a) SOI -30 CA deg ATDC

(b) SOI 30 CA deg ATDC
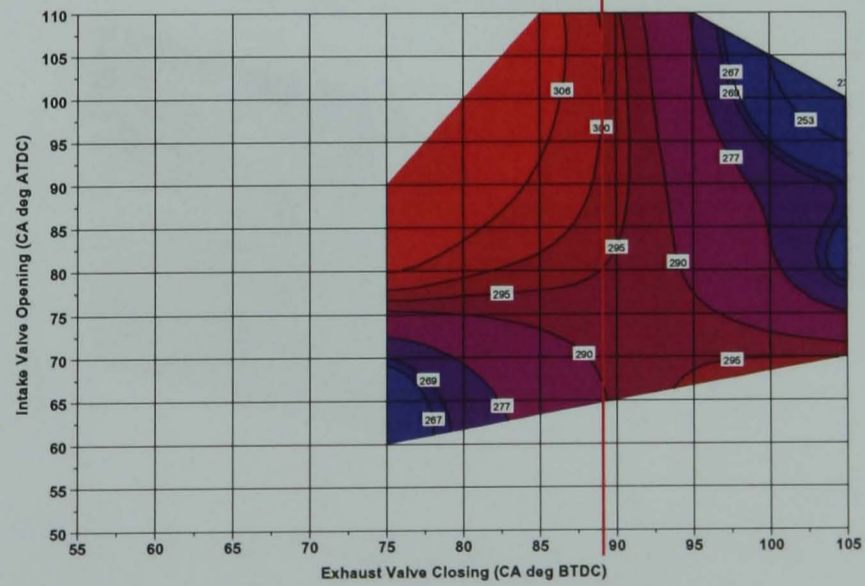
(c) SOI 120 CA deg ATDC

Figure 5.38 (a-c) ISFC (g/kW.h) at EVC versus IVO timings for the shorter CAI camshaft at lambda 1.0

SI combustion ←→ CAI combustion

(a) SOI -30 CA deg ATDC

(b) SOI 30 CA deg ATDC

(c) SOI 120 CA deg ATDC

Figure 5.39 (a-c) ISFC (g/kW.h) at EVC versus IVO timings for the longer CAI camshaft at lambda 1.0

121

5.5.5 Summary of Results at Lambda = 1.0

It was found that for the lambda 1.0 operation, the shorter CAI camshafts could lead to CAI operation at higher NIMEP values compared with the longer CAI camshafts. There are two reasons for the difference in NIMEP values. The first is that the exhaust camshaft with the 20 CA deg longer opening is experiencing Exhaust Valve Opening 20 CA deg before the shorter exhaust camshaft for a given EVC leading to reduced expansion work. The second reason for the difference in NIMEP values is due to the fact that at similar EVC timing, exhaust residuals are approximately 7% higher for the longer CAI camshaft as compared with the shorter CAI camshaft. The extra residual results in less inducted fresh charge and lower NIMEP values. Furthermore, the lower effective compression ratio associated with the longer CAI camshaft contributed to lower NIMEP values.

ISNOx values were found to be lower for the longer CAI camshafts compared with the shorter CAI camshafts due to lower in-cylinder temperatures. CAI operation produces much lower NOx emission than the SI operation. Furthermore due to lower in-cylinder temperatures for the longer CAI camshafts, both ISCO and ISHC values were higher as compared with the shorter CAI camshaft. In addition CAI operation produces higher uHC emissions than SI operation due to low combustion temperature. However, CO emissions could be increased or decreased as the engine changed from SI to CAI operation, depending on the burned gas temperature for post oxidation during the exhaust stroke.

ISFC was the final performance characteristic that was studied. Since ISFC is based on NIMEP, it stands to reason that higher NIMEP values led to lower ISFC values for the shorter CAI camshafts compared with the longer CAI camshafts.

It was found that there was an overlap of NIMEP values between SI and CAI operation. Since SI and CAI operation can be achieved at the same NIMEP values, transition can be realized between the two modes of operation with seamless transition. In addition, it has been noticed that spark-assisted CAI combustion is sometimes present between SI and CAI operation regions, as it will be shown in the subsequent sections.

5.6 Effects of Camshaft Design and Injection Timing at Lambda = 1.2

5.6.1 Introduction

A benefit of CAI combustion is that operation can be achieved at lean and diluted conditions and benefits of improved fuel economy realized. With production SI engines operation is restricted to lambda 1.0 since three-way catalysts are only functional at stoichiometric conditions; thus limiting any benefits of improved fuel economy at lean conditions. CAI combustion produces low levels of NOx emissions and eliminates the need for a NOx trap catalyst. A catalyst is needed for reducing exhaust HC emissions; however HC catalysts can operate at lean conditions. Testing had previously been carried out at lambda 1.2 with the shorter CAI camshafts and the effects on CAI combustion investigated, it was of further interest to study the effects of intake and exhaust valve opening duration on CAI combustion. Similar to lambda 1.0, testing was carried out for all possible IVO-EVC valve timing combinations including SI combustion, spark-assisted combustion and CAI combustion. Figure 5.40 shows a contour map of NIMEP for IVO versus EVC at lambda 1.2 and 1500 rpm for the shorter duration camshafts, on the map the three different regions are indicated. For the spark-assisted and spark-ignition region the ignition timing was taken as 20 CA deg BTDC (combustion) since it was found that this yielded optimized NIMEP and emissions. For the longer CAI camshafts at SOI 120 CA deg ATDC, it was not possible to operate the engine at any EVC timings advanced of 75 CA deg BTDC. This was due to the fact that at EVC 85 CA deg BTDC, exhaust valve opening occurs at 215 CA deg BTDC, causing charge to be forced out early and leading to engine misfire.

5.6.2 Effects of Camshaft Design and Injection Timing on Engine Performance at Lambda = 1.2

The initial performance characteristic investigated was NIMEP, it was found that for both the shorter and longer CAI camshafts as injection timing is retarded, the NIMEP increases (Figures 5.40 (a-c) and Figure 5.41 (a-c)). The maximum NIMEP value observed in the CAI region for the shorter CAI camshafts at SOI -30 CA deg ATDC is 2.81 bar; whereas at SOI 30 CA deg ATDC, the NIMEP value is 3.38 bar. For the longer CAI camshafts, the maximum NIMEP value observed in the CAI region is 2.67 bar; while at SOI 30 CA deg ATDC, the maximum NIMEP is 2.70 bar. For both valve durations, there is a general trend of NIMEP increasing as start of injection is retarded from the NVO re-compression period to the NVO re-expansion period. There are two reasons why NIMEP increases as SOI is retarded. This is likely to be caused by the combustion phasing with SOI -30 CA ATDC, the start of combustion is advanced and causes NIMEP to drop. The reason why the PMEP value is higher at lambda 1.2 as start of injection is retarded can be attributed to a minor heat release event. During the NVO period in a GDI engine, the process of charge cooling is realized due to the vaporization of fuel when injected directly into the hot exhaust gas residual. In the presence of excess oxygen, a minor heat release event is realized. The charge cooling effect reduces compression work during the NVO re-compression period, but the minor heat release aids work output during the NVO re-expansion period. The minor heat release event experienced during the NVO period therefore tends to lower the PMEP. Pumping losses are lower with injection during the NVO re-compression period compared with injection during the NVO re-expansion period (Figure 5.42 (a-c) and Figure 5.43 (a-c)); this is true for both the shorter and longer CAI camshafts. This is unlike lambda 1.0, where PMEP tends to increase with early injection during the negative valve overlap period.

It is apparent that when comparing the NIMEP between the shorter CAI camshafts and longer CAI camshafts that NIMEP is higher for the shorter CAI camshafts. This is due to the fact that similar to lambda 1.0, the longer duration camshafts experience lower expansion work compared with the shorter duration camshafts, as the longer CAI camshafts

open the exhaust valves 20 CA deg earlier than the shorter CAI camshafts. Furthermore, the exhaust valve lift has an extra 1mm for the longer CAI camshafts compared with the shorter CAI camshafts. These two factors cause a higher percentage of charge to exit through the exhaust valves at EVO and decrease the available expansion pressure. Hence greater work has to be done to overcome this loss of expansion pressure, leading to lower NIMEP values for the longer CAI camshafts.

Similar to lambda 1.0, NIMEP values are higher for SI combustion compared with CAI combustion; this is true for both the shorter and longer CAI camshafts. For the shorter CAI camshafts, NIMEP values range from 2.6 to 3.82 bar for SI combustion and 2.6 to 3.72 bar for CAI combustion. For the longer CAI camshafts, NIMEP values range from 2.67 to 3.06 bar for SI combustion and 1.94 to 2.7 bar for CAI combustion. Again higher NIMEP values for SI combustion are due to the fact that there is less trapped residual and more inducted fresh charge.

It can also be observed, similar to lambda 1.0, that some NIMEP values in the SI region overlap with values within the CAI region. This proves an effective method for achieving transitioning from SI to CAI combustion and back to SI combustion. For example, at EVC 55 CA deg BTDC, IVO 80 CA deg ATDC for the shorter CAI camshafts, the NIMEP value is 2.6 bar, at EVC 105 CA deg BTDC, IVO 85 CA deg BTDC, the NIMEP value is also 2.6 bar. Therefore using these two points a transition can be made from SI mode to CAI mode without any noticeable load jump.

Last but not the least, it is noted that a spark-assisted combustion mode is present between the SI and CAI operation, where combustion is initially triggered by spark discharge and then becomes dominated by the multiple auto-ignition heat release process. A detailed analysis of spark-assisted CAI operation will be presented in Chapter 6.

Figure 5.44 (a-c) and Figure 5.45 (a-c) shows that Trapped Residuals do not vary significantly with variation in injection timing, however, as discussed Trapped Residuals influence NIMEP.
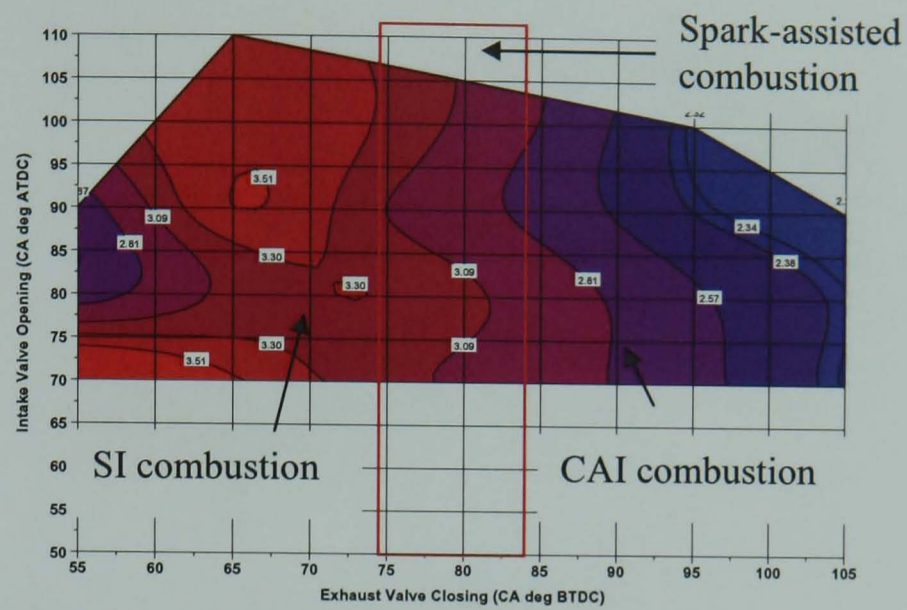
(a) SOI -30 CA deg ATDC
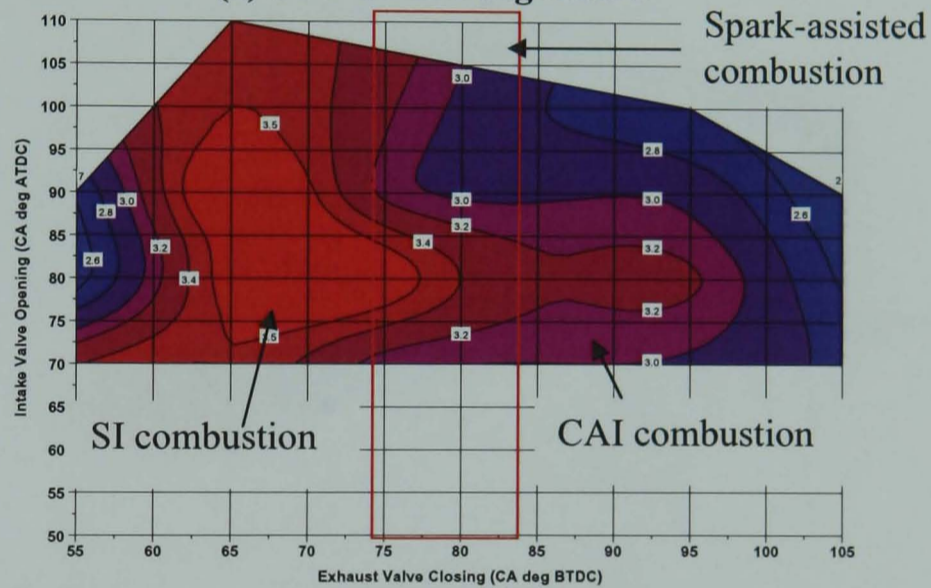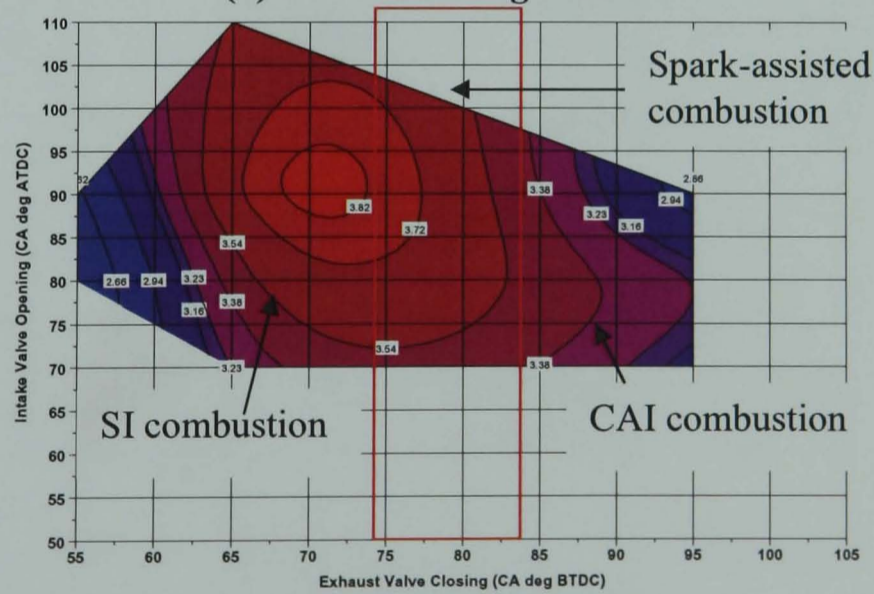
(b) SOI 30 CA deg ATDC

(c) SOI 120 CA deg ATDC

Figure 5.40 (a-c) NIMEP (bar) at EVC versus IVO timings for the shorter CAI camshaft at lambda 1.2
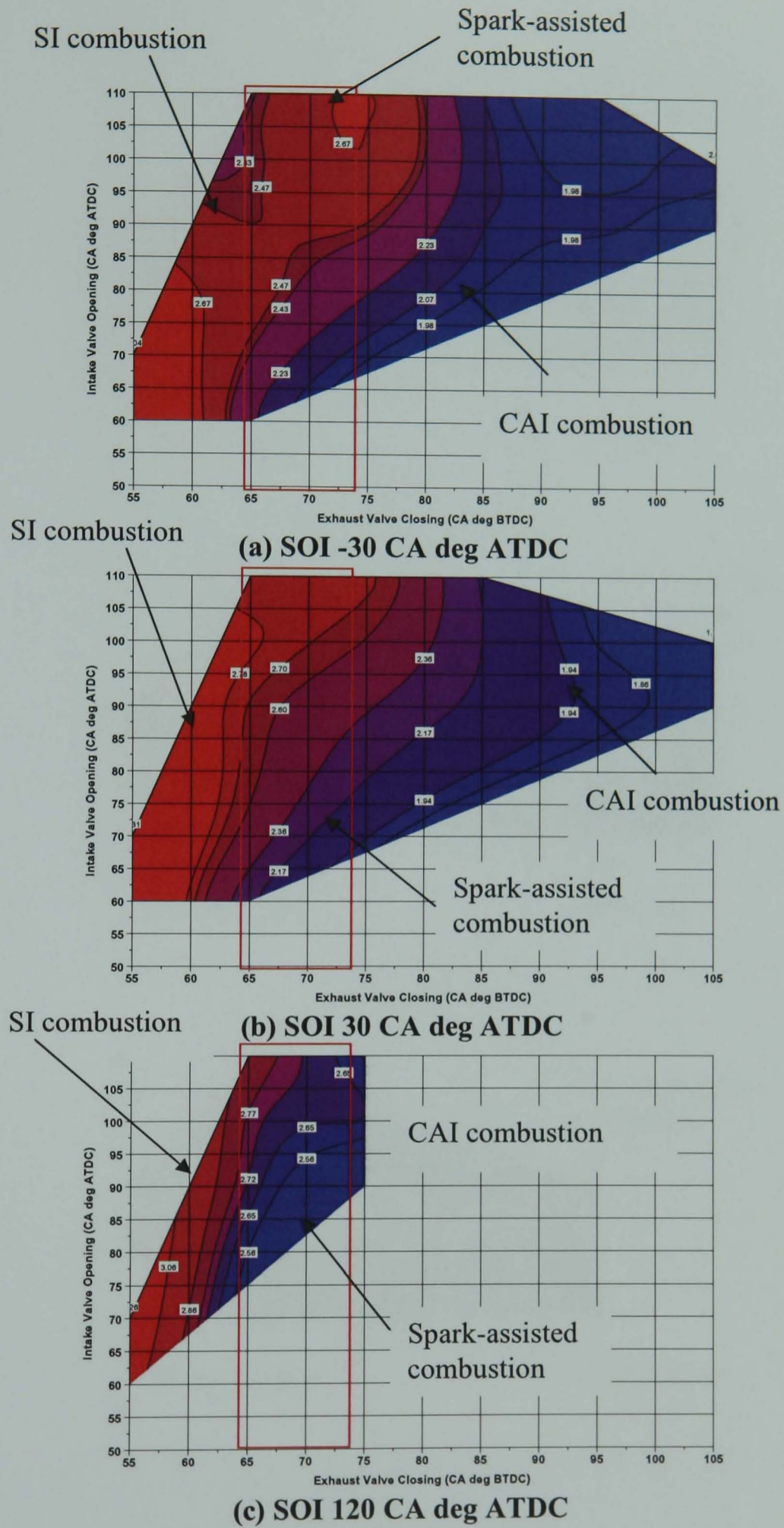
Figure 5.41 (a-c) NIMEP (bar) at EVC versus IVO timings for the longer CAI camshaft at lambda 1.2

127
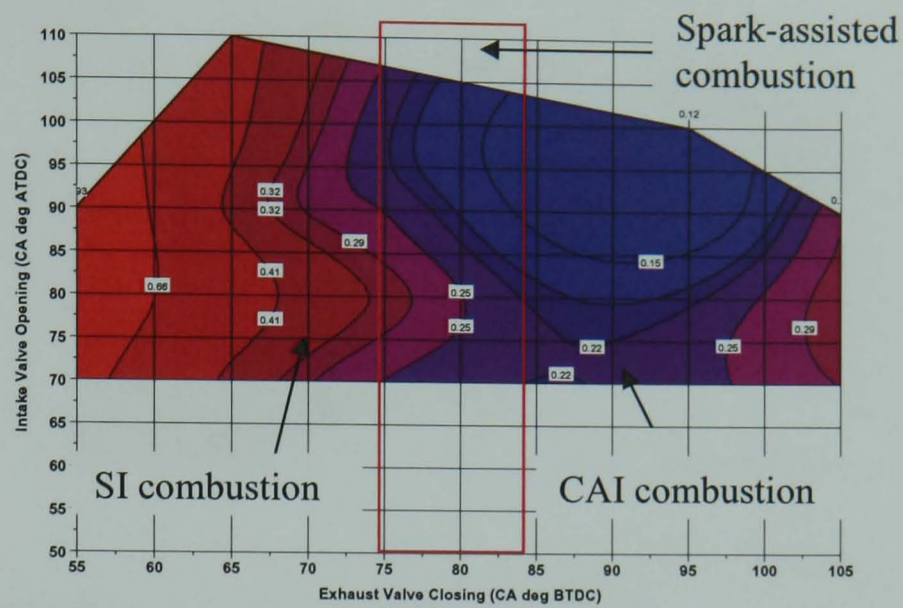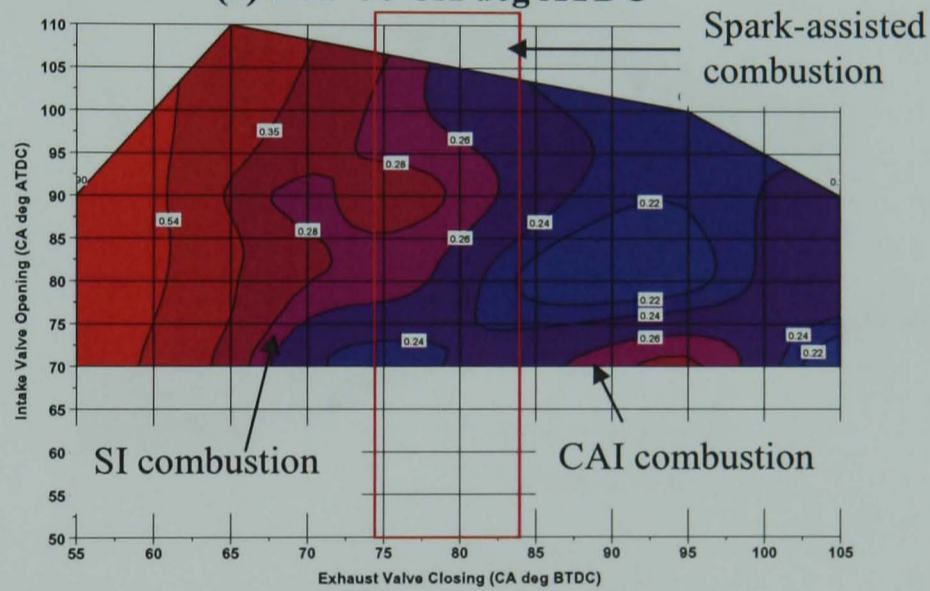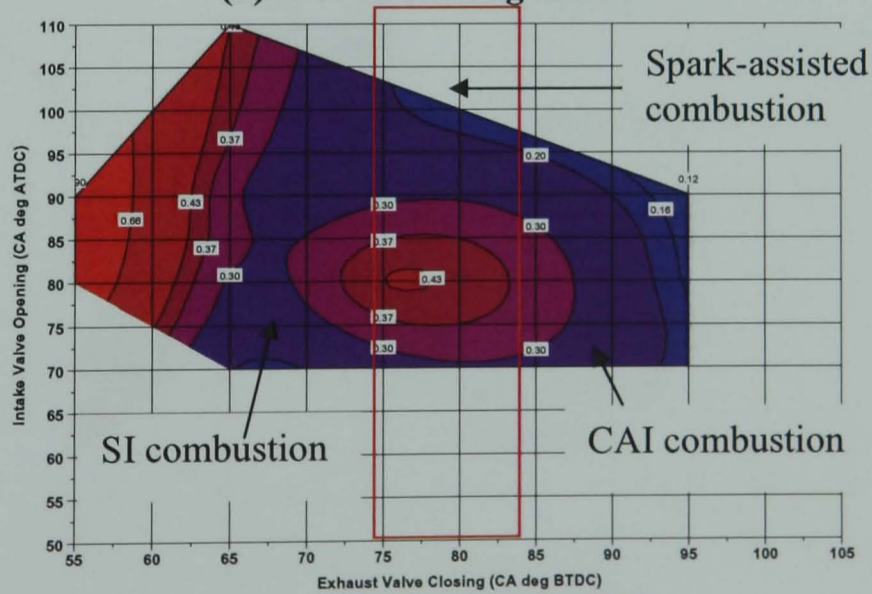
Figure 5.42 (a-c) PMEP at EVC versus IVO timings for the shorter CAI camshaft at lambda 1.2
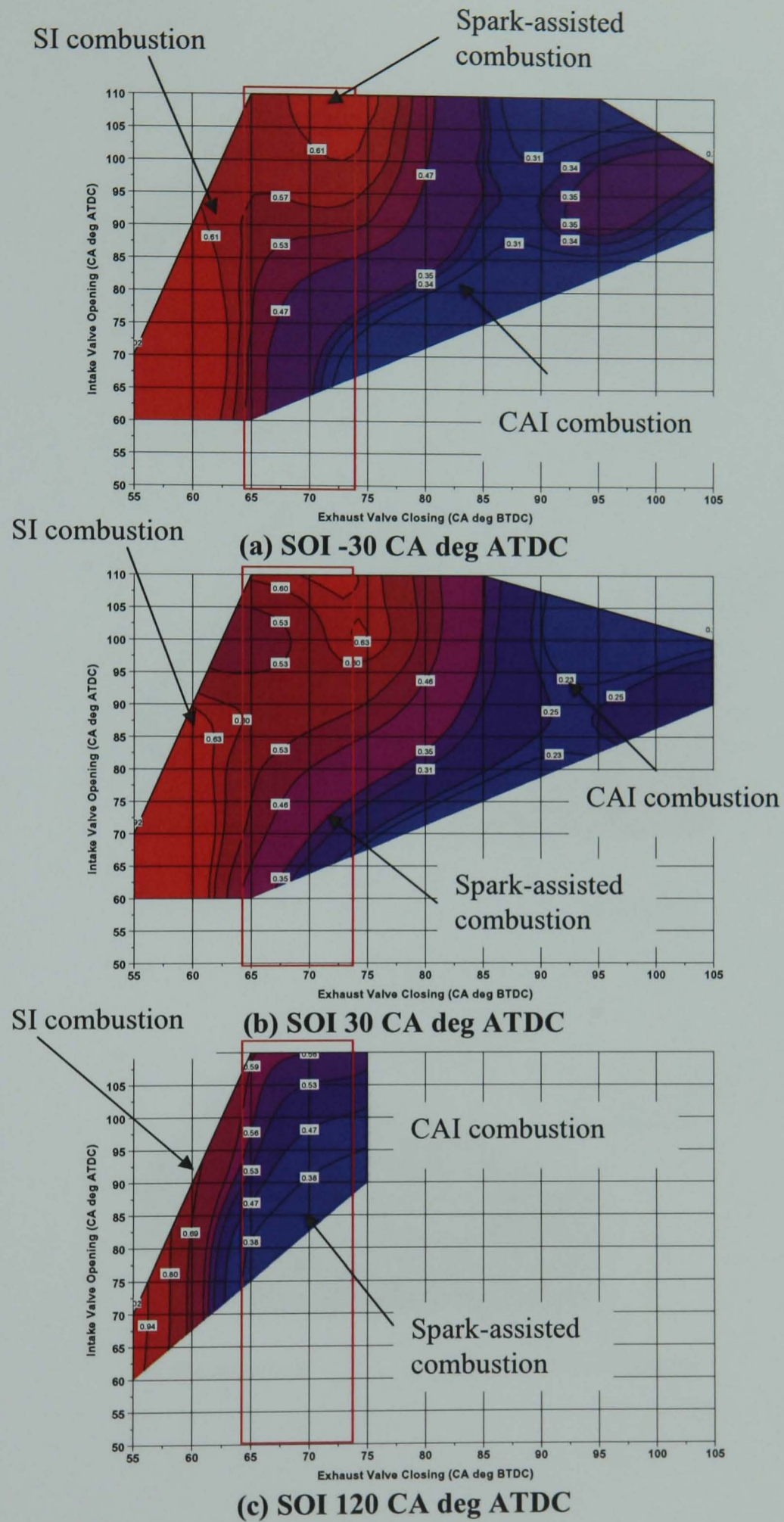
Figure 5.43 (a-c) PMEP at EVC versus IVO timings for the longer CAI camshaft at lambda 1.2
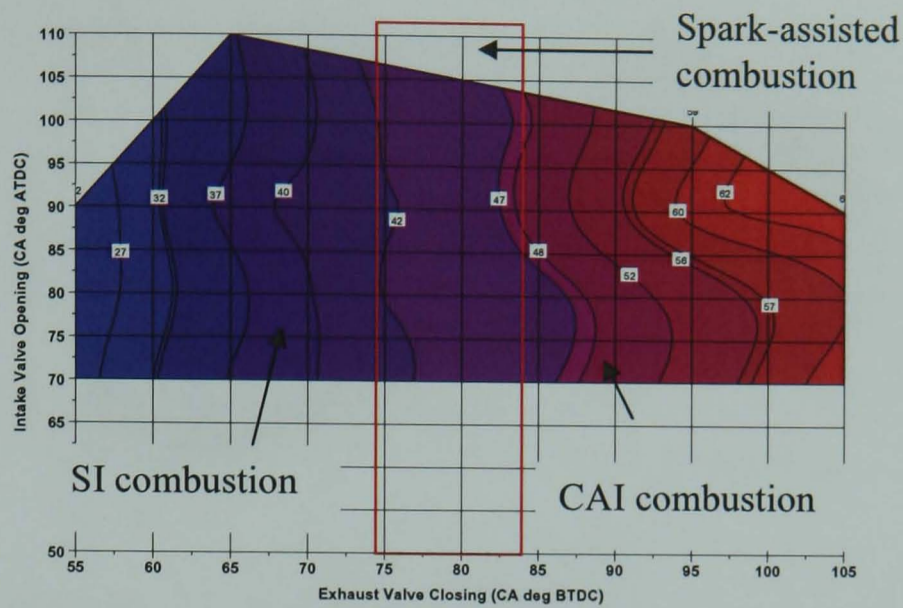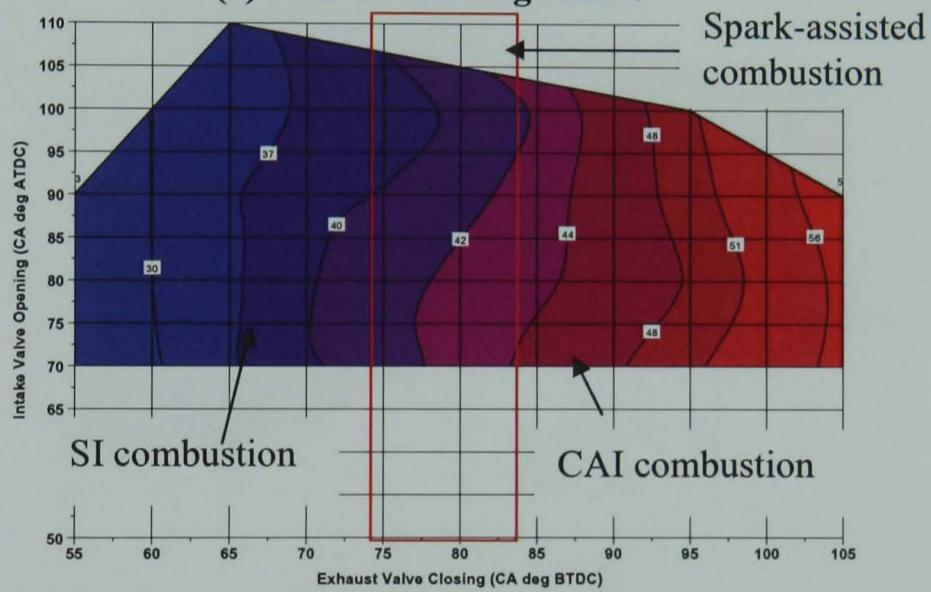
(a) SOI -30 CA deg ATDC

(b) SOI 30 CA deg ATDC
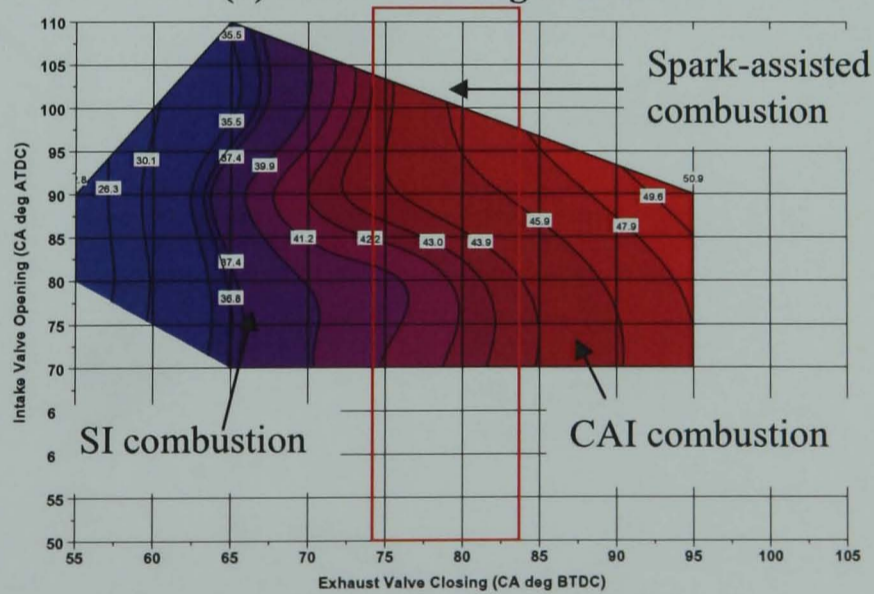
(c) SOI 120 CA deg ATDC

Figure 5.44 (a-c) Percentage of Trapped Residual at EVC versus IVO timings for the shorter CAI camshaft at lambda 1.2
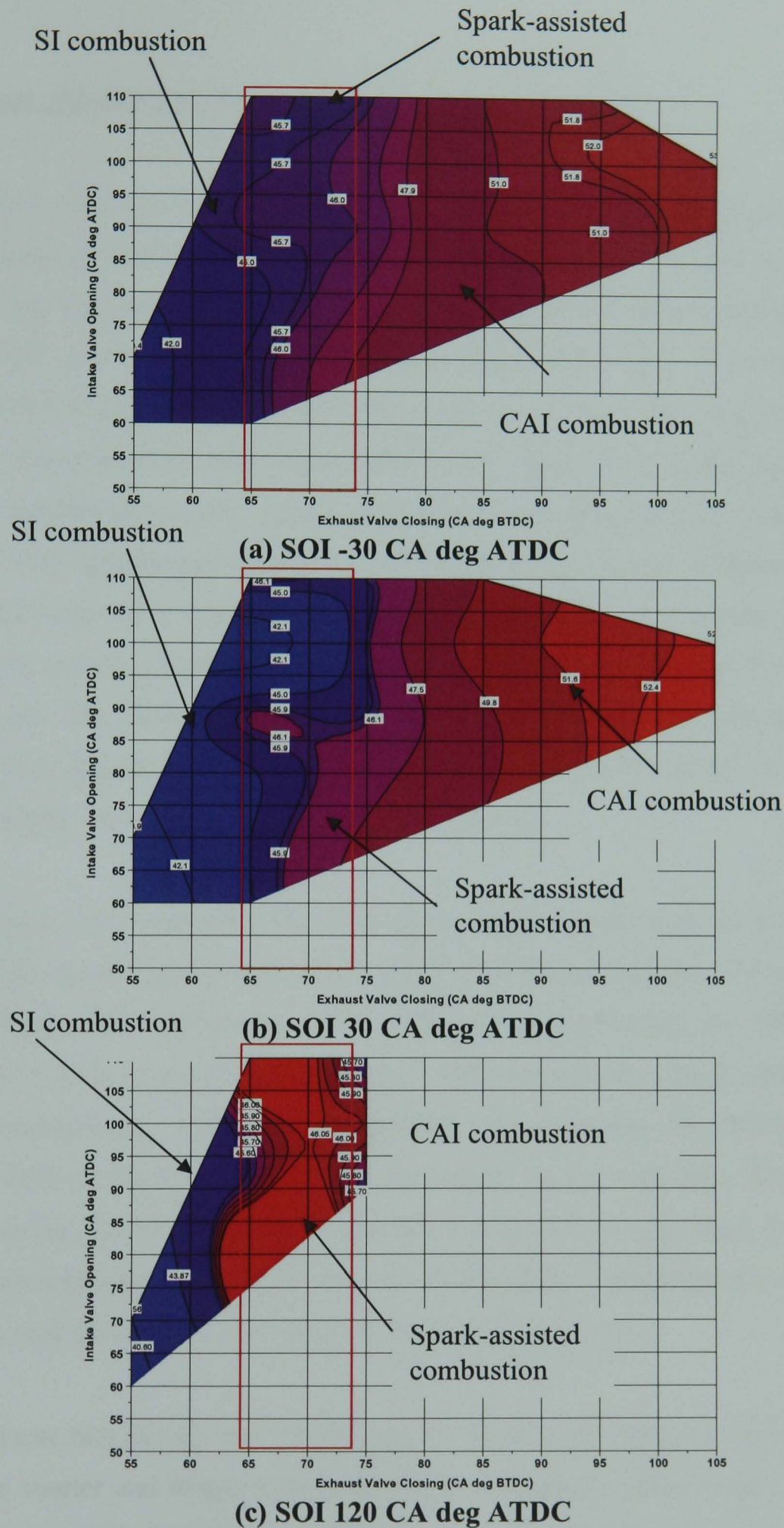
Figure 5.45 (a-c) Percentage of Trapped Residual at EVC versus IVO timings for the longer CAI camshaft at lambda 1.2

5.6.2.1 Effects of Injection Timing on Combustion at lambda = 1.2

Table 5.8-5.13 indicates the 10% and 90% MFB angle, burn duration, peak in-cylinder pressure and the peak heat release rate for each valve timing at 1500 rpm and lambda 1.2, for both the shorter and longer CAI camshafts. For the short duration camshafts at EVC 55 CA deg BTDC, the burn duration (10 – 90% MFB) is 63 CA deg. The 10% MFB angle appears at 373 CA deg ATDC, the 90% MFB angle appears at 436 CA deg ATDC. The late 10% MFB angle indicates that combustion at this point is occurring purely by spark ignition; as combustion occurs by flame propagation from the spark plug location, there is a delay after TDC (expansion) before the 10% MFB angle occurs. Furthermore, the burn angle is very long, 63 CA degrees in this case, this further supports the argument that combustion is occurring only by spark ignition. For other valve timings, EVC 65-105 CA deg BTDC, the 10% MFB angle appears closer to TDC (expansion), even for combustion which has been judged to occur by spark ignition (EVC 65,75 and 85 CA deg BTDC); suggesting that to some degree auto-ignition is occurring.

For the longer CAI camshafts, the 10% MFB angle occurs near 10 CA deg BTDC (expansion) for spark ignition and shifts towards TDC (expansion) for CAI combustion. At EVC 65 CA deg, IVO 70 CA deg ATDC, SOI -30 CA deg ATDC, the 10% MFB angle occurs at 347 CA deg suggesting that the spark aids the underdeveloped auto-ignition sites and causes combustion to commence immediately. In comparison, the 10% MFB angle for the shorter CAI camshaft at EVC 55 CA deg BTDC occurs well after TDC (expansion) exemplifying the fact that pure spark ignition combustion is occurring. In addition, the spark-assisted combustion seems to occur in the SI mode as highlighted in Tables 5.8 – 5.13, where combustion duration is shorter for flame propagation.

The heat release rate (J/deg) was plotted against crank angle (degree), Figure 5.46 – 5.53 for both the shorter and longer CAI camshaft at a particular valve timing. For all valve timing graphs, at SOI -30 CA deg ATDC, combustion phasing is the most advanced and the heat release rate peak is the highest, compared with SOI 30 and 120 CA deg ATDC. As Cao et al. [58] have shown, through numerical studies, the early injection into the NVO

period increases the charge temperature and promotes auto-ignition reactions, hence leading to advanced combustion.

On inspection of peak pressure values from Table 5.8 – 5.13, the lowest peak pressure for the shorter duration camshaft appears to occur at EVC 55 CA deg BTDC during spark ignition, thereafter the peak pressure values seem to vary between 29 and 40 bar for EVC 65, 75, 85, 95 and 105 CA deg. The low peak pressure values at EVC 55 CA deg BTDC can be explained by the fact that combustion is occurring purely by flame propagation, characterized by the long burn duration. Cylinder pressure does not increase rapidly at TDC (expansion) but rather follows a steady pressure rise for flame propagation. For EVC 65, 75, 85, 95 and 105 CA deg BTDC, combustion occurs either by pure CAI or part auto-ignition resulting in a high peak pressure value.

For the longer CAI camshafts, the peak pressure value tends to decrease as EVC is advanced. At EVC 55 CA deg BTDC, IVO 70 CA deg ATDC and SOI 30 CA deg ATDC, the peak pressure is 39 bar, at EVC 105 CA deg BTDC, IVO 100 CA deg and SOI 30 CA deg ATDC, the peak pressure decreases to 25 bar. The decrease in peak pressure can be attributed to the fact that as EVC is advanced, EVO advances into the expansion stroke and hence causes peak pressure to decrease.

Table 5.8 10%, 90% MFB, burn duration and peak in-cylinder pressure for the shorter CAI camshaft at SOI -30 CA deg ATDC

SI combustion- Ignition Timing 20 CA deg BTDC												
EVC (CA deg BTDC)	55	55	55	65	65	65	65	75	75	75	85	85
IVO (CA deg ATDC)	70	80	90	80	90	100	110	70	80	90	80	100
10 % MFB (CA ATDC)	370	377	379	359	360	361	360	353	356	356	356	360
90 % MFB (CA ATDC)	407	432	432	379	373	383	380	379	384	370	372	369
Burn Duration (CA)	37	55	53	20	13	22	20	26	28	14	16	9
Peak In-cylinder Pressure, bar	21	20	20	33	39	30	30	34	43	37	32	36
Peak heat release rate (J/CA)	14	24	11	24	41	22	22	28	56	38	32	42
COV (%)	5.12	11.6	13.1	4.5	2.39	4.52	8.7	2.59	3.56	1.98	1.03	0.96

CAI combustion					
EVC (CA deg BTDC)	95	95	105	105	105
IVO (CA deg ATDC)	90	100	70	80	90
10 % MFB (CA ATDC)	356	357	360	359	359
90 % MFB (CA ATDC)	368	369	371	369	370
Burn Duration (CA)	12	12	11	10	11
Peak In-cylinder Pressure, bar	34	33	34	36	34
Peak heat release rate (J/CA)	32	28	36	34	30
COV (%)	1.26	1.37	1.68	1.24	1.70

Table 5.9 10%, 90% MFB, burn duration and peak in-cylinder pressure for the shorter CAI camshaft at SOI 30 CA deg ATDC

SI combustion- Ignition Timing 20 CA deg BTDC												
EVC (CA deg BTDC)	55	55	55	65	65	65	65	65	75	75	75	85	85
IVO (CA deg ATDC)	70	80	90	70	80	90	100	110	70	80	90	80	100
10 % MFB (CA ATDC)	372	373	375	359	358	361	361	363	353	357	357	357	360
90 % MFB (CA ATDC)	419	436	433	390	385	382	381	380	382	370	391	383	369
Burn Duration (CA)	53	63	58	31	27	21	20	17	29	13	34	26	30
Peak In-cylinder Pressure, bar	20	20	20	31	31	31	28	28	29	41	30	26	28
Peak heat release rate (J/CA)	14	13	12	19	19	22	16	16	26	45	20	22	22
COV (%)	5.0	13	12	6.5	11	5.1	10	11	11	2.4	10	8.3	8.7

CAI combustion						
EVC (CA deg BTDC)	95	95	95	95	105	105	105
IVO (CA deg ATDC)	70	80	90	100	70	80	90
10 % MFB (CA ATDC)	365	364	361	359	364	364	363
90 % MFB (CA ATDC)	384	383	380	385	379	376	379
Burn Duration (CA)	19	19	19	26	15	12	16
Peak In-cylinder Pressure, bar	29	29	30	27	30	32	29
Peak heat release rate (J/CA)	32	21	48	34	23	31	21
COV (%)	6.51	8.19	5.96	7.52	6.85	2.65	7.12

Table 5.10 10%, 90% MFB, burn duration and peak in-cylinder pressure for the shorter CAI camshaft at SOI 120 CA deg ATDC

SI combustion- Ignition Timing 20 CA deg BTDC									CAI combustion		
EVC (CA deg BTDC)	55	55	65	65	65	65	65	75	95	95	95
IVO (CA deg ATDC)	80	90	70	80	90	100	110	80	70	80	90
10 % MFB (CA ATDC)	365	371	353	354	357	358	360	354	365	363	360
90 % MFB (CA ATDC)	435	434	387	387	377	388	391	376	382	383	385
Burn Duration (CA)	70	63	34	33	20	30	31	22	17	20	25
Peak In-cylinder Pressure, bar	20	20	30	32	38	29	29	40	29	29	28

Peak heat release rate (J/CA)	21	12	16	18	30	18	18	28	34	26	15
COV (%)	8.74	10.7	14.2	8.15	6.53	12.5	14.4	4.65	7.0	8.2	9.01

Table 5.11 10%, 90% MFB, burn duration and peak in-cylinder pressure for the longer CAI camshaft at SOI -30 CA deg ATDC

SI combustion- Ignition Timing 20 CA deg BTDC										
EVC (CA deg BTDC)	55	55	65	65	65	65	65	65		
IVO (CA deg ATDC)	60	70	60	70	80	90	100	110		
10 % MFB (CA ATDC)	360	358	344	350	352	347	347	346		
90 % MFB (CA ATDC)	375	370	371	381	374	384	379	376		
Burn Duration (CA)	15	12	27	31	22	37	32	30		
Peak In-cylinder Pressure (bar)	36	43	27	31	37	39	41	42		
Peak heat release rate (J/CA)	58	64	18	20	31	39	41	46		
COV (%)	5.97	2.09	6.9	1.7	1.57	1.73	2.20	2.50		
CAI combustion										
EVC (CA deg BTDC)	75	75	75	85	85	85	95	95	95	105	105
IVO (CA deg ATDC)	90	100	110	90	100	110	90	100	110	90	100
10 % MFB (CA ATDC)	356	353	360	363	361	359	358	360	357	357	359
90 % MFB (CA ATDC)	375	371	376	381	383	384	384	383	379	380	382
Burn Duration (CA)	19	18	16	18	22	25	26	23	22	23	23
Peak In-cylinder Pressure (bar)	27	32	34	30	31	30	26	29	29	26	27
Peak heat release rate (J/CA)	46	35	37	32	23	22	25	22	31	15	18
COV (%)	11.3	2.84	1.19	3.64	3.66	3.41	12.4	10.3	9.62	9.49	6.84

Table 5.12 10%, 90% MFB, burn duration and peak in-cylinder pressure for the longer CAI camshaft at SOI 30 CA deg ATDC

SI combustion- Ignition Timing 20 CA deg BTDC								
EVC (CA deg BTDC)	55	55	65	65	65	65	65	65
IVO (CA deg ATDC)	60	70	60	70	80	90	100	110
10 % MFB (CA ATDC)	360	359	342	347	350	350	352	353
90 % MFB (CA ATDC)	380	374	378	384	382	378	373	373
Burn Duration (CA)	20	15	36	37	32	28	21	20
Peak In-cylinder Pressure (bar)	33	39	24	28	25	35	40	39
Peak heat release rate (J/CA)	29	27	23	24	31	26	32	33
COV (%)	3.05	3.19	6.29	7.55	3.83	1.41	4.93	1.73
CAI combustion								
EVC (CA deg BTDC)	75	75	75	85	85	85	95	105	105
IVO (CA deg ATDC)	90	100	110	90	100	110	100	90	100
10 % MFB (CA ATDC)	358	362	362	360	359	361	360	360	363
90 % MFB (CA ATDC)	377	381	385	383	381	381	379	380	379
Burn Duration (CA)	19	19	23	23	22	20	19	20	16
Peak In-cylinder Pressure (bar)	26	26	28	26	27	27	25	24	25
Peak heat release rate (J/CA)	49	43	24	24	26	24	30	22	23
COV (%)	11.69	12.58	4.70	7.24	5.64	14.9	9.2	7.11	12.35

Table 5.13 10%, 90% MFB, burn duration and peak in-cylinder pressure for the longer CAI camshaft at SOI 120 CA deg ATDC

SI combustion- Ignition Timing 20 CA deg BTDC							CAI combustion		
EVC (CA deg BTDC)	55	55	65	65	65	65	75	75	75
IVO (CA deg ATDC)	60	70	80	90	100	110	90	100	110
10 % MFB (CA ATDC)	356	357	349	354	354	356	362	358	357

90 % MFB (CA ATDC)	381	372	376	379	382	379	379	377	378
Burn Duration (CA)	25	15	27	25	28	23	17	19	21
Peak In-cylinder Pressure (bar)	32	38	29	33	35	38	24	26	26
Peak heat release rate (J/CA)	32	35	26	20	22	31	35	20	23
COV (%)	12.16	3.2	9.74	11.59	4.76	1.57	4.67	2.71	5.26
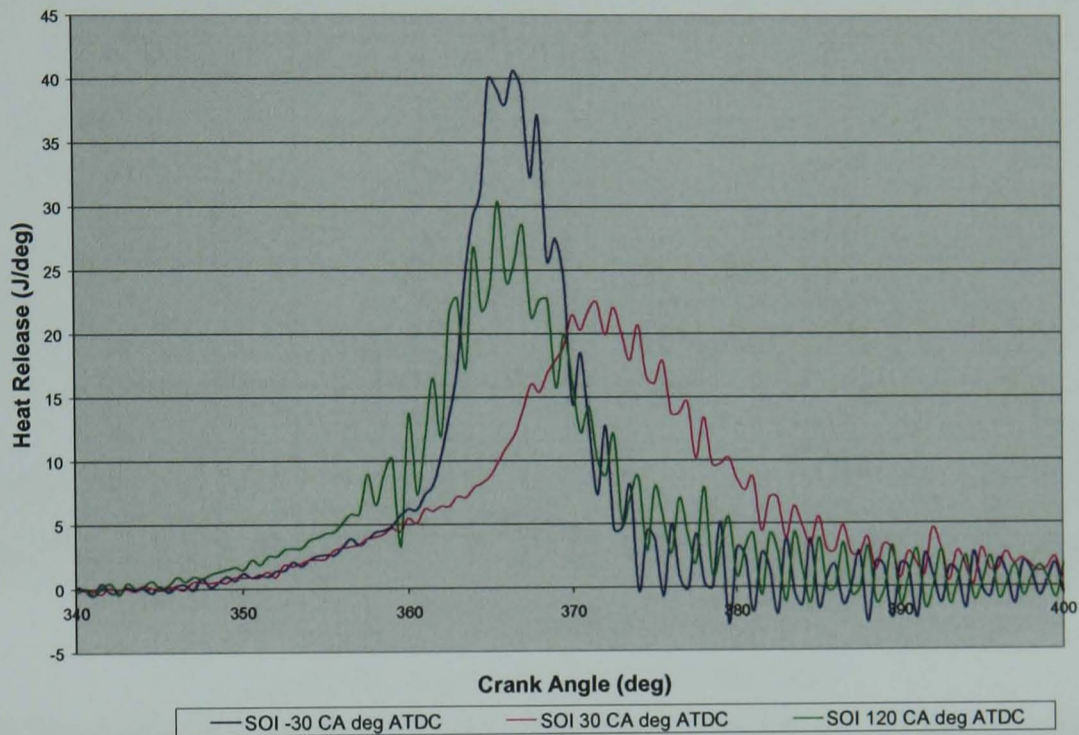
Figure 5.46 Heat Release versus Crank angle for the shorter CAI camshafts at EVC 65 CA deg BTDC, IVO 70 CA deg ATDC, 1500 rpm, lambda 1.2
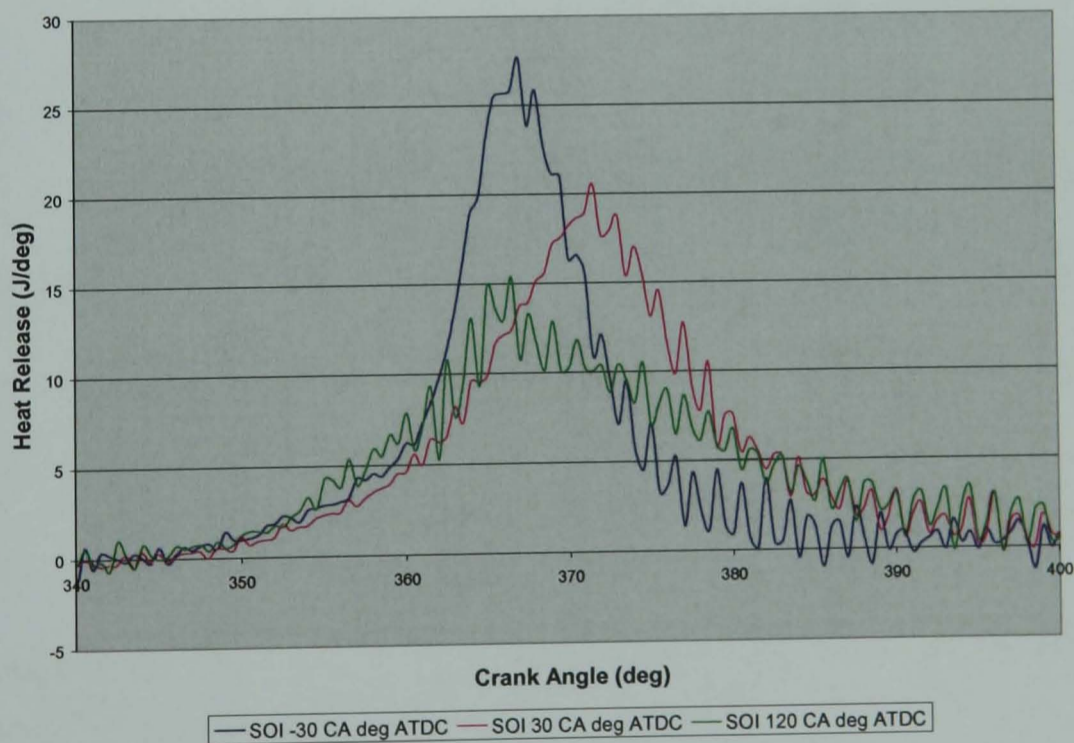
Figure 5.47 Heat Release versus Crank angle for the shorter CAI camshafts at EVC 75 CA deg BTDC, IVO 80 CA deg ATDC, 1500 rpm, lambda 1.2
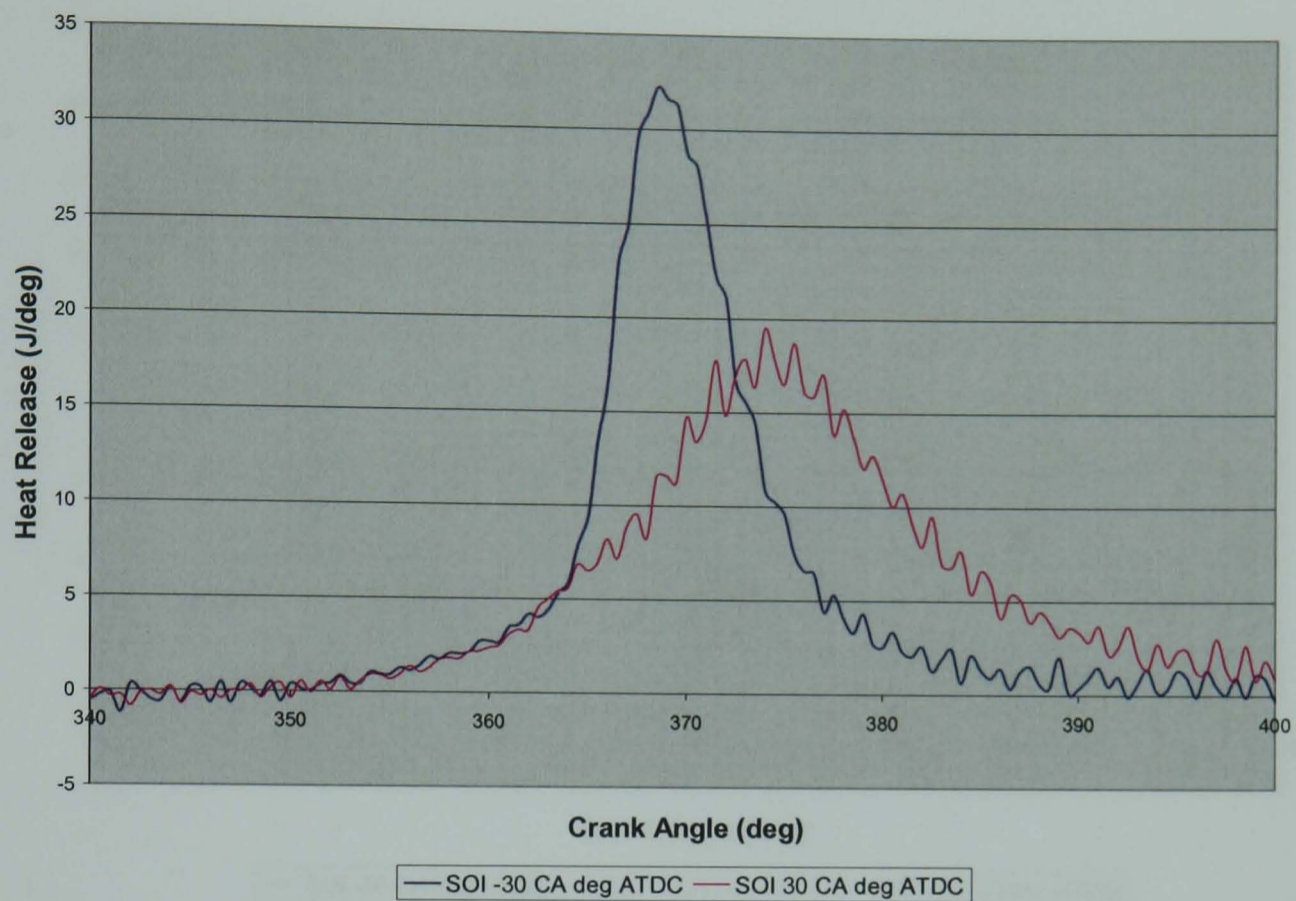
Figure 5.48 Heat Release versus Crank angle for the shorter CAI camshafts at EVC 85 CA deg BTDC, IVO 80 CA deg ATDC, 1500 rpm, lambda 1.2
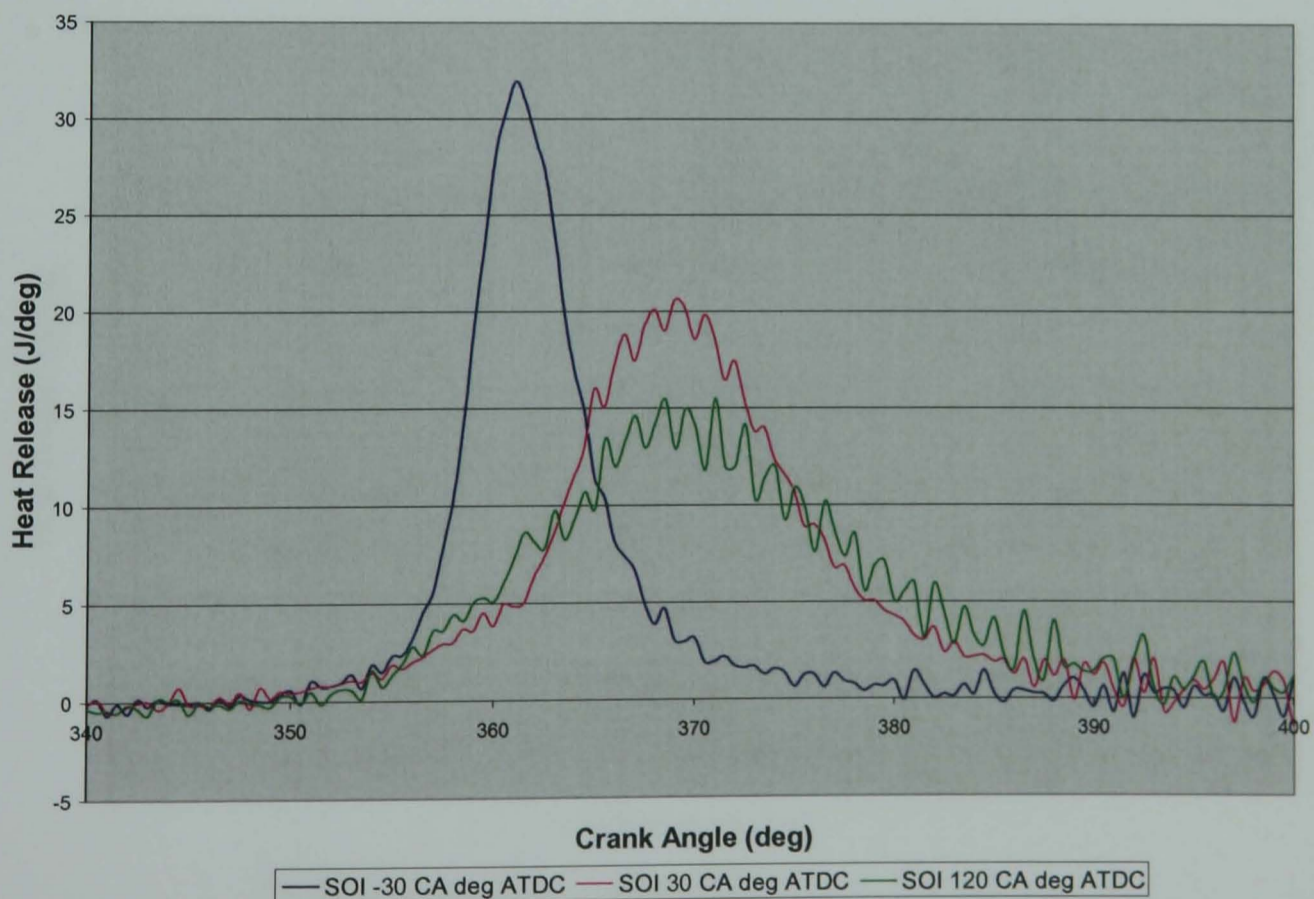
Figure 5.49 Heat Release versus Crank angle for the shorter CAI camshafts at EVC 95 CA deg BTDC, IVO 90 CA deg ATDC, 1500 rpm, lambda 1.2
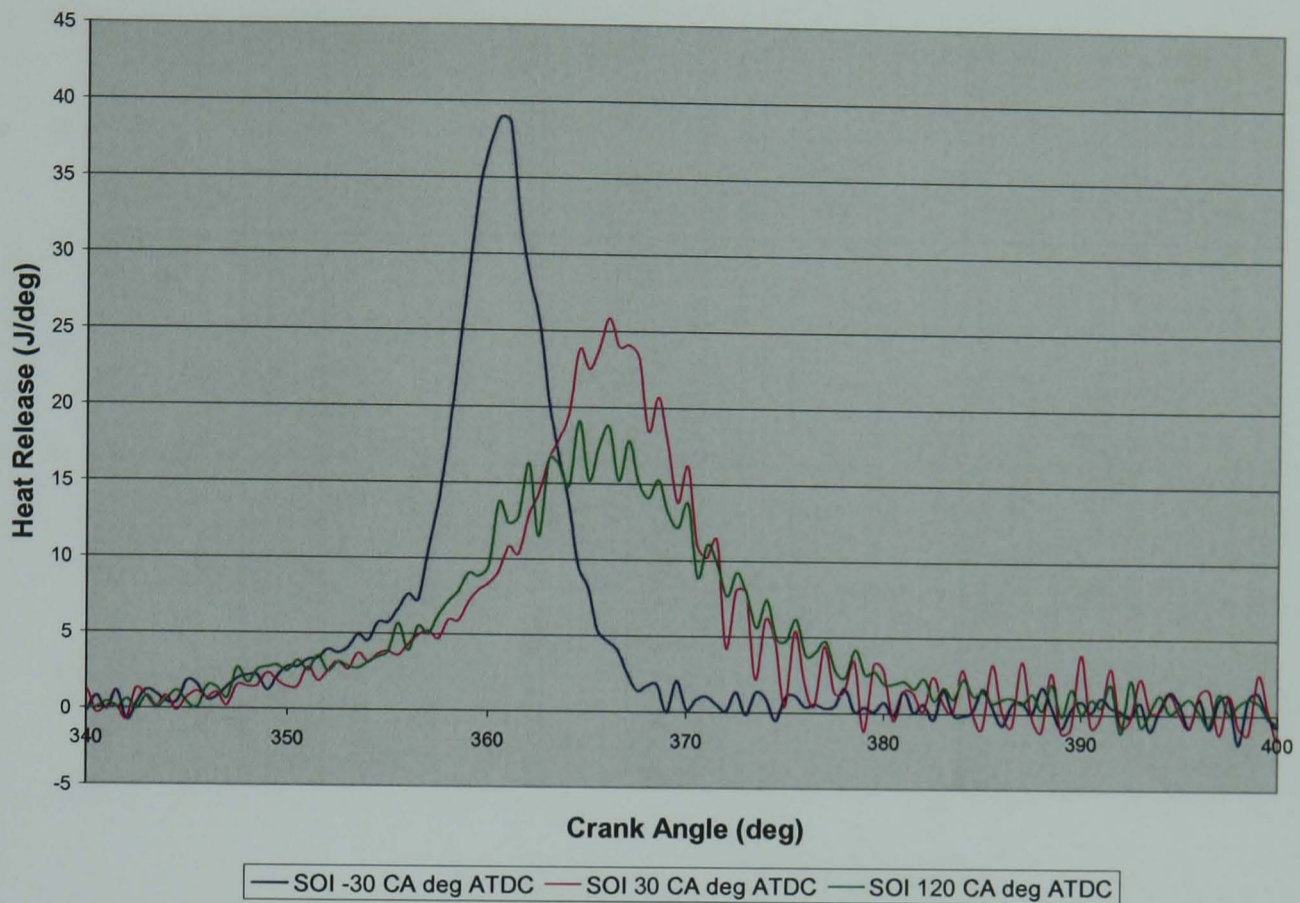
Figure 5.50 Heat Release versus Crank angle for the longer CAI camshafts at EVC 65 CA deg BTDC, IVO 90 CA deg ATDC, 1500 rpm, lambda 1.2
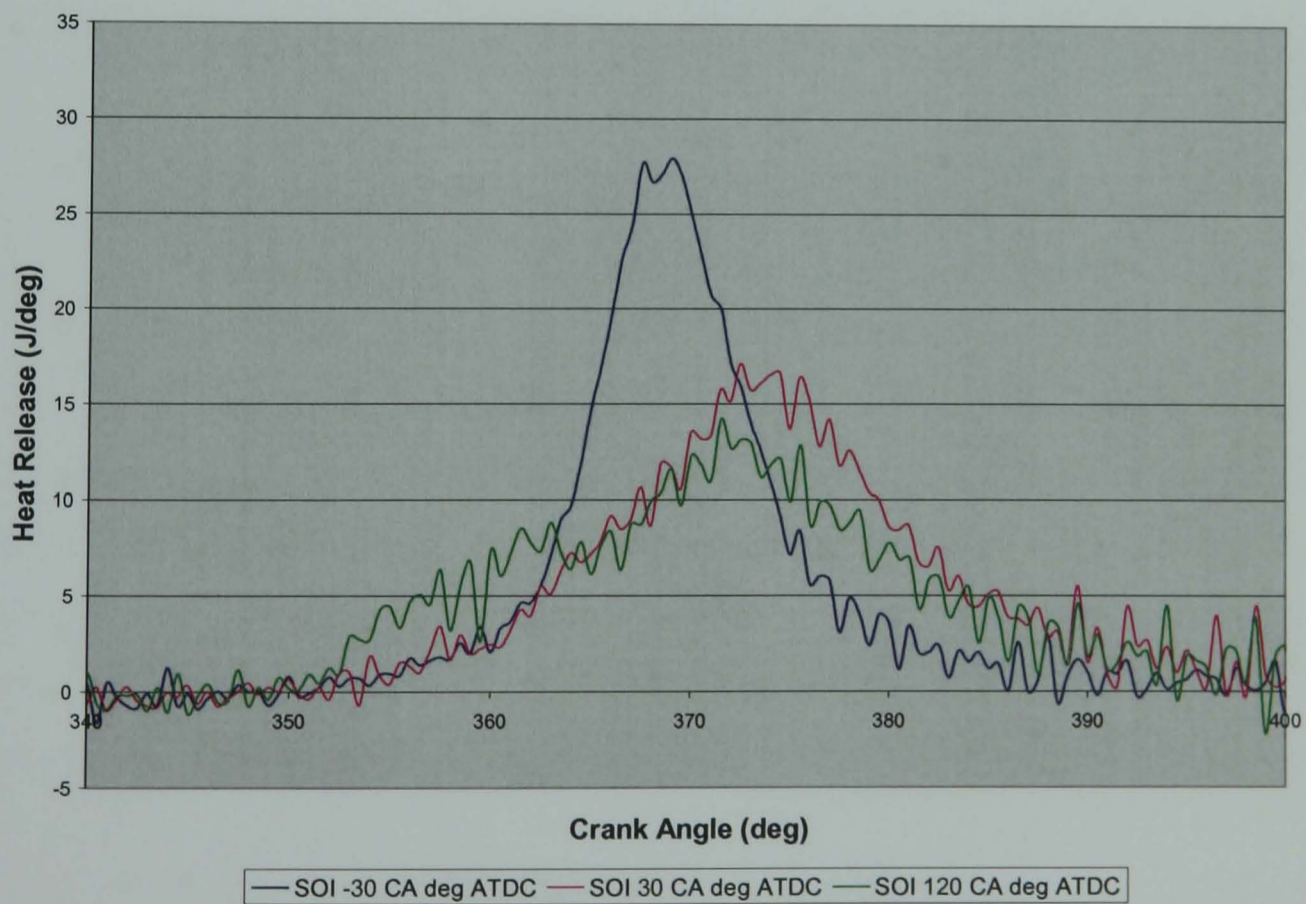
Figure 5.51 Heat Release versus Crank angle for the longer CAI camshafts at EVC 75 CA deg BTDC, IVO 90 CA deg ATDC, 1500 rpm, lambda 1.2
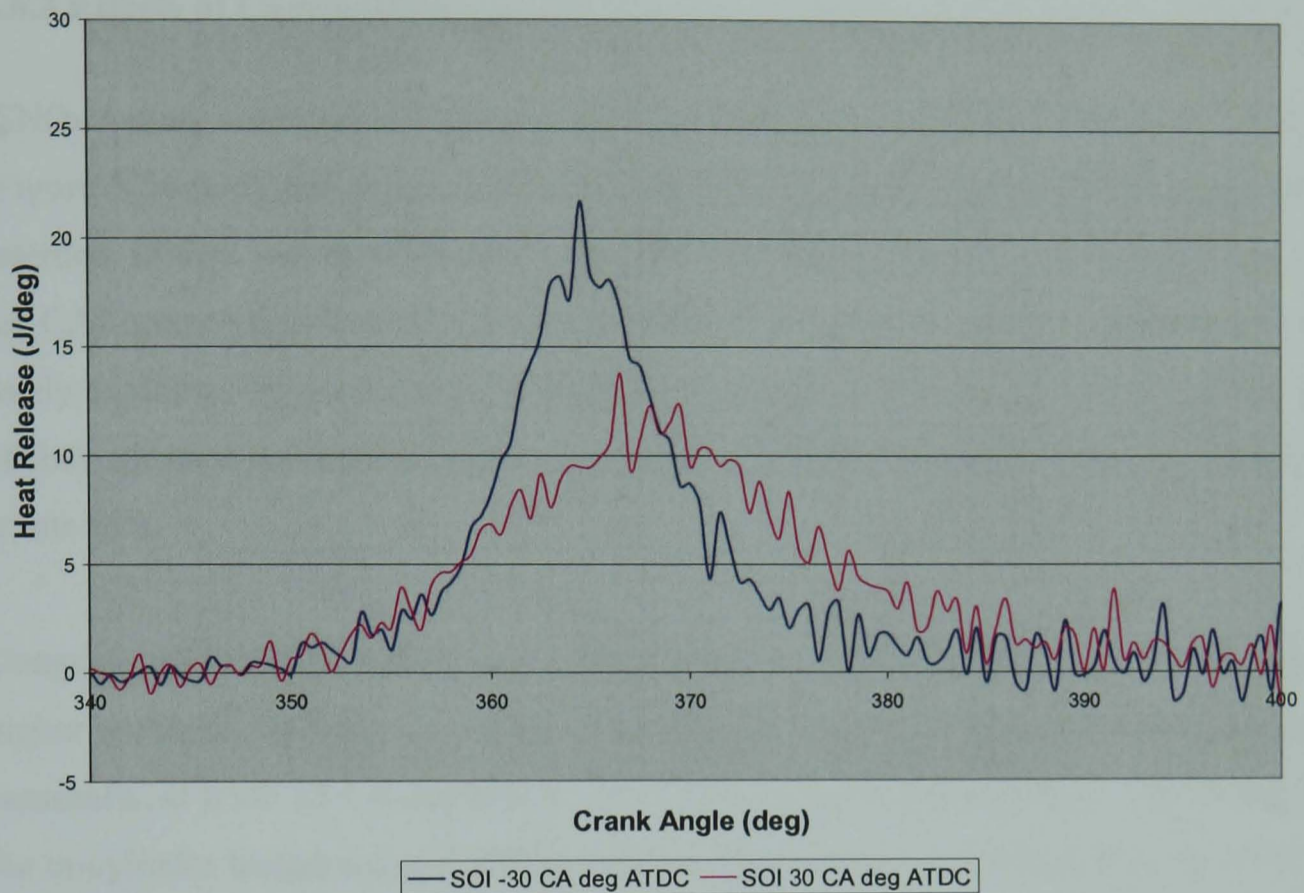
Figure 5.52 Heat Release versus Crank angle for the longer CAI camshafts at EVC 85 CA deg BTDC, IVO 90 CA deg ATDC, 1500 rpm, lambda 1.2
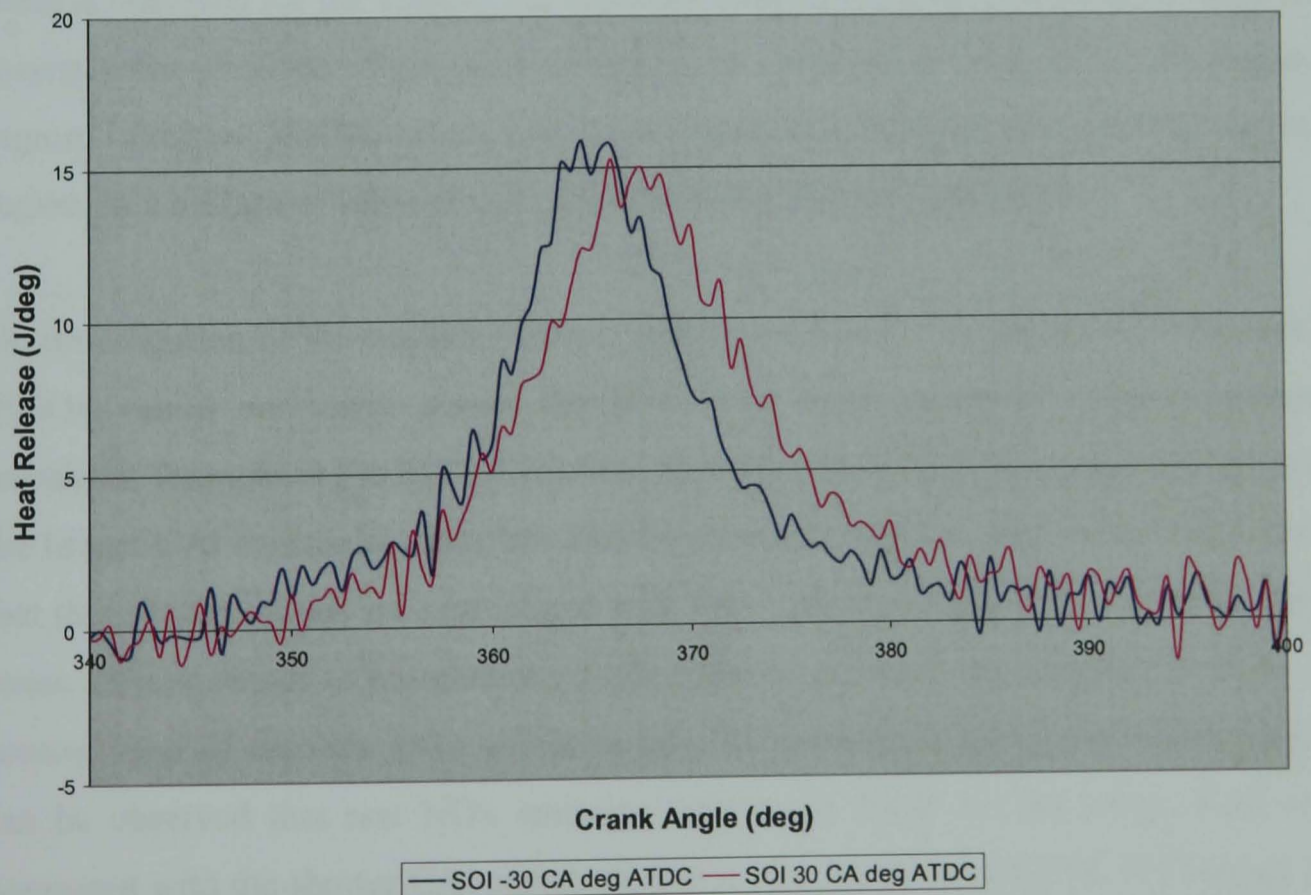
Figure 5.53 Heat Release versus Crank angle for the longer CAI camshafts at EVC 95 CA deg BTDC, IVO 100 CA deg ATDC, 1500 rpm, lambda 1.2

5.6.3 Effects of Camshaft Design and Injection Timing on Emissions at Lambda = 1.2

ISNOx values increased as SOI was retarded for both the shorter and longer CAI camshafts (Figure 5.54 (a-c) and Figure 5.55 (a-c)). At lambda 1.0, it was observed that as SOI was retarded, ISNOx values decreased in the CAI operational region. This trend is the opposite for CAI operation at lambda 1.2, where ISNOx increases as SOI is retarded. This may be partly explained by the increase in spatially averaged peak cylinder temperature as the start of fuel injection is retarded (Figure 5.58 (a-c) and Figure 5.59 (a-c)) and less homogeneity at late SOI.

Comparison of ISNOx values within the SI and CAI region indicate that ISNOx values are higher within the SI region compared with the CAI region as expected. For the shorter CAI camshafts, at EVC 55 CA deg BTDC, IVO 80 CA deg ATDC and SOI -30 CA deg ATDC, the in-cylinder temperature is 2185K and the ISNOx value is 1.67 g/kW.h. At EVC 90 CA deg BTDC, IVO 85 CA deg ATDC and SOI -30 CA deg ATDC, the in-cylinder temperature drops to 1500K causing the ISNOx value to drop to 0.11 g/kW.h. A similar trend is observed for the longer CAI camshafts, the in-cylinder temperatures range from the lowest value of 995K within the CAI region, to a maximum value of 1760K within the SI region. Likewise, ISNOx values vary from a maximum value of 4.53 g/kW.h, within the SI region, to a minimum value of 0.22 g/kW.h, within the CAI region.

On investigation of the contour maps, it is apparent that for the shorter CAI camshafts, the ISNOx values are lower across the EVC-IVO range compared with the longer CAI camshafts throughout the SI/CAI regions. However, In-cylinder temperatures are lower for the longer CAI camshafts, therefore ISNOx values should also be lower. This is due to the fact that ISNOx values are normalized with ISFC values, therefore a large ISFC value will cause ISNOx values to be relatively high. Figure 5.56 (a-c) and Figure 5.57 (a-c) show a contour map of absolute NOx values in ppm for the shorter and longer CAI camshafts. It can be observed that raw NOx emission values are lower for the longer CAI camshaft compared with the shorter CAI camshaft; this is true for the entire EVC-IVO range. For the longer CAI camshafts, at EVC 95 CA deg BTDC, IVO 80 CA deg ATDC and SOI -30 CA

deg ATDC the NOx value is 26 ppm. For the shorter CAI camshafts at the same valve timing and injection timing the NOx value is 46 ppm. Therefore, the lower in-cylinder temperature observed for the longer CAI camshafts cause lower NOx emissions, however this is not reflected fully in the ISNOx value since ISNOx values are normalized with ISFC.

It was observed that ISHC values increased as fuel injection timing was retarded; this was true for both the shorter and longer CAI camshafts (Figure 5.60 (a-c) and Figure 5.61 (a-c)). The reason for this is that there is less mixing time at retarded fuel injection times (SOI 30 and 120 CA deg ATDC). The lack of mixing time leads to fuel rich zones within the combustion chamber and hence an increase in unburned hydrocarbons at late injections. It is apparent that ISHC values are higher for the longer CAI camshafts compared with the shorter CAI camshafts. This is due to lower peak in-cylinder temperatures and a shorter expansion stroke observed for the longer CAI camshafts (Figure 5.59 (a-c)). Raw uHC emission data was also plotted in Figure 5.62 (a-c) and Figure 5.63 (a-c), raw uHC values are also higher for the longer CAI camshafts which collaborates with the trend for ISHC values.

Values of ISHC are higher for the CAI region compared with the SI region for both the shorter and longer CAI camshafts due to lower combustion temperatures.

It was found that ISCO values increased as start of fuel injection was retarded first from -30 CA deg ATDC to 30 CA deg ATDC and then to 120 CA deg ATDC. This was true for both the shorter and longer CAI camshafts (Figure 5.64 (a-c) and Figure 5.65 (a-c)). The reason for the increase in ISCO values as fuel injection timing is retarded is due to mixing time decreasing. With a decrease in mixing time, fuel rich pockets are formed in certain parts of the combustion chamber. All the fuel in these fuel rich pockets does not undergo complete combustion, leading to incomplete combustion products such as ISCO. ISCO values are higher for the longer CAI camshafts compared with the shorter CAI camshafts at any given valve timing. The reason for this trend is that for the longer CAI camshafts, EVO is occurring 20 CA deg earlier compared with the shorter CAI camshaft. This means that the charge is being forced out through the exhaust valve while undergoing oxidation. This

141

leads to incomplete combustion and the production of greater volumes of CO for the longer CAI camshafts compared with the shorter CAI camshafts. Again Raw CO emission data was also plotted in Figure 5.66 (a-c) and Figure 5.67 (a-c), to confirm that raw CO values are in correspondence with ISCO values.

The majority of the lowest ISCO values are observed within the SI region compared with the CAI region. However, there is not a clear trend observed when transition is made from the SI region to the CAI region.
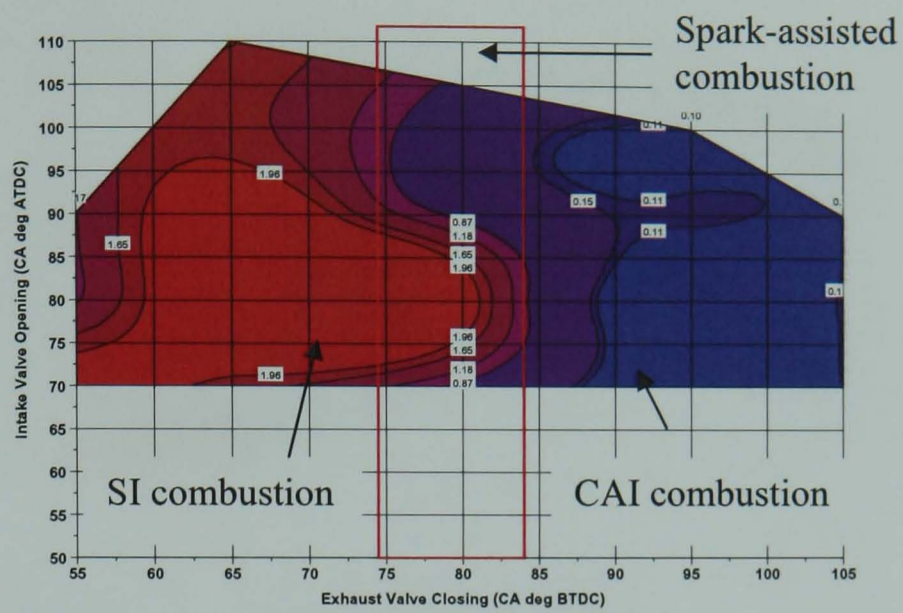
(a) SOI -30 CA deg ATDC
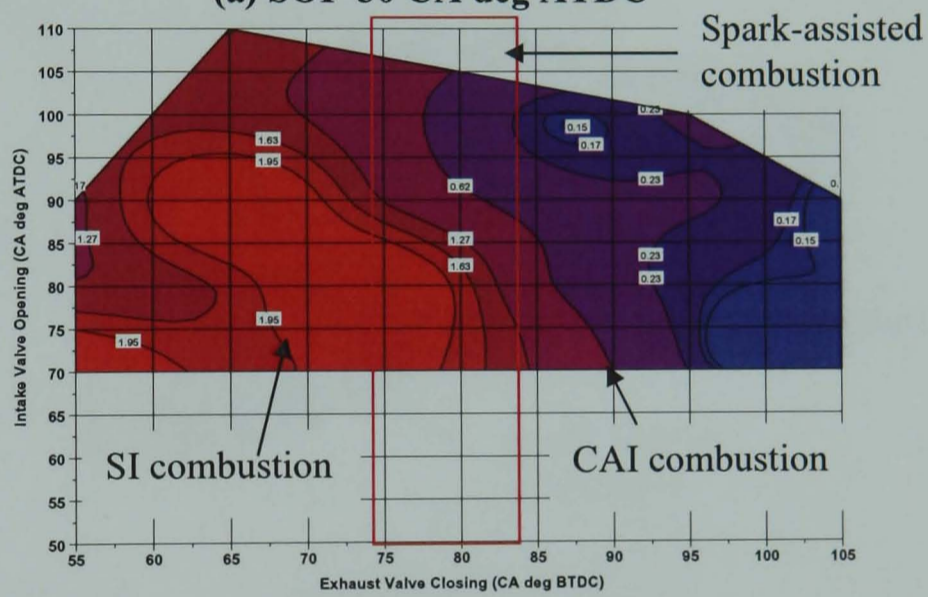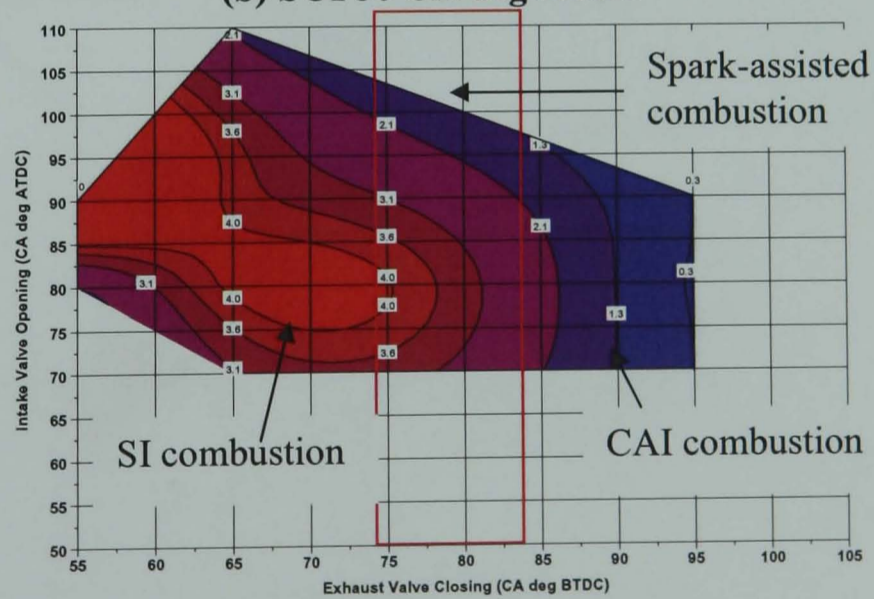
(b) SOI 30 CA deg ATDC

(c) SOI 120 CA deg ATDC

Figure 5.54 (a-c) ISNOx (g/kW.h) at EVC versus IVO timings for the shorter CAI camshaft at lambda 1.2
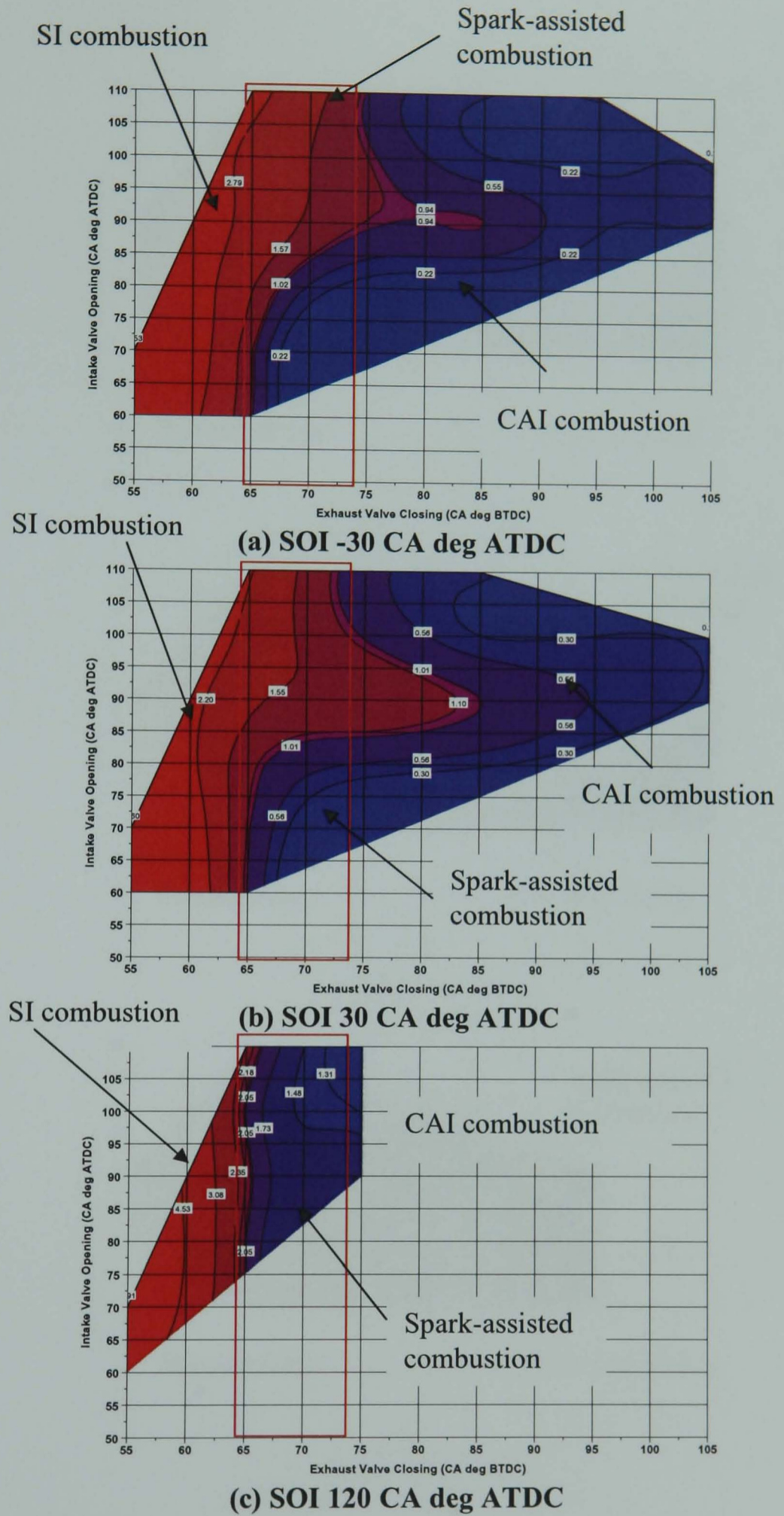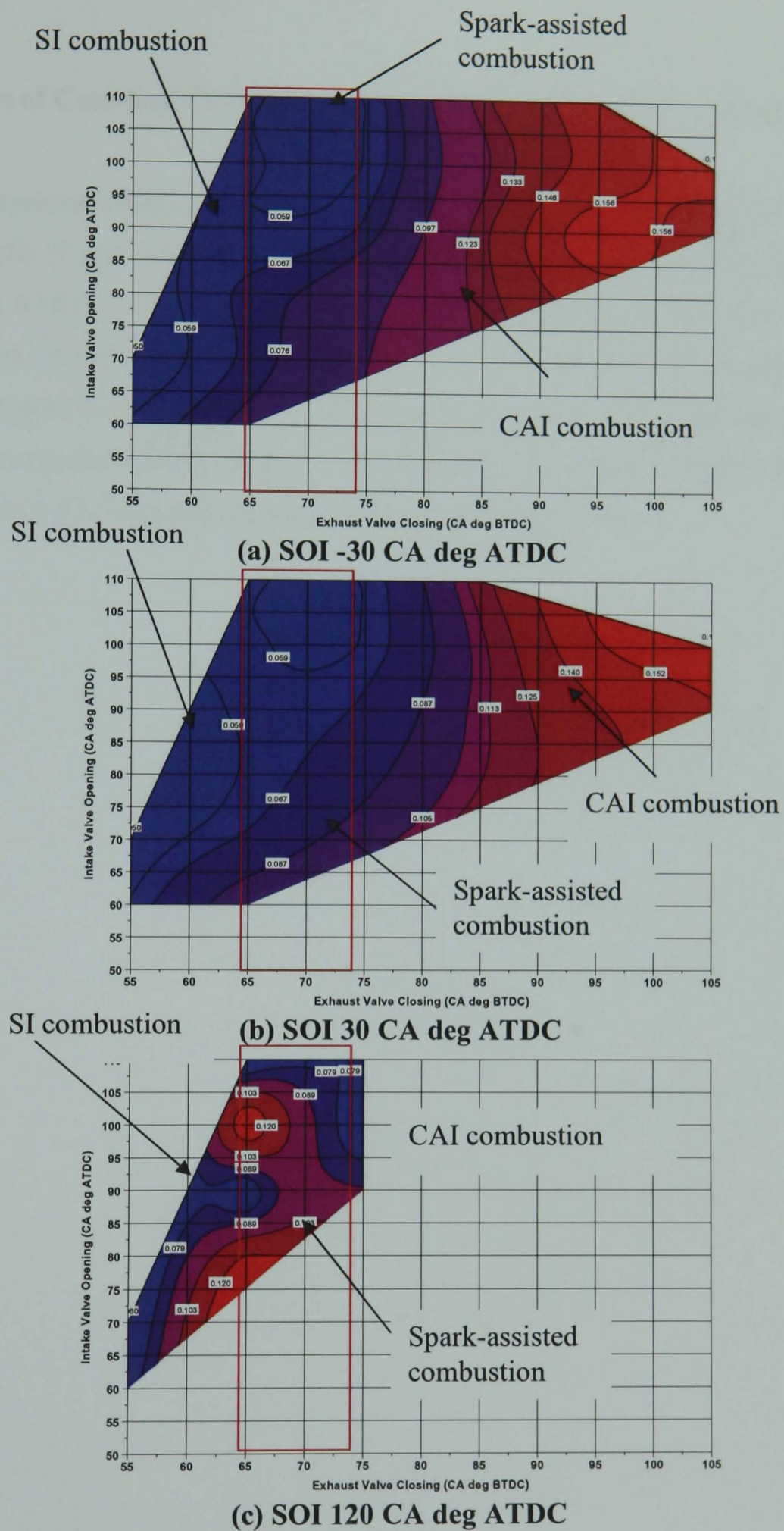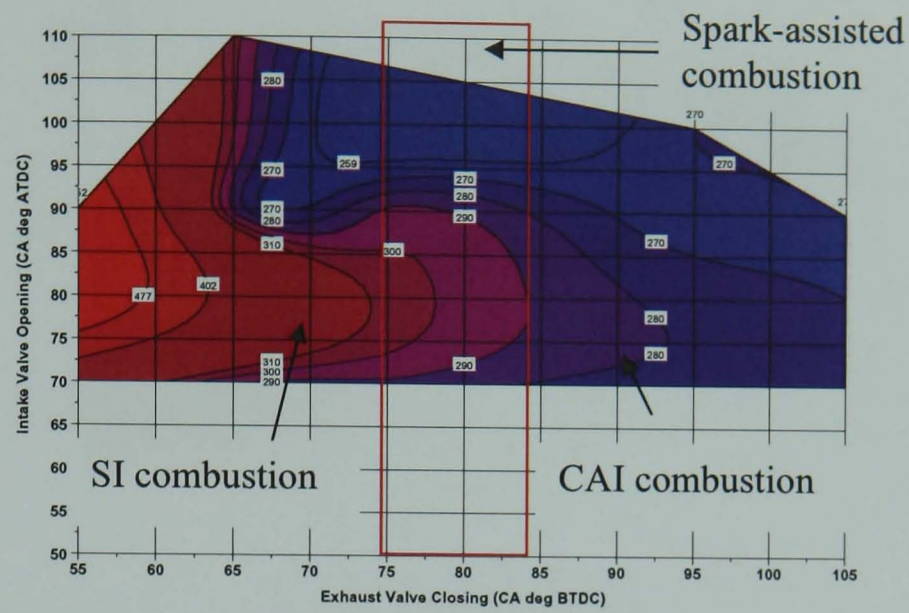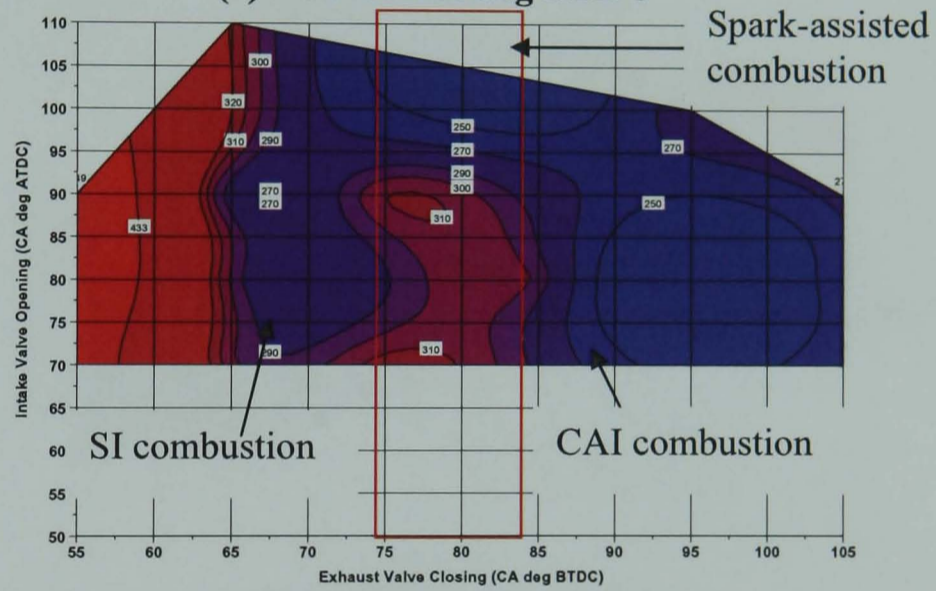
Figure 5.55 (a-c) ISNOx (g/kW.h) at EVC versus IVO timings for the longer CAI camshaft at lambda 1.2

144
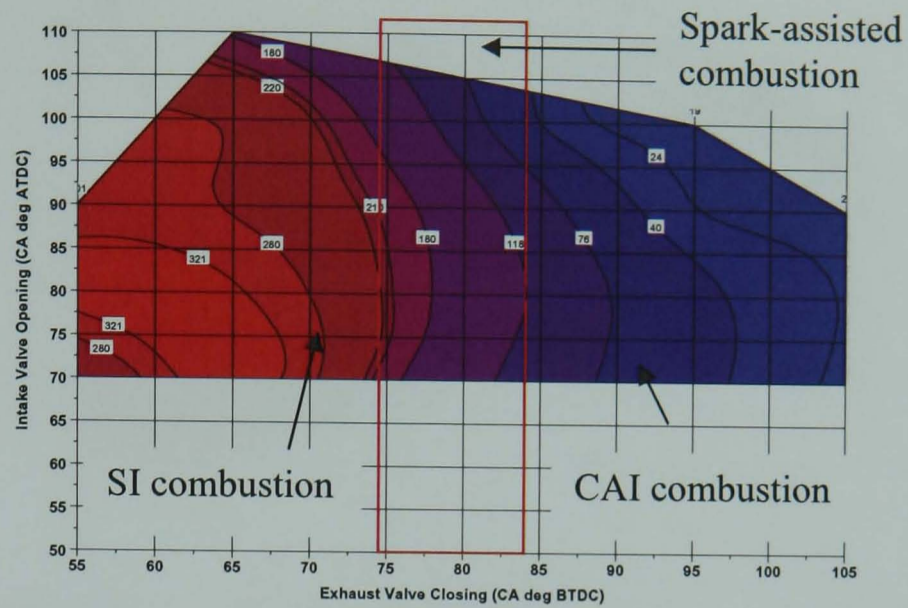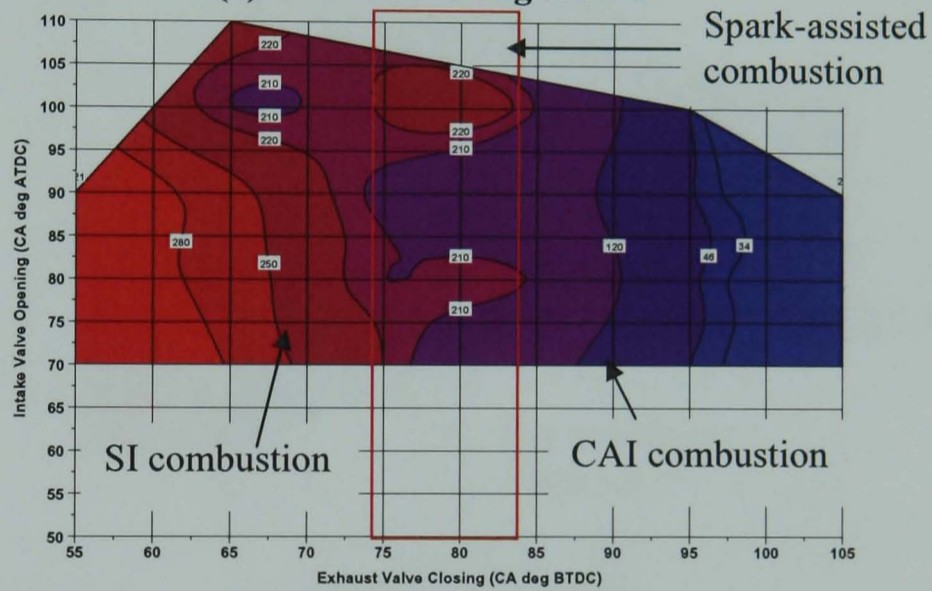
(a) SOI -30 CA deg ATDC
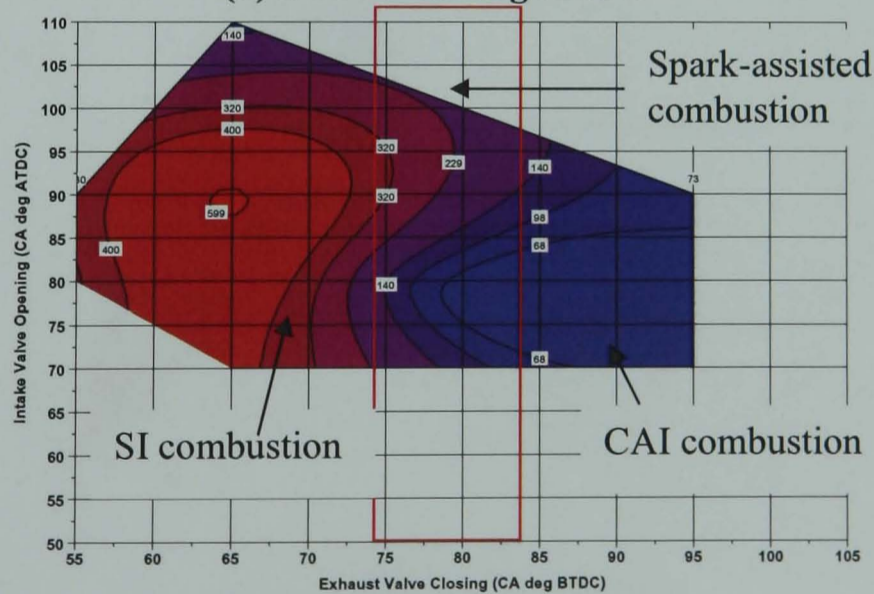
(b) SOI 30 CA deg ATDC

(c) SOI 120 CA deg ATDC

Figure 5.56 (a-c) NOx values (ppm) at EVC versus IVO timings for the shorter CAI camshaft at lambda 1.2
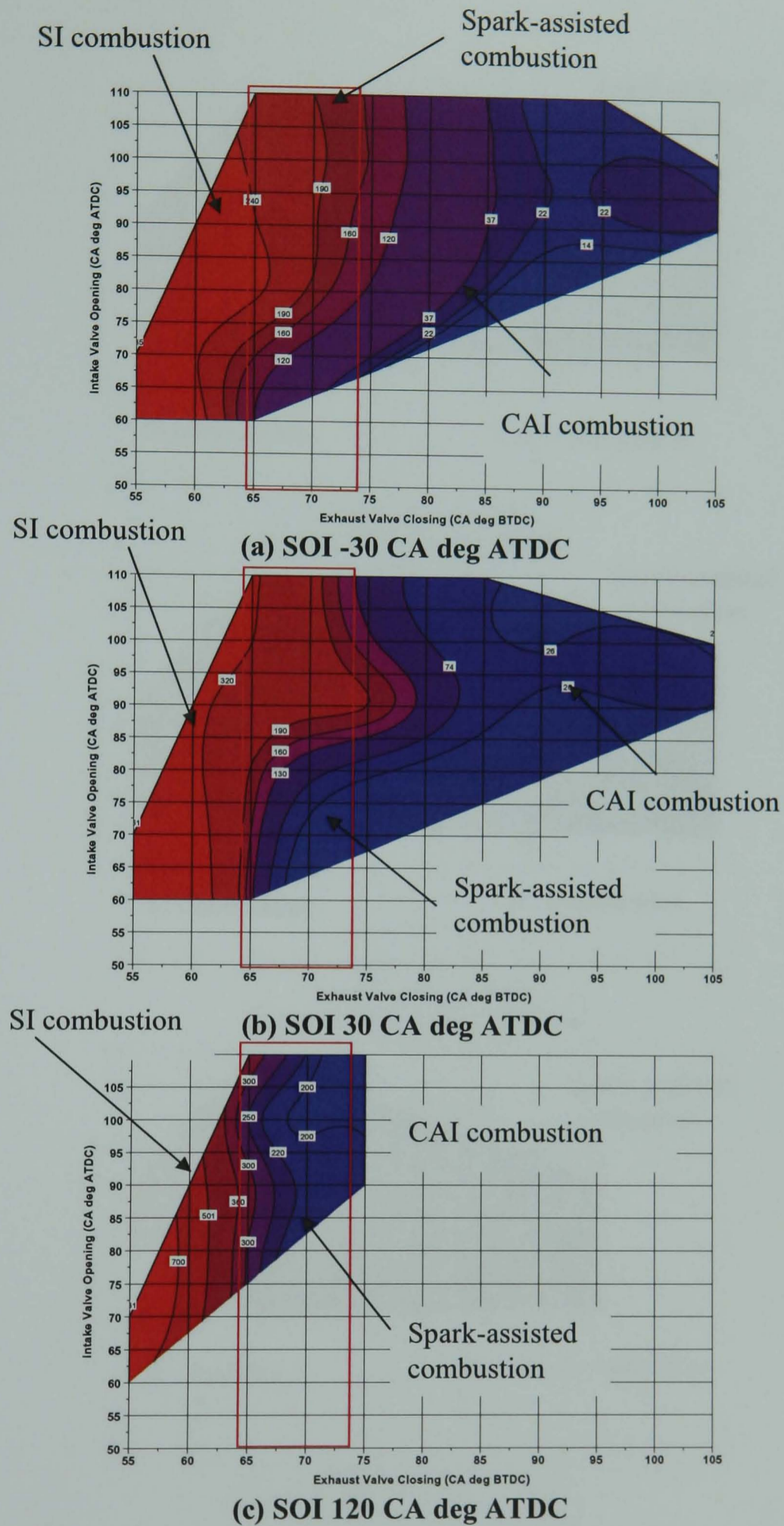
Figure 5.57 (a-c) NOx values (ppm) at EVC versus IVO timings for the longer CAI camshaft at lambda 1.2
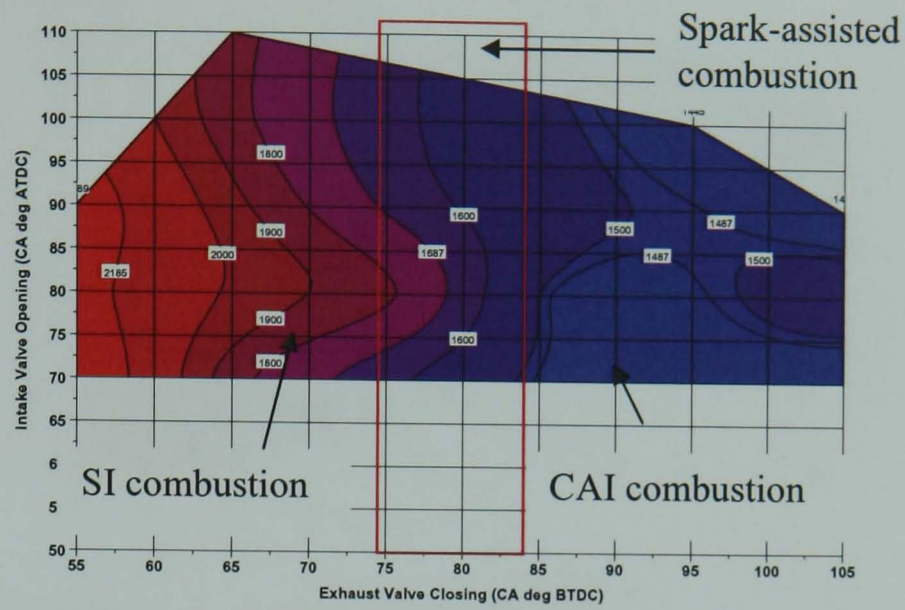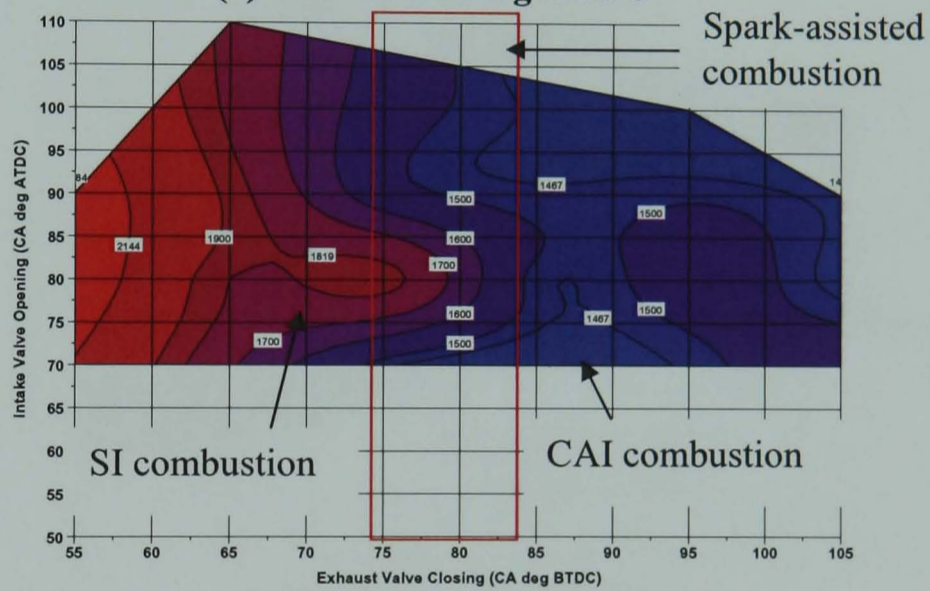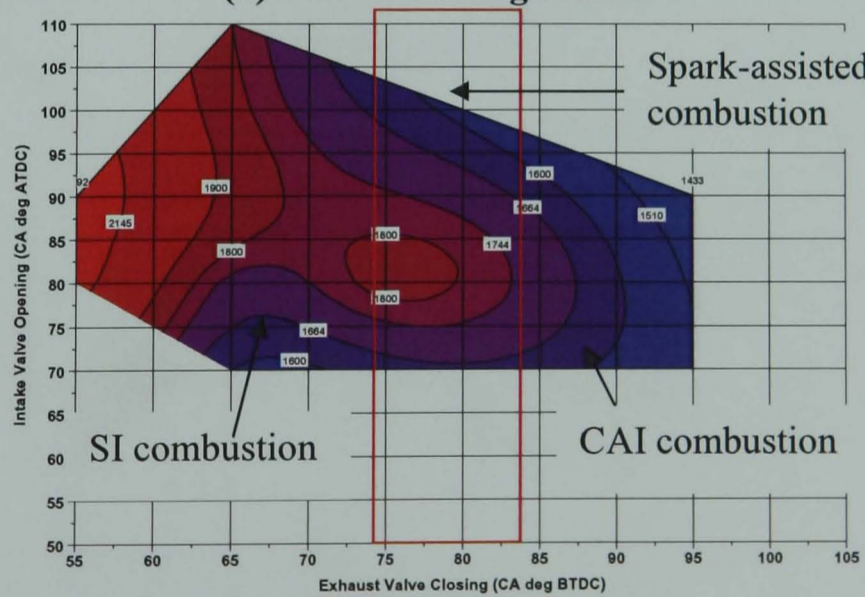
Figure 5.58 (a-c) In-cylinder Temperature [K] at EVC versus IVO timings for the shorter CAI camshaft at lambda 1.2
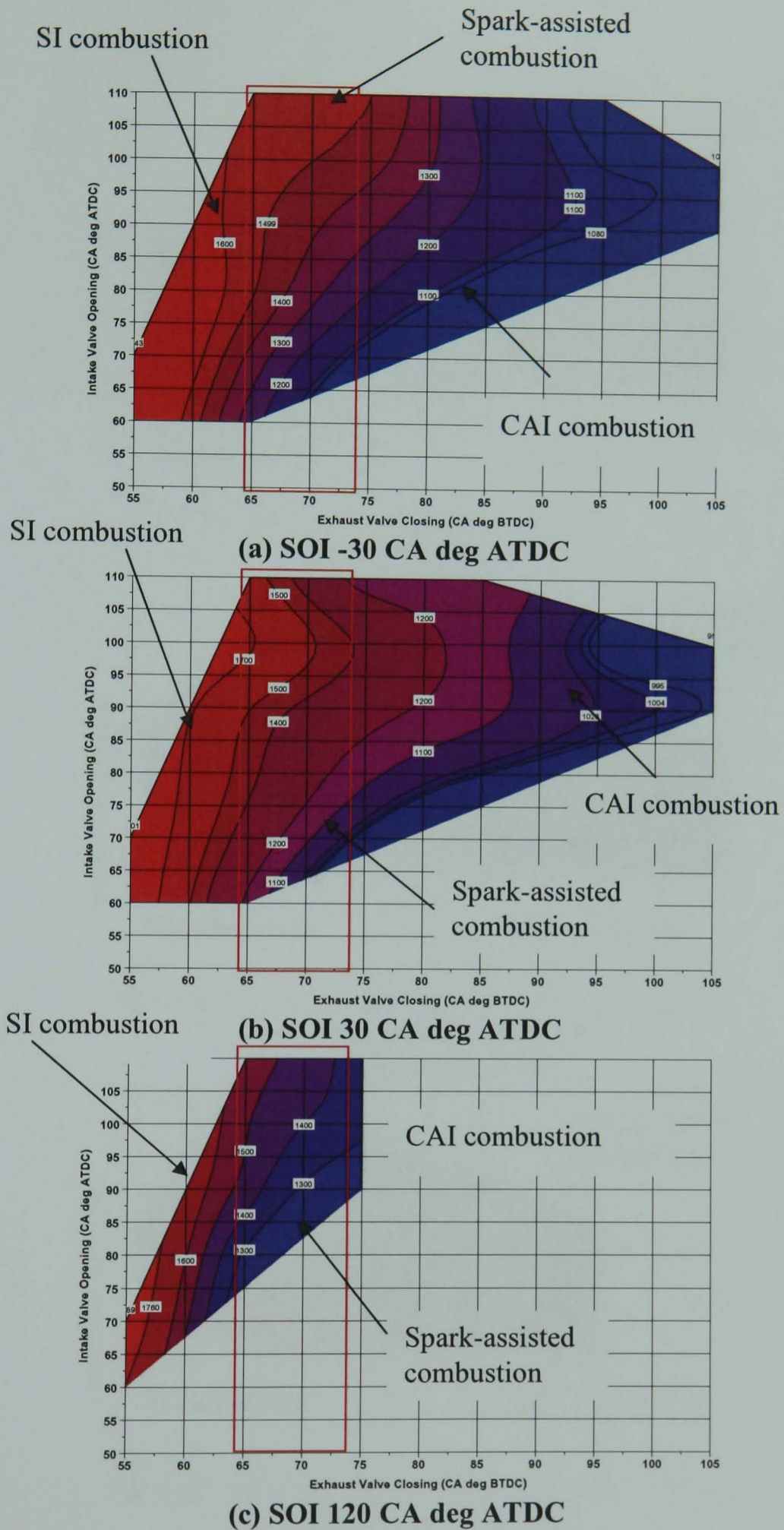
Figure 5.59 (a-c) In-cylinder Temperature [K] at EVC versus IVO timings for the longer CAI camshaft at lambda 1.2
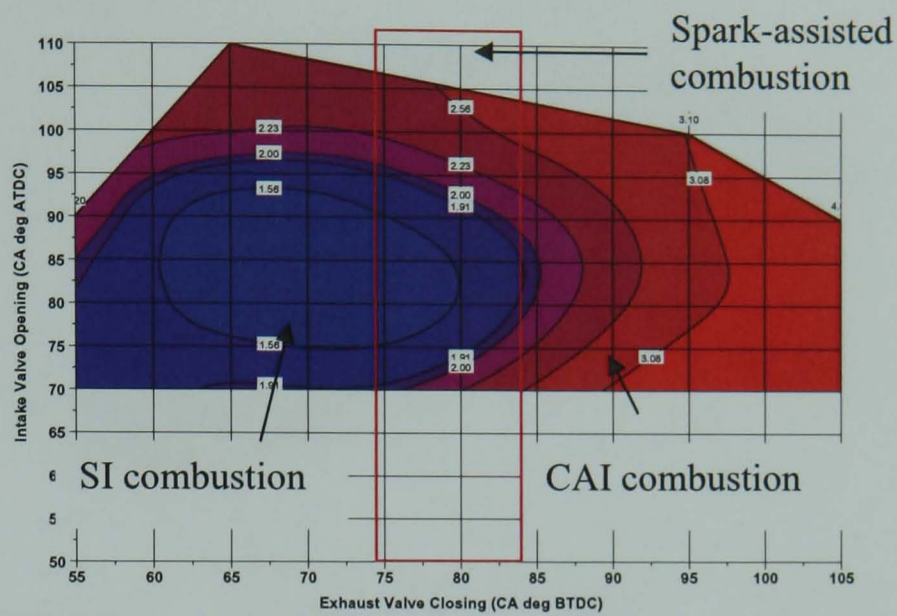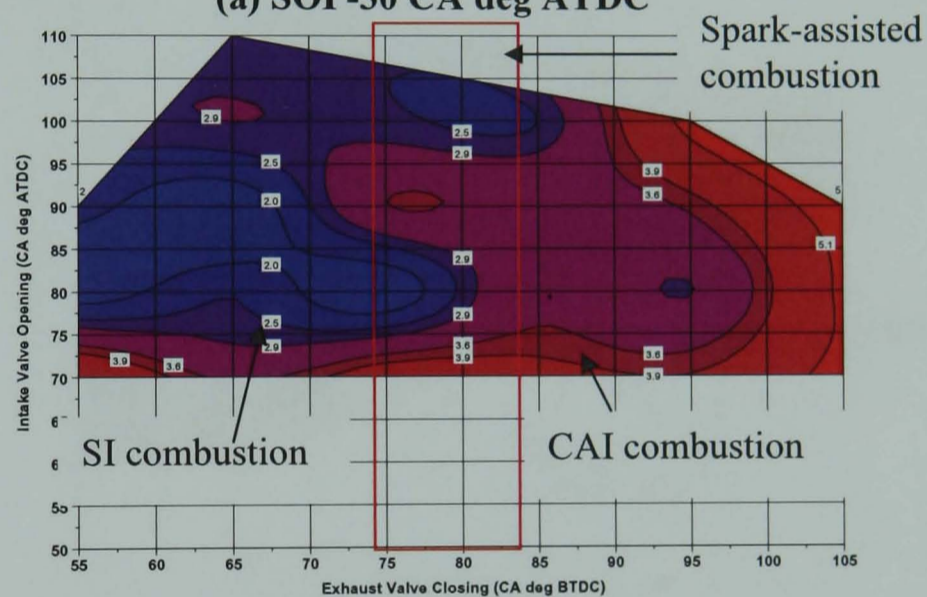
(a) SOI -30 CA deg ATDC
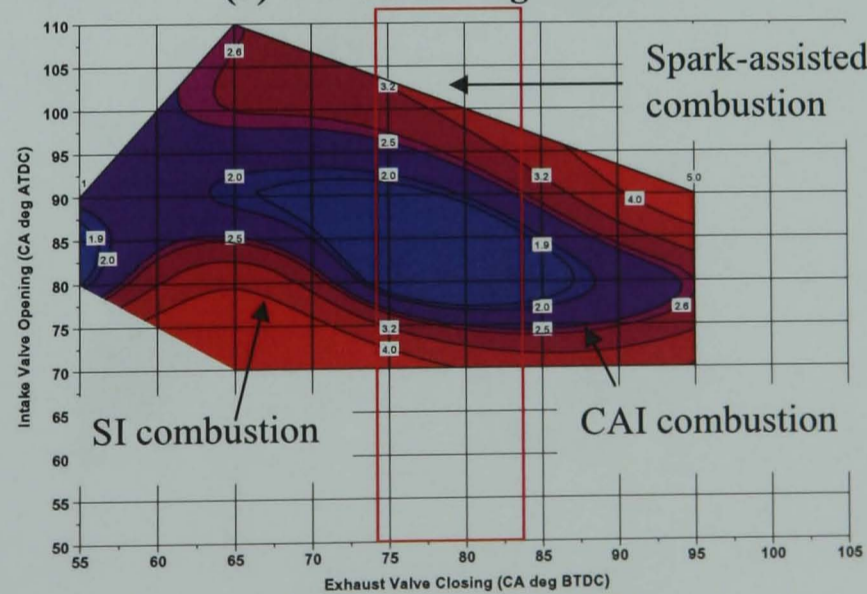
(b) SOI 30 CA deg ATDC

(c) SOI 120 CA deg ATDC

Figure 5.60 (a-c) ISHC (g/kW.h) at EVC versus IVO timings for the shorter CAI camshaft at lambda 1.2
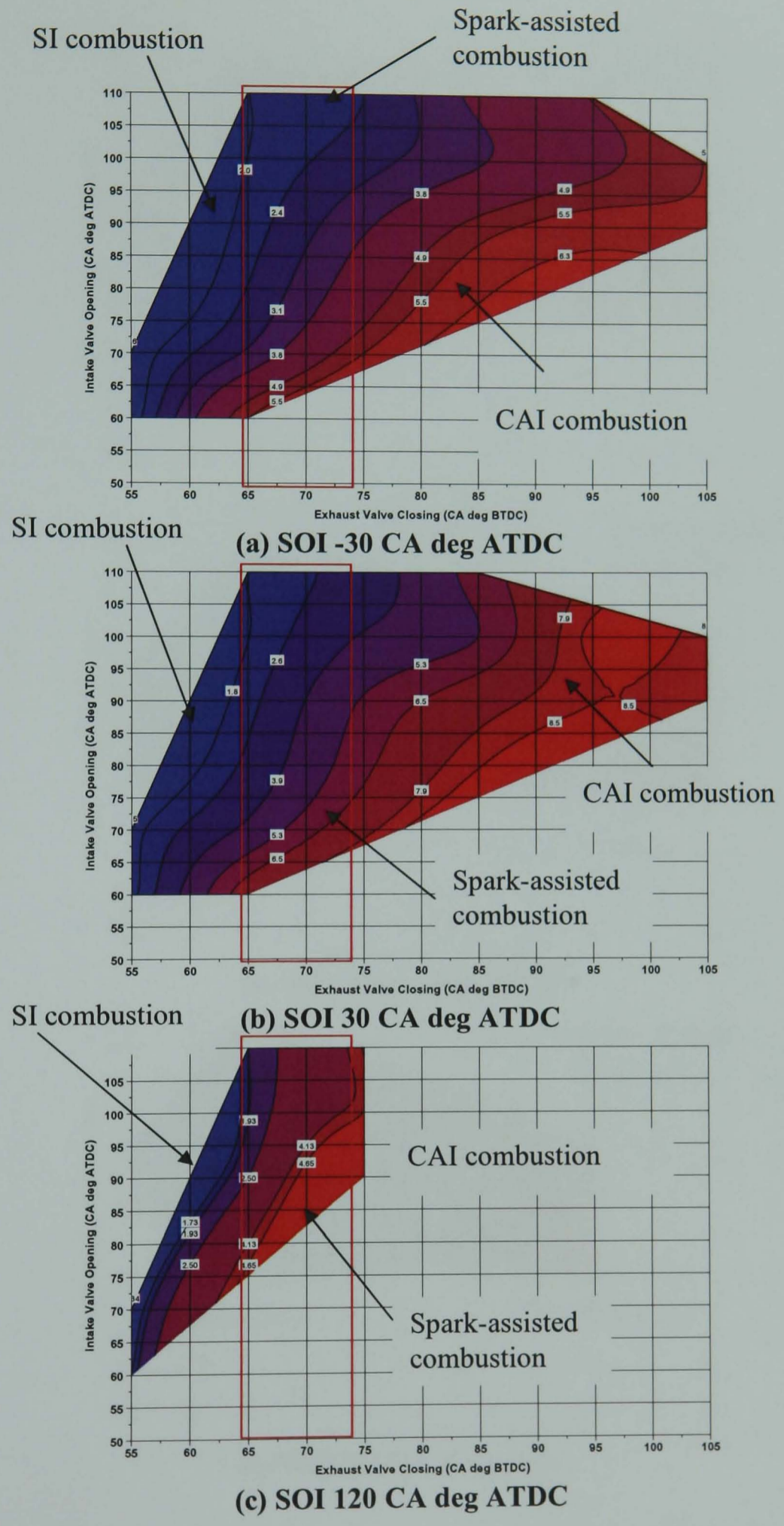
Figure 5.61 (a-c) ISHC (g/kW.h) at EVC versus IVO timings for the longer CAI camshaft at lambda 1.2
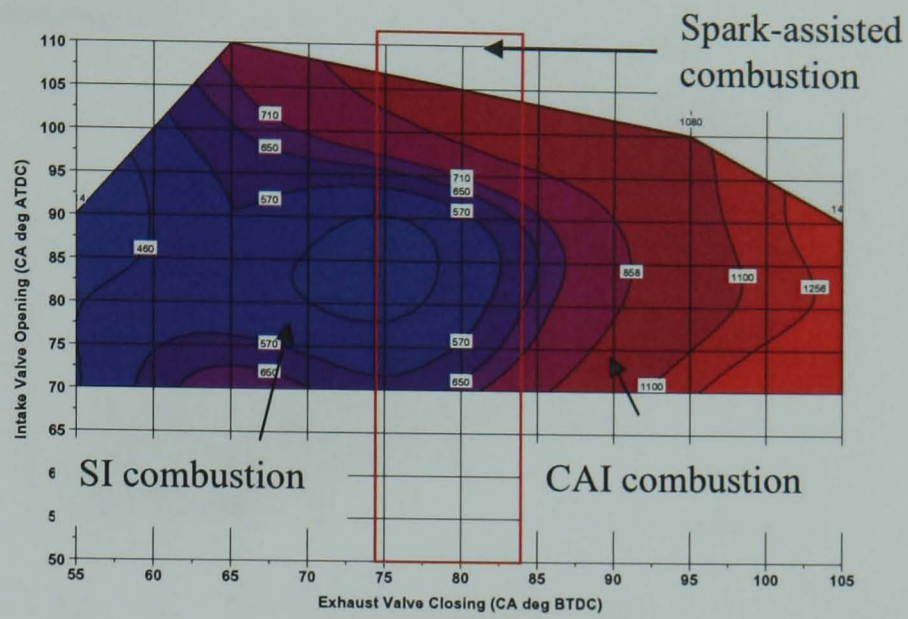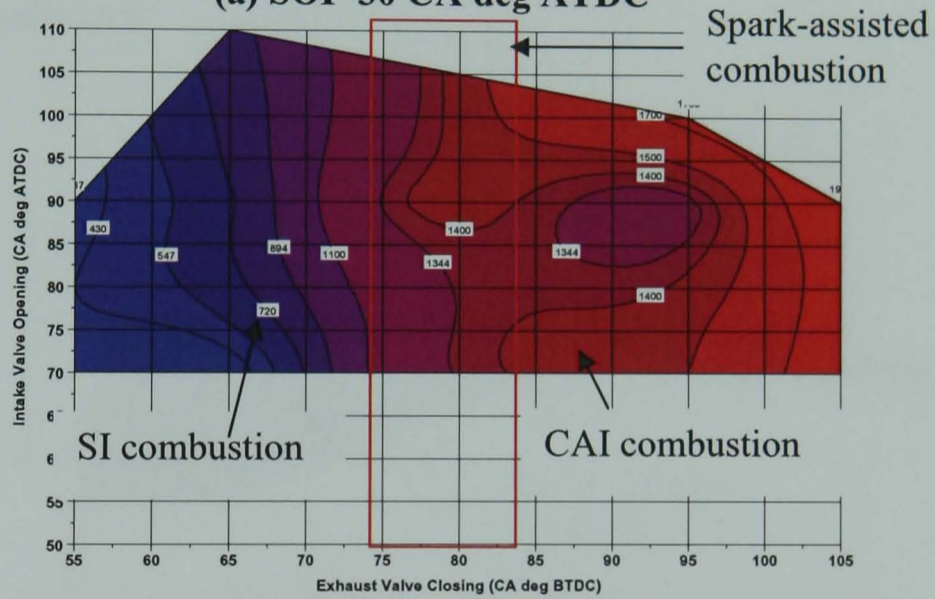
(a) SOI -30 CA deg ATDC
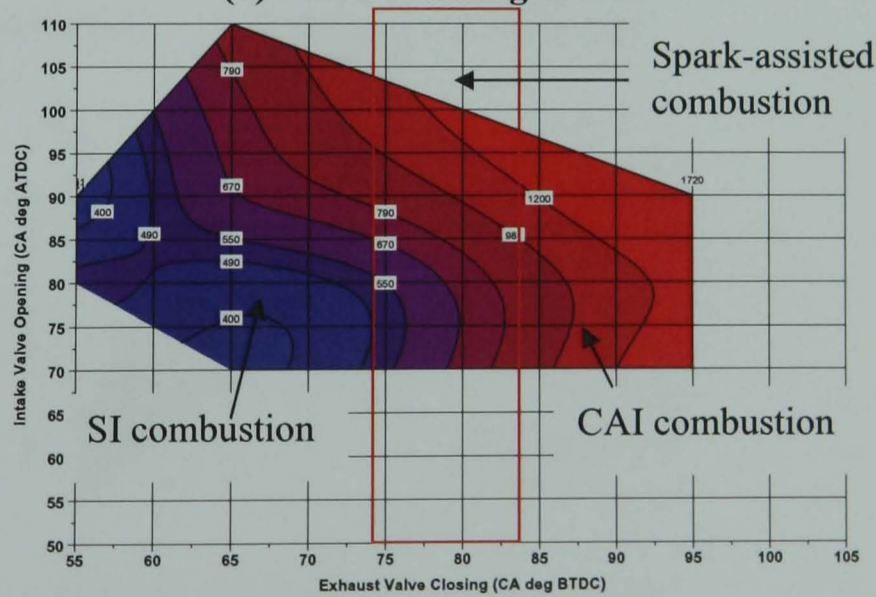
(b) SOI 30 CA deg ATDC

(c) SOI 120 CA deg ATDC

Figure 5.62 (a-c) uHC values (ppm) at EVC versus IVO timings for the shorter CAI camshaft at lambda 1.2
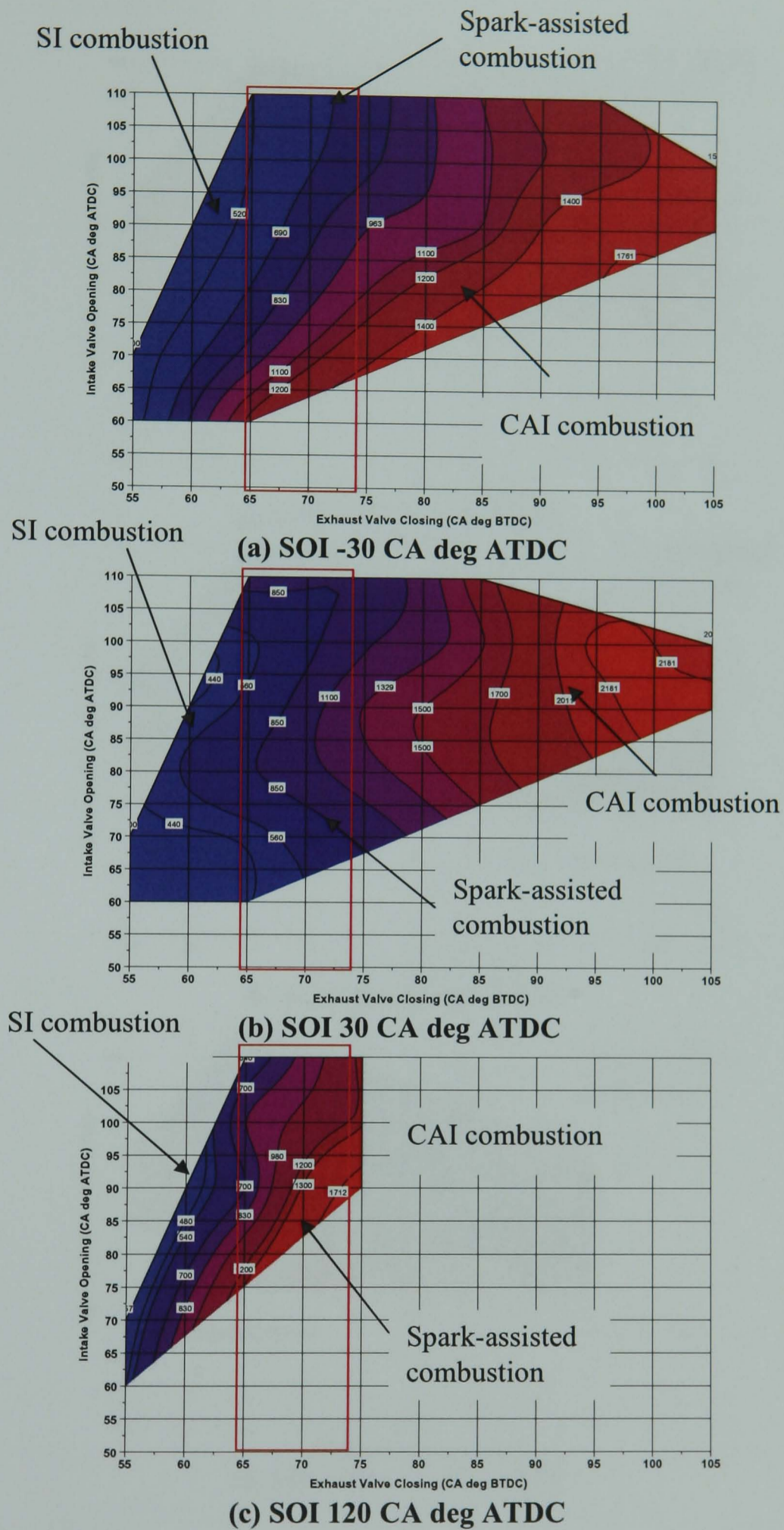
Figure 5.63 (a-c) uHC values (ppm) at EVC versus IVO timings for the longer CAI camshaft at lambda 1.2
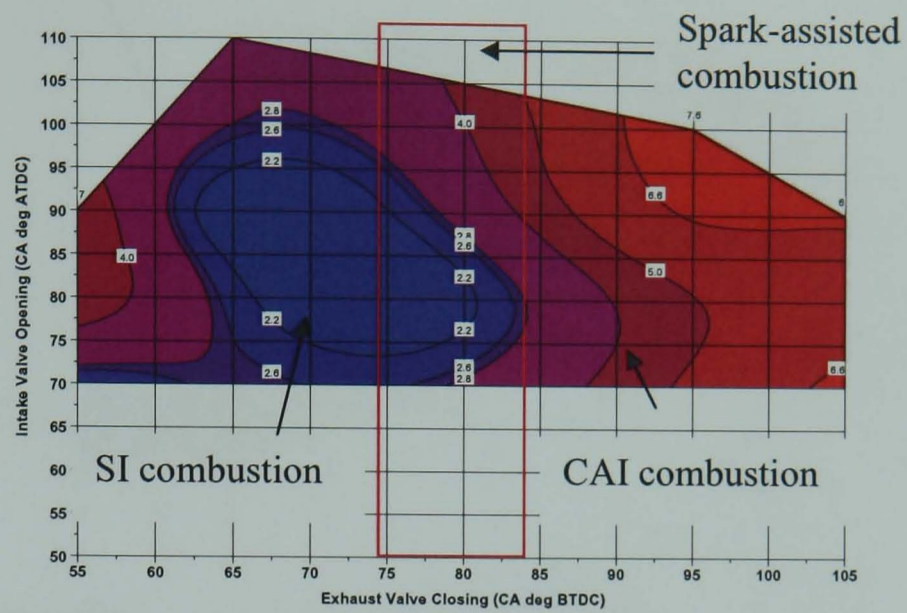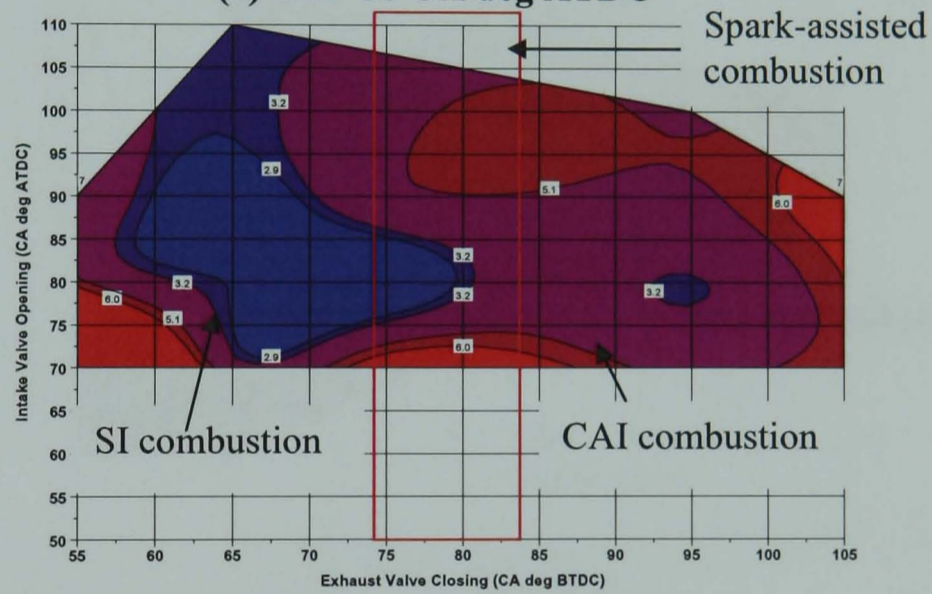
(a) SOI -30 CA deg ATDC
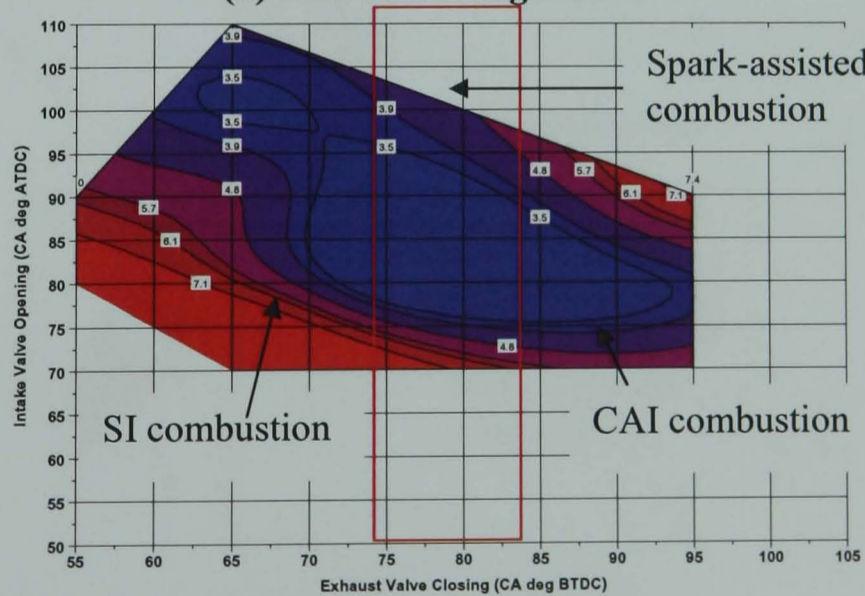
(b) SOI 30 CA deg ATDC

(c) SOI 120 CA deg ATDC

Figure 5.64 (a-c) ISCO (g/kW.h) at EVC versus IVO timings for the shorter CAI camshaft at lambda 1.2
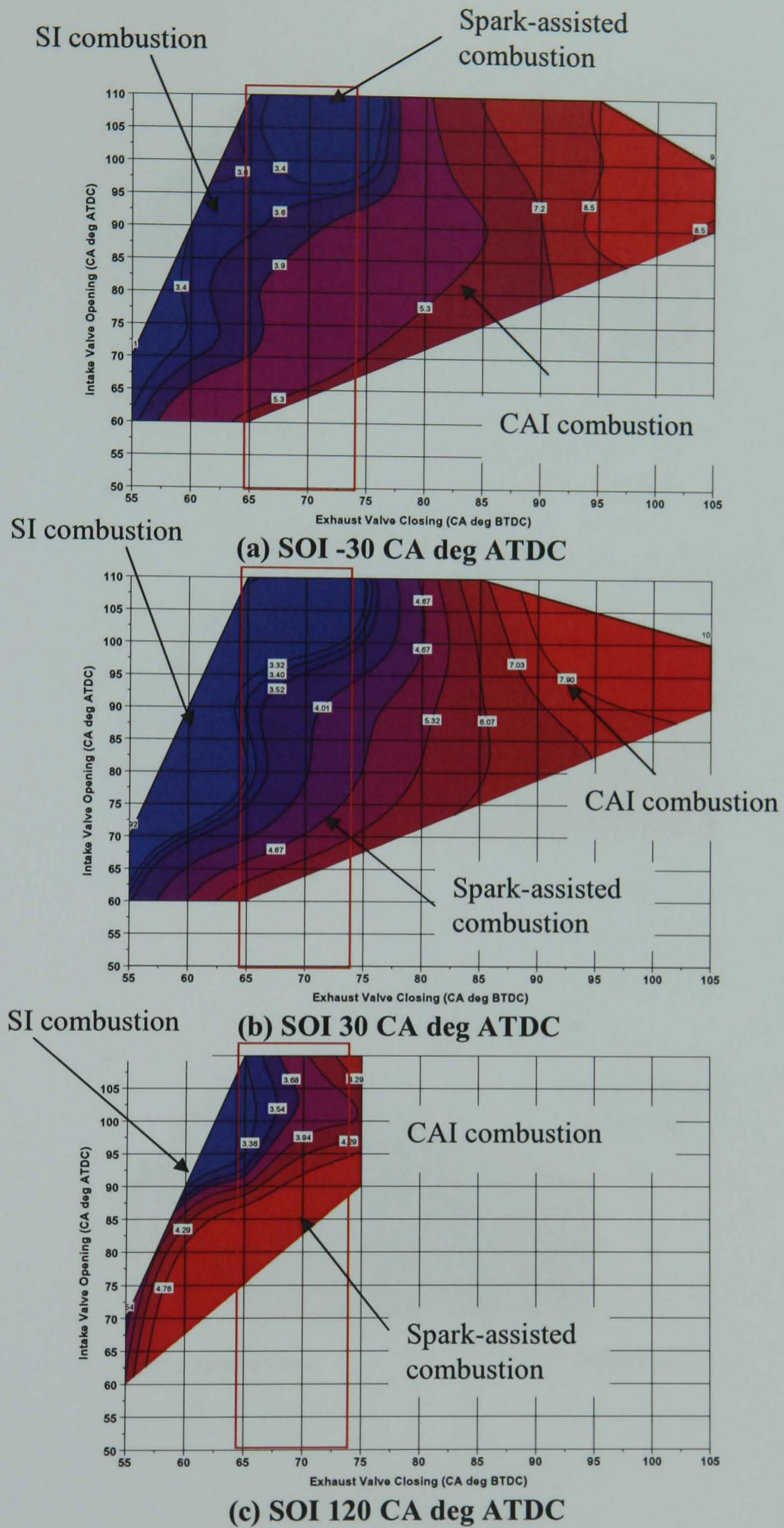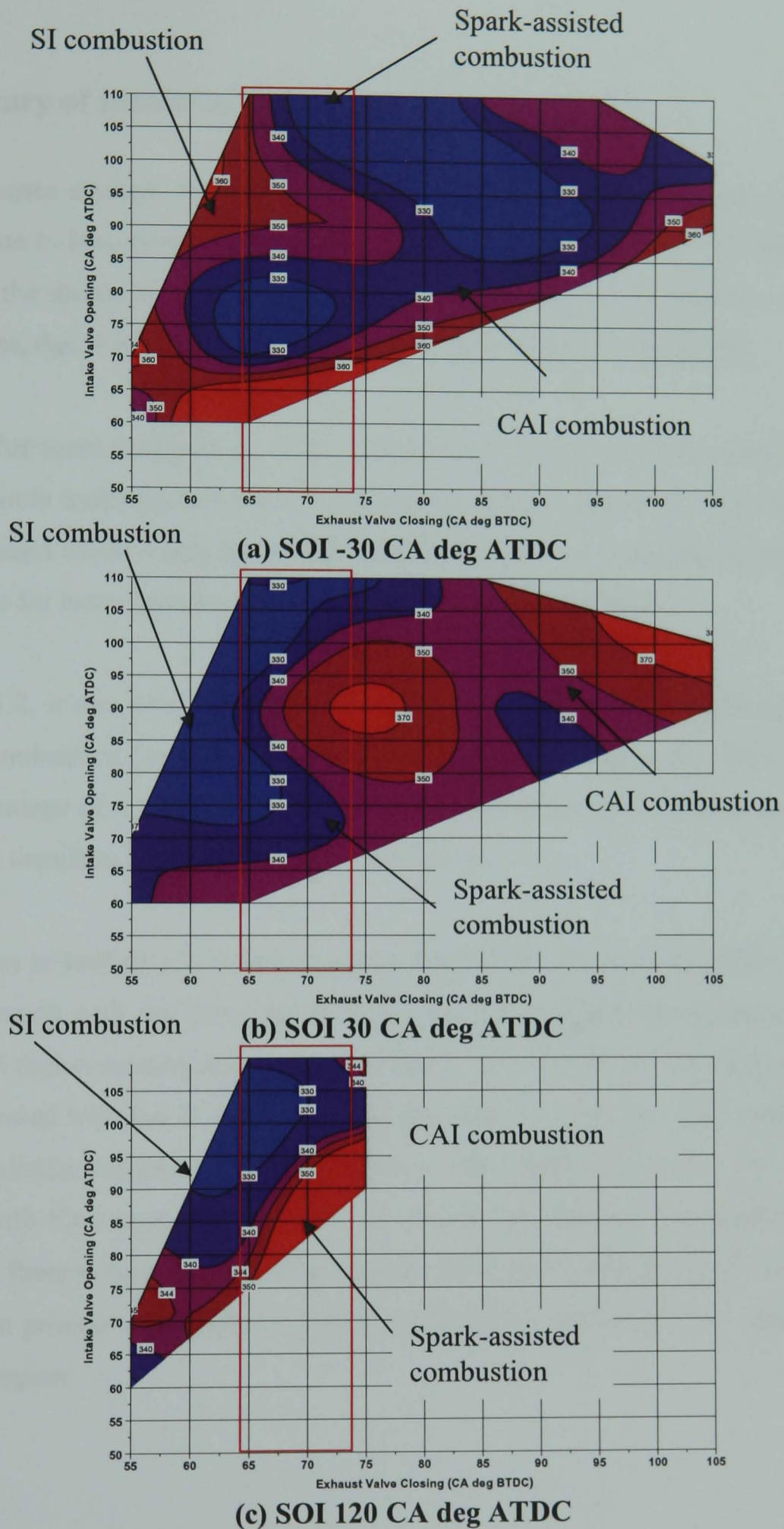
Figure 5.65 (a-c) ISCO (g/kW.h) at EVC versus IVO timings for the longer CAI camshaft at lambda 1.2
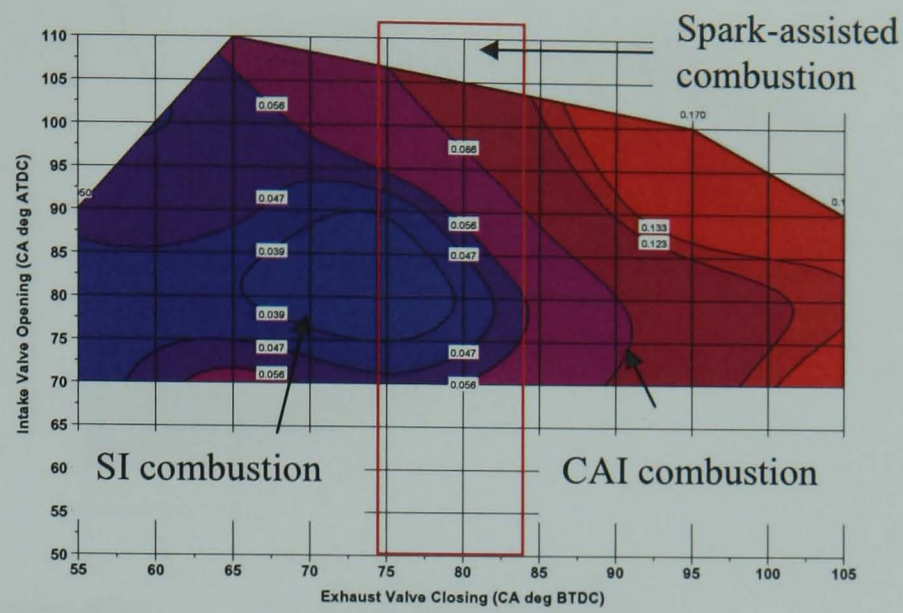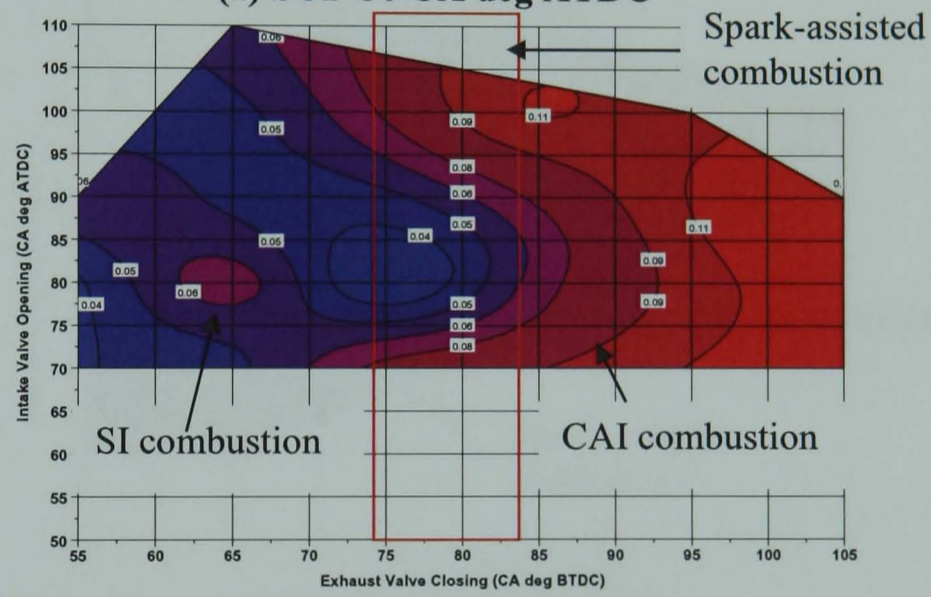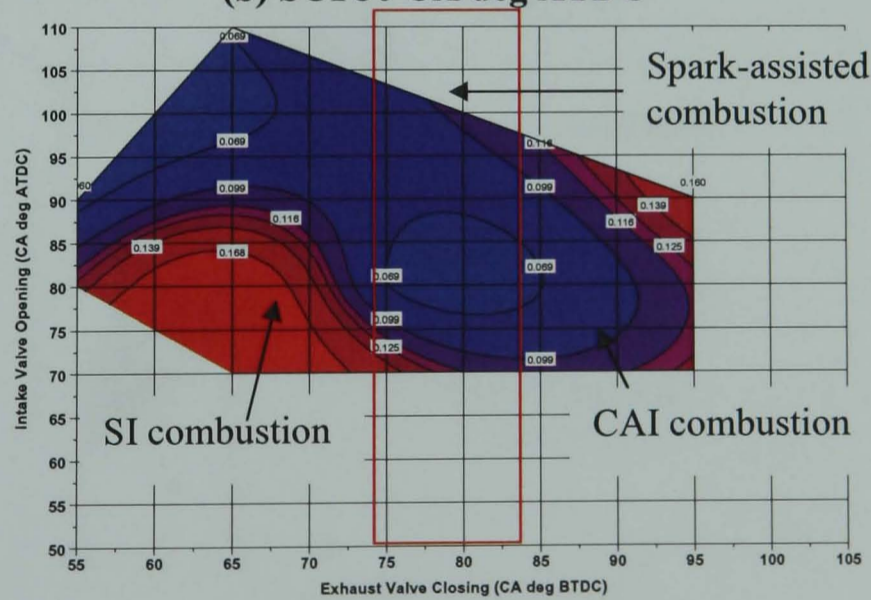
Figure 5.66 (a-c) CO values (%) at EVC versus IVO timings for the shorter CAI
camshaft at lambda 1.2

Figure 5.67 (a-c) CO values (ppm) at EVC versus IVO timings for the longer CAI camshaft at lambda 1.2

5.6.4 Effects of Camshaft Design and Injection Timing on ISFC at Lambda = 1.2

As start of injection timing is retarded, ISFC values increase for both the shorter and longer CAI camshafts (Figure 5.68 (a-c) and Figure 5.69 (a-c)). The lower values observed at SOI -30 CA deg ATDC is due to lower pumping losses. Less work is needed to overcome the exhaust gases and therefore fuel consumption also drops at injection during the NVO re-compression period. The shorter CAI camshafts have lower ISFC values across the EVC-IVO range compared with the longer CAI camshafts. This is due to higher NIMEP values for the shorter CAI camshaft coupled with lower expansion work.

(a) SOI -30 CA deg ATDC

(b) SOI 30 CA deg ATDC
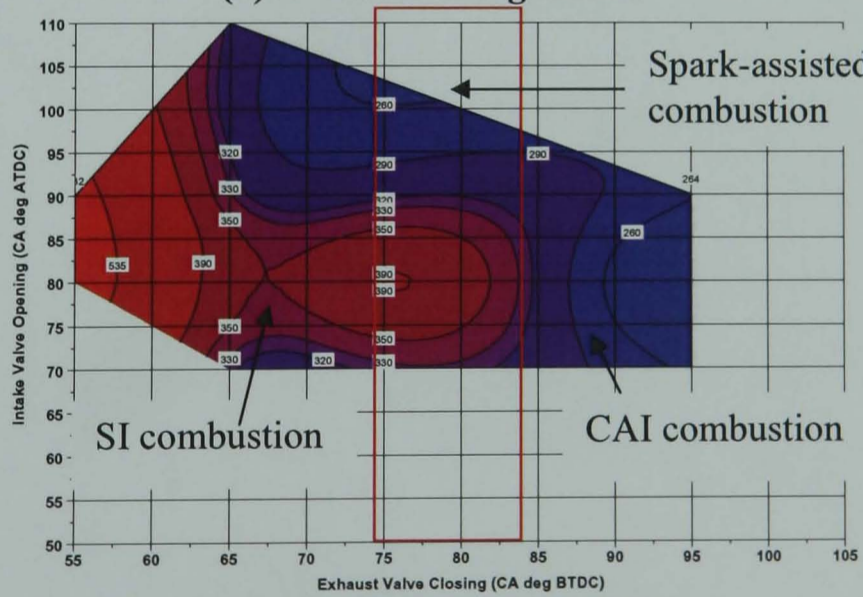
(c) SOI 120 CA deg ATDC

Figure 5.68 (a-c) ISFC (g/kW.h) at EVC versus IVO timings for the shorter CAI camshaft at lambda 1.2

Figure 5.69 (a-c) ISFC (g/kW.h) at EVC versus IVO timings for the longer CAI camshaft at lambda 1.2

5.7 Summary of results at lambda = 1.2

For all the cases studied, the shorter CAI camshafts could achieve higher load with CAI operation, due to less expansion work associated with the longer CAI camshafts. At some load points, the shorter CAI camshafts produce more NOx in the cylinder but less uHC and CO emissions, due to higher combustion temperature present in the cylinder.

It is noted that some load points can be operated with SI or CAI mode, providing a sound basis for smooth transition between SI/CAI operations. It is also noted that a spark-assisted CAI combustion mode is present between the SI and CAI valve settings, providing another useful means for better transition control between CAI/SI operations.

At lambda 1.2, it was found that NIMEP values were higher for SI combustion compared with CAI combustion for both the shorter and longer CAI camshafts. This was due to a higher percentage of residual gas being trapped for advanced EVC timing and hence CAI combustion; therefore NIMEP values would be lower.

For emissions at lambda 1.2, it was observed that ISNOx values were higher within the SI region compared with the CAI region. This was due to higher in-cylinder temperatures within the SI region causing higher ISNOx values. Values of ISHC were higher for the CAI region compared with the SI region for both the shorter and longer CAI camshafts due to higher in-cylinder temperatures. ISCO values were generally lower for SI operation compared with CAI operation for both the shorter and longer CAI camshafts. For CAI combustion, there is less inducted fresh charge and hence a lack of oxygen which restricts the oxidation process and results in higher ISCO values within the CAI region compared with the SI region.

Chapter 6

CAI Combustion Region Enlargement

Chapter 6 CAI Combustion region enlargement

6.1 Introduction

In order for CAI combustion to see use within an automotive engine, the operational region has to be expanded. As mentioned, a CAI/SI hybrid engine is the most likely method which can utilize the low ISNOx production and improved fuel economy of CAI combustion. Therefore methods which can help the transition from SI to CAI combustion and increase either the low or mid-range loads were investigated. After much consideration and observation the chosen areas of research which could be used as a potential method of CAI operational region enlargement were: spark-assistance, high speed operation and late injection.

It has been observed that for the boundary region between CAI and SI combustion, then the use of a spark can promote combustion and enlarge the CAI combustion region particularly near the misfire limit. Using spark suggests that combustion is occurring through the means of flame propagation. However, it is shown in this section that the spark is in fact aiding auto-ignition combustion. Results for longer duration intake and exhaust camshafts were compared against shorter ones, with a view to see if camshaft duration had any effect on spark-assisted CAI operation.

In the previous Chapter, results at a fixed engine speed of 1500 rpm were analyzed and discussed. In this chapter, the effect of engine speed is examined for the longer CAI camshafts as the speed range of the shorter CAI camshafts was restricted to 1750 rpm.

Finally the effects of very late injection on CAI combustion were investigated. The motivation for studying late injection was to see if there are any benefits of split injection for CAI combustion. It was envisaged that the ultra late injection would replicate the main injection of a split injection strategy. The Bosch engine management system offers the capability of undertaking split injection, however, time was a limiting factor and therefore implementing and undertaking split injection could not be realized. A comparison was

162

made between the effects of very late injection with shorter and longer duration camshafts on CAI combustion.

6.2 Spark Assisted CAI combustion

6.2.1 Introduction

As mentioned in Chapter 5 there is an area sandwiched between SI operation and CAI operation, where the engine can operate in such a way that the combustion is initiated by a spark but the main combustion process is characterized with fast heat release and low NOx associated with CAI operation. It is believed that the spark helps the chemical kinetics process to facilitate the auto-ignition to take place. Figure 6.1 shows a chart of lambda against trapped residuals, the spark-assisted area is typically at lean conditions with a moderate amount of residuals. Ultimately, the use of a spark leads to ISNOx values which are slightly higher than normal CAI combustion but much lower than normal SI combustion values. Figures 6.2, 6.4 and 6.6 show graphs of EVC versus IVO plotted for ISNOx, trapped residual and NIMEP respectively, for the shorter CAI camshafts, on the graph is an indication of the SI and CAI operating regions. It can be seen that based on ISNOx values, any EVC timing retarded beyond 80 CA deg BTDC is undergoing combustion by SI since ISNOx values are high and trapped residual is low. Whereas any EVC timing advanced further than 80 CA deg BTDC is undergoing combustion by CAI since ISNOx values are low and the trapped residual level is moderate. Figures 6.3, 6.5 and 6.7 show graphs of EVC versus IVO plotted for ISNOx, trapped residual and NIMEP respectively, for the longer CAI camshafts. The region retarded beyond EVC 70 CA deg BTDC is undergoing SI combustion, the region advanced beyond EVC 70 CA deg BTDC is undergoing CAI combustion.
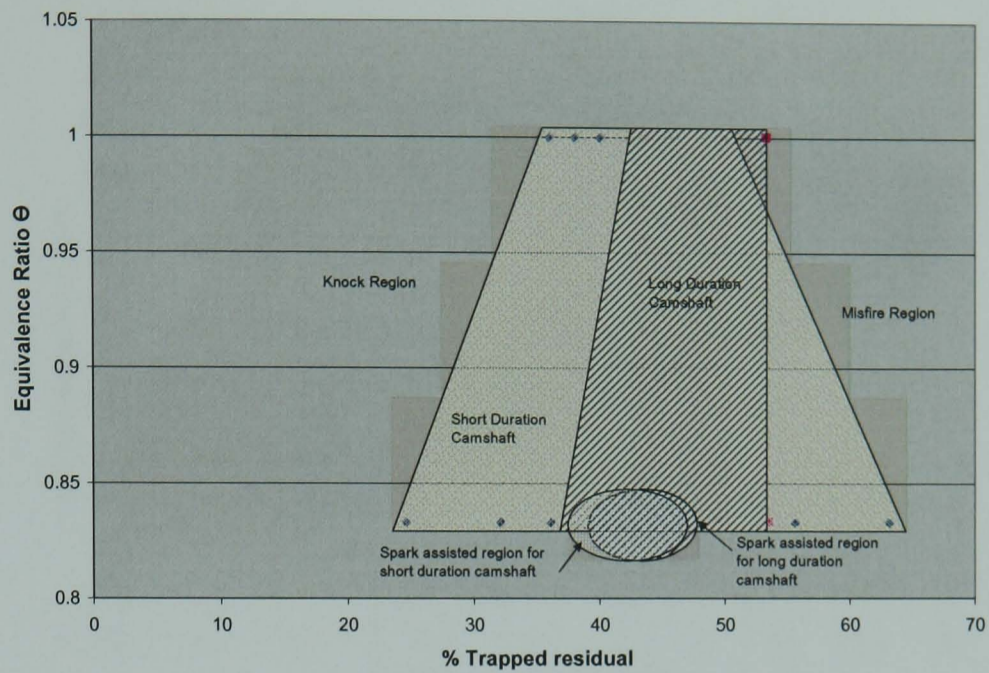
Figure 6.1 Indication of the Spark-Assisted area for the shorter and longer CAI camshafts at 1500 rpm and SOI -30, 30 and 120 CA deg ATDC.
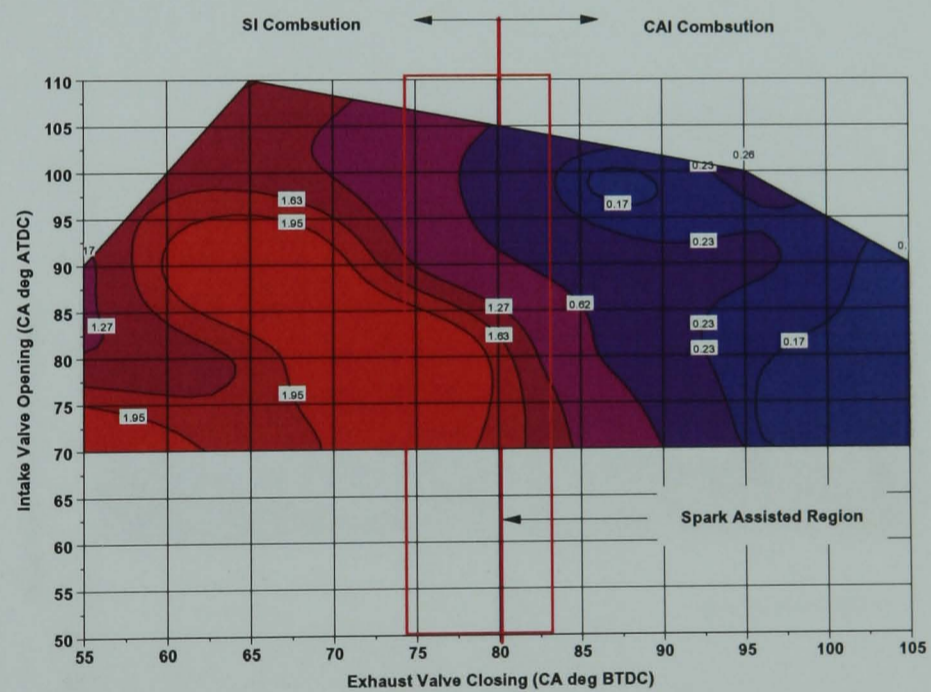
Figure 6.2 Indication of spark-assisted area on ISNOx (g/kW.h) contour map of EVC versus IVO timings at SOI 30 CA deg ATDC, lambda 1.2 and 1500 rpm for the shorter CAI camshafts
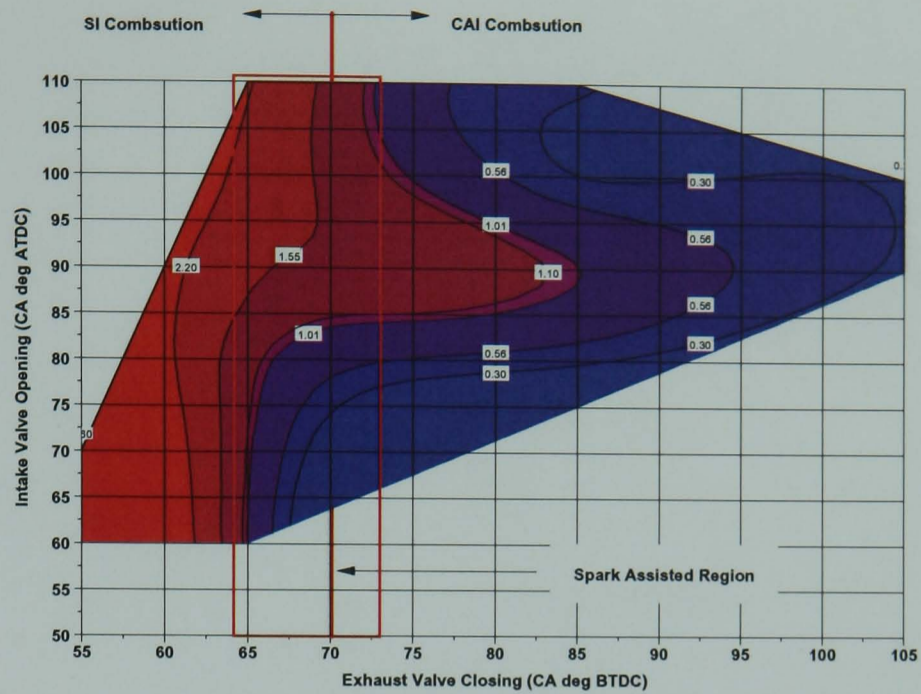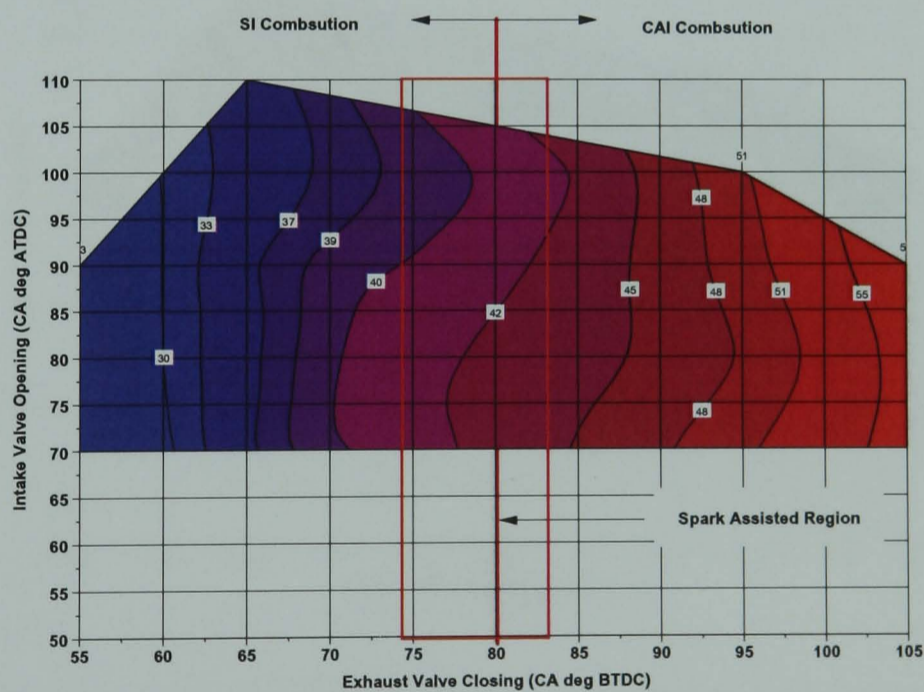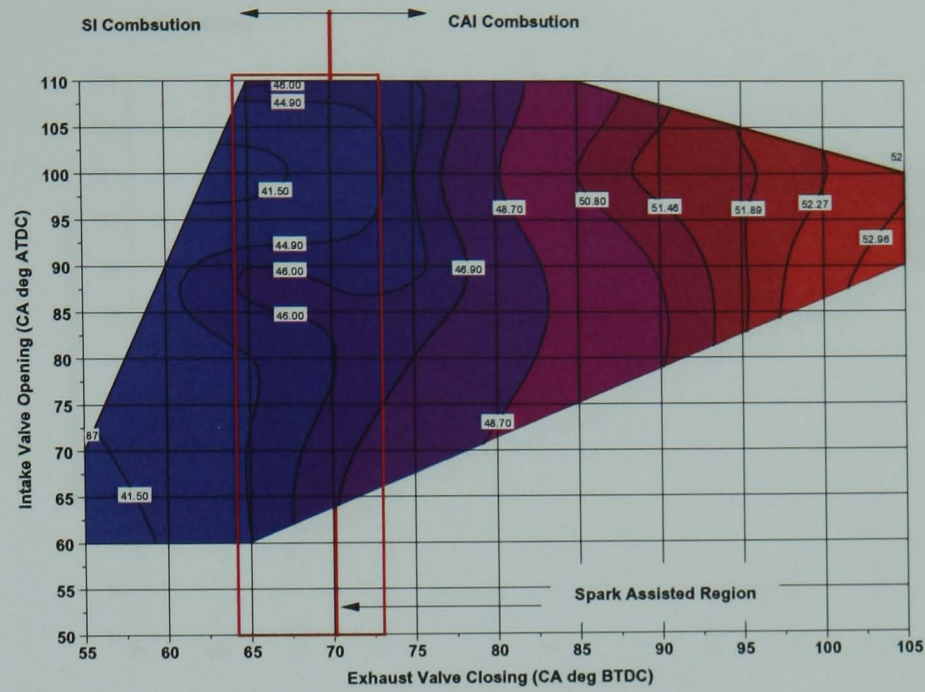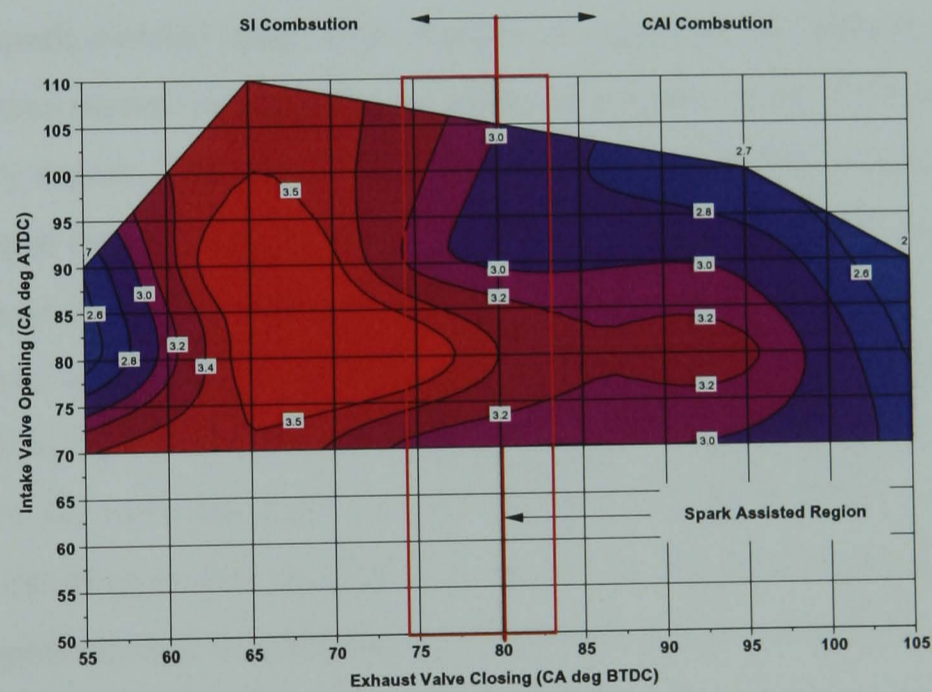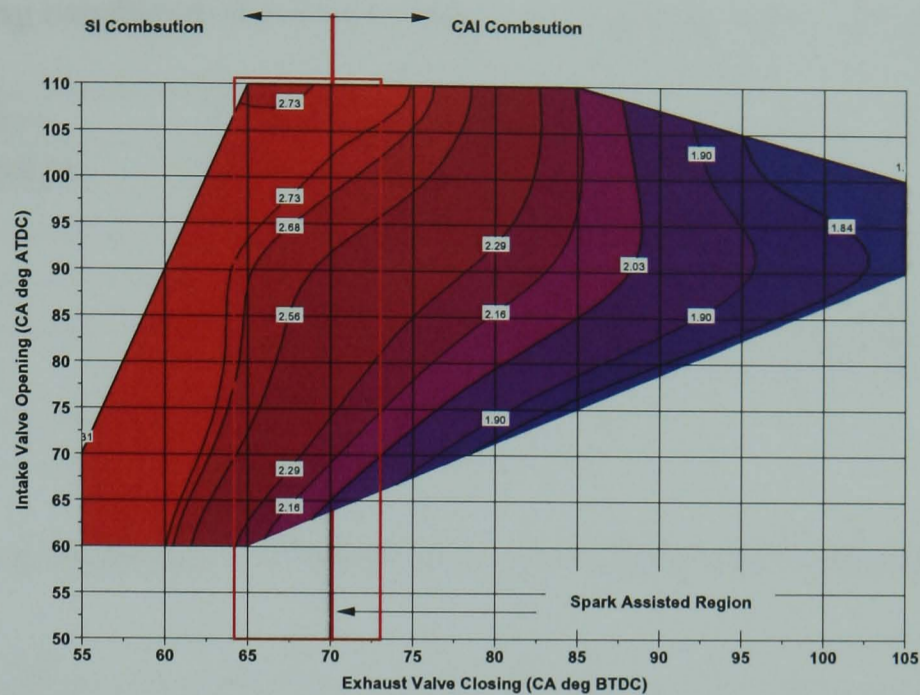
Figure 6.3 Indication of spark-assisted area on ISNOx (g/kW.h) contour map of EVC versus IVO timings at SOI 30 CA deg ATDC, lambda 1.2 and 1500 rpm for the longer CAI camshafts

Figure 6.4 Indication of spark-assisted area on trapped residual (%) contour map of EVC versus IVO timings at SOI 30 CA deg ATDC, lambda 1.2 and 1500 rpm for the shorter CAI camshafts

165

Figure 6.5 Indication of spark-assisted area on trapped residual (%) contour map of EVC versus IVO timings at SOI 30 CA deg ATDC, lambda 1.2 and 1500 rpm for the longer CAI camshafts

Figure 6.6 Indication of spark-assisted area on IMEP (bar) contour map of EVC versus IVO timings at SOI 30 CA deg ATDC, lambda 1.2 and 1500 rpm for the shorter CAI camshafts

Figure 6.7 Indication of spark-assisted area on IMEP (bar) contour map of EVC versus IVO timings at SOI 30 CA deg ATDC, lambda 1.2 and 1500 rpm for the longer CAI camshaft

Four different spark-assisted cases were studied as specified in Table 6.1 and 6.2. The main emphasis was placed on studying the effect of a spark on the CAI process near the CAI/SI boundary region. The use of a spark here helps to stabilize combustion. The four cases were grouped into two test groups, the first test group investigated the effect of EVC timing on spark-assisted CAI operation for the shorter CAI camshafts. The second test group investigated whether a longer intake and exhaust valve duration had any effect on spark-assisted CAI operation. For this test both cases were studied on the respective CAI/SI boundary for each camshaft. For the shorter CAI camshaft this was EVC 80 CA deg BTDC, for the longer CAI camshaft this was 70 CA deg BTDC. For both test groups, three different spark timings were chosen: TDC, 20 CA deg BTDC and 40 CA deg BTDC. These spark timing were then compared with fully auto-ignition combustion where combustion occurred without spark. Lambda was maintained at 1.2 and the start of injection was varied from -30 to 120 CA deg ATDC.

167

Table 6.1 Operating conditions for Test Group 1 with different EVC timings

Intake Valve Duration	120 CA deg
Exhaust Valve Duration	110 CA deg
Lambda	1.2
Speed	1500 rpm
Case [A]	**EVC 80 CA deg BTDC and IVO 85 CA deg ATDC**
Case [B]	**EVC 95 CA deg BTDC and IVO 70 CA deg ATDC**

Table 6.2 Operating conditions for Test Group 2 with different Camshafts

Lambda	1.2
Speed	1500 rpm
Case [C]	**EVC 80 CA deg BTDC and IVO 75 CA deg ATDC** **Intake Valve Duration: 120 CA, Exhaust Valve Duration: 110 CA**
Case [D]	**EVC 70 CA deg BTDC and IVO 75 CA deg ATDC** **Intake Valve Duration: 140 CA, Exhaust Valve Duration: 130 CA**

6.3 Effects of Spark Ignition on CAI Combustion at different EVC Timings (Case A and Case B in Test Group 1)

6.3.1 Effects of Spark Ignition on NIMEP

As can be seen from Figure 6.8 and Figure 6.9, with spark assisted CAI the achievable NIMEP is higher than conventional CAI. Furthermore, as ignition timing is advanced the achievable NIMEP increases. For all load cases, NIMEP at early injection is lower compared with later fuel injection. When fuel injection begins to infringe upon BDC (intake) the NIMEP falls again.

The actual higher NIMEP with spark ignition is attributable to the combustion phasing. For the early fuel injection cases (Figure 6.10 and Figure 6.11), as the ignition timing is advanced from TDC (compression) to 40 CA deg BTDC, the start of combustion consequently advances towards TDC. The maximum NIMEP is reached with a spark

168

timing of 20 CA deg BTDC at SOI 30 CA deg ATDC. As the spark ignition is advanced to 40 CA deg ATDC, the NIMEP drops due to early combustion.

For EVC 80 CA deg BTDC, the effect of spark is more pronounced with late injection at 90 CA deg ATDC (Figure 6.12) than the early injection at 30 CA deg ATDC (Figure 6.10). This is due to two reasons, firstly the later injection creates a more stratified charge and hence a more ignitable combustible charge near the spark plug for initial flame propagation, secondly due to the shorter time available for fuel/air mixing and auto-ignition reactions. For EVC 95 CA deg BTDC, the presence of spark improves the combustion process as evidenced by the higher heat release rate at SOI 90 CA deg ATDC, as well as more advanced combustion. For the late fuel injection, the effect of ignition timing on the start of combustion is even more pronounced as shown in Figure 6.12 and 6.13

Table 6.3 compares two valve timing cases for SOI 60 CA deg ATDC. Investigation of the 10%-50% MFB and 50%-90% MFB reveals that spark has a more profound effect on the 50%-90% MFB rather than the earlier stage. The 50%-90% MFB stage of CAI main combustion has the characteristics of typical CAI operation with very fast heat release, as the auto-ignition combustion takes place simultaneously across the unburned mixture.

Furthermore, since the combustion is taking place earlier at higher pressures and temperatures the 50%-90% stage of combustion is accelerated as the heat release takes place near TDC within a smaller volume.

For the advanced exhaust valve timing case (EVC 95 CA deg BTDC), the burn duration variation between spark-assisted and conventional CAI is only 4 CA deg (Table 6.3), smaller than Case A. This is because there is a greater volume of trapped residual and a greater threshold of thermal energy with the more advanced EVC. Therefore assisting CAI with spark has limited effect as there is enough thermal energy to initiate CAI combustion.

On inspection of trapped residuals (%) from Table 6.3, it appears that spark timing has little effect on the volume of trapped residuals. The trapped residual (%) for both cases are within 2% for different spark timings. As expected for the more advanced valve timing

case (EVC 95 BTDC), the volume of trapped residuals are greater than the retarded case (EVC 80 BTDC).

It appears that spark-ignition improves the COV_{IMEP} value, from Table 6.3, it can be noted that without spark-ignition, the COV_{IMEP} value is lower compared with ignition without spark.
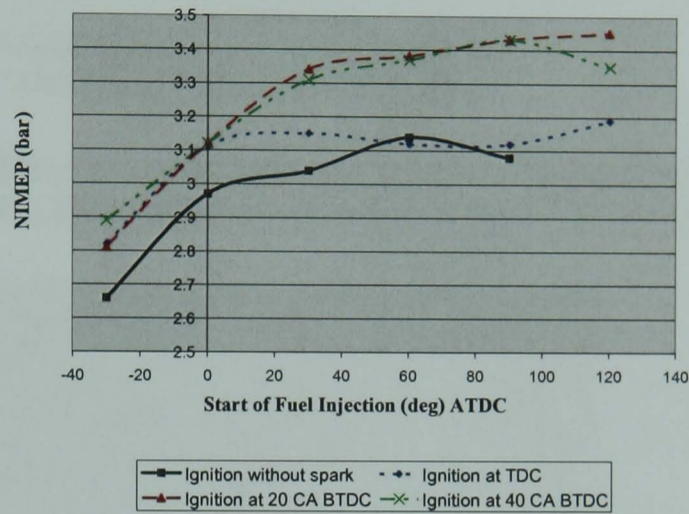

Figure 6.8 NIMEP against injection timing at different Ignition Timings, EVC 80 CA BTDC, IVO 85 CA deg ATDC, 1500 rpm, lambda 1.2
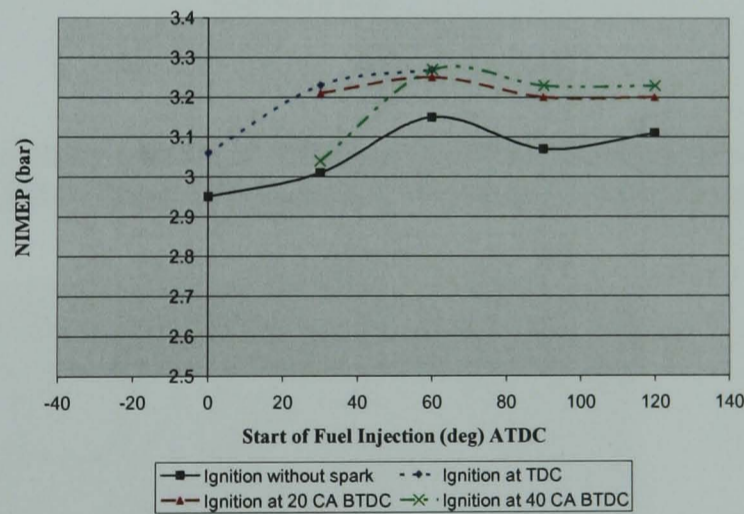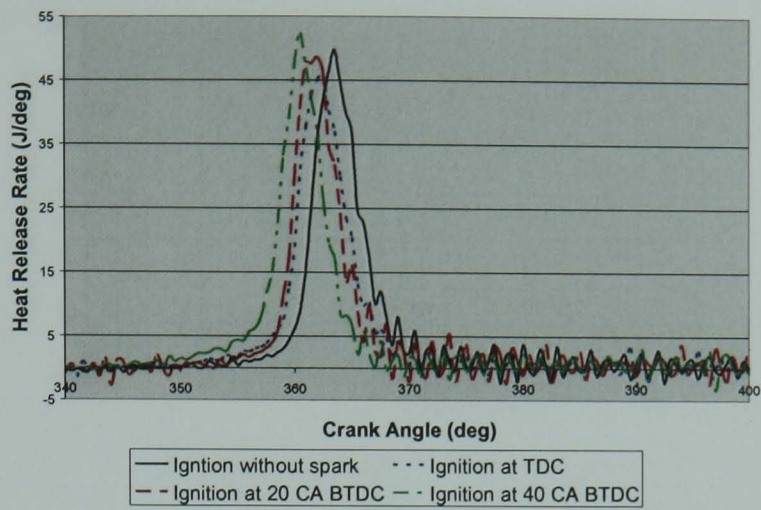

Figure 6.9 NIMEP against injection timing at different Ignition Timings, EVC 95 CA deg BTDC, IVO 70 CA deg ATDC, 1500 rpm, lambda 1.2

Figure 6.10 Heat Release Rate curves at different Ignition Timings EVC 80 CA deg BTDC, IVO 85 CA deg ATDC, Start of Injection = 30 CA deg ATDC (intake)
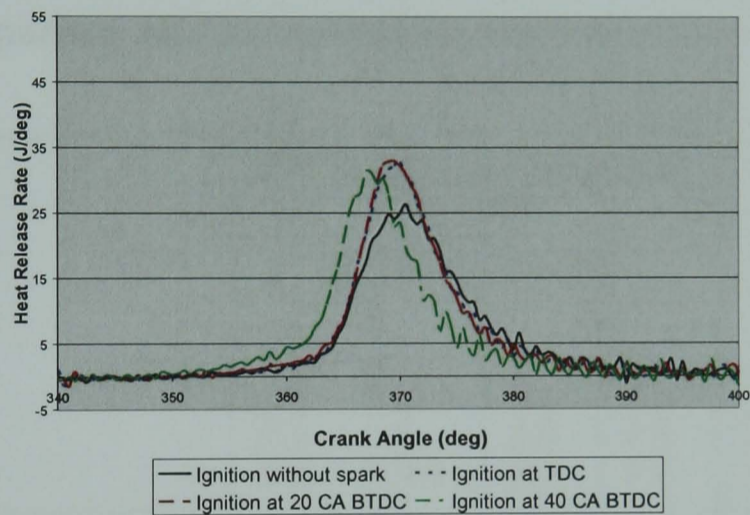
Figure 6.11 Heat Release Rate curves at different Ignition Timings EVC 95 CA deg BTDC, IVO 70 CA deg ATDC, Start of Injection = 30 CA deg ATDC (intake)
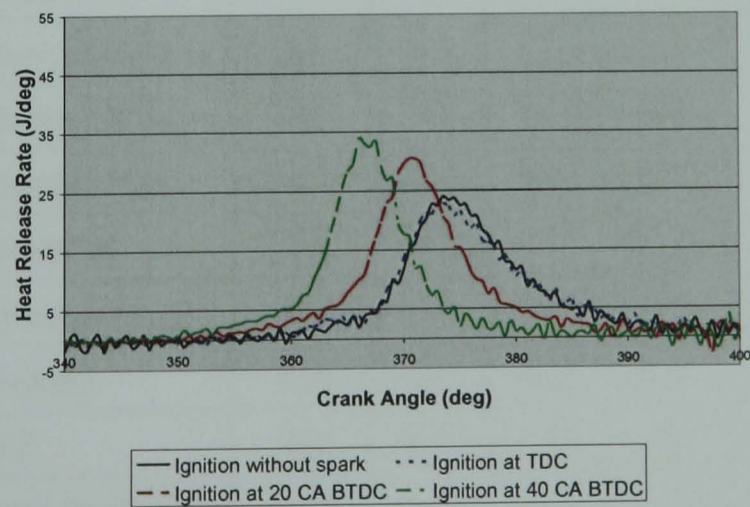
Figure 6.12 Heat Release Rate curves at different Ignition Timings EVC 80 CA deg BTDC, IVO 85 CA deg ATDC Start of Injection = 90 CA deg ATDC

171
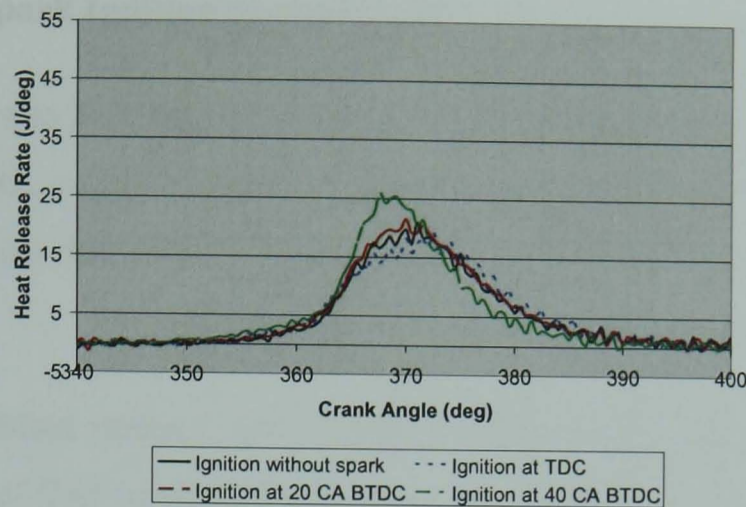
Figure 6.13 Heat Release Rate curves at different Ignition Timings EVC 95 CA deg BTDC, IVO 70 CA deg ATDC, Start of Injection = 90 CA deg ATDC

Table 6.3: Comparison of CAI combustion characteristics at two different valve timings.

	EVC 80 CA deg BTDC, IVO 85 deg ATDC				EVC 95 deg BTDC, IVO 70 deg ATDC			
	SOI 60 CA deg ATDC				SOI 60 CA deg ATDC			
	Ignition without spark	Ignition at TDC	Ignition at 20 CA BTDC	Ignition at 40 CA BTDC	Ignition without spark	Ignition at TDC	Ignition at 20 CA BTDC	Ignition at 40 CA BTDC
10% mass burned (CA)	368.0	366.6	363.7	359.9	366	363.5	365.5	361.5
50% mass burned (CA)	375.4	376.1	370.7	366.1	371.5	372	371.5	368
90% mass burned (CA)	394.1	390.3	381.9	378.0	384	384.5	381	377.5
10%-50% burn duration (CA)	7.4	9.5	7	6.2	5.5	8.5	6	6.5
50%-90% burn duration (CA)	18.7	14.2	11.2	11.9	12.5	12.5	9.5	9.5
10%-90% burn duration (CA)	26.1	23.8	18.2	18.1	19	21	15.5	15.5
Peak pressure (MPa)	26.4	24.8	32.3	37.2	30.3	29.1	30.8	34.5
Location of peak pressure (CA)	379	378.5	374.5	370	375.5	376	375.5	373
NET IMEP (MPa)	3.14	3.12	3.38	3.37	3.15	3.15	3.25	3.27
T_{exh} (K)[a]	413	425	384	384	384.5	374.7	372.8	370.8
Trapped Residuals (%) (Predicted)	44.91	43.27	45.86	46.42	48.98	47.53	48.48	48.61
COV_{imep} (%)	9.06	3.518	1.736	1.172	6.513	5.003	3.88	2.138

[a]T_{exh} for experimentation refers to the exhaust temperature of exhaust gases measured from the exhaust port

6.3.2 Effects of Spark Ignition on emissions

From Figure 6.14 and Figure 6.15 it is apparent that as spark timing is advanced for spark assisted CAI, $ISNO_x$ values increase as compared with conventional CAI for EVC 80 CA deg BTDC, whereas the ISNOx values change little with spark for EVC 95 CA deg BTDC.

The measured exhaust temperatures (Table 6.3) show that compared with conventional CAI, spark-assisted CAI temperature is lower. The reason for this is that the combustion process is advanced as spark is advanced for spark-assisted CAI as shown in Figures 6.10 - 6.13. Therefore, the expansion ratio, taken as end of combustion to exhaust valve opening increases, causes the exhaust temperature to decrease.

Figure 6.16 and Figure 6.17 show the variation of calculated peak in-cylinder temperature against the start of fuel injection. It is important to stress that this is the calculated in-cylinder temperature based on the ideal gas law. However in-cylinder gases may not be ideal and homogeneous, due to the complicated gas exchange processes and inhomogeneous combustion mixture. But it is still viable to analyse the general trend. Examining the pressure plots (Figure 6.18 and 6.19), the peak pressure during the combustion process increases as spark is advanced for spark assisted CAI and is higher than the conventional CAI case. As seen in Figure 6.10 to Figure 6.13, the heat release rate peak increases as spark is advanced and again is higher than for conventional CAI.

On inspection of the calculated in-cylinder temperature (K) profiles (Figure 6.16 and Figure 6.17), it can clearly be seen that higher $ISNO_x$ values with advanced spark timing are due to higher in-cylinder temperatures caused by a fast heat release rate as discussed previously.

173
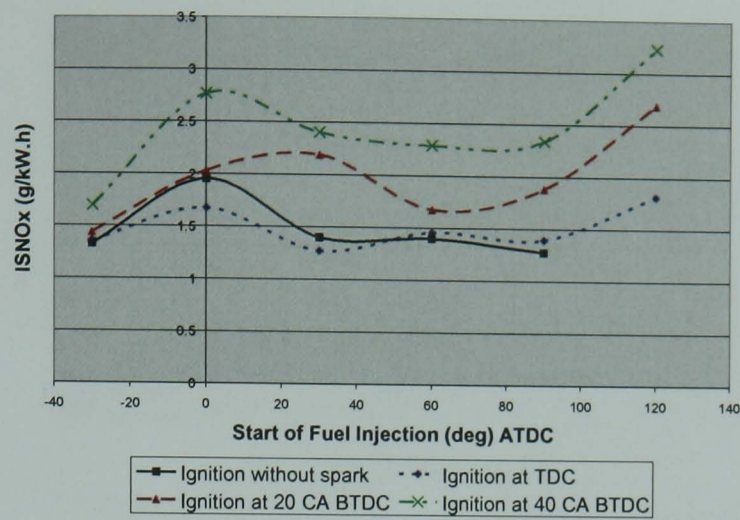
Figure 6.14 ISNOx against injection timing at different Ignition Timings, EVC 80 CA BTDC, IVO 85 CA deg ATDC
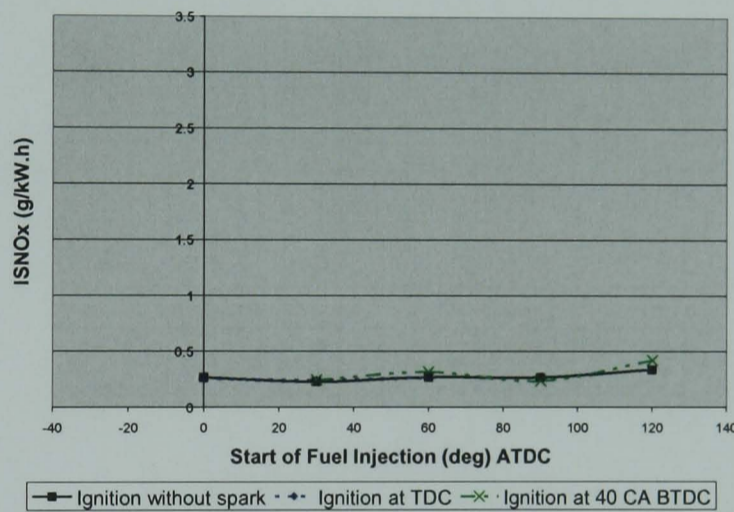

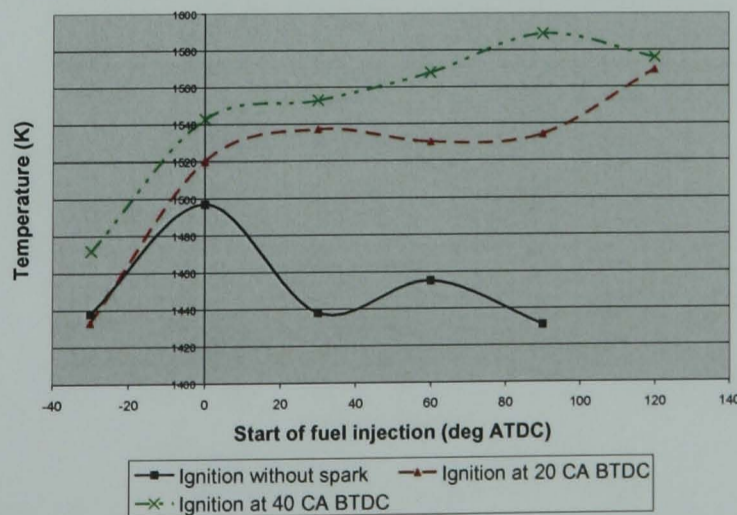**Figure 6.15 ISNOx against injection timing at different Ignition Timings, EVC 95 CA BTDC, IVO 70 CA deg ATDC**

Figure 6.16 Calculated peak In-cylinder Temperature against injection timing at different Ignition Timings, EVC 80 CA BTDC, IVO 85 CA deg ATDC
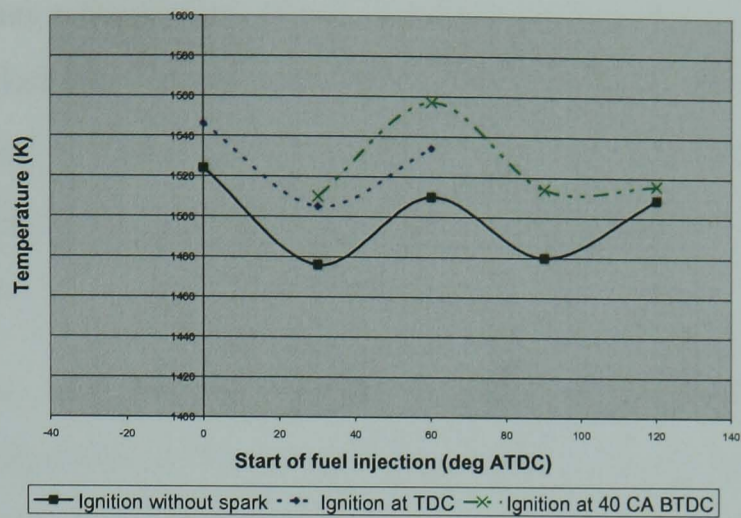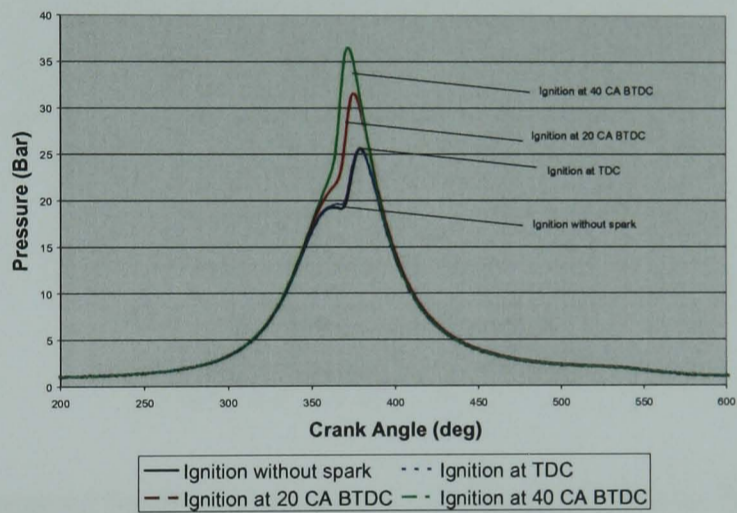
Figure 6.17 Calculated peak In-cylinder Temperature against injection timing at different Ignition Timings, EVC 95 CA BTDC, IVO 70 CA deg ATDC

Figure 6.18 Pressure against Crank Angle during the Combustion phase, EVC 80 CA deg BTDC, IVO 85 CA deg ATDC Start of Injection = 60 CA deg ATDC (Intake)
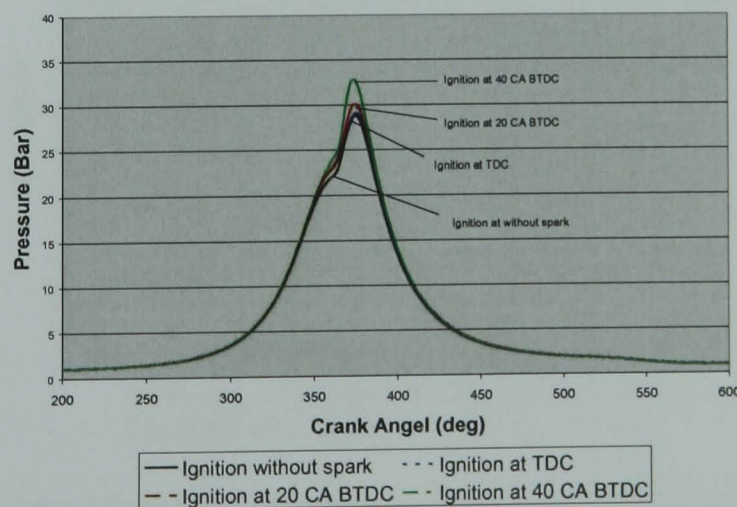
Figure 6.19 Pressure against Crank Angle during the Combustion phase, EVC 95 CA deg BTDC, IVO 70 CA deg ATDC Start of Injection = 60 CA deg ATDC (Intake)

Spark-assisted CAI has a favourable effect on ISHC values. From Figure 6.20 and Figure 6.21, it can be seen that ISHC values are lower for spark-assisted CAI than conventional CAI. The reason for lowered (HC) emissions for spark assisted CAI is because combustion is taking place at higher pressures and temperatures, leading to more complete combustion.

For the same reason, with the introduction of spark ignition, ISCO values decrease throughout the fuel injection timing range (Figure 6.22 and Figure 6.23). Moreover, as the ignition timing is advanced further, the ISCO values drop even more.
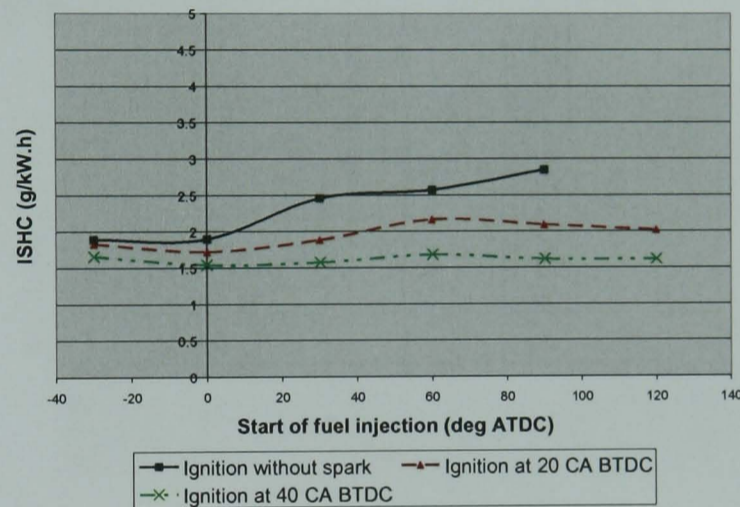
Figure 6.20 ISHC against injection timing at different Ignition Timings, EVC 80 CA BTDC, IVO 85 CA deg ATDC
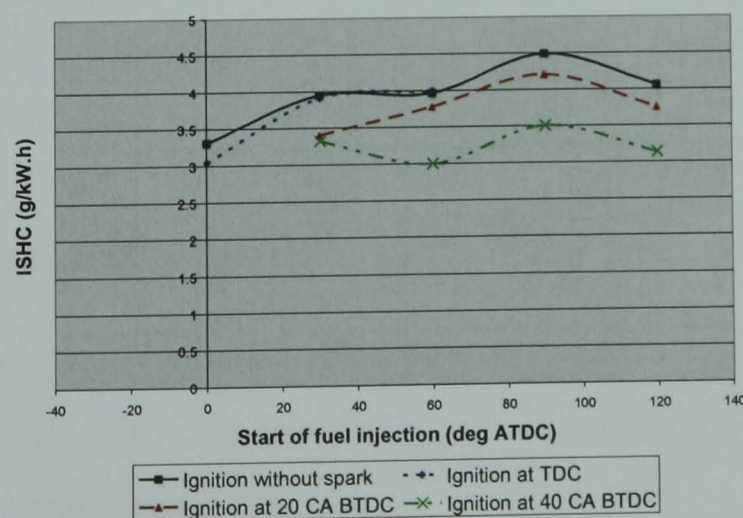
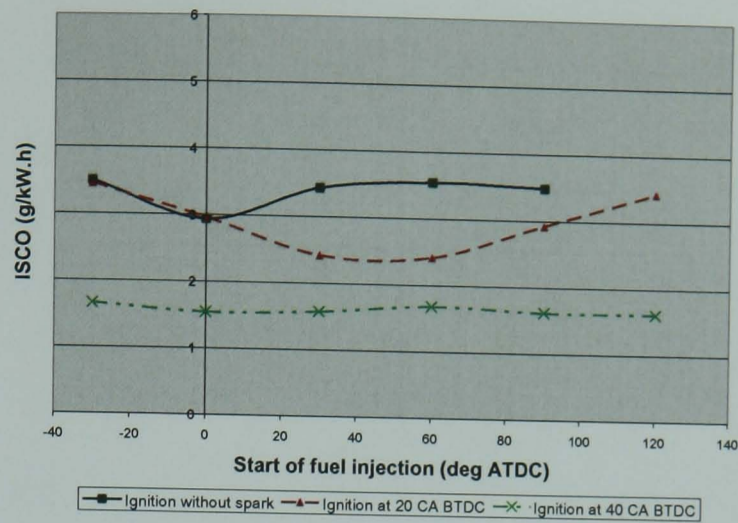**Figure 6.21 ISHC against injection timing at different Ignition Timings, EVC 95 CA BTDC, IVO 70 CA deg ATDC**

Figure 6.22 ISCO against injection timing at different Ignition Timings, EVC 80 CA deg BTDC, IVO 85 CA deg ATDC
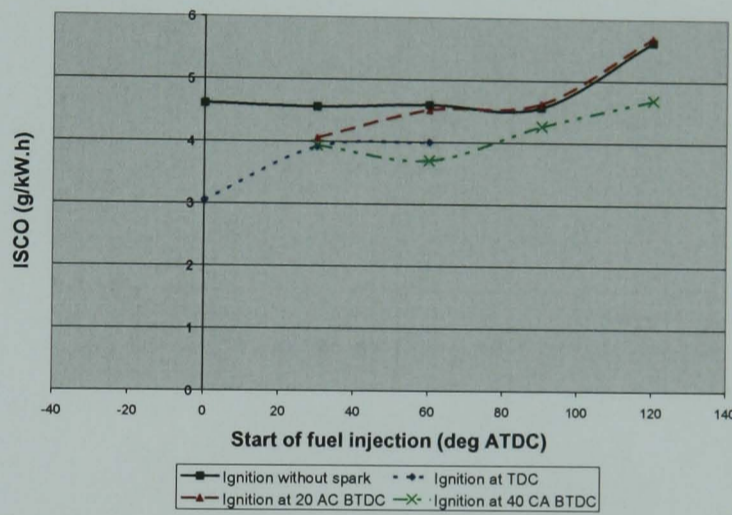

Figure 6.23 ISCO against injection timing at different Ignition Timings, EVC 95 CA deg BTDC, IVO 70 CA deg ATDC

6.3.3 Effects of Spark Ignition on ISFC

For both valve timing cases as spark is advanced for spark-assisted CAI, ISFC values (Figure 6.24 and Figure 6.25) decrease. This can be attributed to higher NIMEP values caused by optimized combustion phasing.
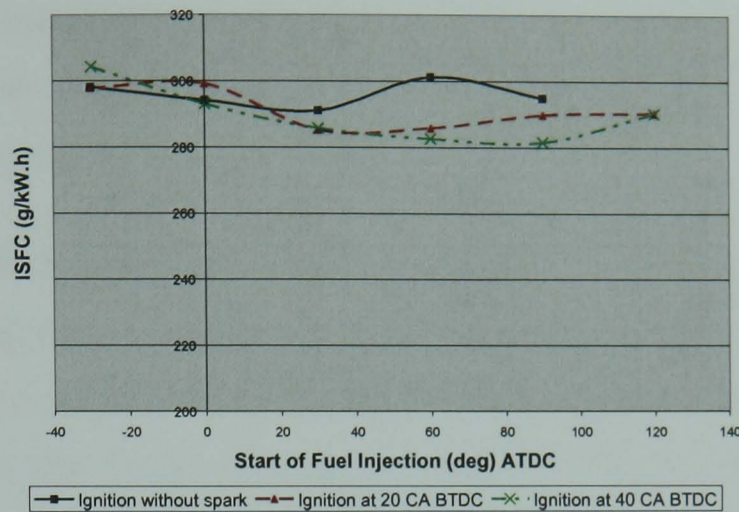
Figure 6.24 ISFC against injection timing at different Ignition Timings, EVC 80 CA BTDC, IVO 85 CA deg ATDC
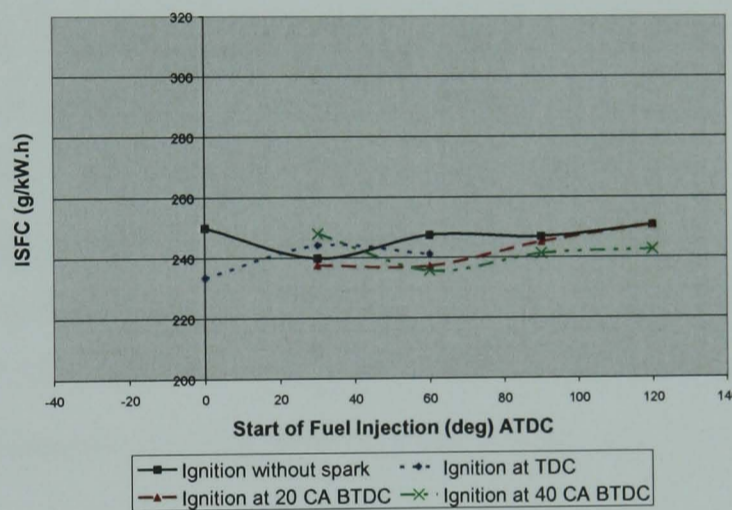

Figure 6.25 ISFC against injection timing at different Ignition Timings, EVC 95 CA BTDC, IVO 70 CA deg ATDC

6.4 Effects of Spark Ignition on CAI Combustion at different valve durations (Case C and Case D in Test Group 2)

6.4.1 Effects of Spark Ignition on NIMEP

For Test Group 2, it was of interest to see the effects of valve duration on spark-assisted CAI. An EVC timing of 80 CA deg BTDC was used for the shorter CAI camshafts. For the longer CAI camshafts, an EVC timing of 70 CA deg BTDC was chosen. Again the three different ignition times of TDC, 20 CA deg BTDC and 40 CA deg BTDC were

compared with CAI combustion without spark. The IVO timing was 75 CA deg ATDC for both cases. Lambda was maintained at 1.2, engine speed of 1500 rpm and the start of injection was varied from -30 to 120 CA deg ATDC.

On inspection of the variation of NIMEP against the start of fuel injection (CA deg ATDC) at different ignition timings (Figure 6.26 and Figure 6.27), it appears that NIMEP is higher for spark-assistance compared with CAI combustion; this is the case for both case C (shorter CAI camshafts) and case D (longer CAI camshafts). For case C the maximum achieved NIMEP for conventional CAI was 2.8 bar at SOI TDC (intake) whereas with ignition at 40 CA BTDC, SOI 120 CA deg ATDC, the NIMEP was 3.3 bar. For case D the maximum NIMEP with CAI combustion was 2.3 bar at SOI at TDC (intake), with the use of spark assistance the maximum NIMEP was 2.47 bar at SOI 60 CA deg ATDC. Spark assistance also allowed combustion to occur at injection timings retarded beyond TDC, for both the shorter and longer CAI camshafts; effectively increasing the operating region. At later injection cases there is less time for charge mixing resulting in stratified charge, the influence of chemical kinetics is not sufficient to allow conventional CAI combustion to occur with stratified charge; with the use of spark-assistance, CAI combustion can be instigated over a wider and retarded injection range.
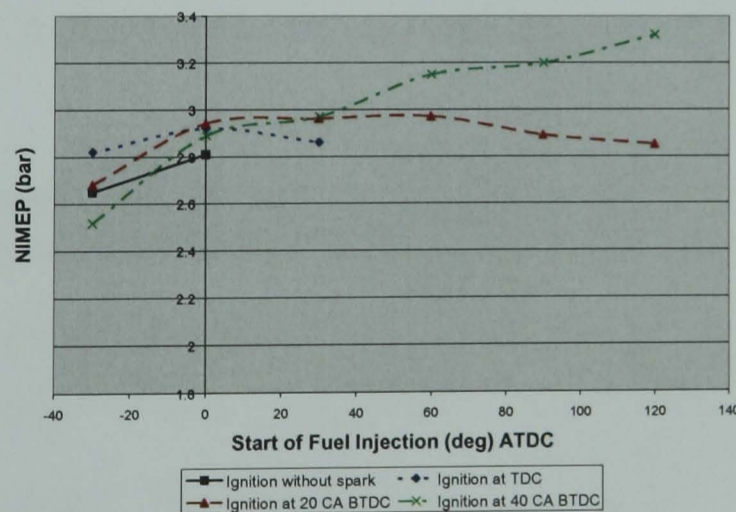

Figure 6.26 NET IMEP against injection timing at different Ignition Timings, EVC 80 CA deg BTDC, IVO 75 CA deg ATDC, shorter CAI camshaft
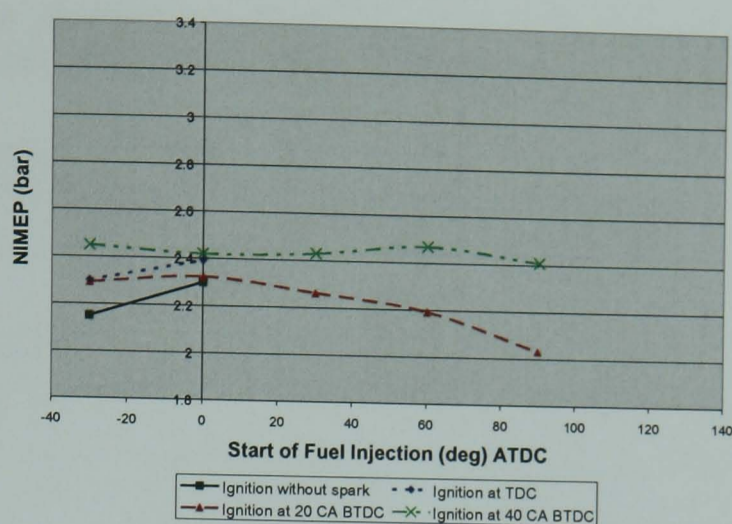
Figure 6.27 NET IMEP against injection timing at different Ignition Timings, EVC 70 CA deg BTDC, IVO 75 CA deg ATDC, longer CAI camshaft

Table 6.4 and Table 6.5, list the trapped residual (%) for Case C and D consecutively. The effects of ignition timing on the percentage of trapped residual, for both the shorter and longer CAI camshafts, are almost negligible. The percentage of trapped residual varies between 44.28% to 47.83% for the shorter CAI camshaft, and varies between 46.18% to 47.33% for the longer CAI camshaft. The effects of spark-assistance are obvious at lean conditions (lambda = 1.2) with sufficient exhaust residuals (~45%), there is not sufficient thermal energy to allow CAI combustion to occur, yet the amount of inducted charge is neither sufficient nor rich enough to allow combustion through flame propagation.

Table 6.4: Trapped Residual against injection timing at different Ignition Timings, EVC 80 CA deg BTDC, IVO 75 CA deg ATDC, shorter CAI camshafts

Injection Timing (deg ATDC)	Trapped Residual (%)			
	Conventional CAI	Ignition at TDC	Ignition at 20 CA deg BTDC	Ignition at 40 CA deg BTDC
-30	46.53	46.10	47.83	
0	44.69	45.33	46.13	46.97
30		43.80	44.51	45.81
60			44.92	45.15
90			44.19	44.34
120			44.28	45.64

Table 6.5: Trapped Residual against injection at different Ignition Timings, EVC 70 CA deg BTDC, IVO 75 CA deg ATDC, longer CAI camshafts

Injection Timing (deg ATDC)	Trapped Residual (%)			
	Conventional CAI	Ignition at TDC	Ignition at 20 CA deg BTDC	Ignition at 40 CA deg BTDC
-30	46.89	46.59	47.02	47.09
0	47.33	46.64	46.23	47.27
30			46.11	47.29
60			45.64	47.15
90			46.18	46.98
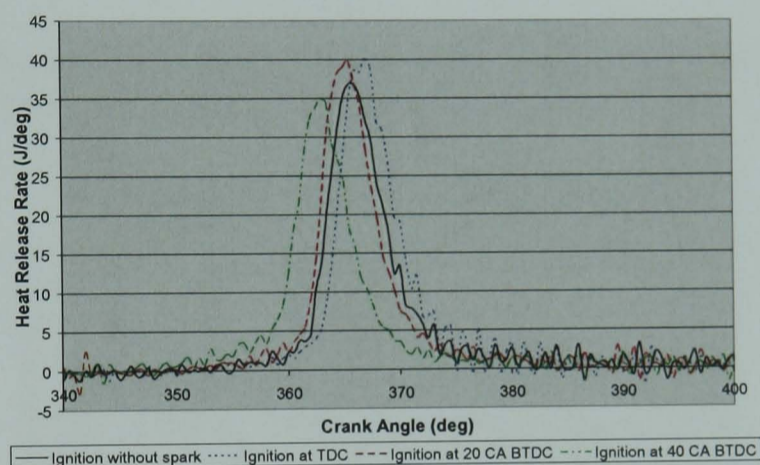
Figure 6.28 Heat Release Rate against crank angle (deg) at injection timing 30 CA deg BTDC, EVC 80 CA deg BTDC, IVO 75 CA deg ATDC, shorter CAI camshafts
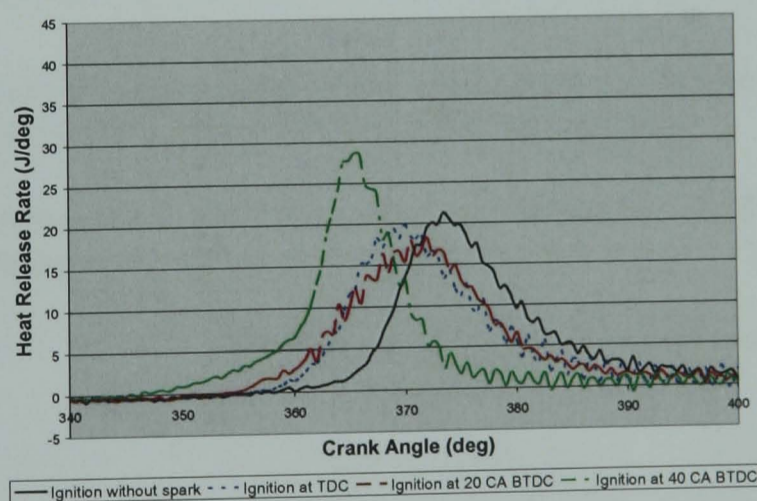

Figure 6.29 Heat Release Rate against crank angle (deg) at injection timing 30 CA deg BTDC, EVC 70 CA deg BTDC, IVO 75 CA deg ATDC, longer CAI camshafts
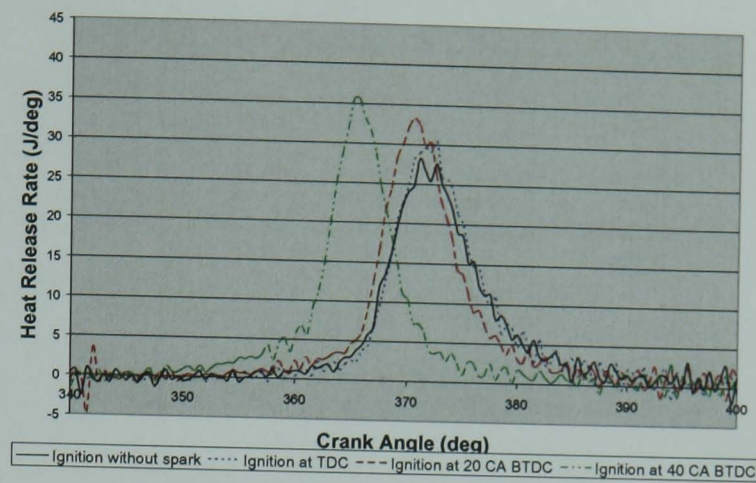
Figure 6.30 Heat Release Rate against crank angle (deg) at injection timing TDC, EVC 80 CA deg BTDC, IVO 75 CA deg ATDC, shorter CAI camshafts
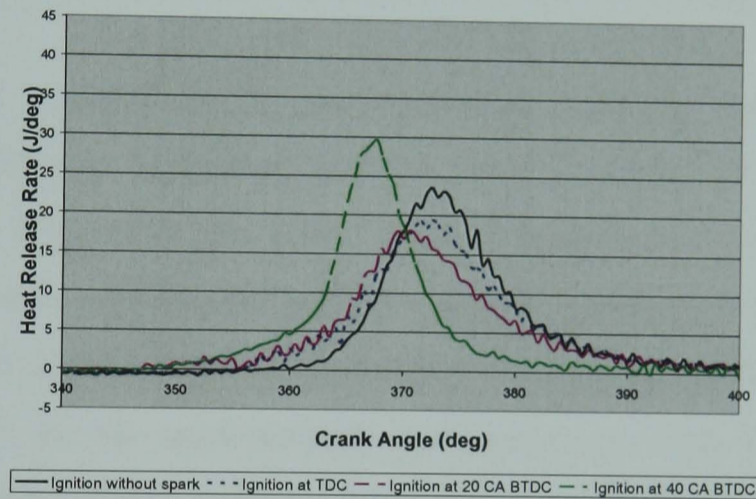

Figure 6.31 Heat Release Rate against crank angle (deg) at injection timing TDC, EVC 70 CA deg BTDC, IVO 75 CA deg ATDC, longer CAI camshafts

Table 6.6 Comparison of CAI combustion characteristics between shorter and longer CAI camshafts

	EVC 80 CA deg BTDC, IVO 75 deg ATDC				EVC 70 deg BTDC, IVO 75 deg ATDC			
	SOI at TDC (intake)				SOI at TDC (intake)			
	Ignition without spark	Ignition at TDC	Ignition at 20 CA BTDC	Ignition at 40 CA BTDC	Ignition without spark	Ignition at TDC	Ignition at 20 CA BTDC	Ignition at 40 CA BTDC
10% mass burned (CA)	361	357	357	356	361	358	359	360

182

50% mass burned (CA)	373	371	372	366	374	373	371	367
90% mass burned (CA)	380	381	384	377	386	387	385	376
10%-50% burn duration (CA)	12	14	15	10	13	15	12	7
50%-90% burn duration (CA)	7	10	12	11	12	14	14	9
10%-90% burn duration (CA)	19	24	27	21	25	29	26	16
COV_{IMEP} (%)	2.07	1.84	1.11	1.06	9.77	8.27	6.0164	5.02
Peak pressure (MPa)	27.18	29.58	27.77	34.31	26.39	26.26	26.92	33.29
Location of peak pressure (CA)	376.5	370.5	377	370	378	376.5	375	371.5
NET IMEP (MPa)	2.81	2.94	2.92	2.86	2.30	2.39	2.32	2.42
Texh (K)	395	393	398	378	403	429	418	399
Trapped Residuals (%) (Predicted)	44.68	46.13	45.33	46.97	47.32	46.63	46.23	47.27

As with Case A and Case B, spark-assistance near the misfire boundary can affect combustion phasing. As ignition is advanced for case C and D, combustion phasing is also advanced (Figures 6.28 – 6.31). Again it appears that the higher NIMEP is due to earlier combustion phasing for both the shorter and longer CAI camshafts. Table 6.6 compares MFB data for both set of camshafts, it can be seen that the 10% MFB angle is more advanced for the spark-assisted cases compared with combustion without spark. Early combustion phasing indicates that there is more time for combustion to commence and hence more energy can be realized from the fuel. However, advancing ignition too much leads to very advanced combustion which does not lead to higher NIMEP. From Table 6.6, it can be seen that for Case C at ignition 20 CA deg BTDC, the NIMEP value is 2.92 bar, this decreases to 2.86 bar when ignition is advanced to 40 CA deg BTDC. The COV_{IMEP} value also decreases as ignition timing is advanced and also when spark-assistance is used, indicating enhanced combustion stability for spark-assistance.

6.4.2 Effects of Spark Ignition on Emissions

The same relationship is observed for Cases C and D with regards to emissions as case A and B. For both Case C and Case D, spark-assistance CAI yields higher $ISNO_x$ values compared with conventional CAI (Figure 6.32 and Figure 6.33). This has been attributed to higher in-cylinder temperature for the spark-assisted cases as indicated by Figure 6.34

183

and Figure 6.35. However, beneath a certain threshold temperature, the effects of oxidation have a detrimental effect on combustion. For Case C at SOI 30 CA deg ATDC, it is evident that although the in-cylinder temperature is lower for spark timing at TDC and 20 CA BTDC, the $ISNO_x$ values are still higher for spark-assisted CAI compared with conventional CAI.

For Case C and Case D, $ISNO_x$ values are approximately between 0.9 g/kW.h to 1.4 g/kW.h. ISNOx values for CAI combustion at lambda 1.2 are usually below 0.4g/kW.h, as shown in Chapter 5, however even ISNOx values close to 1 g/kW.h are still relatively low compared with SI combustion.
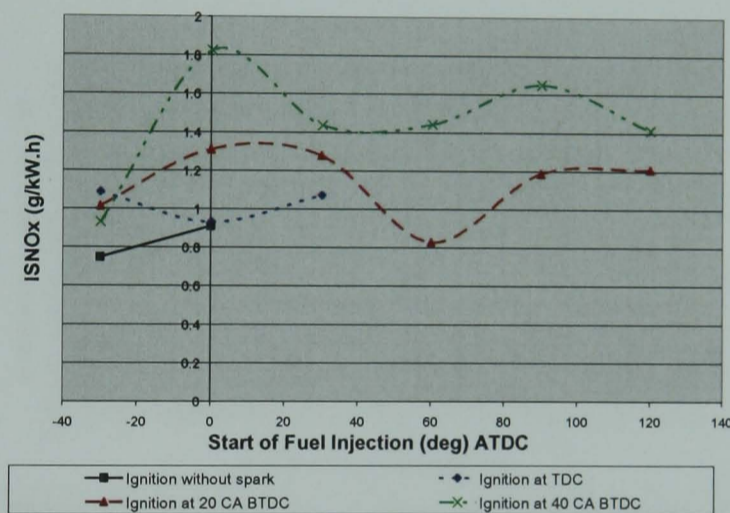
Figure 6.32 ISNOx against injection timing at different Ignition Timings, EVC 80 CA deg BTDC, IVO 75 CA deg ATDC, shorter CAI camshafts
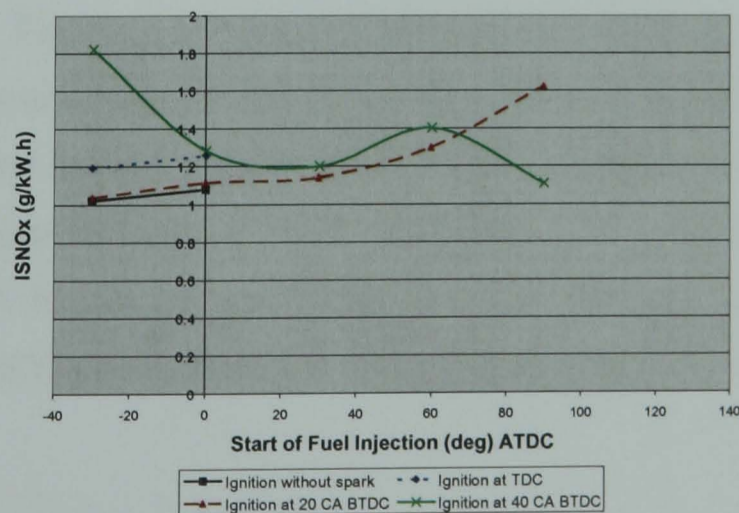

Figure 6.33 ISNOx against injection timing at different Ignition Timings, EVC 70 CA deg BTDC, IVO 75 CA deg ATDC, longer CAI camshafts
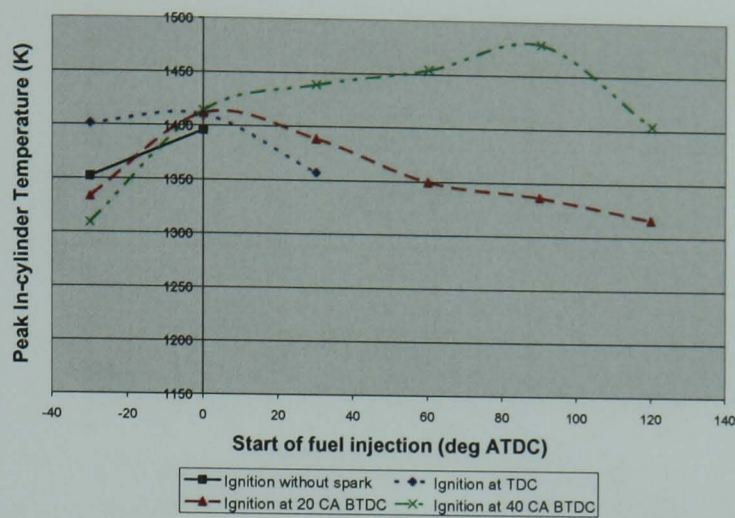
184

Figure 6.34 Calculated In-cylinder temperature against injection timing at different Ignition Timings, EVC 80 CA deg BTDC, IVO 75 CA deg ATDC, shorter CAI camshafts
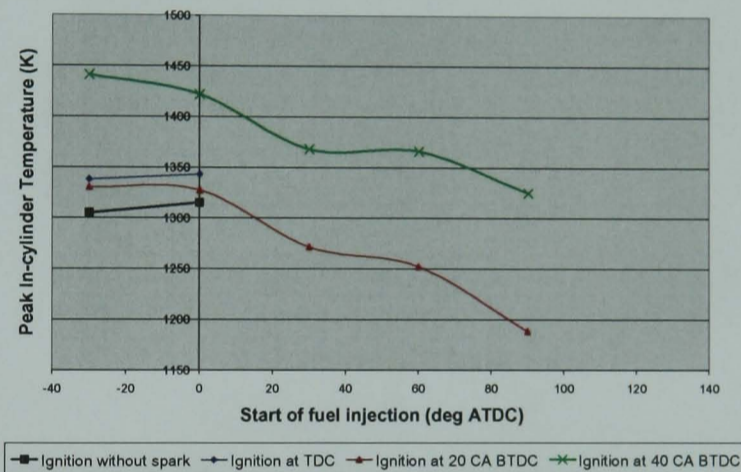

Figure 6.35 Calculated in-cylinder temperature against injection timing at different Ignition Timings, EVC 70 CA deg BTDC, IVO 75 CA deg ATDC, longer CAI camshafts

Figure 6.34 and Figure 6.35 supports the general trend of higher in-cylinder temperatures for spark-assisted CAI compared with conventional CAI. As a result, the ISHC values are lower for spark-assisted CAI compared with conventional CAI across the fuel injection range as shown in Figure 6.36 and 6.37. ISCO follows a similar trend with higher in-cylinder temperatures from the spark-assisted cases leading to lower ISCO values (Figure 6.38 and Figure 6.39).
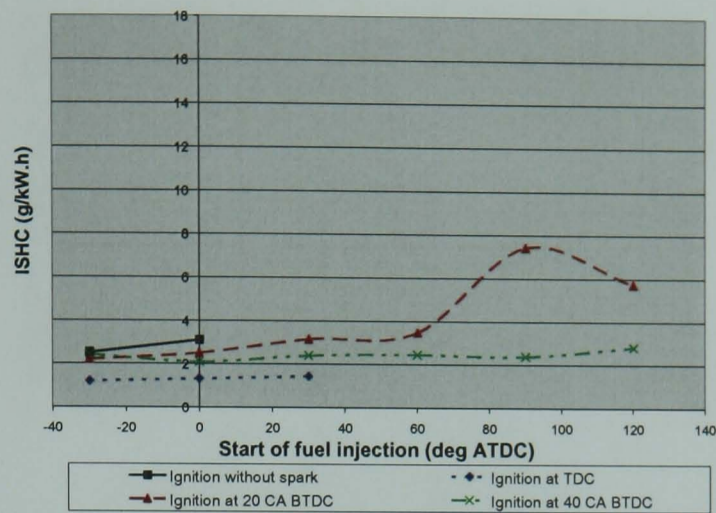
185

Figure 6.36 ISHC against injection timing at different Ignition Timings, EVC 80 CA deg BTDC, IVO 75 CA deg ATDC, shorter CAI camshafts
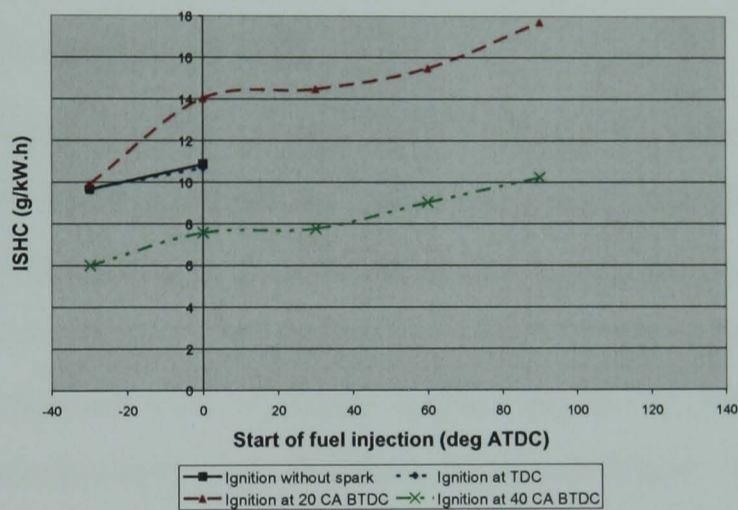

Figure 6.37 ISHC against injection timing at different Ignition Timings, EVC 70 CA deg BTDC, IVO 75 CA deg ATDC, longer CAI camshafts
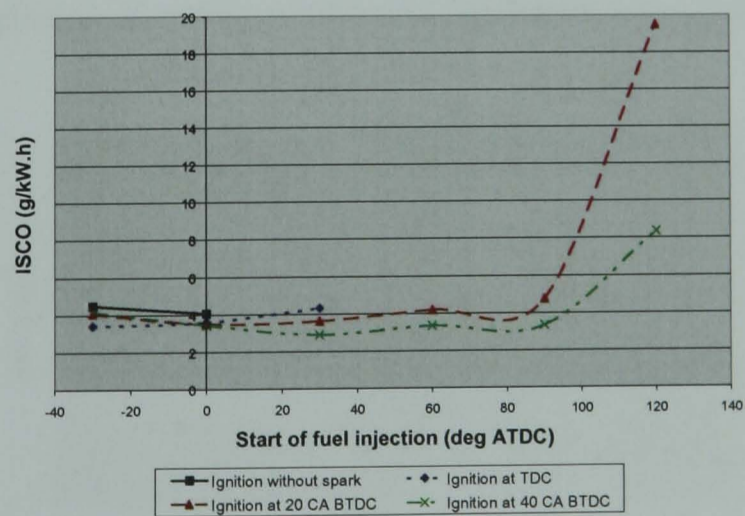

Figure 6.38 ISCO against injection timing at different Ignition Timings, EVC 80 CA deg BTDC, IVO 75 CA deg ATDC, shorter CAI camshafts
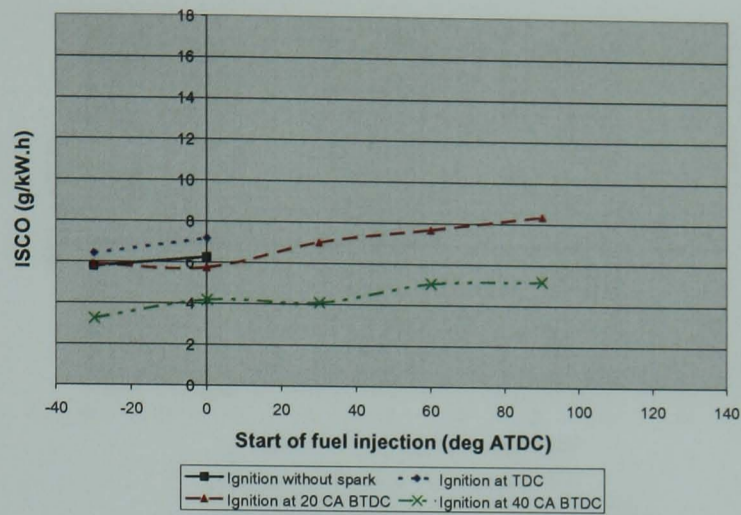
Figure 6.39 ISCO against injection timing at different Ignition Timings, EVC 70 CA deg BTDC, IVO 75 CA deg ATDC, longer CAI camshafts

6.4.3 Effects of Spark Ignition on ISFC

It appears that SOI 30, 60 and 90 CA deg ATDC delivers the lowest ISFC (g/kW.h) for spark timing at 40 CA deg BTDC for both Case C and Case D (Figure 6.40 and Figure 6.41). For injection during the NVO re-compression process at SOI -30 deg ATDC, ISFC values for Case C are higher for spark timing at 40 CA deg BTDC compared with conventional CAI. It would appear that the re-compression process affects the charge composition and therefore spark-assistance has limited effect. During SOI at TDC (intake) for Case D, the ISFC values for conventional CAI are higher than spark-assisted CAI at spark timing 40 CA deg BTDC. This is due to higher in-cylinder pressures and hence less inducted fresh air and less injected fuel.
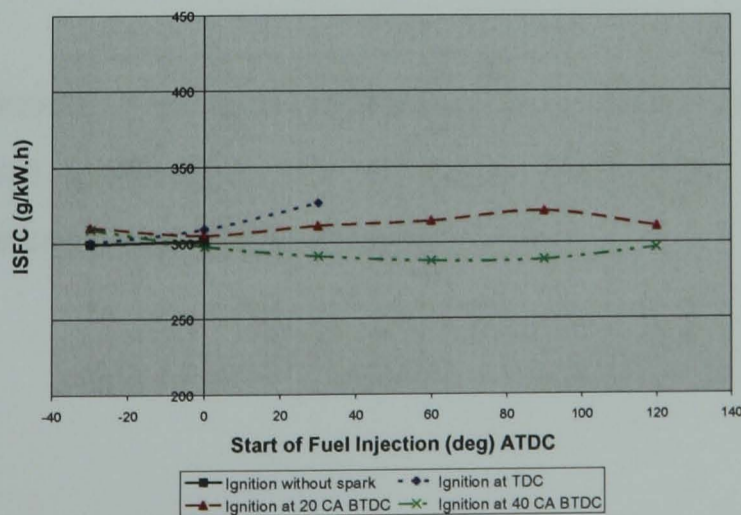

Figure 6.40 ISFC against injection timing at different Ignition Timings, EVC 80 CA deg BTDC, IVO 75 CA deg ATDC, shorter CAI camshafts
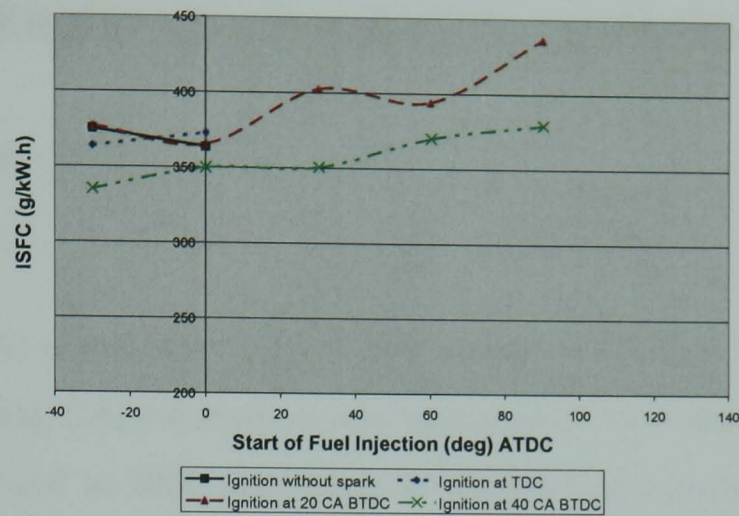
187

Figure 6.41 ISFC against injection timing at different Ignition Timings, EVC 70 CA deg BTDC, IVO 75 CA deg ATDC, longer CAI camshafts

6.4.4 Summary of spark-assisted CAI Combustion

It was observed that for spark-assisted CAI operation, higher NIMEP values were obtained. Furthermore as spark timing was advanced NIMEP increased. On inspection of the heat release rate, it was noticed that spark-assistance advanced the start of combustion and also increased the peak of heat release rate, due to optimized combustion phasing. As a result ISFC values decrease and the cyclic variation is reduced.

On inspection of the 10%-90% MFB, it is noticeable that spark-assistance has a greater effect on the 50%-90% MFB stage, as well as being responsible for the early start of combustion.

ISNOx values increased with spark-assistance due to higher in-cylinder temperatures caused by advanced combustion. Due to earlier combustion phasing, HC and CO emissions are lower compared with spark-assisted CAI.

6.5 Effects of Engine speed on Engine combustion

6.5.1 Introduction

In order to study CAI combustion further and attempt to increase the boundary region, the engine speed during CAI combustion was increased to 2000 rpm. It was only possible to increase engine speed to 2000 rpm using the longer CAI camshaft. Since, the longer CAI camshaft had higher intake valve lift than the shorter CAI camshaft, it was possible to induct more fresh charge needed for operation at higher speeds.

In order to study the effect of engine speed, tests were conducted for a valve timing of EVC 65 CA deg BTDC, IVO 70 CA deg ATDC at two engine speeds: 1500 rpm and 2000 rpm. It was also of interest to investigate if start of fuel injection timing at different speeds offered any flexibility of control over load and the consequent effect on emission and fuel consumption. Therefore, graphs of NIMEP, ISFC, ISNOx, ISHC and ISCO were plotted against start of injection. Furthermore, in order to investigate CAI combustion characteristics at 2000 rpm, the 10%, 50% and 90% MFB, percentage of trapped residual and heat release data were analyzed. In order to see if lambda had any effect on CAI combustion at high speed, three cases were studied at SOI -40, 40 and 120 CA deg ATDC:

[I] EVC 65 CA deg BTDC, IVO 70 CA deg ATDC, 2000 rpm, Lambda = 1.0

[II] EVC 65 CA deg BTDC, IVO 70 CA deg ATDC, 2000 rpm, Lambda = 1.1

[III] EVC 65 CA deg BTDC, IVO 70 CA deg ATDC, 1500 rpm, Lambda = 1.0

6.5.2 Effects of speed on engine performance at valve timing EVC 65 CA deg BTDC, IVO 70 CA ATDC

Figure 6.42 and Figure 6.43 show charts of ISNOx and trapped residual values against speed respectively. It can be seen that at EVC 65 CA deg BTDC, IVO 70 CA deg ATDC at 2000 rpm and SOI 40 CA deg ATDC, CAI combustion is occurring; at 1500 rpm SI combustion is taking place. To achieve CAI operation at 1500 rpm, more advanced EVC timing has to be used. ISNOx values are low at 2000 rpm and the percentage of trapped residual is high; at 1500 rpm, ISNOx values are high and percentage of trapped residuals is low. Figure 6.44 shows a chart of NIMEP against speed for the longer duration CAI camshaft i.e. intake duration 140 CA, exhaust duration 130 CA. It can be seen that at 1500 rpm the highest NIMEP can be achieved with SI operation, at 2000 rpm the lowest NIMEP is realized.

From Figure 6.45, it is apparent that as engine speed is increased from 1500 rpm (Case III) to 2000 rpm (Case I and Case II), the NIMEP decreases. At high engine speeds, the gas exchange process has less time to take place, the higher residual is obtained as shown in Figure 6.46, limiting the amount of inducted fresh charge and hence restricting the highest attainable NIMEP. Furthermore, increasing the lambda value from 1.0 (case I) to 1.1 (case II) at high speed, causes a further decrease in the NIMEP (Figure 6.45).

Start of injection timing does not seem to affect NIMEP very much. At 2000 rpm, the NIMEP value is almost constant at 2.68 bar at lambda = 1.0. At lambda = 1.1, the NIMEP value varies between 2.64 bar to 2.11 bar and at 1500 rpm, NIMEP varies between 2.9 bar to 3.05 bar.
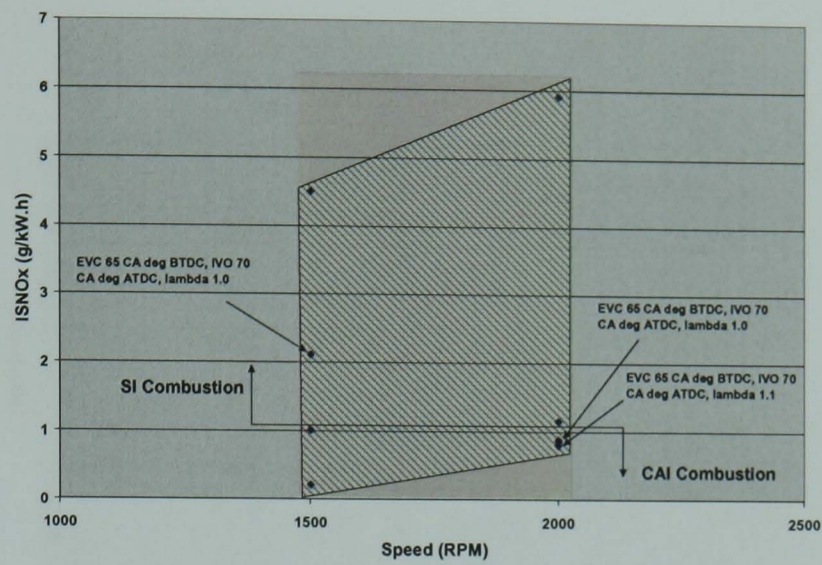
190

Figure 6.42 Chart of ISNOx against speed indicating CAI and SI operational area using long CAI camshafts, SOI 40 CA deg ATDC
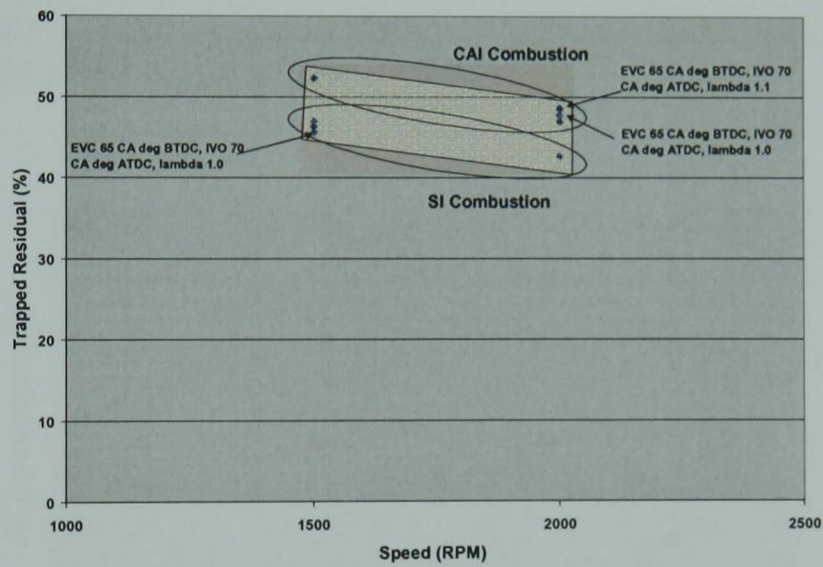

Figure 6.43 Chart of trapped residual against speed indicating CAI and SI operational area using long CAI camshafts, SOI 40 CA deg ATDC
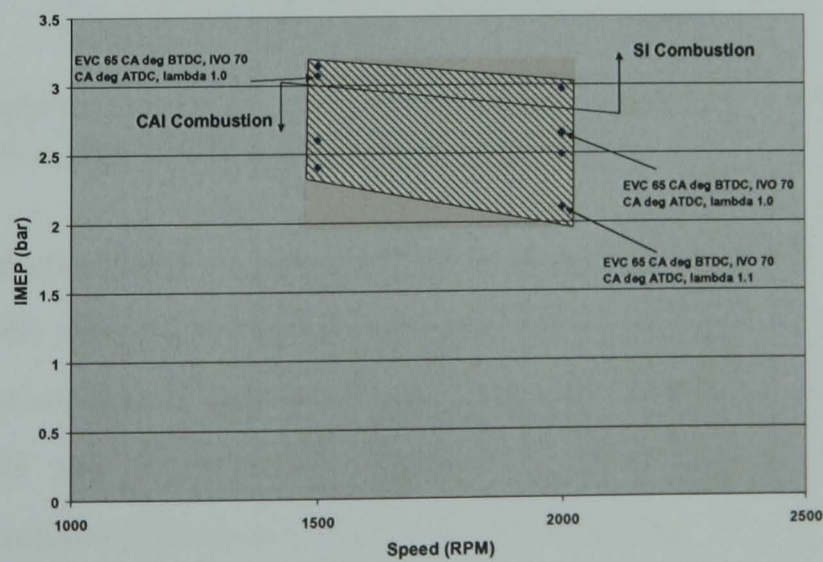

Figure 6.44 Chart of IMEP against speed indicating CAI and SI operational area using long CAI camshafts, SOI -40 CA deg ATDC
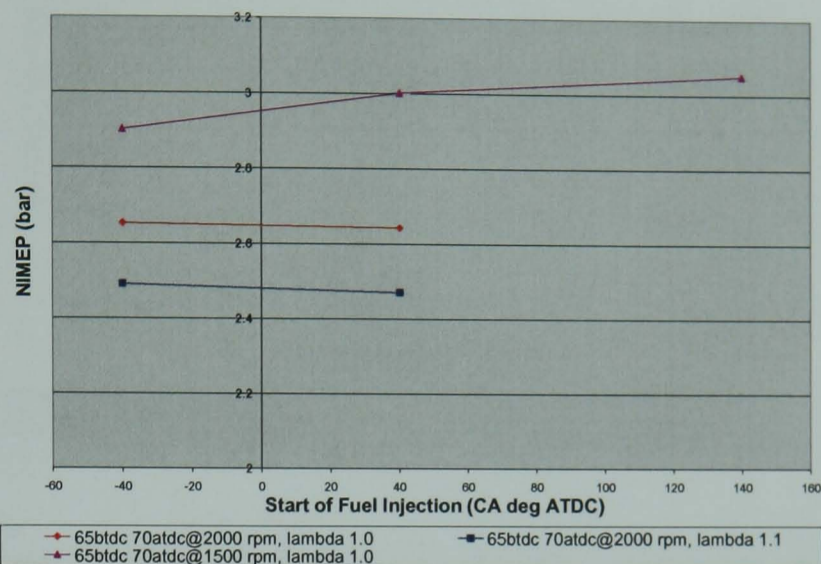
Figure 6.45 NIMEP against injection timing at different speed and lambda, EVC 60 CA deg BTDC, IVO 70 CA deg ATDC
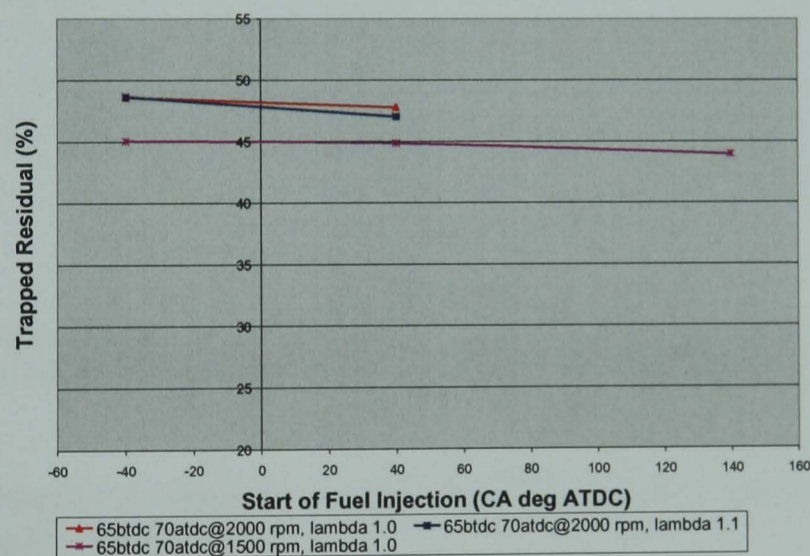

Figure 6.46 Trapped Residual against injection timing at different speed and lambda, EVC 60 CA deg BTDC, IVO 70 CA deg ATDC

It can be seen that operations at 2000 rpm have advanced 10% MFB and retarded 90% MFB compared with that at 1500 rpm (Figure 6.47). The burn duration increases at high speed and at lean conditions (Figure 6.48) and the peak cylinder pressure decreases with speed (Figure 6.49 and Figure 6.50). Highest in-cylinder temperature coupled with highest peak pressure result in short burn duration at 1500 rpm. As speed is increased, the volume of trapped residuals increase due to a faster gas exchange process, this leads to longer burn duration and eventually misfire.
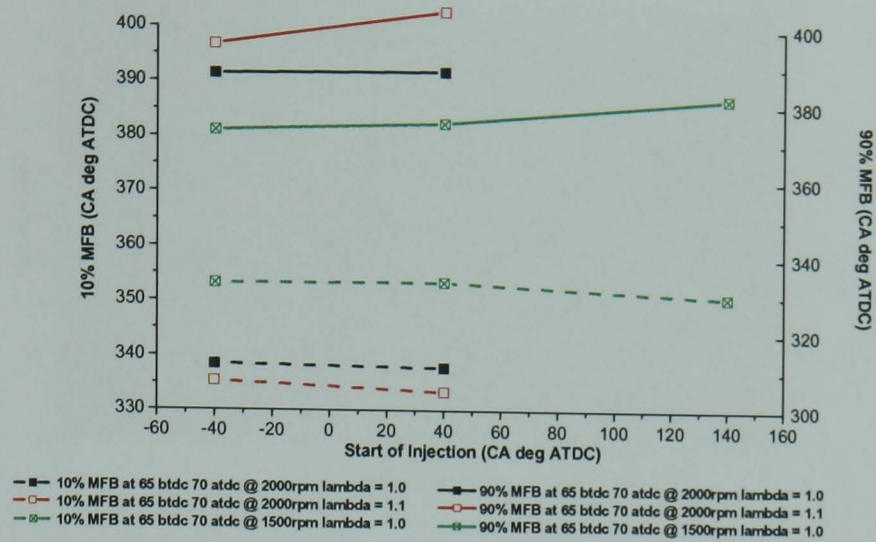
192

Figure 6.47 10%, 90% MFB against injection timing at different speed and lambda
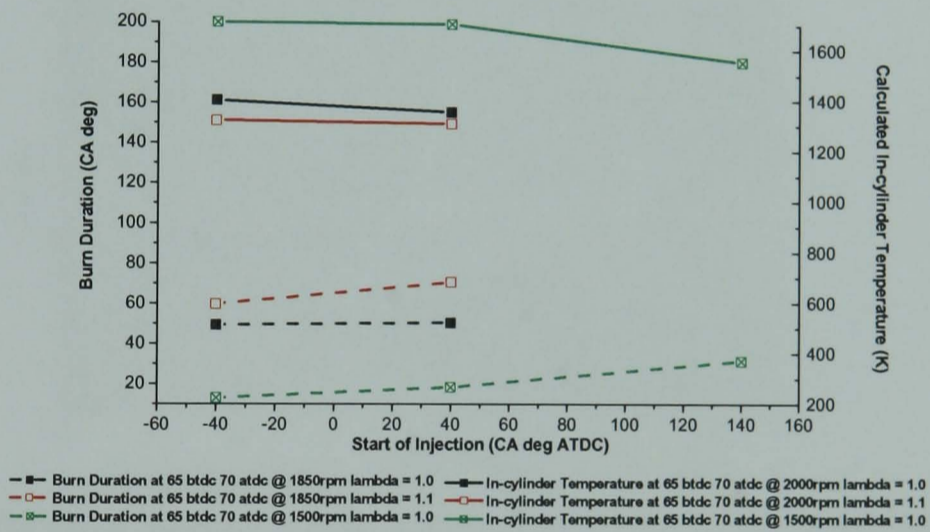
Figure 6.48 In-cylinder temperature, burn duration against injection timing at different speed and lambda
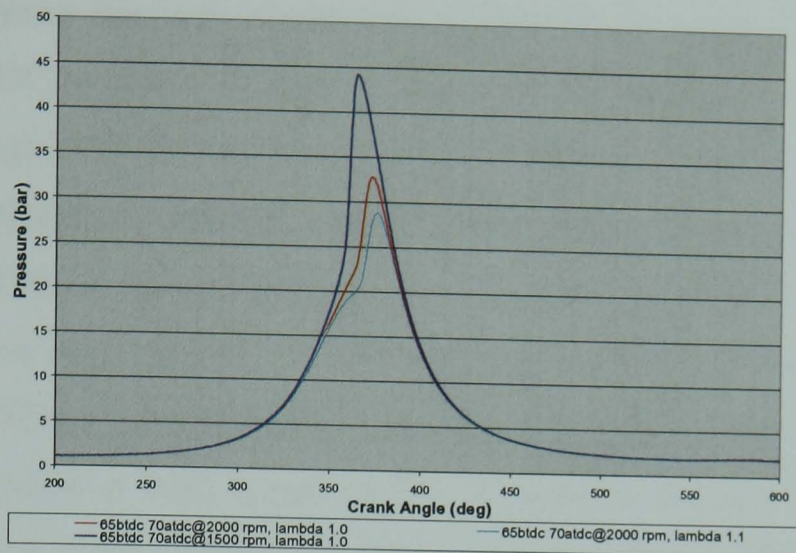
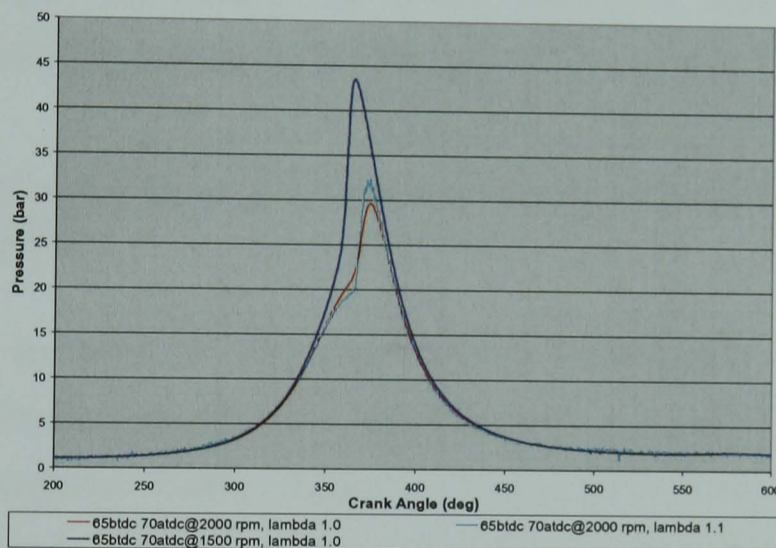**Figure 6.49 Pressure against crank angle at different speed and lambda, SOI at -40 CA deg ATDC**

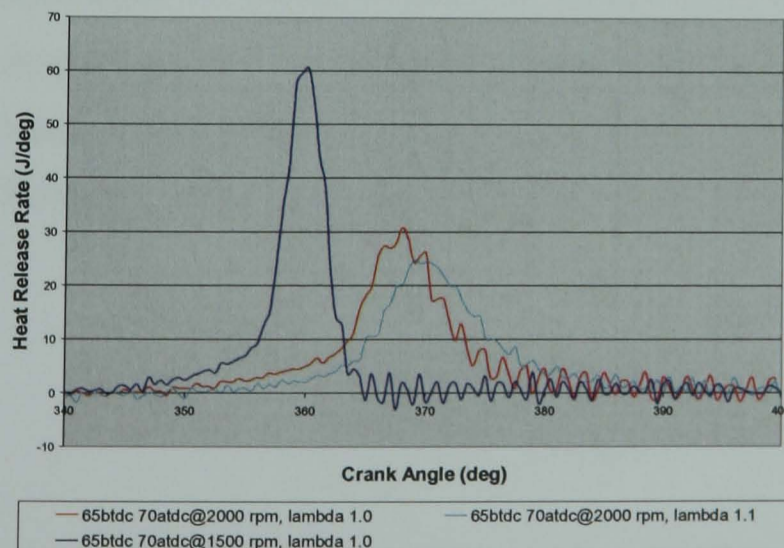**Figure 6.50 Pressure against crank angle at different speed and lambda, SOI at 40 CA deg ATDC**

Figure 6.51 Heat Release Rate against crank angle at different speed and lambda, EVC 60 CA deg BTDC, IVO 70 CA deg ATDC, SOI at -40 CA deg ATDC

194

Figure 6.51 shows the heat release rate against crank angle, combustion at 1500 rpm occurs near TDC, whereas for Case I and Case II (2000 rpm), combustion occurs after TDC. Zhao et al. [59] offer an explanation and state that theoretically, the ignition delay of HCCI combustion depends largely on mixture chemistry, and it is relatively independent of engine speed. However, the ignition time of HCCI combustion relative to the engine crank angle will be retarded when the engine speed increases. When ignition occurs before TDC, the temperature rise from compression will compensate the relative ignition retardation at high engine speed. If ignition appears after TDC, the relative ignition delay caused by high engine speed will be further retarded by expansion which slows the temperature rise. Since combustion is occurring after TDC for the high speed cases, in-cylinder temperatures are lower leading to drastically retarded ignition compared with HCCI combustion at 1500 rpm.

6.5.3 Effects of speed on engine emissions at valve timing EVC 65 CA deg BTDC, IVO 70 CA ATDC

ISNO$_x$ values are lower at 2000 rpm compared with 1500 rpm (Figure 6.52). This corresponds with Li et al. [60] who found the same general trend that increasing engine speed led to decreased BSNO$_x$ values. Li et al. also found that variation for BSNO$_x$ at high speed between lambda 1.0 and 1.1 is quite miniscule. The reason for the drop in ISNOx values at high speed is due to the drop of in-cylinder temperatures as shown in Figure 6.48. Furthermore, as SOI is varied from -40 CA deg ATDC to 40 CA deg ATDC, ISNOx values drop for all three cases. Injecting during the recompression period (-30 CA deg ATDC) causes combustion to start early, leading to slightly higher combustion temperatures. However, even this slight change in temperature causes higher ISNOx values.
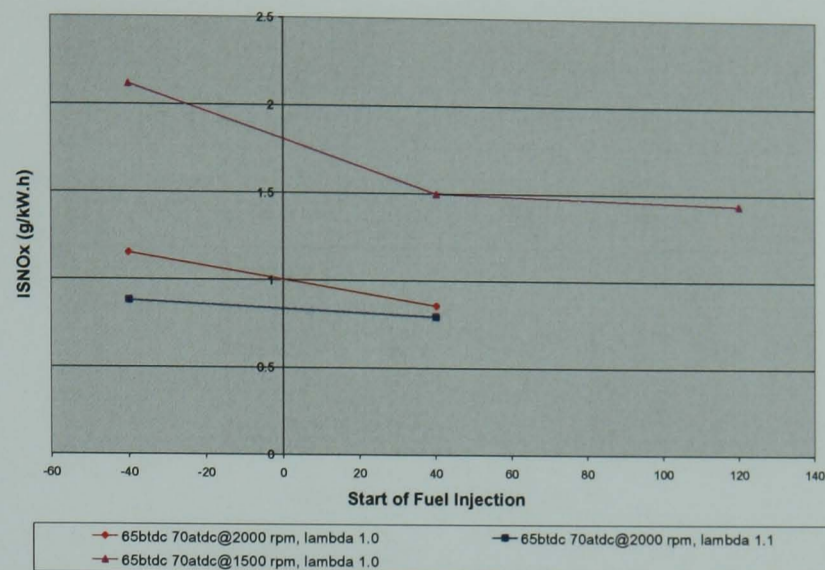
Figure 6.52 ISNOx against injection timing at different speed and lambda

From Figure 6.53 it can be seen that the ISHC values are higher for 2000 rpm compared with 1500 rpm. Furthermore, lambda 1.1 (Case II) has higher ISHC values compared with lambda 1.0 (Case I), due to lower combustion temperatures shown in Figure 6.48. The ISHC values remain constant over the injection range.
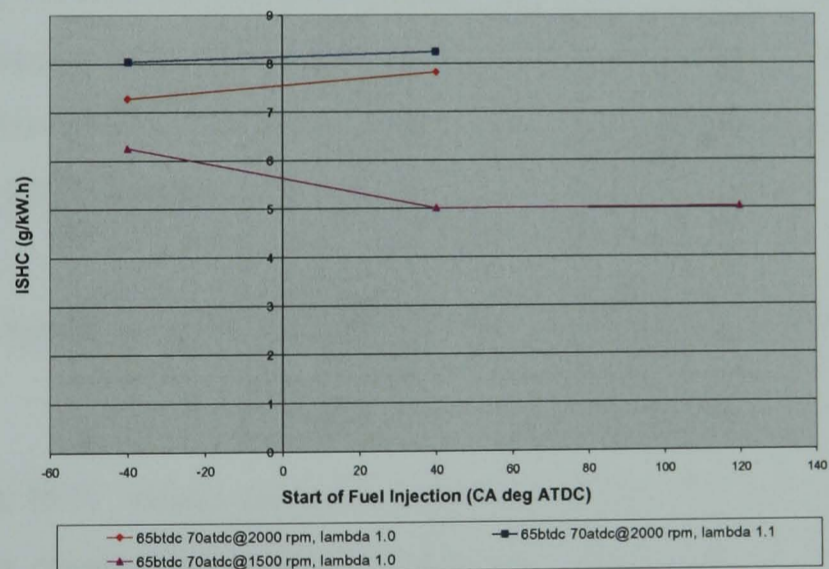

Figure 6.53 ISHC against injection timing at different speed and lambda

In contrast, ISCO values are higher at 1500 rpm than those at 2000 rpm (Figure 6.54) and at a leaner mixture which produces less CO emissions, probably due to extended and delayed combustion at 2000 rpm for more complete CO oxidation.
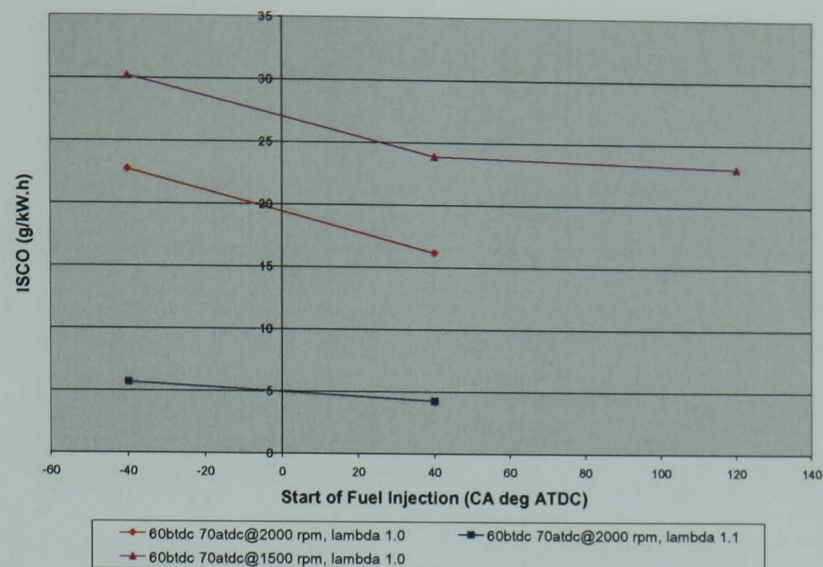
Figure 6.54 ISCO against injection timing at different speed and lambda

Retarding the injection timing, from -40 to 40 CA deg ATDC causes ISCO values to drop for all three cases, a possibility is that injection at 40 CA deg ATDC allows better mixing due to the piston moving downwards and introducing a swirl motion. At SOI -40 CA deg ATDC, the piston is moving upwards, injecting at this time causes fuel to be sprayed onto the cylinder wall and piston causing fuel rich pockets. As injection timing is retarded to SOI 120 CA deg ATDC, for Case III (1500 rpm), ISCO values decrease further. This is due to better mixing, when the piston is near BDC, fuel injection has more cylinder volume to disperse within; this better mixing and avoidance of wall and piston wetting allows for lower ISCO values.

6.5.4 Effects of speed on ISFC at valve timing EVC 65 CA deg BTDC, IVO 70 CA ATDC

At 1500 rpm, the ISFC values are lower compared with 2000 rpm (Figure 6.55). This is due to inefficient combustion phasing, Figure 6.51 shows that combustion is occurring near TDC whereas for higher speed the combustion is retarded. The injection timing has little effect on ISFC as it does on NIMEP.
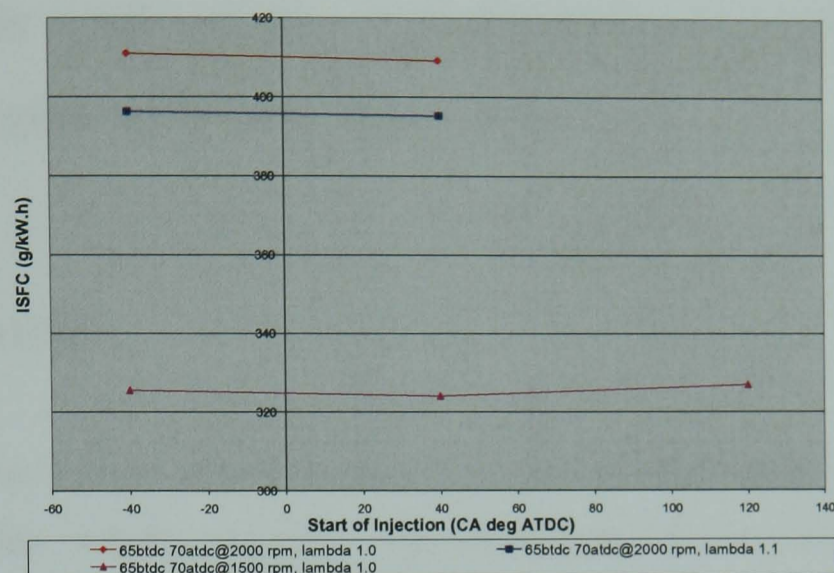
Figure 6.55 ISFC against injection timing at different speed and lambda

6.5.5 Summary of effects of speed at valve timing EVC 65 CA deg BTDC, IVO 70 CA deg ATDC

It has been shown that for a given valve timing, increasing speed allows CAI combustion to be realized. At EVC 65 CA deg BTDC, at 1500 rpm, the engine operates in SI combustion mode, increasing speed to 2000 rpm allows the engine to trap more residuals and achieve CAI combustion.

The effects of start of injection timing on CAI combustion were investigated at 2000 rpm. It was found that varying the SOI from -40 to 40 CA deg ATDC had little effect on NIMEP at 2000 rpm. Likewise, ISFC values also did not drastically vary over the injection range.

ISNOx values are lower at a speed of 2000 rpm compared with 1500 rpm at EVC 65 CA deg ATDC, due to lower in-cylinder temperatures. At lambda 1.1 ISNOx values are even lower due to even lower in-cylinder temperatures.

ISHC values increases with engine speed as combustion changes from SI at 1500 rpm to CAI operation at 2000 rpm, whereas CO emissions decreases.

6.6 Analysis of CAI Combustion at lambda 1.2 in DI Gasoline Engine with Late Injections

6.6.1 Introduction

Results in Chapter 5 have shown that that fuel injection at different periods during the engine cycle has various benefits and drawbacks. Early injection during the recompression period can promote the auto-ignition process and cause combustion to start early. Late injection during the compression stroke can produce stratified charge and hence a different combustion process. It becomes apparent that a combination of injection timing strategies is needed to optimize fuel economy and emissions i.e. split injection strategies. The Bosch VS100 management system has capabilities to undergo split injections, where injection volume is split in percentage between the pre and main injections. However, due to limited information on the Bosch VS100 system, it was not possible to implement and test any split injection cases. It was deemed that investigating late injection would provide a useful indication of engine behaviour during the main injection phase of a split injection strategy. It has been reported that auto-ignition can be accelerated by the presence of stratified charge and commences into fuel-lean zones allowing control over ignition timing [58]. Therefore, it was also of interest to see if late injection allowed any control over ignition timing. Start of injection was varied from 170 CA deg ATDC to 290 CA deg ATDC (intake) in increments of 30 CA deg and engine performance and emission data was recorded. Again the engine was allowed to warm up and reach an operating temperature of 85°C. The throttle was left wide open, the AFR was kept at lambda 1.2 and engine speed was maintained at 1500 rpm.

Two different valve timing combinations were selected, to investigate the effect of intake and exhaust valve duration on CAI combustion and whether late SOI influenced any part of combustion. For the shorter CAI camshaft an EVC time of 85 CA deg BTDC at 1500 rpm was chosen, as more retarded EVC could only be operated with SI and advanced

EVC led to misfire. For the longer CAI camshaft, an EVC time of 75 CA deg BTDC was chosen, again retarding the EVC time led to SI combustion and advancing EVC caused misfire. The spark was left on for both cases, however, it was deemed that CAI combustion was occurring since ISNOx values were low. For comparison purposes engine performance and emissions were plotted against start of fuel injection timing for the full range of injection timings permissible with the engine management system. The full range was SOI -40 to 290 CA deg ATDC and plotted for the shorter CAI camshafts at an EVC timing of 85 CA deg BTDC. It is possible to inject earlier than -40 CA deg ATDC and inject later than 290 CA deg ATDC for CAI combustion, however the Bosch VS100 had been coded to only operate within this injection window. The two valve cases tested are given in Table 6.7:

Table 6.7 Operating conditions and valve timings for late injection testing

Lambda	1.2
Speed	1500 rpm
Case 1 with shorter CAI camshafts	**EVC 85 CA deg BTDC and IVO 60 CA deg ATDC** **Intake Valve Duration: 120 CA, Exhaust Valve Duration: 110 CA**
Case 2 with longer CAI camshafts	**EVC 75 CA deg BTDC and IVO 110 CA deg ATDC** **Intake Valve Duration: 140 CA, Exhaust Valve Duration: 130 CA**

6.6.2 Effects of EVC and Valve duration on NIMEP at late Injection

As shown in Figure 6.56, late injections have little effect on NIMEP values for both the shorter and longer CAI camshafts. Furthermore, there is little effect of fuel injection from SOI 170 to 290 CA deg ATDC on the percentage of trapped residual (Figure 6.58). But early injection during the intake stroke led to higher NIMEP (Figure 6.57) due to the charge cooling effect. The charge cooling effects also result in a lower percentage of trapped residuals for early injection (Figure 6.61), as more fresh charge is inducted. Figure 6.59 and Figure 6.60 shows that late injection is characterized with advanced start

of combustion but longer combustion duration. Whereas the opposite occurs for the early injection (Figure 6.62 and Figure 6.63).

Cao et al. [6] have shown that such a large difference in combustion characteristics between the early and later injections is due to charge stratification. As shown in Figure 6.64 and Figure 6.65, the mixture is homogeneous throughout the combustion chamber when injection takes place during the intake stroke. As the injection is retarded, there is a significant stratification in mixture distribution. There are more regions of very lean mixture as injection is retarded. Such lean mixtures will burn slower resulting in a longer combustion duration, while the start of combustion is advanced due to the presence of richer mixtures.
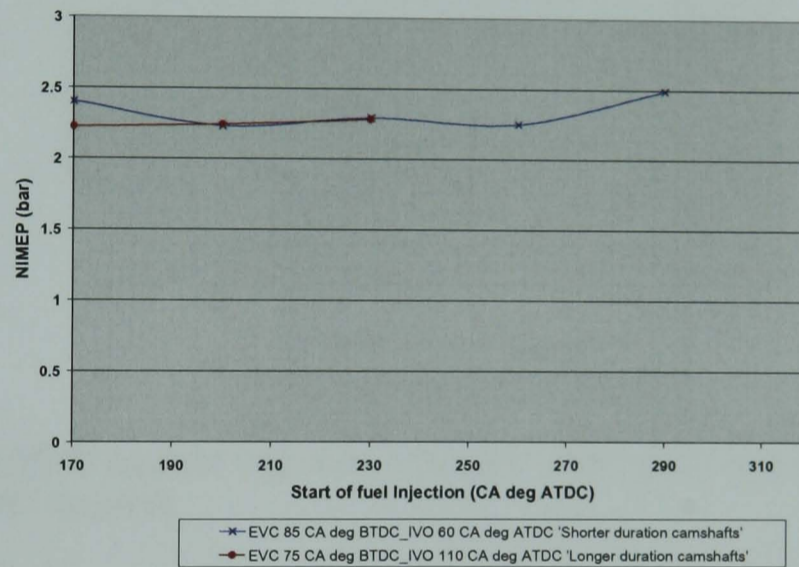

Figure 6.56 Net IMEP against injection timing at different valve timings for SOI 170 to 290 CA deg ATDC (intake)

Figure 6.57 Net IMEP against injection timing for the shorter CAI camshafts, SOI - 40 to 290 CA deg ATDC (intake), EVC = 85 CA deg BTDC, IVO = 60 CA deg ATDC

201

Figure 6.58 Trapped Residual against injection timing at different valve timings, SOI 170 to 290 CA deg ATDC (intake)

Figure 6.59 10% MFB against injection timing at different valve timings, SOI 170 to 290 CA deg ATDC (intake)

Figure 6.60 Burn Duration against injection timing at different valve timings, SOI 170 to 290 CA deg ATDC (intake)

Figure 6.61 Trapped Residual against injection timing for the shorter CAI camshafts, SOI -40 to 290 CA deg ATDC (intake), EVC = 85 CA deg BTDC, IVO = 60 CA deg ATDC
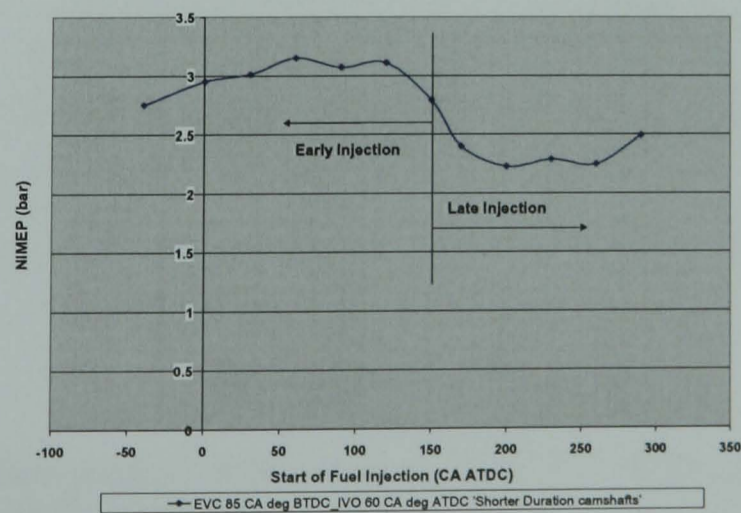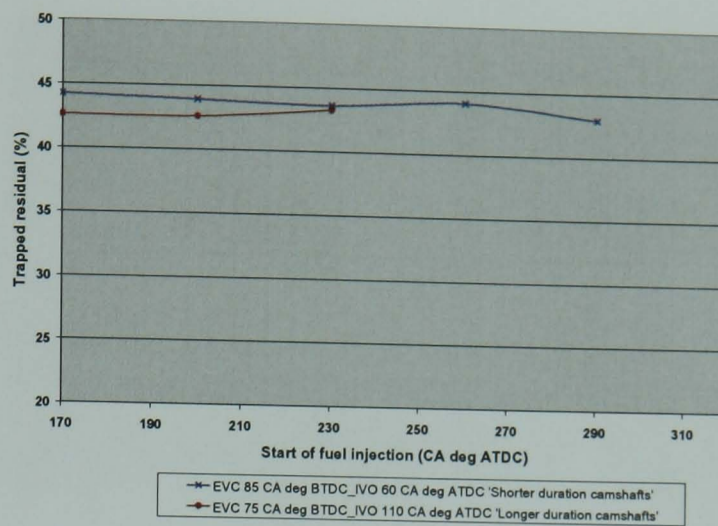

Figure 6.62 10% MFB against injection timing for the shorter CAI camshafts, SOI -40 to 290 CA deg ATDC (intake), EVC = 85 CA deg BTDC, IVO = 60 CA deg ATDC
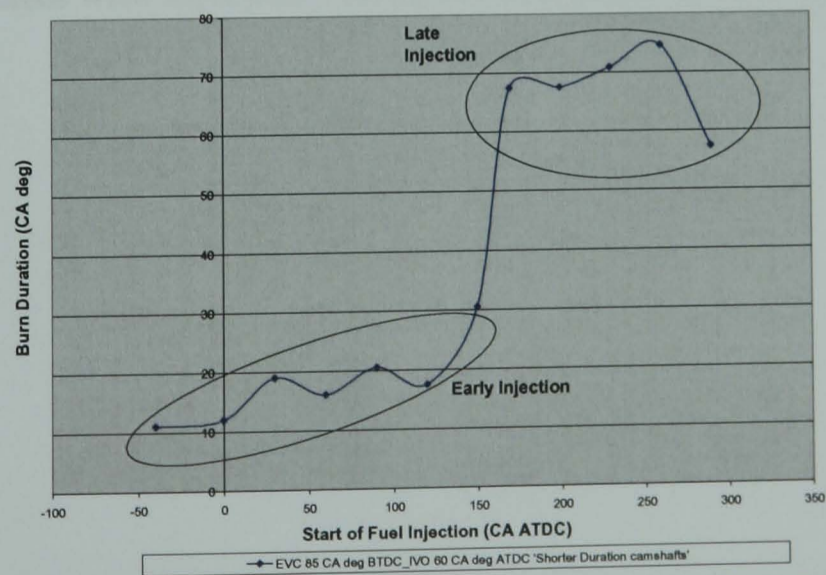
Figure 6.63 Burn Duration against injection timing for the shorter CAI camshafts, SOI -40 to 290 CA deg ATDC (intake), EVC = 85 CA deg BTDC, IVO = 60 CA deg ATDC

203
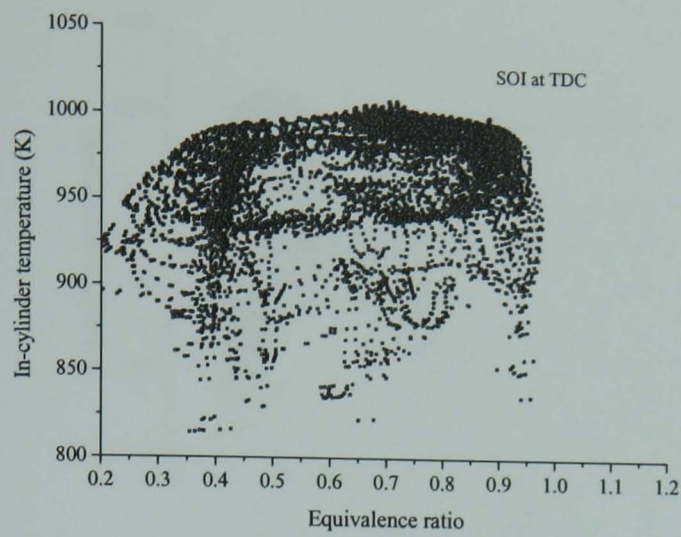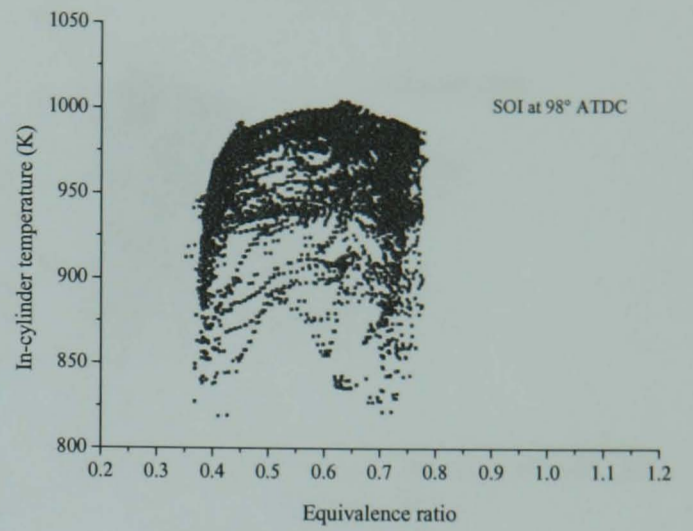
(a) TDC

(b) SOI at 98° ATDC
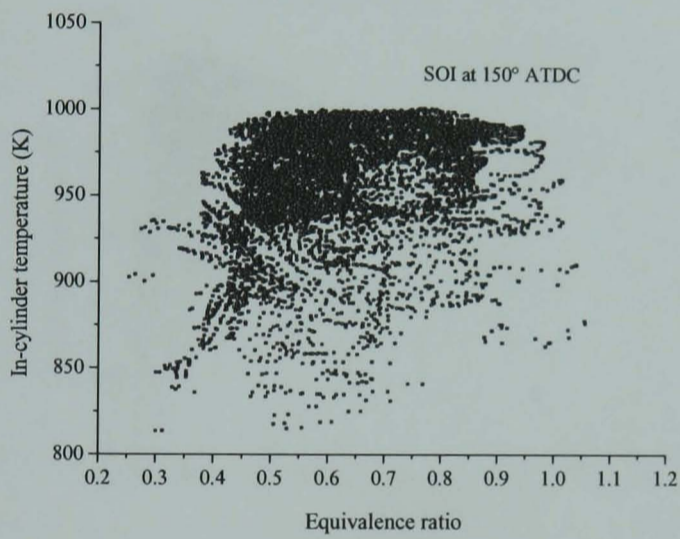
(c) SOI at 150° ATDC

Figure 6.64 Equivalence ratio-temperature distribution at the end of compression stroke for the cases with injection during the re-expansion and intake periods [58]

(d) SOI at 218° ATDC

(e) SOI at 250° ATDC

(f) SOI at 260° ATDC

(g) SOI at 270° ATDC
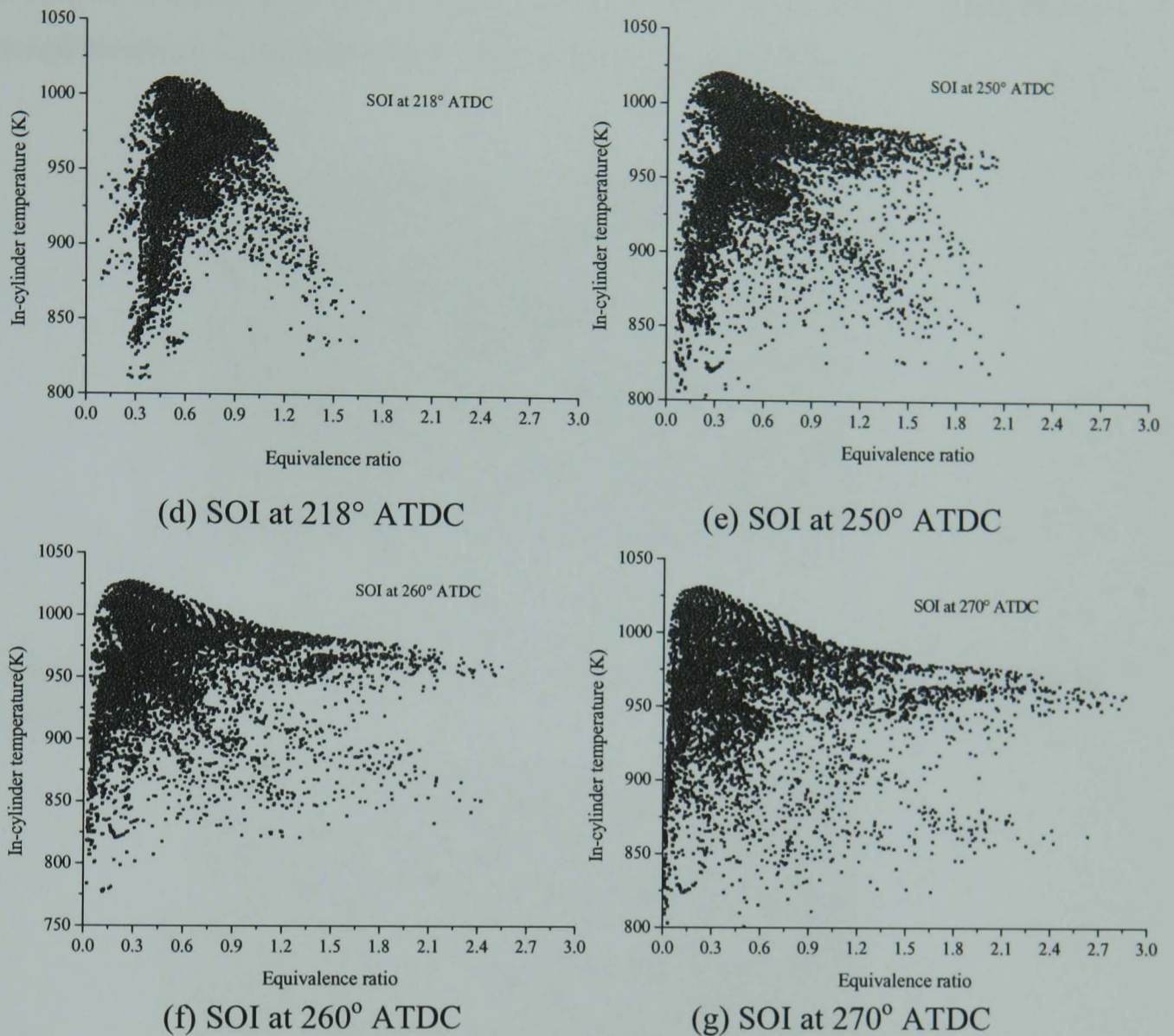
Figure 6.65 Equivalence ratio-temperature distribution at the end of compression stroke for the cases with injection after IVC [58]

6.6.3 Effects of EVC and Valve duration on emissions at late Injection

SOI between 170 to 290 CA deg ATDC has a minimal effect on ISNOx values for both valve timing cases (Figure 6.66), or in-cylinder peak gas temperature (Figure 6.68). Figure 6.67, shows the variation of ISNOx along the complete injection range permissible for the engine (-40 CA deg to 290 CA deg ATDC) for valve timing case of EVC 80 BTDC, IVO 60 ATDC. As can be observed, at early injection cases ISNOx values are extremely low and gradually increase for late injection. For late injection ISNOx values are higher than early injection, even though in-cylinder temperatures are lower for late

205

injection (Figure 6.69). Higher ISNOx values are due to the lower NIMEP values of late injection and localized high temperature regions of fuel rich mixtures.
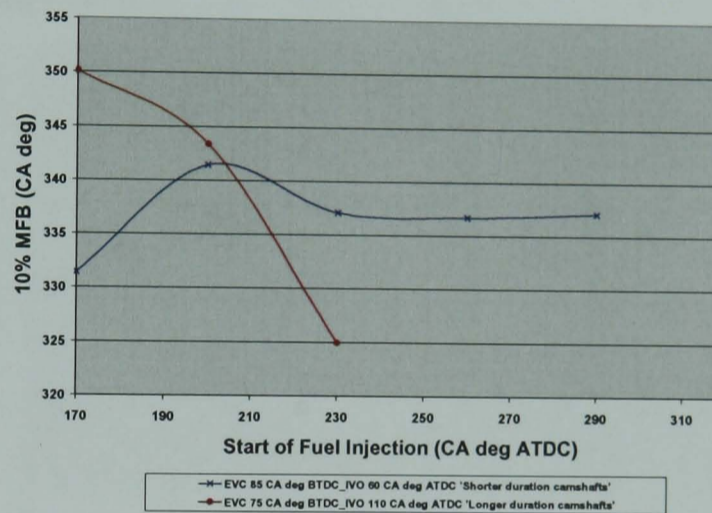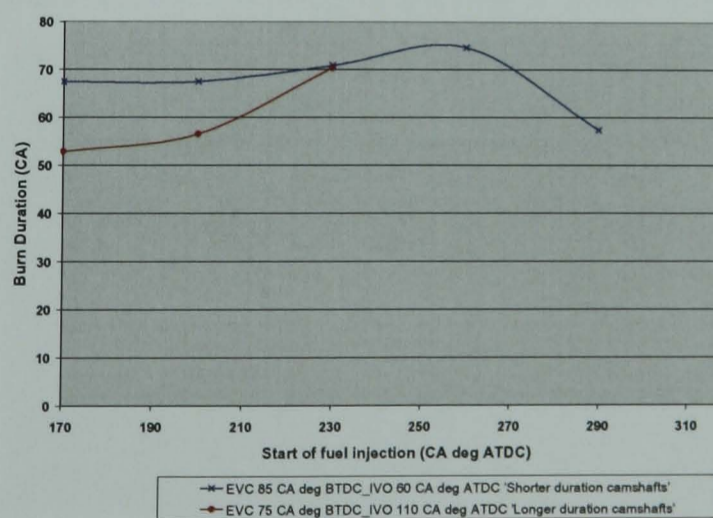

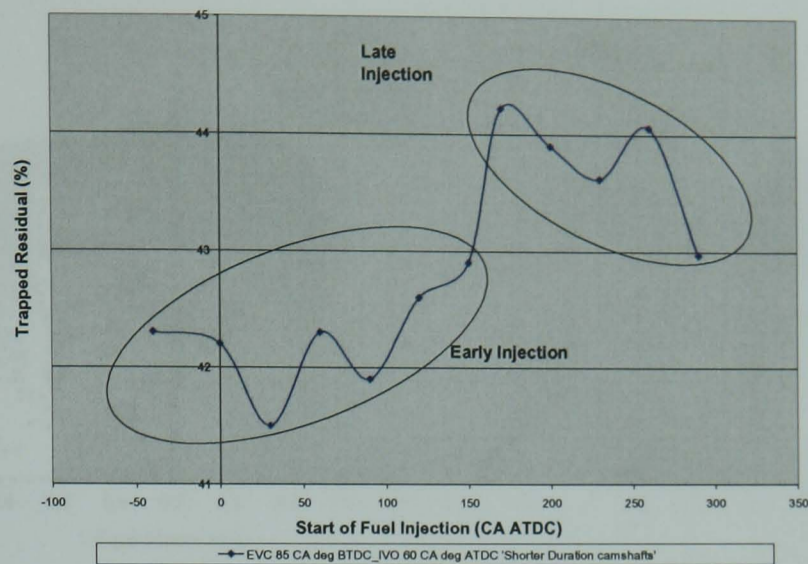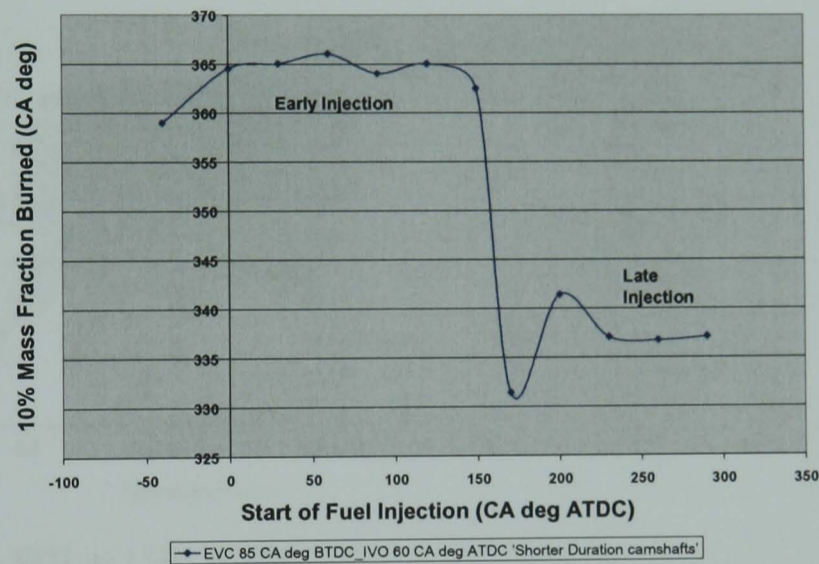**Figure 6.66 ISNOx against injection timing at different valve timings, SOI 170 to 290 CA deg ATDC (intake)**

Figure 6.67 ISNOx against injection timing for the shorter CAI camshafts, SOI -40 to 290 CA deg ATDC (intake), EVC = 85 CA deg BTDC, IVO = 60 CA deg ATDC
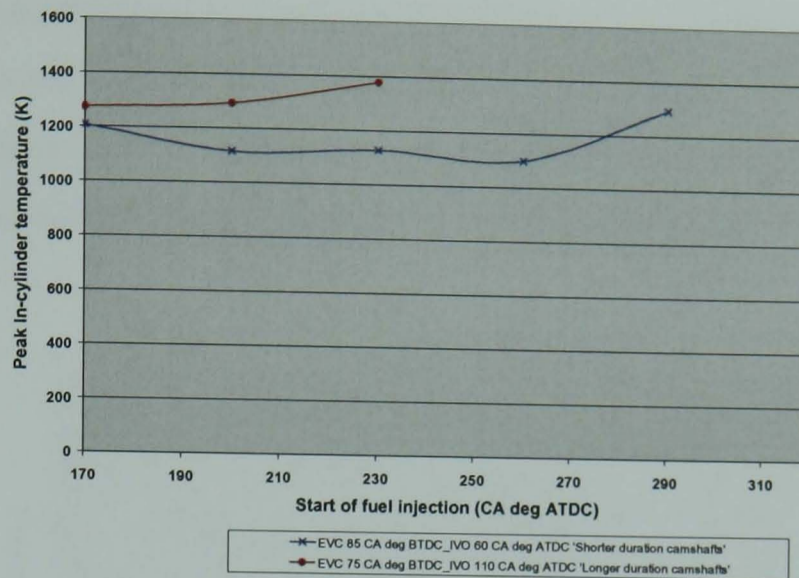
Figure 6.68 Peak In-cylinder temperature against injection timing at different valve timings, SOI 170 to 290 CA deg ATDC (intake)

Figure 6.69 Peak In-cylinder temperature against injection timing for the shorter CAI camshafts, SOI -40 to 290 CA deg ATDC (intake), EVC = 85 CA deg BTDC, IVO = 60 CA deg ATDC

For the shorter CAI camshafts, the intake air has been fully inducted when SOI takes place, reducing potential mixing effects by the motion of the intake air. For the longer duration camshafts, SOI occurs during the induction of intake air allowing for more homogeneous-like mixing to occur. This mixing results in lower ISHC from the longer CAI camshaft engine operation due to absence of fuel rich regions, as seen in Figure 6.70.

207

ISHC values (Figure 6.71) show a general trend of increasing with retarded injection as stratification becomes noticeable as discussed before. The presence of over lean/rich mixtures will increase uHC emissions. As expected the peak temperature is lower with late injection as the combustion duration was longer (Figure 6.69).

Figure 6.70 ISHC against injection timing at different valve timings, SOI 170 to 290 CA deg ATDC (intake)
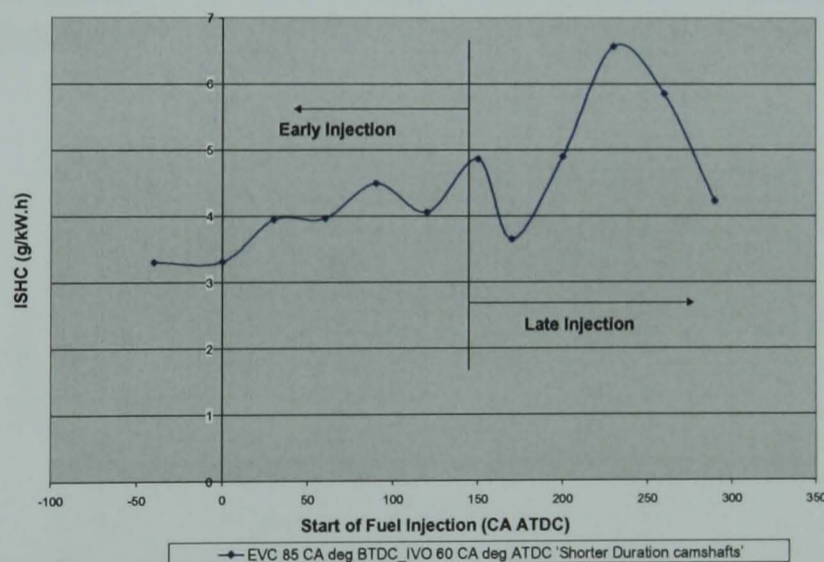
Figure 6.71 ISHC against injection timing for the shorter CAI camshafts, SOI -40 to 290 CA deg ATDC (intake), EVC = 85 CA deg BTDC, IVO = 60 CA deg ATDC

There is an increase in ISCO values as injection is retarded from 170 CA deg ATDC to 290 CA deg ATDC for both camshafts. As start of injection timing moves towards TDC (expansion) there is less time for mixing and incomplete oxidation increases drastically.

ISCO values were vastly greater at late injection compared with early injection (Figure 6.73). At early injection, ISCO values varied between 3 g/kWh to 6 g/kWh. Whereas at late injection ISCO values varied from 38 g/kWh to 58 g/kWh. ISCO values were extremely high due to late injection causing incomplete oxidation. Again this is due to the stratification effect as discussed before.
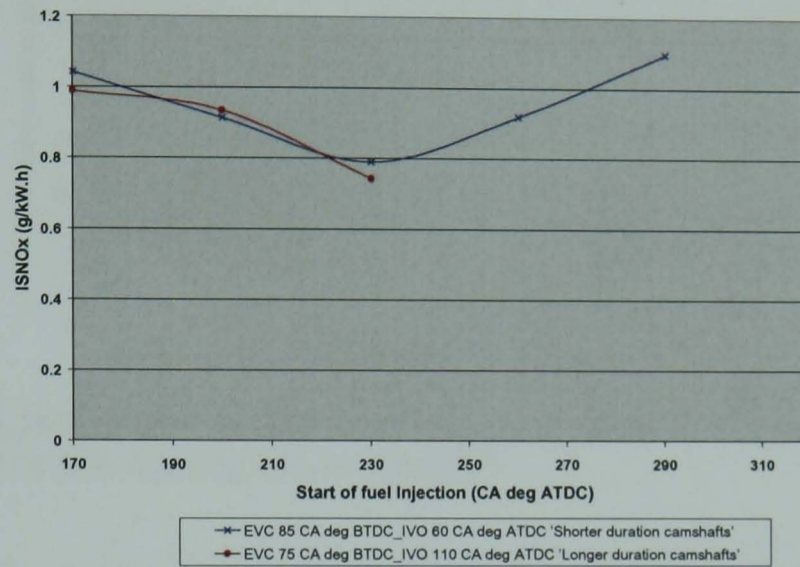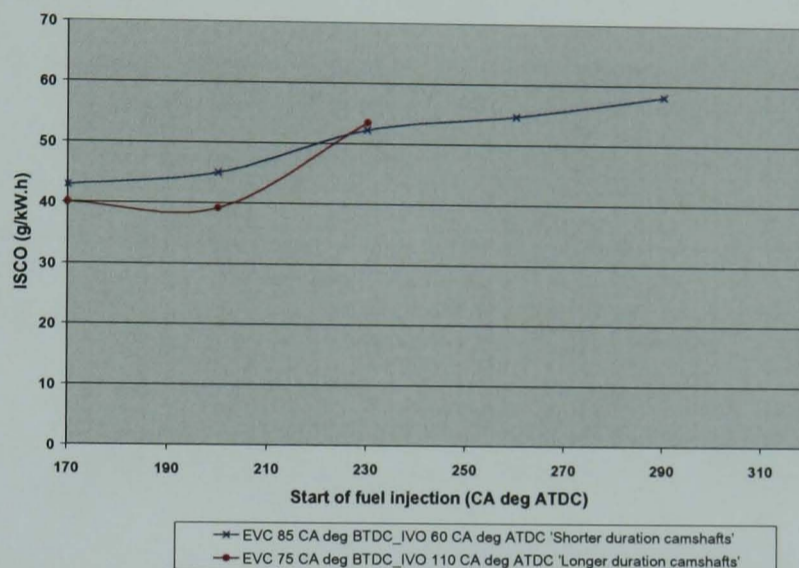

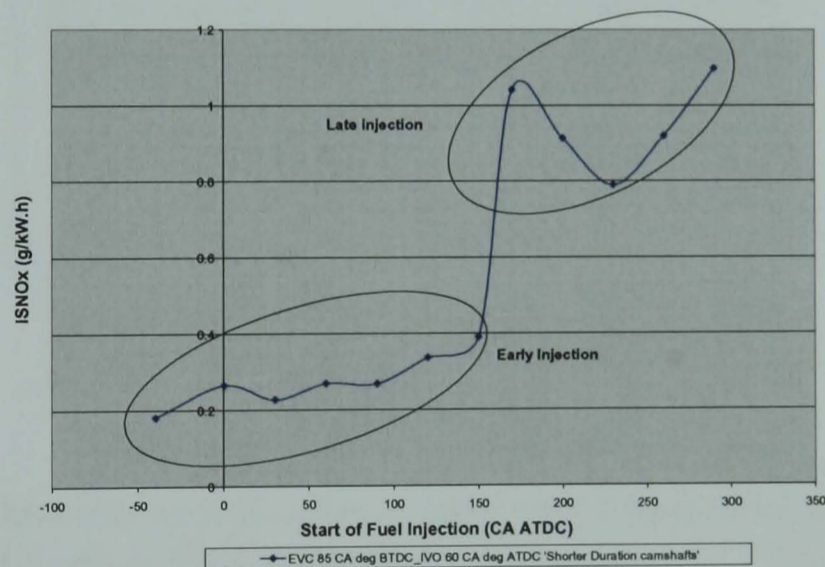Figure 6.72 ISCO against injection timing at different valve timings, SOI 170 to 290 CA deg ATDC (intake)
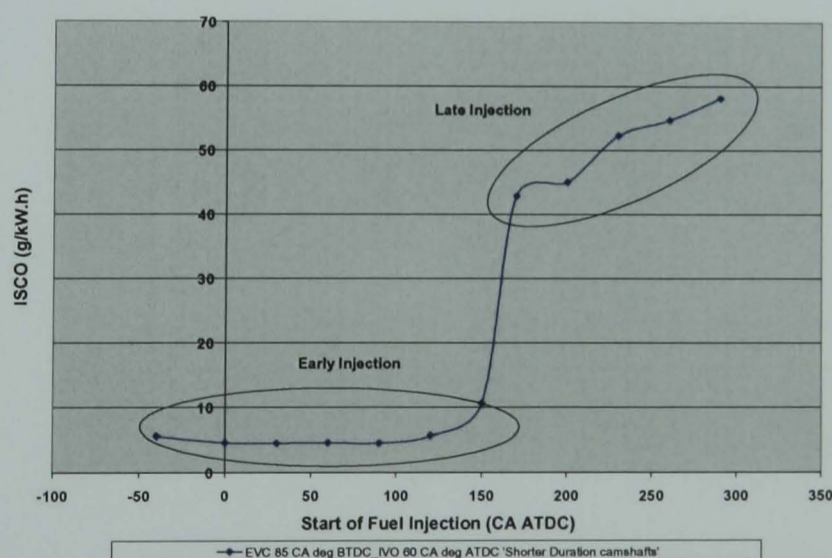
Figure 6.73 ISCO against injection timing for the shorter CAI camshafts, SOI -40 to 290 CA deg ATDC (intake), EVC = 85 CA deg BTDC, IVO = 60 CA deg ATDC

6.6.4 Effects of EVC and Valve duration on ISFC at late Injection

The longer CAI camshafts have higher ISFC values, for SOI 170 to 290 CA deg ATDC, compared with the shorter CAI camshafts (Figure 6.74), due to reduced expansion work as explained previously. The higher ISFC values of late injection (Figure 6.75) are expected as combustion is much slower and incomplete compared with early injections.

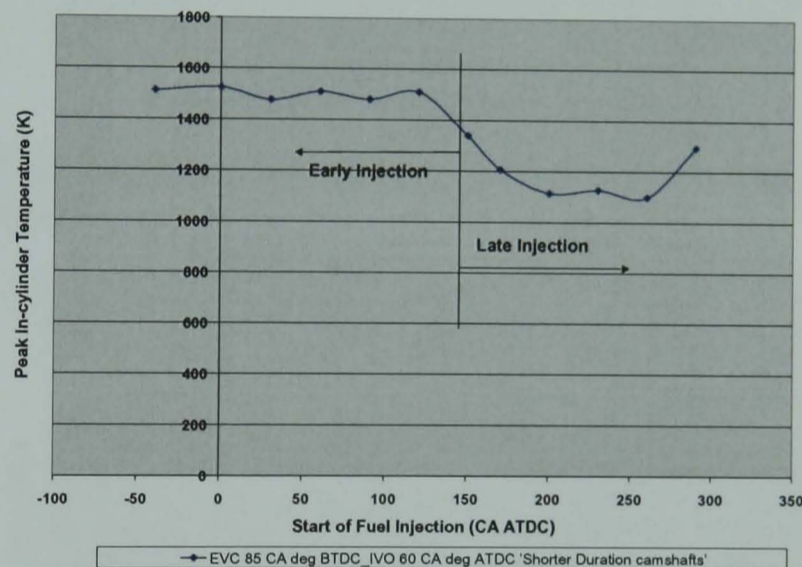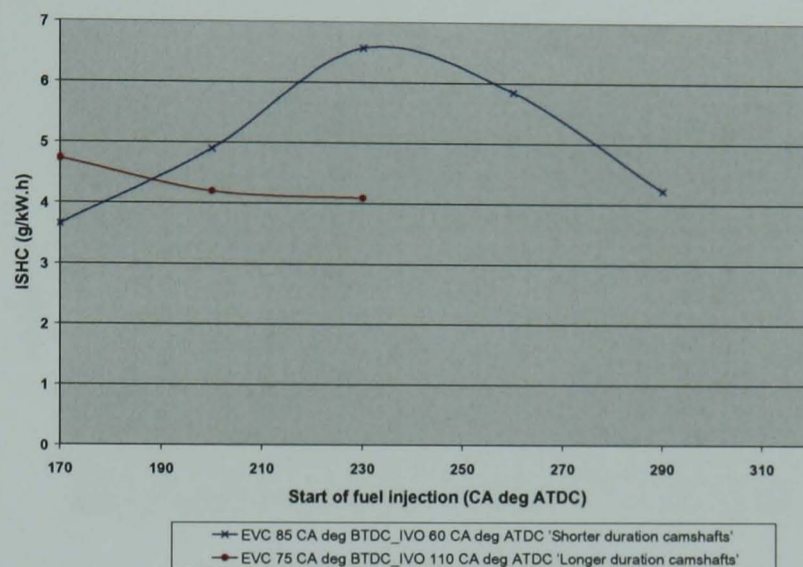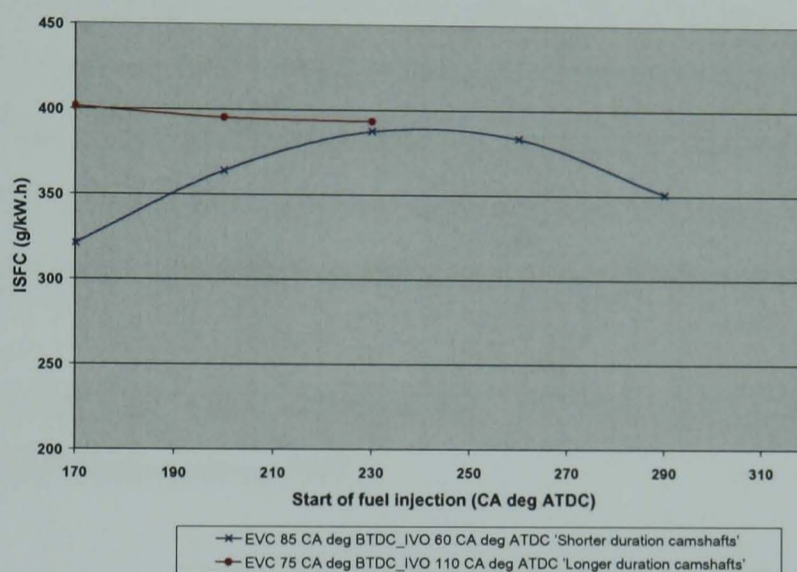**Figure 6.74 ISFC against injection timing at different valve timings, SOI 170 to 290 CA deg ATDC (intake)**
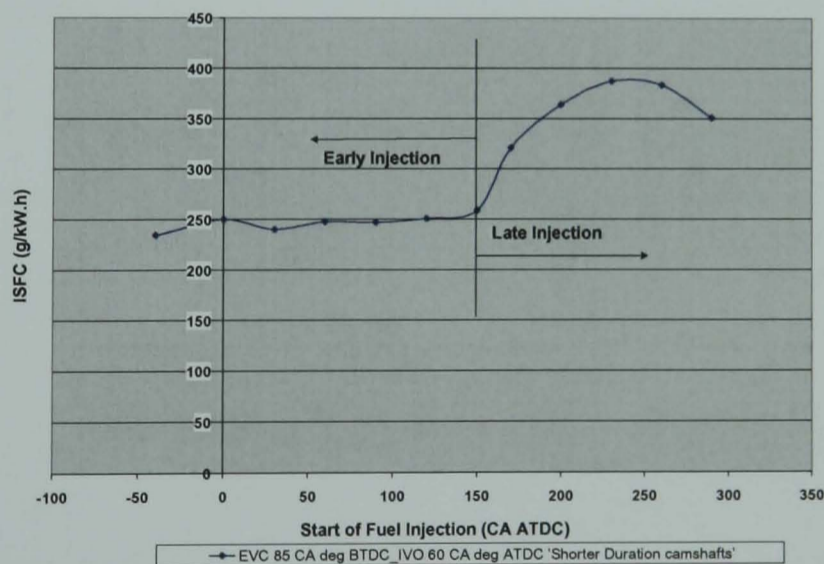
Figure 6.75 ISFC against injection timing for the shorter CAI camshafts, SOI -40 to 290 CA deg ATDC (intake), EVC = 85 CA deg BTDC, IVO = 60 CA deg ATDC

6.6.5 Summary of Late Injection on Engine Performance and Emissions

It was found that late injection leads to advanced combustion, but long combustion duration or partial burn due to the charge stratification effect. As a consequence of low NIMEP values at late injection, ISFC values were higher compared with early injection.

It was also observed at late injection that emissions increased compared with early injection. It was found that fuel rich pockets affected emissions in different ways. For ISNOx, it was found that that fuel rich pockets had locally high temperatures that caused ISNOx values to increase at late injection. ISHC and ISCO values were also higher at late injections due to unburnt fuel within rich regions of the combustion chamber.

Finally it was found that valve duration did not have any significant effect at late injection on NIMEP, emissions or ISFC.

Chapter 7

Conclusions and Recommendations for Further Work

Chapter 7   Conclusions and Recommendations for

Further Work

7.1 Introduction

A Ford 1.6 L multi-cylinder Direct Injection Gasoline engine was commissioned and modified to operate with Controlled Auto-Ignition combustion. The prototype engine fundamentally only differed from a conventional SI engine in that it had lower-than-normal valve lift and shorter-than-normal valve duration set in a negative valve overlap configuration. The engine was modified to incorporate a variable valve timing system which could be used to achieve CAI. EVC timing was advanced and hence a high percentage of exhaust gas was trapped, this provided the thermal energy to initiate auto-ignition of the fuel and the dilution of charge to control the subsequent heat release. As a consequence of reduced valve lift and duration, there was a limitation on inducted fresh charge, it was therefore envisaged that increasing intake and exhaust valve duration and lift would have an effect on the operational region. Through this research some interesting concepts were uncovered which provided possible solutions for seamless transitioning, future research is required to prove the viability of these concepts.

7.2 Engine Performance and Emissions whilst Utilizing SI and CAI combustion

7.2.1 Effect of Valve Duration on Engine Performance whilst using low-lift, short-duration CAI camshafts

It was found that at lambda 1.0, at the most retarded SOI timing that the NIMEP value was the highest for both the shorter and longer CAI camshafts. This was due to higher pumping losses resulting from heat loss occurring from SOI during the negative valve overlap. The

heat loss at early injection results in lower expansion pressure and hence higher pumping losses.

At lambda 1.2, it was also found that as injection timing was retarded, NIMEP increased. This was due to two reasons, the first being that combustion phasing was advanced with early injection causing NIMEP to drop. The second was due to a minor heat release event reducing compression work and increasing expended expansion work during the NVO period.

At both lambda 1.0 and 1.2, it was found that NIMEP values were higher for SI combustion compared with CAI combustion for both the shorter and longer CAI camshafts. This was due to a higher percentage of residual being trapped for advanced EVC timing and hence CAI combustion; therefore NIMEP values would be lower. However, it was found that at both lambda 1.0 and 1.2, some NIMEP values in the SI region overlap with values within the CAI region. This proves an effective method for achieving transitioning from low-lift SI to CAI combustion and back to low-lift SI combustion.

At lambda 1.0, for the entire SOI range, the shorter CAI camshafts had higher NIMEP values compared with the longer CAI camshafts. Firstly EVO for the longer CAI camshaft occurs 20 CA deg before EVO for the shorter CAI camshafts. The exhaust valve opened earlier during the power stroke resulting in positive work being displaced and causing higher pumping losses for the longer CAI camshafts. The second reason for lower NIMEP values was due to a higher percentage of trapped residual for the longer CAI camshafts at the same valve timing compared with the shorter CAI camshafts. This was due to higher in-cylinder pressure at EVC for the longer CAI camshafts leading to higher in-cylinder pressure at IVO and hence less inducted fresh charge. The other reason for the lower NIMEP values at lambda 1.0 for the longer CAI camshafts was due to a lower effective compression ratio for the same IVO, as IVC is retarded by 20 CA deg.

At lambda 1.2, the longer duration camshafts experience higher pumping losses compared with the shorter duration camshafts causing NIMEP values to be lower. For the longer CAI

camshafts, EVO is occurring 20 CA deg in advance, at a given valve timing, when compared with the shorter CAI camshafts. Furthermore, the valve lift is an extra 1mm for the longer CAI camshafts compared with the shorter CAI camshafts. These two factors cause a higher percentage of charge to exit through the exhaust valves and decrease the available expansion pressure. Hence greater work has to be done to overcome this loss of expansion pressure, leading to lower NIMEP values for the longer CAI camshafts at lambda 1.2.

7.2.2 Effect of Valve Duration on Engine Emissions whilst using low-lift, short-duration CAI camshafts

ISNOx emissions

At lambda 1.0, it was found that for both the shorter and longer CAI camshaft, at the most retarded SOI timing ISNOx values were the lowest. At lambda 1.2, the opposite effect was observed, for both the shorter and longer CAI camshafts as SOI timing was retarded the ISNOx values increased. This could be explained by the increase in spatially averaged peak in-cylinder temperature as SOI is retarded.

For both the shorter and longer CAI camshafts, at lambda 1.0 and 1.2, it was observed that ISNOx values were higher within the SI region compared with the CAI region. This was due to higher in-cylinder temperatures within the SI region causing higher ISNOx values.

On comparison of ISNOx values between the shorter and longer CAI camshafts at lambda 1.0, it was found that lower values of ISNOx existed for the longer CAI camshafts. This was due to the 20 CA deg earlier EVO opening for the longer CAI camshafts causing lower in-cylinder pressures and hence lower bulk in-cylinder temperatures. This allowed lower ISNOx values for the longer CAI camshafts.

For lambda 1.2, a similar trend was observed, it was found that the raw NOx emission values are lower for the longer CAI camshafts compared with the shorter CAI camshafts. This was due to lower in-cylinder temperatures observed for the longer CAI camshafts.

ISHC emissions

At lambda 1.0 and 1.2, for both the shorter and longer CAI camshafts, it was found that as SOI was retarded ISHC values increased. This was due to less mixing time at retarded fuel injection times. The lack of mixing time leads to fuel rich zones within the combustion chamber and hence an increase in unburned hydrocarbons at late injections.

Values of ISHC are higher for the CAI region compared with the SI region for both the shorter and longer CAI camshafts. ISHC values are based on in-cylinder temperatures, a higher in-cylinder temperature indicates less unburned fuel and hence a decreased production of unburnt hydrocarbons.

ISHC values are higher for the longer CAI camshafts, at lambda 1.0 and 1.2, compared with the shorter CAI camshafts. This is due to lower peak in-cylinder temperatures and a shorter expansion stroke observed for the longer CAI camshafts.

ISCO emissions

At lambda 1.0 and 1.2, as SOI is retarded ISCO values increase drastically. This can be explained by the fact that there is less time for charge mixing at later injections, decreasing homogeneity and increasing locally rich combustion.

ISCO values were generally lower for SI operation compared with CAI operation for both the shorter and longer CAI camshafts. However, it was observed that at lambda 1.0 for the longer CAI camshaft, CO values were lower for CAI operation compared with SI operation. ISCO values are not entirely based on in-cylinder temperature but are also based on the oxidation process. For CAI combustion, there is less inducted fresh charge and hence a lack

of oxygen which restricts the oxidation process and results in higher ISCO values within the CAI region compared with the SI region.

ISCO values are higher for the longer CAI camshafts compared with the shorter CAI camshafts, due to higher in-cylinder temperatures for the shorter CAI camshafts. The higher in-cylinder temperatures result in lower ISCO values due to a more favorable environment for CO to be oxidized to CO_2.

7.2.3 Effect of Valve Duration on Fuel Consumption whilst using low-lift, short-duration CAI camshafts

As SOI is retarded for both the shorter and longer CAI camshafts at lambda 1.0, ISFC values decrease. This is due to the fact that injection during the re-compression period initiates charge cooling which allows injection of more fuel, however, this is expended on higher pumping losses during the cycle. Injection during the re-expansion process allows less fuel to be injected due to lower expansion pressure and hence ISFC values are lower.

At lambda 1.2, as SOI is retarded, ISFC values increase for both the shorter and longer CAI camshafts. The lower values observed at early SOI timing is due to lower pumping losses. Less work is needed to overcome the exhaust gases and therefore fuel consumption also drops at injection during NVO re-compression period.

At both lambda 1.0 and 1.2, ISFC values are greater for the longer CAI camshafts compared with the shorter CAI camshafts. The reason for this is that higher pumping losses are associated with longer CAI camshafts.

7.3 Effects of Spark-Assistance on CAI combustion

It was found that there was an area sandwiched between spark-ignition combustion at low-lift and CAI combustion. This area, identified as spark-assisted combustion, is initiated by spark but has the characteristics of CAI operation. After undertaking testing it was found

that spark-assistance exhibited certain universal characteristics; true for both shorter and longer CAI camshafts. It was found that for spark-assisted combustion for both shorter and longer CAI camshafts that higher NIMEP values were obtained. Furthermore as ignition timing was advanced NIMEP increased. Ultimately, spark-assistance advanced the start of combustion and increased the heat release rate peak due to optimized combustion phasing. As a result of increased NIMEP, the ISFC values decreased for the spark-assisted cases again due to optimized combustion phasing.

For both the shorter and longer CAI camshafts, ISNOx values increased with spark-assistance due to higher in-cylinder temperatures caused by advanced combustion. Likewise due to higher in-cylinder temperatures it was found that ISHC and ISCO values decreased compared with conventional CAI combustion; again this trend was found for both the shorter and longer CAI camshafts.

7.4 Effects of operation at 2000 rpm on CAI combustion

The effects of operation at 2000 rpm on CAI combustion while varying SOI timing were investigated. It was found that varying SOI had little effect on NIMEP at 2000 rpm. It appears that at higher speed, there is less time for the charge temperature and pressure to be altered through fuel injection and so NIMEP does not change significantly over the injection range. Furthermore, since NIMEP did not change over the injection range at 2000 rpm, ISFC values did not drastically vary over the injection range.

ISNOx values are lower at a speed of 2000 rpm compared with 1500 rpm at EVC 65 CA deg ATDC. The reason for lower ISNOx values at 2000 rpm is due to lower in-cylinder temperatures. Due to these lower in-cylinder temperatures ISHC values are higher at 2000 rpm.

It was found that ISCO values were highest at 1500 rpm due to incomplete oxidation and poor charge mixing. Increasing engine speed to 2000 rpm caused ISCO values to decrease.

7.5 Effects of late injection on CAI combustion

It was of interest to investigate if late injection timings, typically 170 CA deg ATDC to 290 CA deg ATDC (intake), had an effect on CAI combustion. It was found that late injection leads to advanced combustion, but long combustion duration or partial burn due to the charge stratification effect. As a consequence of low NIMEP values at late injection, ISFC values were higher compared with early injection.

It was also observed at late injection that emissions increased compared with early injection. It was found that fuel rich pockets affected emissions in different ways. For ISNOx, it was found that fuel rich pockets had locally high temperatures that caused ISNOx values to increase at late injection. ISHC and ISCO values were also higher at late injections due to unburnt fuel within rich regions of the combustion chamber.

Finally it was found that valve duration did not have any significant effect at late injection on NIMEP, emissions or ISFC.

7.6 Recommendations for Future Work

Analysis work of the engine test data presented some interesting discoveries, some of which provided a method for seamless transition. Furthermore, research work highlighted certain avenues of interest which would be worthwhile exploring in order to push HCCI engines closer to production status. The author feels that work in the following areas should provide some useful and interesting results:

i)   It was found that similar NIMEP values were found for spark-ignition operation at low-lift and CAI operation. Therefore, it is apparent that by controlling injection timing, ignition timing, air/fuel ratio and valve timing that transition can be made from SI to CAI operation. Using an advanced engine management system, it should be possible to control these four parameters and change between SI and CAI operation. Work should be undertaken to implement and

evaluate the feasibility of using this method of transitioning and any noticeable condition change.

ii)   It was shown that SOI timing has a major effect on CAI combustion engine performance and emissions. Various benefits can be achieved by injecting at certain times with regard to valve events. However, for all research presented in this thesis, injection timing could be varied from -40 CA deg ATDC to 290 CA deg ATDC (intake) using only single injections. The effects of different injection strategies with numerous injections within the same cycle could prove useful and allow the advantages of early and late injection to be simultaneously realized.

iii)   Ultimately, for an HCCI engine to be capable of meeting the load demands of current production engines, an engine has to be produced which has the ability of switching between SI high-lift operation, SI low-lift operation and CAI operation. SI high-lift operation would be used for high loads, SI low-lift operation would be used for cold start and CAI operation would be used for low and mid loads. Therefore, the most realistic solution would be in the form of a Cam Profile Switching engine which could switch between the different modes. It would be useful to observe the effects on emissions and any discernible torque jump during transitioning with such an engine.

References

1. "Consultation on the review of the UK Climate Change Programme", DEFRA, March 2005.

2. "Gasoline Supply and Prices: Why are gas prices rising", United States Environmental Protection Agency (EPA), obtained from http://www.epa.gov/otaq/gasoline/informayion.htm

3. Euro III-V legislated emission levels, Vehicle Certification Agency (VCA), obtained from http://www.carfueldata.org.uk/June 2004.

4. "California Exhaust Emissions Standards and Test Procedures for 2004 and Subsequent Model Passenger Cars. Light Duty Trucks and Medium Duty Vehicles, California Environmental Protection Agency Air Resources Board", (CARB), June 2004.

5. Searles, R.A,. "Introduction to internal combustion engines", Third edition, Macmillian Press, ISBN 0-333-86058 322 9, 2000, p171.

6. Onishi, s., Jo, S.H., Shoda, K., Jo, P.D., and Kato, S., "Active Thermo-Atmosphere Combustion (ATAC) – A New Combustion Process for Internal Combustion Engines", SAE Paper 79050, 1979.

7. Stone, R., "Introduction to internal combustion engines", Third Edition, Macmillan Press, ISBN 0-333-74013 0, 2000, pp171.

8. Searles, R. A., "Emission catalyst technology-challenges and opportunities in the 21st century", International conference on 21st century emission technology, IMECH, conference transactions 2000-2, ISBN 1 86058 322 9, 2000.

9. Aoyama, T., Hattori, Y., Mizuta, J., (Toyota Central Research and Development Labs., Inc.) Sato, Y., (Toyota Motor Corp.) "An Experimental Study on Premixed-Charge Compression Ignition Gasoline Engine", SAE Paper 960081, 1996.

10. Willand, J., Nieberding, R.G., Vent, G., Enderle, C., "The Knocking Syndrome – Its Cure and Its Potential", SAE Paper 982483, 1998.

11. Urushihara, T., Hiraya, K., Kakuhou, A., Itoh, T., "Expansion of HCCI Operating Region by the Combination of Direct Fuel Injection, Negative Valve Overlap and Internal Fuel Reformation", SAE Paper 2003-01-0749, 2003.

12. Yamaoka, S., Kakuya, H., Nakagawa, S., Nogi, T., (Hitachi Research Laboratory, Hitachi, Ltd) Shimada, A., Kihara, Y., "A Study of Controlling the Auto-Ignition and Combustion in a Gasoline HCCI Engine", SAE Paper 2004-01-0942, 2004.

13. Xu, H., T. Wilson, S. Wallace, S. Richardson, M. Wyszynski, T. Megaritis, D. Yap, S. Golunski, and S. Peucheret, "Progress in FORESIGHT Homogeneous Auto-ignition Engines", JSAE paper 20055496, JSAE paper 20055496, JSAE Annual Congress (Spring), May 18-20, Yokohama (Japan), 2005.

14. Stanglmaier, R.H., Roberts C.E., "Homogeneous Charge Compression Ignition (HCCI): Benefits, Compromises, and Future Engine Applications", SAE Paper 1999-01-3682, 1999.

15. Ciatti, S.A., Hessler, J.P., Lee, K.O., Tentner, A.M., and Zhu, J., "Investigation of Nano-Particulate Production from Low Temperature Combustion", SAE paper 2005-01-0128, 2005.

16. Zhao, F.Q. et al., "Homogeneous Charge Compression Ignition (HCCI) engines – Key research and developement issues", ISBN 0-7680-1123-X, 2003, pp1

17. Fuerhapter, A., Piock, W.F., and Fraidl G.K., "CSI – Controlled Auto Ignition – the best Solution for the fuel Consumption – Versus Emission Trade-Off?", SAE paper 2003-01-0754, 2003.

18. Yang, J., Culp, T., "Development of a Gasoline Engine System Using HCCI Technology – The Concept and the Test Results", SAE paper 2002-01-2832, 2002.

19. Au, M.Y., Girard, J.W., Dribble, R., Flowers, D., Aceves, S.M., Martinez-Frias, J., Smith, R., Seibel, C., Maas, U., "1.9-Liter Four Cylinder HCCI Engine Operation with Exhaust Gas Recirculation", SAE paper 2001-01-1894, 2001.

20. Li J., Zhao, H., and Ladommatos, N., "Research and development of controlled auto-ignition (CAI) combustion in a four-stroke multi-cylinder gasoline engine", SAE paper 2001-01-3608, 2001.

21. Najt, P. M. and Foster, D.E., "Compression-ignited homogeneous charge combustion", SAE paper 830264, 1983.

22. Marriott, C., and Reitz, R., "Experimental Investigation of direct injection-gasoline for premixed compression ignited combustion phasing control", SAE 2002-01-0418, 2002.

23. Milovanovic, N., and Chen, R., "A review of Experimental and Simulation Studies on Controlled Auto-Ignition Combustion", SAE paper 2001-01-1890, 2001.

24. Jun, D., Ishii, K., Lida, N., "Combustion Analysis of Natural Gas in a Four Stroke HCCI Engine Using Experimental and Elementary Reactions Calculation", SAE paper 2003-01-1089, 2003.

25. Yap, D., S.M. Peucheret, A. Megaritis, M.L. Wyszynski, and H. Xu, "Natural Gas HCCI Engine Operation with Exhaust Gas Fuel Reforming. Int J Hydrogen Energy", 2006. 31: pp587 - 595

26. Pucher, G.R., Gardiner, D.P., Bardon, M.F., and Battista V., "Alternative Combustion Systems for Piston Engines involving Homogeneous Charge Compression Ignition Concepts - A review of Studies using Methanol, Gasoline and Diesel Fuel", SAE Paper 962063, 1996.

27. Gong, X., Johnson, R., Miller, D.L., and Cemansky, N.P., "Effects of DTBP on the HCCI Combustion Characteristics of SI Primary Reference Fuels", SAE Paper 2005-01-3740, 2005.

28. Thring, R. H., "Homogeneous Charge-Compression Ignition (HCCI) Engines", SAE Paper 892068, 1989.

29. Yap, D., A. Megaritis, M.L. Wyszynski, and H. Xu, "Effect of inlet valve timing on boosted gasoline HCCI with residual gas trapping", SAE 2005-01-2136, SAE Fuels and Lubricants Meeting, Rio de Janeiro, May 2005, 2005.

30. Lavy, J., Dabadie, J.C., Angelberger, C., Duret, P., Willand, J., Juretzka, A., Schaflein, J., Ma, T., Lendresse, Y., Satre, A., Schulz, C., Kramer, H., Zhao, H., and Damiano, L., "Innovative Ultra-low NOx controlled auto-ignition combustion process for gasoline engines: the 4-SPACE project", SAE paper 2000-01-1873, 2000.

31. Kimura, S., et al. "New combustion concept for ultra-clean and high-efficiency small DI diesel engines", SAE paper 1999-01-3681, 1999.

32. Christensen, M., Hultqvist, A, and Johansson, B., "Demonstrating the multi fuel capability of a homogeneous charge compression ignition engine with variable compression ratio," SAE paper 1999-01-3679, 1999.

33. Koopman, L., Strom, H., Lundgren, S., Backland, O., (Volvo Car Corporation) Denbratt, I., (Chalmers University of Technology) "Demonstrating a SI-HCCI-SI mode change on a Volvo 5-Cylinder Electronic Valve Control Engine", SAE Paper 2003-01-0753, 2003.

34. Kaahaaina, N.B., Simon, A.J., Caton, P.A., Edwards, C.F., "Use of Dynamic Valving to Achieve Residual-Affected Combustion", SAE Paper 2001-01-0549, 2001.

35. Urushihara, T., Hiraya, K., Kakuhou, A., Itoh, T., "Expansion of HCCI Operating Region by the Combination of Direct Fuel Injection, Negative Valve Overlap and Internal Fuel Reformation", SAE Paper 2003-01-0749, 2003.

36. Dec, J.E., Sjoberg, M., A., "Parametric Study of HCCI Combustion – the Sources of Emissions at Low Loads and the Effects of GDI Fuel Injection", SAE Paper 2003-01-0752, 2003.

37. Martinez-Frias, J., Aceves S.M., Flowers, D., Smith, J.R.(Lawrence Livermore National Laboratory), Dibble, R.(University of California at Berkley), "Equivalence Ratio-EGR Control of HCCI Engine Operation and the Potential for Transition to Spark-Ignited Operation", SAE paper 2001-01-3613, 2001.

38. Yelvington, P.E., and Green, W.H., "Prediction of the Knock Limit and Viable Operating Range for a Homogeneous-Charge Compression-Ignition (HCCI) Engine", SAE Paper 2003-01-1092, 2003.

39. Olsson, J., and Johansson, B., "Boosting for High Load HCCI", SAE Paper 2004-01-0940, 2004.

40. Xu, H., S. Rudolph, Z. Liu, S. Wallace, S. Richardson, M.L. Wyszynski, and A. Megaritis, "An Investigation into the Operating Mode Transitions of a Homogeneous Charge Compression Ignition Engine Using EGR Trapping. SAE Transactions", (SAE 2004- 01-1911), 2004.

41. Koopman, L., Strom, H., Lundgren, S., Backland, O., (Volvo Car Corporation) Denbratt, I., (Chalmers University of Technology) "Demonstrating a SI-HCCI-SI mode change on a Volvo 5-Cylinder Electronic Valve Control Engine", SAE Paper 2003-01-0753, 2003.

42. Sun, R., Thomas, R., and Gray, C.L. Jr., "An HCCI Engine: Power Plant for a Hybrid Vehicle", SAE Paper 2004-01-0933, 2004.

43. Milovanovic, M., Blundell, D., Pearson, R., Turner, J., (Lotus Engineers), Chen, R., (Department of Aeronautical and Automotive Engineering, Loughborough University), "Enlarging the Operational Range of a Gasoline HCCI Engine by Controlling the Coolant Temperature", SAE Paper 2005-01-0157, 2005.

44. Haraldsson, G., Tunestal, P., Johansson, B., and Hyvonen, J., "Transient Control of a Multi Cylinder HCCI Engine During a Drive Cycle", SAE Paper 2005-01-0153, 2005.

45. Matthews, J., Santoso, H., and Cheng, W.K., "Load Control for an HCCI Engine", SAE Paper 2005-01-0150, 2005.

46. Hyvonen, J.,(Fiat-GM Powertrain Sweden) Haraldson, G., Johansson, B., (Division of Combustion Engines, Lund Institute of Technology) "Operating Conditions Using Spark Assisted HCCI Combustion during Combustion Mode Transfer to SI in a Multi-Cylinder VCR-HCCI engine", SAE Paper 2005-01-0109, 2005.

47. Milovanovic, M., Blundell, D., Pearson, R., Turner, J., (Lotus Engineers), Chen, R., (Department of Aeronautical and Automotive Engineering, Loughborough University), "Enlarging the Operational Range of a Gasoline HCCI Engine by Controlling the Coolant Temperature", SAE Paper 2005-01-0157, 2005.

48. Aroonsrisopon, T., Werner, P., Waldman, J.O., Sohm, V., Foster, D.E., Morikawa, T., and Lida, M., "Expanding the HCCI Operation With the Charge Stratification", SAE Paper 2004-01-1756, 2004.

49. Urushihara, T., Yamaguchi, K., Yoshizawa, K., and Itoh, T., "A study of a Gasoline-Fuelled Compression Ignition Engine ~ Expansion of HCCI Operation range Using SI Combustion as a Trigger of Compression Ignition", ~ SAE 2005-01-0180, 2005.

50. Osbourne, R.J., Li, G., Sapsford, S.M., Stokes, J., Lake, T.H., and Heikal, M.R., "Evaluation of HCCI for Future Gasoline Powertrains", SAE Paper 2003-01-0750, 2003.

51. Plint. M., and Martyr. A., "Engine Testing Theory and Practice", Second Edition, Butterworth-Heinemann ISBN 0 7680 03148, 1999, pp125.

52. Robert Bosch GmbH, 2001. "Gasoline Systems: Gasoline Direct Injection", [CD ROM]. Bentley Publishers Robert Bosch GmbH, "Gasoline-engine Management" First edition, SAE International ISBN 0 7680 05108, 1999.

53. Zhao. H., and Ladommatos. N., "Engine Combustion Instrumentation and Diagnostics" First Edition SAE International, 2001, pp25

54. Kistler 6061B Thermocomp® Quartz Pressure Sensor, Kistler Instruments Ltd., Obtained from http://www.kistler.com/mediaaccess/ml/000-020m-09.95.pdf, 2001.

55. Robert Bosch GmbH, "Gasoline Engine Management", Second Edition, Professional Engineering Ltd, ISBN 1 8605 84349, 2004, pp268

56. Heywood, J.B., "Internal combustion engine fundamentals", McGraw-Hill Book Company, ISBN 0-07-100499-8, 1988, pp384

57. Standing, R.H., "Controlled Auto-Ignition in a Multi-Cylinder Direct Injection Gasoline Engine", PhD Thesis, Brunel University, 2005.

58. Cao, Li., "Numerical Study of Controlled Auto-ignition Combustion in Port and Direct Fuel Injections Gasoline Engine", PhD Thesis, Brunel University, 2005.

59. Zhao, F., Asmus, T.W., Assanis, D.N., Dec, J.E., Eng, J.A., Najt, P.M., Homogeneous Charge Compression Ignition (HCCI) Engines: Key Research and Development Issues, 2003, pp338.

60. Li, J., Zhao, Z., Ladommatos, N., and Ma, T., "Research and development of Controlled auto-ignition (CAI) Combustion in a 4-Stroke multi-cylinder gasoline engine", SAE Paper 2001-01-3608, 2001.

Appendix A   Values for LabVIEW™ Knock Detection Program

Parameter	Value
Trigger Position	252.5 or 612.5
Samples/Rev	720
Calibration Factor	10 bar
Low Pass Filter	13,000
High Pass Filter	18,000
Sampling Rate	40,000
Crank Radius	4.07 cm
Cylinder Bore	7.9 cm
Con-Rod Length	13.63
Compression Ratio	11.5
Swept Volume	399 cm^3
Clearance Volume	38 cm^3
IVC	300
EVO-IVC	132
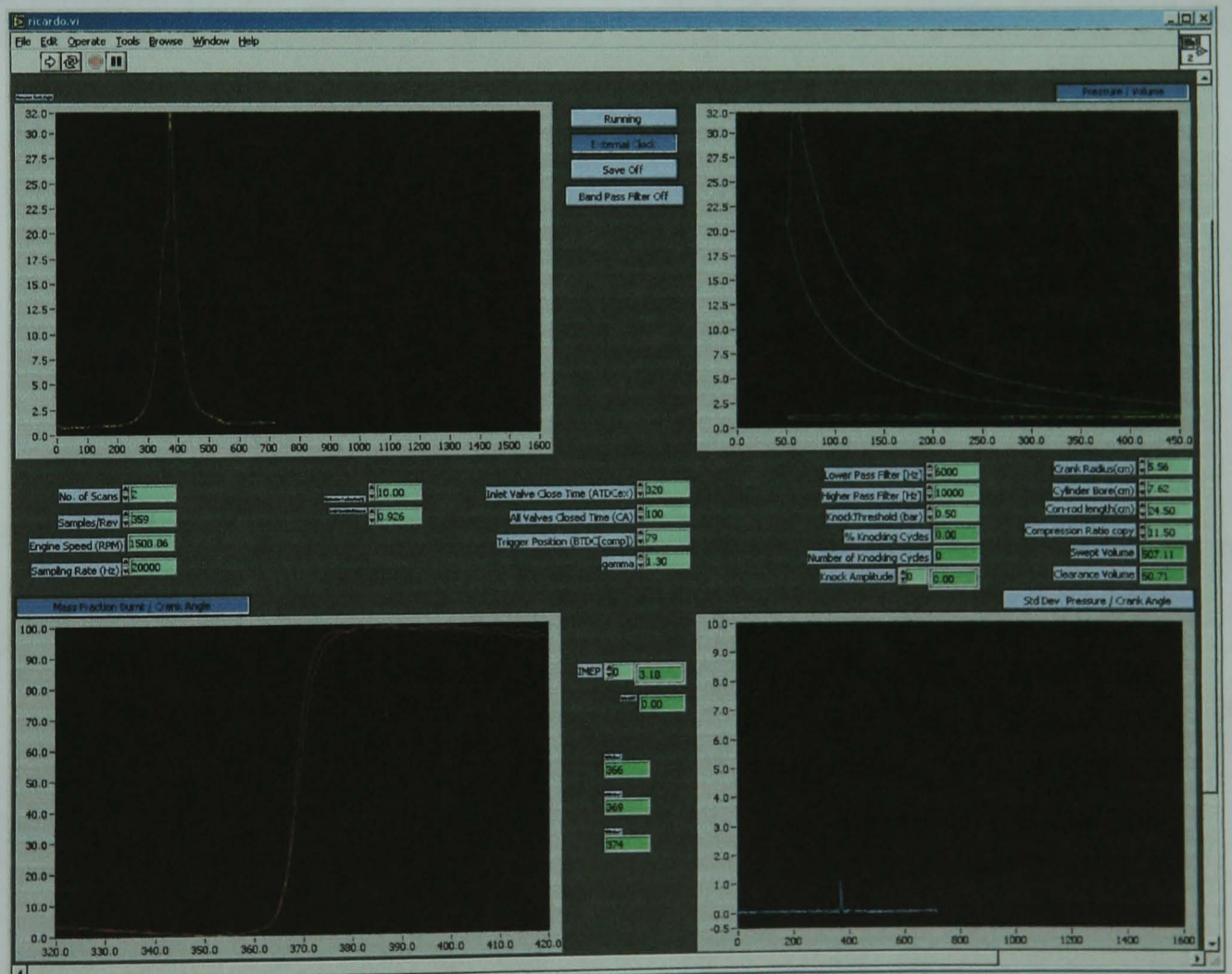
Front Panel of LabVIEW™ Knock Detection Program